

Air Force Institute of Technology

**AFIT Scholar**

---

Theses and Dissertations

Student Graduate Works

---

12-1995

## Validation of the Articulated Total Body Model Data Set Describing the Large Advanced Dynamic Anthropomorphic Manikin

Joel J. Hagan

Follow this and additional works at: <https://scholar.afit.edu/etd>



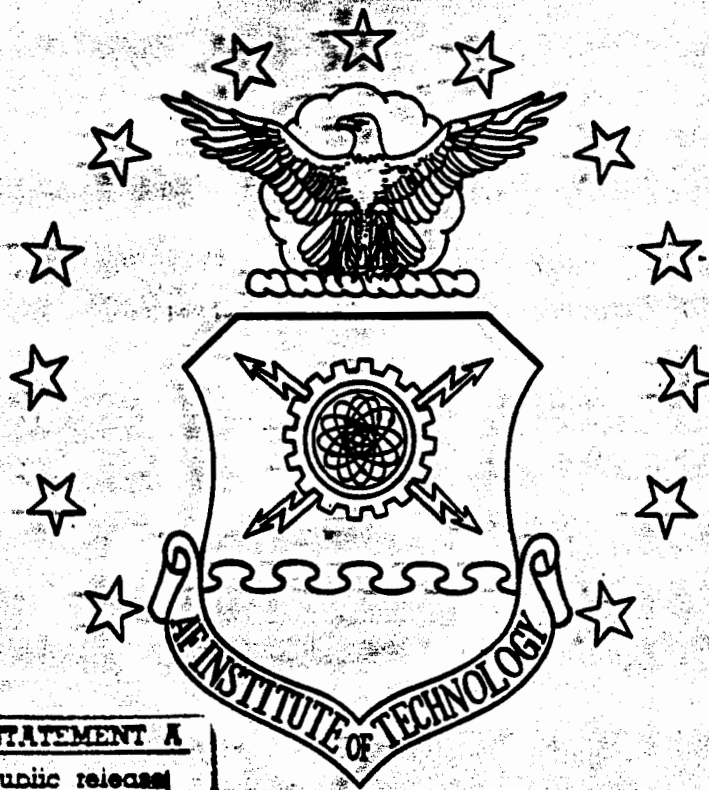
Part of the [Aerospace Engineering Commons](#)

---

### Recommended Citation

Hagan, Joel J., "Validation of the Articulated Total Body Model Data Set Describing the Large Advanced Dynamic Anthropomorphic Manikin" (1995). *Theses and Dissertations*. 6096.  
<https://scholar.afit.edu/etd/6096>

This Thesis is brought to you for free and open access by the Student Graduate Works at AFIT Scholar. It has been accepted for inclusion in Theses and Dissertations by an authorized administrator of AFIT Scholar. For more information, please contact [AFIT.ENWL.Repository@us.af.mil](mailto:AFIT.ENWL.Repository@us.af.mil).



**DISTRIBUTION STATEMENT A**  
Approved for public release  
Distribution Unlimited

VALIDATION OF THE ARTICULATED TOTAL  
BODY MODEL DATA SET DESCRIBING THE LARGE  
ADVANCED DYNAMIC ANTHROPOMORPHIC MANIKIN

THESIS

Joel J. Hagan, Captain, USAF

AFIT/GAE/ENY/95D-11

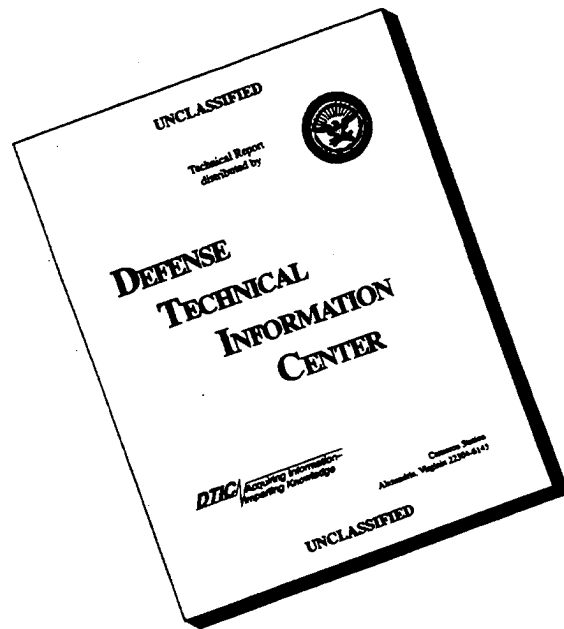
19960327 004

DEPARTMENT OF THE AIR FORCE  
AIR UNIVERSITY  
**AIR FORCE INSTITUTE OF TECHNOLOGY**

Wright-Patterson Air Force Base, Ohio

DTIC QUALITY INSPECTED 1

# DISCLAIMER NOTICE



**THIS DOCUMENT IS BEST QUALITY AVAILABLE. THE COPY FURNISHED TO DTIC CONTAINED A SIGNIFICANT NUMBER OF PAGES WHICH DO NOT REPRODUCE LEGIBLY.**

AFIT/GAE/ENY/95D-11

VALIDATION OF THE ARTICULATED TOTAL  
BODY MODEL DATA SET DESCRIBING THE LARGE  
ADVANCED DYNAMIC ANTHROPOMORPHIC MANIKIN

THESIS

Joel J. Hagan, Captain, USAF

AFIT/GAE/ENY/95D-11

Approved for public release; distribution unlimited

The views expressed in this thesis are those of the author and do not reflect the official policy or position of the United States Air Force, Department of Defense, or the United States Government.

AFIT/GAE/ENY/95D-11

VALIDATION OF THE ARTICULATED TOTAL BODY MODEL DATA SET  
DESCRIBING THE LARGE ADVANCED DYNAMIC ANTHROPOMORPHIC  
MANIKIN

THESIS

Presented to the Faculty of the School of Engineering  
of the Air Force Institute of Technology

Air University

In Partial Fulfillment of the Requirements for the Degree of  
Master of Science in Aeronautical Engineering

Joel J. Hagan, B.S.

Captain, USAF

December 1995

Approved for public release; distribution unlimited

## Acknowledgments

The purpose of this thesis is to validate the Articulated Total Body (ATB) model data set describing the Large Advanced Dynamic Anthropomorphic Manikin (ADAM). The importance of this research stems from the need to maintain the current standard of Air Force ejection seat safety in light of decreasing *defense dollars*. With less and less money, the U.S. Air Force is continually expected to do more with less. The validation of the ADAM data set will allow Armstrong Laboratory to perform more extensive ejection seat testing while spending less money on full scale ejection seat sled track testing.

Without a doubt, I could not have accomplished this research without the aid of many patient, intelligent individuals who took the time to guide me in a year of intense research. Many of these individuals I would like to thank. First of all, I would like to thank my advisor, Dr. Christopher Hall, who gave me direction when I needed it, but also allowed me free reign to stand and fall on my own. Second, I would like to thank the sponsors of my thesis at the Vulnerability Branch of the Air Force's Armstrong Laboratory. There are many individuals at Armstrong Laboratory who made significant contributions to my research. I would like to thank Ms. Jeanne Smith and Staff Sergeant Jennie Rachauskas for the invaluable computer support they provided. I would like to thank Mr. Greg Thompson, Mr. Chris Albery, and Ms. Donna Baughn for providing ADAM technical expertise. Measurement data on the ADAM which they provided considerably helped in the development of the ATB simulations used in this research. I

would also like to thank Mr. John Plagha for his support in providing and deciphering the AMIT test data.

There are two people at Armstrong Laboratory I would like to thank specifically. The first is Dr. Louise Obergefell. Dr. Obergefell, with her extensive knowledge of the ATB model and background in ejection seat modeling, was always available to answer any questions I had, from the most basic to the most complex. Her direction in performing this research was invaluable. Second, and most importantly, I wish to thank Ms. Annette Rizer. Annette was instrumental in explaining to me the many intricacies involved with the ATB software and in developing an ATB simulation of the ADAM. On a daily basis, she took every opportunity to help me when ever I needed it. Without her patience and hard work, and I assure you, working with me on a daily basis is hard work, I could not have accomplished the research presented in this thesis.

Finally, I wish to thank both my parents, Jim Hagan and Rosie Hagan, for their staunch support and ceaseless encouragement of my education. Some days when the school work becomes overwhelming and the research project isn't working, you need to be able to look up to someone else and say to yourself, "If that person believes in me, I should also believe in me." Both my parents have always believed in me and given me the support I needed to get me to where I am today - Thank you.

Joel J. Hagan

## Table of Contents

	Page
Acknowledgments.....	ii
Table of Contents.....	iv
List of Figures.....	viii
List of Tables.....	xi
List of Acronyms.....	xii
Abstract.....	xiii
I. Introduction.....	1
Background.....	1
Automotive Manikins.....	3
Ejection Seat Manikins.....	4
Advanced Dynamic Anthropomorphic Manikin.....	5
Motivation For This Research.....	7
Articulated Total Body Model.....	7
Ellipses and Connecting Joints.....	8
Ellipses.....	9
Joints.....	11
Planes.....	14
Objective.....	16
Methodology.....	17
Organization.....	18
II. Articulated Total Body Input File Development For AMIT 79E-G2A.....	19
AMIT 79E-G2A Test Description.....	20
Ejection Seat and Cockpit.....	20
Wind Plane.....	22
Wind Force Calculation.....	23
Addition of Flight Helmet and Boots to the ADAM Data Set .....	23
Placement and Balancing of the Body in the Ejection Seat.....	25
Approved Segment/Segment and Segment/Plane Contacts.....	26
Force Deflection Functions.....	26
Filtering and Conditioning Ejection Seat Accelerometer Data.....	27
Removal of Acceleration and Velocity Biases.....	27
Filtering Acceleration and Velocity Data Prior to <i>Seat First Motion</i> ....	31
Ejection Seat Trajectory Simulation Data.....	35
Filtering Ejection Seat Trajectory Simulation Data.....	37

Integrating Linear Acceleration Data.....	41
Calculating Velocities at the Seat Reference Point.....	43
Employing Mean of All Accelerometers in ATB Model.....	44
III. Result of the First ATB Simulation of AMIT 79E-G2A.....	48
Incomplete Simulation.....	48
Joint Angular Displacement Comparisons.....	49
Overall Similarity Between ATB Modeled and Measured Joint Motions ...	52
Excessive Joint Oscillations.....	53
Solutions to Joint Oscillation Problem.....	54
IV. Modifications to the ADAM Data Set.....	56
Joint Resistive Torque Function Measurement Procedure .....	56
Joint Resistive Torque Function Modifications.....	57
Constant Torque Addition.....	57
Torque Function Addition.....	58
Implementation.....	60
V. Results of the Second ATB Modeling of AMIT 79E-G2A .....	62
Euler Angle Comparison.....	62
Quaternion Comparison.....	64
Three Dimensional Comparison.....	66
Overall Similarity Between ATB Modeled and Measured Joint Motions...	68
VI. ATB Input File Development For the AMIT 79E-F1 Test.....	70
AMIT 79E-F1 Test Description.....	70
Modifications to AMIT 79E-G2A Input File.....	71
Removal of Acceleration and Velocity Biases.....	71
Filtering Ejection Seat Trajectory Simulation Data.....	73
Calculating Linear and Angular Velocities at SRP.....	73
Modifications to Ejection Seat Trajectory Data.....	76
VII. Results of the ATB Modeling of AMIT 79E-F1.....	77
Joint Angular Displacement Comparison.....	77
Overall Similarity Between Modeled and Measured Joint Motions.....	79
VIII. Conclusions and Recommendations.....	81
Conclusions.....	81
Recommendations.....	83
Appendix A: ATB Input File Card Definitions.....	86
Appendix B: Planes Describing the ACESII Ejection Seat in the Articulated Total Body Model.....	87

Appendix C:	Planes Describing the F-16A cockpit in the Articulated Total Body Model.....	88
Appendix D:	Measurements Required to Modify the ADAM Model to Account For a Flight Helmet.....	89
Appendix E:	Segment/Segment Contacts.....	90
Appendix F:	Plane/Segment Contacts.....	91
Appendix G:	Raw and Filtered Linear Acceleration and Angular Velocity Data Prior To <i>Seat First Motion</i> .....	92
Appendix H:	MATHCAD® Code to Filter Ejection Seat Data.....	97
Appendix I:	Raw and Filtered Linear Acceleration and Angular Velocity Data Between <i>Seat First Motion</i> and <i>Seat-ADAM Separation</i> .....	99
Appendix J:	AMIT 79E-G2A Cut-off Frequencies.....	104
Appendix K:	SIMULINK™ Block Diagram Used to Integrate Linear Acceleration Data.....	105
Appendix L:	Integrated Linear Accelerations.....	106
Appendix M:	MATLAB® Code to Transform Ejection Seat Linear Velocities From the Location of the Accelerometers to the Seat Reference Point.....	110
Appendix N:	Linear Velocities at Seat Reference Point.....	114
Appendix O:	ADAM Joint Angular Displacement Comparisons For the First ATB Simulation of AMIT 79E-G2A (Raw Data).....	118
Appendix P:	Explanation of the Terms - Flexion/Extension, Abduction/Adduction, Medial/Lateral, and Supination/Pronation.....	125
Appendix Q:	ADAM Joint Angular Displacement Comparisons For the First ATB Simulation of AMIT 79E-G2A (Shifted, Polarized Data)...	130
Appendix R:	ADAM Joint Motion With the Coulomb Friction Multiplied By a Factor of 10.....	137

Appendix S:	ADAM Joint Angular Displacement Comparisons For the Second ATB Simulation of AMIT 79E-G2A.....	143
Appendix T:	Comparison of Joint Angular Displacements For the First and Second ATB Simulation of AMIT 79E-G2A.....	150
Appendix U:	ADAM Joint Angular Displacements For the Second ATB Simulation of AMIT 79E-G2A in Terms of Quaternion Elements.....	156
Appendix V:	MATLAB® Code Written In Order to Describe Joint Angular Displacements in Three Dimensions.....	164
Appendix W:	AMIT 79E-F1 Cut-off Frequencies.....	170
Appendix X:	ADAM Joint Angular Displacement Comparisons For the ATB Simulation of AMIT 79E-F1.....	171
Appendix Y:	ATB Model of ADAM, ACES II Ejection Seat and F-16 Cockpit.....	178
Appendix Z:	ATB Simulation of AMIT 79E-F1.....	179
Bibliography.....		180
Vita.....		182

## List of Figures

Figure	Page
1.1 Third Generation Ejection Seats and Aircraft Performance Comparison.....	1
1.2 Fourth Generation Ejection Seat and Aircraft Performance Comparison.....	2
1.3 Large ADAM.....	6
1.4 Ellipsoid Geometric Centers and Centers of Mass.....	10
1.5 Ellipsoid Coordinate Systems.....	11
1.6 Segment Local & Principal Moment of Inertia Coordinate Systems.....	11
1.7 Euler Joint.....	12
1.8 Joint Structure.....	12
1.9 Joint Resistive Torque Function.....	13
1.10 Contact Plane.....	15
2.1 Raw Linear Acceleration and Angular Velocity Data Prior to <i>Seat First Motion</i> .....	28
2.2 Raw and Filtered Linear Acceleration Data Prior to <i>Seat First Motion</i> .....	32
2.3 Raw and Filtered Angular Velocity Data Prior to <i>Seat First Motion</i> .....	33
2.4 Raw Ejection Seat Trajectory Simulation Data.....	36
2.5 Raw and Filtered Linear Acceleration Ejection Seat Trajectory Simulation Data.....	39

2.6	Raw and Filtered Angular Velocity Ejection Seat Trajectory Simulation Data.....	40
2.7	Integrated Linear Accelerations.....	42
2.8	Velocity at Seat Reference Point.....	45
2.9	Average Linear Velocity at Seat Reference Point.....	46
2.10	Angular Velocity at Seat Reference Point.....	47
3.1	ADAM Right and Left Elbow Flexion.....	50
3.2	ADAM Right Elbow Flexion After Shifting and Polarization.....	52
3.3	Left and Right Elbow Supination/Pronation With Coulomb Friction Multiplied by a Factor of 10.....	55
4.1	Modified Joint Resistive Torque Function.....	59
5.1	ADAM Left and Right Elbow Flexion.....	63
5.2	Comparison of ADAM Left and Right Elbow Flexion For Runs 1 and 2.....	64
5.3	Quaternion Elements of the Left Elbow.....	65
5.4	Initial State of 3-D Comparison.....	67
5.5	3-D Comparison During Joint Motion.....	67
6.1	Linear Velocities At Seat Reference Point.....	74
6.2	Angular Velocity At Seat Reference Point.....	75

7.1	AMIT 79E-F1 Joint Motions Prior to Polarity Reversal.....	78
7.2	AMIT 79E-F1 Joint Motions After Polarity Reversal.....	78
8.1	U.S. Naval Aircraft Ejections.....	84

## List of Tables

Table	Page
1.1 Ellipsoid Axes Subscript Definitions.....	10
1.2 Coordinates Defining Ejection Seat Bottom.....	14
2.1 Biases in Raw Linear Accelerations and Angular Velocities.....	30
2.2 Biases in Filtered Linear Accelerations and Angular Velocities.....	34
4.1 Joint Functions Modified By a Constant Torque Increase.....	58
4.2 Joint Functions Modified By a Linearly Increasing Function.....	60
6.1 Biases in Raw Linear Accelerations and Angular Velocities.....	72

## List of Acronyms

AAMRL	Armstrong Aerospace Medical Research Laboratory
ACES	Advanced Concept Ejection Seat
ADAM	Advanced Dynamic Anthropomorphic Manikin
AFB	Air Force Base
AMIT	ADAM/MASE Integration Test
ATB	Articulated Total Body
CG	Center of Gravity
CVS	Crash Victim Simulator
GARD	Gruman-Alderson Research Dummy
HIA	Horizontal Impact Accelerator
KEAS	Knots Equivalent Airspeed
KIAS	Knots Indicated Airspeed
MASE	Multi-Axis Seat Ejection
MDT	Mountain Daylight Time
MST	Mountain Standard Time
SRL	Systems Research Laboratories, Inc.
SRP	Seat Reference Point
USAF	United States Air Force

## Abstract

As aircraft are developed for the 21<sup>st</sup> century, improvements in flight hardware such as engines employing *Super Cruise* and thrust vectoring will translate into ever expanding aircraft flight envelopes. Increasing flight envelopes results in increased danger to the pilot associated with high speed ejections. Unfortunately, decreasing *defense dollars* limit the extent to which aircraft ejection systems can be tested to ensure pilot safety. A low cost, effective solution to this dilemma is the use of computer modeling to augment full scale ejection seat sled track testing. To this end, the U.S. Air Force's Armstrong Laboratory has developed a data set describing the Advanced Dynamic Anthropomorphic Manikin (ADAM) for use in conjunction with the Articulated Total Body (ATB) model for the purpose of simulating the dynamics of the ADAM during sled track ejections. The purpose of this thesis is to validate the ADAM data set by graphically comparing ADAM joint angular displacements calculated by the ATB model with those measured during ejection seat sled track tests. Results of initial comparisons indicate oversimplifications in original joint resistive torque function calculations. These oversimplifications result in excessive joint oscillations as simulated by the ATB model. A certain amount of success in damping these joint oscillations is realized as a result of modifications to these joint resistive torque functions. Overall, the ATB model accurately simulates ADAM motion for the first 400 milliseconds of each simulation. Beyond this time, simulation versus AMIT 79E-F1 test results correlate relatively well. Nonetheless, excessive oscillations in certain joints continue to persist. These results indicate that the current ADAM data set is not completely valid.

VALIDATION OF THE ARTICULATED TOTAL BODY MODEL DATA SET  
DESCRIBING THE LARGE ADVANCED DYNAMIC ANTHROPOMORPHIC  
MANIKIN

I. Introduction

Background

As future military aircraft are developed, operational flight envelopes will be characterized by higher speeds and higher altitudes. With these increased performance capabilities comes an increased danger to the pilot. Figure 1.1 presents a comparison of proposed third generation ejection seat operating envelopes to the flight envelopes of future Department of Defense (DoD) aircraft.

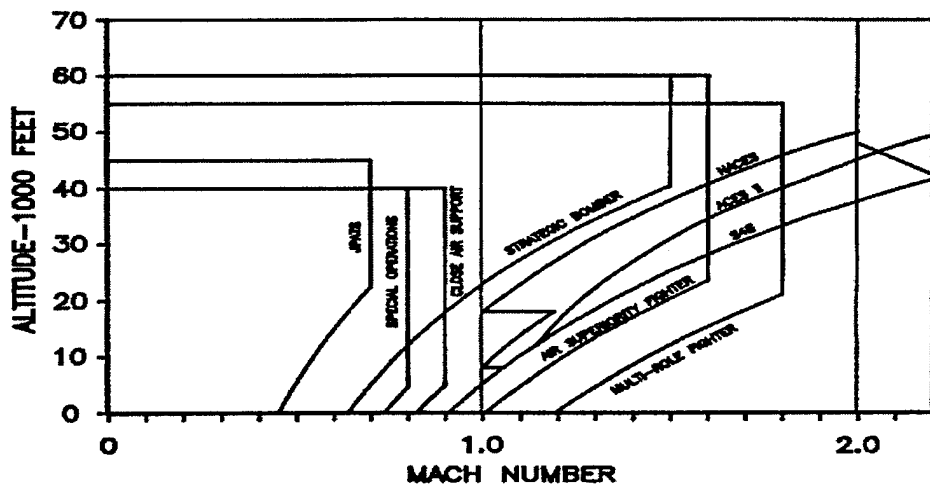


FIGURE 1.1 Third Generation Ejection Seats and Aircraft Performance Comparison (Zegler, 1993)

The aircraft envelopes are based on proposed aircraft designs such as the Advanced Tactical Fighter (ATF), the Multi-Role Fighter, and the Joint Primary Aircraft Training

System (JPATS). Similarly, ejection seat envelopes are based on the existing Advanced Concept Ejection Seat II (ACES II) as well as designs of the Naval Aircrew Common Ejection Seat (NACES) and the S4S ejection seat (Zegler, 1993). Figure 1.1 displays the borderline capability third generation ejection seats will have in adequately protecting tomorrow's pilots. Figure 1.2 depicts how even fourth generation ejection seats, defined by specifications developed by the Crew Escape Systems Technologies (CREST) program office, may not sufficiently ensure the safety of pilots in certain regimes of the flight envelope (Zegler, 1993).

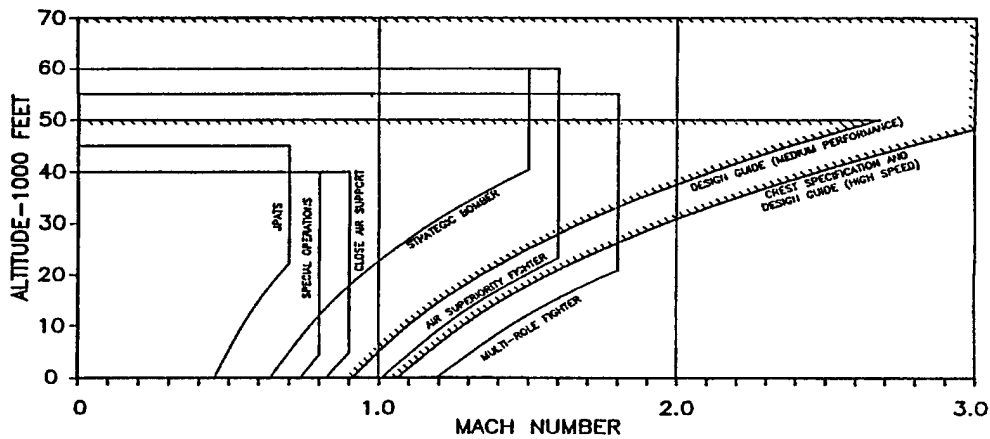


FIGURE 1.2 Fourth Generation Ejection Seat and Aircraft Performance Comparison (Zegler, 1993)

Clearly, then, Figures 1.1 and 1.2 provoke the question, "How will improvements in future aircraft performance affect the safety of pilots in the event of an ejection?" Although one would prefer to test every regime of the flight envelope to ensure the safety of the flight crew, the use of full scale, man-in-the-loop testing is prohibitively expensive, and prohibitively dangerous. Borrowing an idea from the automotive industry, the

United States Air Force (USAF) has found it useful to simulate various ejection scenarios by ejecting human-like manikins from high speed sled track ejection seats.

This chapter delineates the evolution of manikins used in the evaluation of aircraft ejection seat safety. This background portrait of ejection seat manikins culminates in the description of the Advanced Dynamic Anthropomorphic Manikin (ADAM) which is the manikin currently employed by the Air Force for ejection seat testing. Following the ADAM description is a definition of the objective of this thesis which is to validate a data set describing the ADAM. The ADAM data set is used by the Articulated Total Body (ATB) computer model to simulate the dynamics of the ADAM during an aircraft ejection. Next, a short description is presented explaining how this validation is accomplished. Finally, an outline of the remaining chapters in the thesis is presented.

### Automotive Manikins

The automotive industry has employed several different types of manikins throughout its history of ensuring passenger safety. Manikins first developed during the 1950's were simply used to simulate the human body's interaction with the car's seat and belts. Inertial properties were of primary concern at this time. Further manikin development was spurred by the public emphasis on automobile safety. In the 1960's and 1970's manikins such as the Hybrid II developed by General Motors, more commonly known as the Part 572, were introduced. These manikins more accurately simulated the motion of the body, specifically the arms, legs, and head. Similarly, in the late 1970's

General Motors developed the Hybrid III manikin with improved joint characteristics and instrumentation capability (Rasmussen and others, 1993:1).

Manikins such as the Hybrid II and Hybrid III were very good at simulating the response of the human body to car-like crashes. Unfortunately, as the aerospace industry realized, car crashes are not very similar to aircraft ejections. Automobile manikins had a certain number of disadvantages with regard to aerospace applications. Shortcomings such as poor modeling of the human spine, the area of the body enduring the greatest impact during an ejection, and insufficient durability to withstand the large forces encountered during aircraft ejections, precluded the use of the Hybrid II and Hybrid III in ejection seat testing (Rasmussen and others, 1993:2). Consequently, the aerospace industry was forced to continue employing existing manikins specifically designed for ejection seat testing.

#### Ejection Seat Manikins.

The manikins developed for the purpose of testing ejection seats, unfortunately, had not advanced as quickly as those manikins developed for the purpose of evaluating automotive safety. Until the late 1980's, the majority of ejections seat tests were accomplished using the Grumman-Alderson Research Dummy (GARD) or Center of Gravity (CG) dummy developed in the early 1950's (Bartol and others, 1990:2). Noting a need to develop a more accurate manikin for the Advanced Concept Ejection Seat (ACES) II Upgrade System, the USAF developed the Limb Restraint Evaluator (LRE). Although the LRE served its purpose of evaluating the limb restraint system for the

ACES II, it still fell short in many areas when it came to accurately modeling the human body during an aircraft ejection. Similar to the Part 572 and Hybrid III manikins, the LRE did not simulate the compressions of the spinal column or the cervical and lumbar sections. It also only modeled the large sized male (Bartol and others, 1990:3).

#### Advanced Dynamic Anthropomorphic Manikin.

These deficiencies in current automobile and ejection seat manikins led the Air Force to initiate the development of the Advanced Dynamic Anthropomorphic Manikin (ADAM) (Rizer and others, 1994). The ADAM was developed by Systems Research Laboratories (SRL) in 1985. There are currently two sizes of the ADAM, small and large. The small ADAM has a mass of 60.40 kilograms and is 1.68 meters in height. The large ADAM has a mass of 98.43 kilograms and is 1.89 meters in height. These sizes are based on surveys taken by the USAF in 1967 to define geometric characteristics of current aviators (Rasmussen and others, 1993:2). A picture of the large ADAM is shown in Figure 1.3.

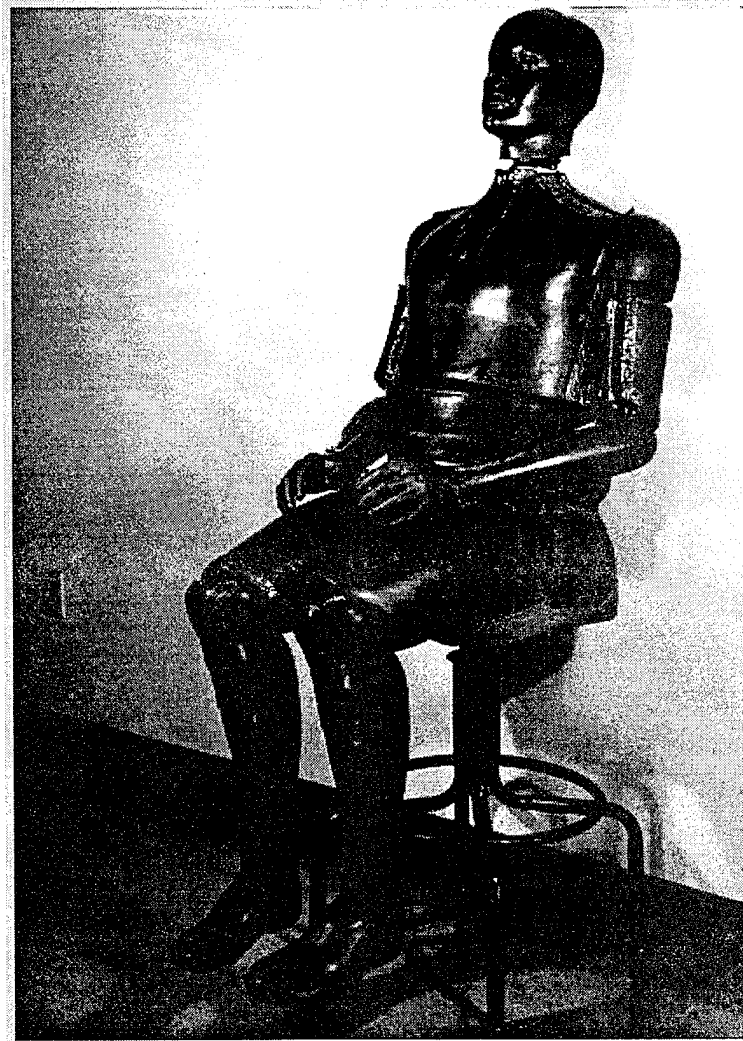


FIGURE 1.3 Large ADAM (Rizer and others, 1994)

The ADAM consists of 17 segments corresponding to the primary divisions of the human body (upper arm, forearm, head, neck, etc.). Joint ranges of motion and joint resistances to motion are representative of human joint characteristics. Detachable skin coverings facilitate an accurate geometrical representation of the human body. An axially deforming spinal structure accurately models the critical dynamics of the human spinal column. Coupled with an onboard data acquisition system capable of reading 128

channels, the ADAM is a tremendous leap forward in the U.S. Air Force's ability to model human body dynamics in the event of an aircraft ejection. A full description of the ADAM is presented in Advanced Dynamic Anthropomorphic Manikin (ADAM) Final Design Report AAMRL-TR-90-023, March 1990 (Bartol and others, 1990).

#### Motivation For This Research

ADAM is a significant step forward in improving the accuracy of modeling the human body during aircraft ejections. Improvements such as this have also lead to increases in the cost of ejection seat sled track tests. Currently, high speed sled track test at Holloman AFB, NM costs approximately \$100,000 per sled track run (Plagha, 1995). Sled track costs and manikin repair and maintenance costs have resulted in a need for a capability to augment full scale ejection seat sled track testing. Current trends toward computer simulation are increasingly becoming the solution of choice to overcome these costs while still providing accurate information regarding the effects of high speed ejections on aviators. The USAF Armstrong Laboratory (AL) is currently developing such computer simulation capability. The Biodynamics and Biocommunications Division of AL employs the Articulated Total Body (ATB) Model to simulate gross human body dynamics during aircraft ejections (Obergefell and others, 1988:1).

#### Articulated Total Body Model.

The ATB model is a derivative of the Crash Victim Simulator (CVS) developed by Calspan Corporation in 1975 for AL. Modifications to the CVS include additions of

harnesses, belts, and wind blast effects. The ATB model is designed to model the three-dimensional dynamics of a system of rigid bodies. Although the human body is the primary system modeled by the ATB simulation, it has also been used to model the motion of billiard balls as well as the transient response of the MX missile suspended from cables in a wind tunnel (Obergefell and others 1988:1-7). A full description of the ATB model is presented in Articulated Total Body Model Enhancements AAMRL-TR-88-043, January 1988 (Obergefell and others 1988:22-25).

In order to simulate the dynamics of a particular body using the ATB, one needs to model both the body and the environment with which the body interacts during a particular event such as an aircraft ejection. In the case of ejection seat simulation, the body is the ejection seat manikin and the environment is the ejection seat and aircraft cockpit. The body is modeled in the ATB as a series of ellipses connected by joints. The environment is modeled as a series of planar surfaces. The following two sections further explain the use of ellipses, joints, and planes in the development of an ATB simulation.

Ellipses and Connecting Joints. Systems, such as the human body, are modeled by the ATB as a series of elliptical structures (ellipsoids) termed segments which are connected by joints. In order for ellipses to accurately model sections of the human body such as the lower arm, upper arm, etc., certain characteristics of the body segments and joints must be known. Elliptical segments are defined by the following characteristics.

1. Ellipsoid semiaxes lengths
2. Location of ellipsoid geometric center
3. Mass and CG location
4. Principal axis orientation and Principal moments of inertia
5. Force deflection functions defining resistance encounter when impacting a segment

Joints connecting each segment are defined by the following characteristics.

1. Joint type (Euler, slip, ball and socket, etc.)
2. Locked/unlocked state of joint rotational axes
3. Location of the joint relative to the adjoining segments
4. Orientation of the joint axes.
5. Joint resistive torque functions defining the resistance in each joint to motion

The properties defined in these two lists for a specific body characterize that body's ATB data set. This data set can then be used to model the dynamics of that particular body.

Ellipses. Although the shape of an ellipse only approximates the geometrical properties of a particular segment of the body, the mass properties of the segment are accurately modeled by defining the true location of the segment's center of mass. Note that the center of mass is normally not located at the center of the ellipsoid.

Defined for each segment are three separate right handed coordinate systems. The first coordinate system is the segment local coordinate system which has its origin at the center of mass and is orientated parallel to the ellipsoid semiaxes. The location of the ellipsoid geometric center is defined relative to the segment local coordinate system. When the body is standing straight up and down, all of the segment coordinate systems have their X axes pointing forward and Z axes pointing down. The second axis system, the ellipsoid axis system, is located at the geometric center of the ellipse and is also orientated parallel to the ellipsoid semiaxes. The third axis system is the principal axis system which is collocated with the segment local coordinate systems at the segment center of mass. The orientation of the principal axis is defined relative to the local segment coordinate system and varies with each segment. The Figure 1.4 through Figure 1.6 present an example of two attached ellipsoids. Shown in this description are the axis

systems described in this section. The subscripts on the X, Y, and Z axes in these three figures are defined in Table 1.1.

TABLE 1.1 Definition of Ellipsoid Axes Subscripts

Subscript	Axis System
I	Inertial
E	Ellipsoid
L	Local
P	Principal

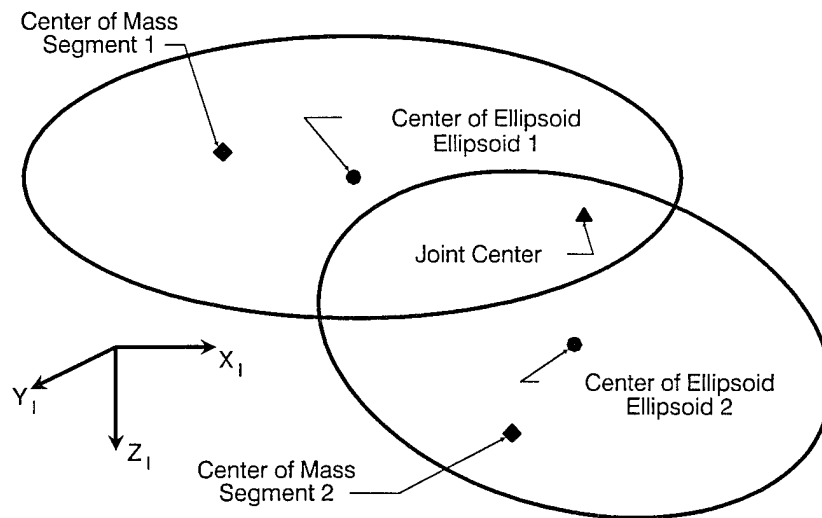


FIGURE 1.4 Ellipsoid Geometric Center and Center of Mass (Obergefell, 1993:11)

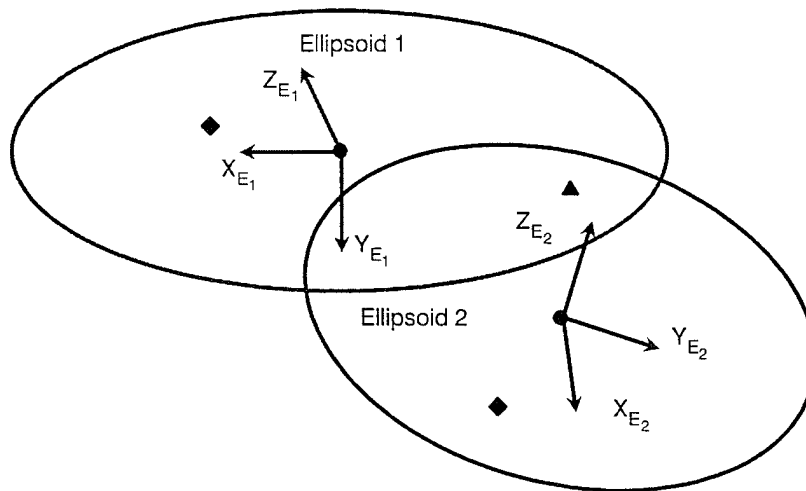


FIGURE 1.5 Ellipsoid Coordinate Systems (Obergefell, 1993:12)

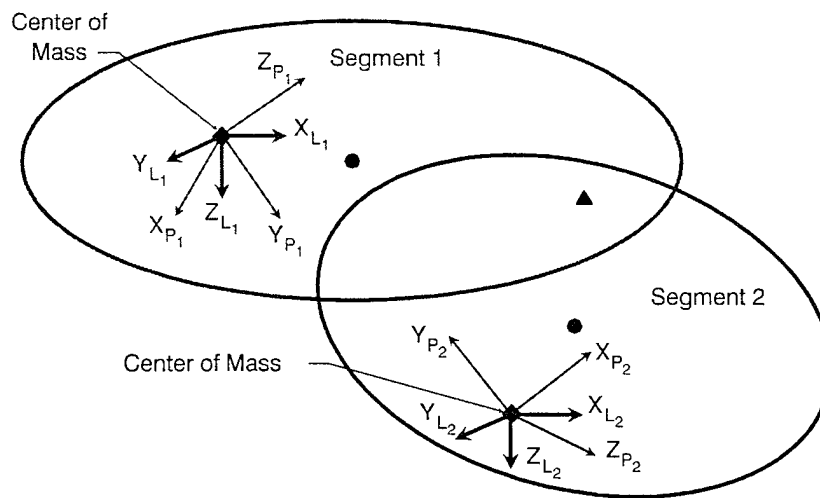


FIGURE 1.6 Segment Local & Principal Moments of Inertia Coordinate Systems (Obergefell, 1993:13)

Joints. Of the many different possible types of joints that can be modeled by the ATB, the data set describing the ADAM almost exclusively employs the Euler joint. The head and neck joints, which use ball and socket joints, are the only exceptions. Figure 1.7 presents a model of an Euler joint.

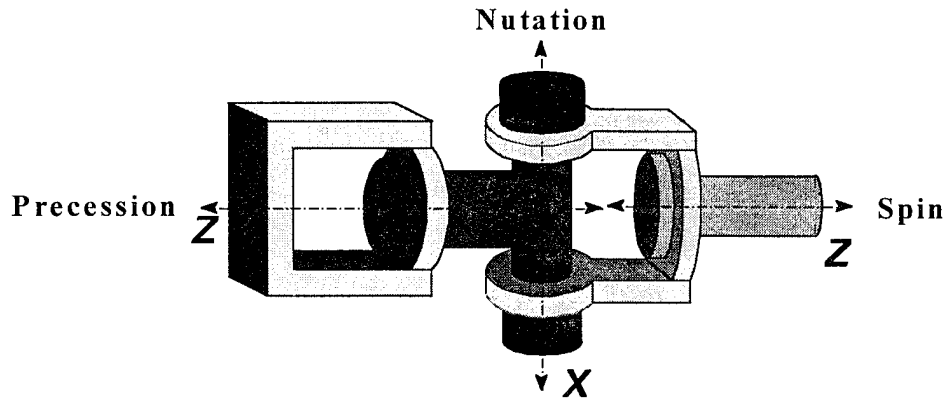


FIGURE 1.7 Euler Joint (Obergefell, 1993:23)

A joint's location and orientation are defined relative to the local coordinate system of each segment the joint is connecting. Two axis systems are collocated at each joint. One joint axis system orientation is defined relative to one of the connected segments and the other joint axis system is defined relative to the other connected segment. The relative angular displacement of these two axis systems defines the rotation the connected segments about that joint. Figure 1.8 presents an example of a typical joint structure depicting these axis systems.

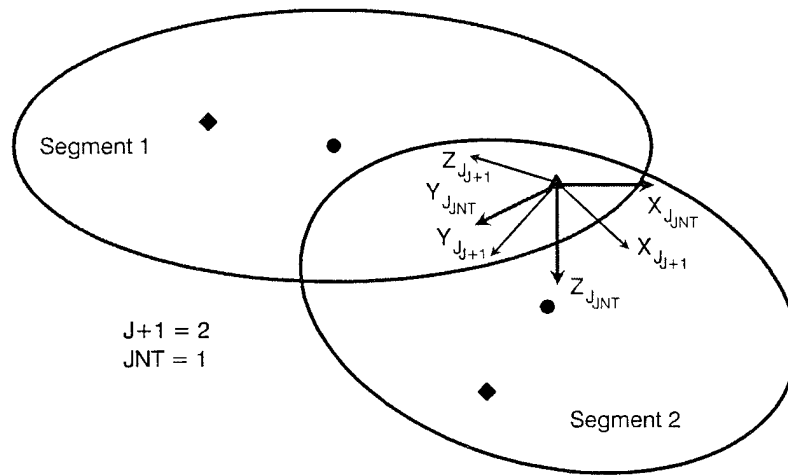


FIGURE 1.8 Joint Structure (Obergefell, 1993:14)

The resistive torque in each joint which opposes joint motion is defined by joint resistive torque functions. Relative to a predefined joint zero angle, joints can rotate one of two directions, positive or negative. Terms describing each joint's positive and negative displacements are defined in Appendix P. Each joint's displacements (positive and negative) are characterized by separate joint resistive torque functions such as the one depicted in Figure 1.9.

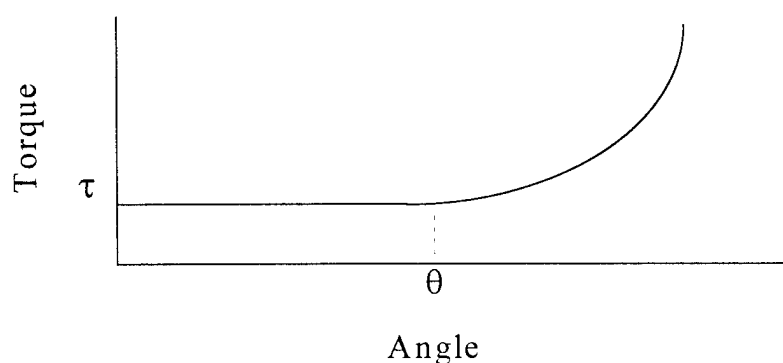


FIGURE 1.9 Joint Resistive Torque Function

The constant coulomb friction torque  $\tau$  models the resistive torque experienced by a particular joint in the range of motion between *soft stops*. The constant coulomb friction torque,  $\tau$ , results from the resistance due to friction plates present in each of the ADAM's joints. *Soft stops* are polyurethane pads which limit the ADAM's range of joint motion. They also serve to model the increasing resistance encountered by a human joint when it reaches its limiting range of motion. Once the joint motion reaches a certain *stop angle*,  $\theta$ , which is when the soft stops are contacted, the joint resistive torque function becomes nonlinear and the resulting resistive torque increases rapidly.

Planes. Along with describing the characteristics of the body modeled by the ATB, the characteristics of the environment in which the body is present must also be modeled. In the case of simulating an aircraft ejection for example, one must model the geometry of the cockpit and the ejection seat. The cockpit and ejection seat are termed “vehicles” in the ATB model. Vehicles are characterized as having their trajectory predefined prior to the start of the simulation. This is in contrast to the body which has its motion calculated throughout the ATB simulation. It is the force resulting from vehicle motion that causes the body to move during the simulation.

Vehicles are modeled primarily using planar surfaces. In order to create a plane in the ATB model, three points in space are specified relative to the inertial reference frame. These three points must characterize two orthogonal vectors which outline two sides of the plane. The vector defined by crossing these two vectors identifies the positive side of the plane. A typical vector set and resulting plane are displayed in Table 1.2 and Figure 1.9 respectively.

TABLE 1.2 Coordinates Defining Ejection Seat Bottom

	Seat Bottom		
1	0.85	-9.10	-0.85
2	0.85	9.10	-0.85
3	18.67	-9.10	-0.85

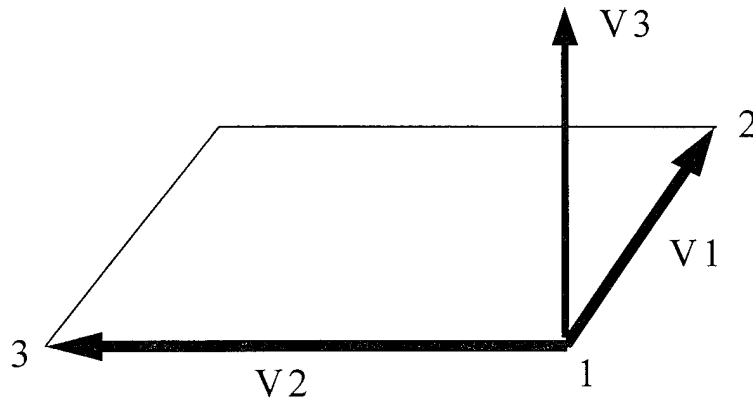


FIGURE 1.10 Contact Plane

Points 1, 2, and 3 are specified by the three ordered triplets defined in Table 1.2. Using the right hand rule, crossing vector V1 with vector V2 results in vector V3 which is normal to the positive face of the plane. If an ellipsoid segment contacts a plane, it will receive a force with a magnitude defined by a particular force-deflection function and in the direction defined by V3. Therefore, if a segment contacts the positive side of a plane, the resulting force will oppose the motion, and the segment will be pushed away from the plane. However, if a segment contacts the negative side of a plane, the contact force will be in the same direction as the segment's velocity, and will pull the segment through the plane (an unrealistic case which should not occur in a normal simulation).

The force imparted on the modeled body resulting from contact with a plane or with another segment is defined in the ATB model by force deflection functions. The magnitude of the force defined by a force deflection function is primarily dependent on a body segment's depth of penetration into a plane or segment. The greater the depth, the greater the reactive force. Force deflection functions can be defined in the ATB model

either in coefficient or tabular form. Specific force deflection functions used in this validation are describe in Chapter II.

Three vehicles, the aircraft cockpit, ejection seat, and camera, are described in the ATB simulation, each vehicle having its own axis system. The camera vehicle is artificially defined for the purpose of viewing the simulation. The modeled body does not interact with the camera segment at any time. At the beginning of an ATB simulation, vehicle axis systems are coincident with the inertial axis system. The ATB model's inertial axis system is oriented with the positive X direction pointing forward, the positive Y direction pointing to the right and the positive Z direction pointing down. The ejection seat's vehicle axis system is centered at the ACES II Seat Reference Point (SRP). The initial orientation of this axis system has the X axis pointing forward and pitched up 30° and the Z axis pointing up and parallel to the seat back. The orientation of the cockpit and camera vehicle axis systems corresponds to the orientation of the inertial axis system.

### Objective

Presented in the section of this chapter titled "Ellipses and Connecting Joints" are two lists describing information about a body that must be known in order to model that particular body using the ATB. This information is known as the body's data set. The current ATB data set describing the large ADAM was developed by Systems Research Laboratories in-house at Wright-Patterson AFB, OH in 1994. Development of a Simulation Database for the Advanced Dynamic Anthropomorphic Manikin (ADAM)

describes the details of how this was accomplished (Rizer and others, 1994). The objective of this thesis is to validate the Articulated Total Body (ATB) data set describing the Advanced Dynamic Anthropomorphic Manikin (ADAM). Validation, as defined in this context, refers to a determination of how accurately the ATB can model the ADAM when employing this data set.

### Methodology

Validation is based on comparisons between the joint angular displacements of the ADAM as modeled by the ATB and the ADAM joint angular displacements recorded during two separate ejection seat tests in which an ADAM was ejected from the Multi-Axis Seat Ejection (MASE) sled track at Holloman AFB, New Mexico (Gragg 1993). The tests used for this validation are the ADAM/MASE Integration Test (AMIT) 79E-G2A and AMIT 79E-F1. The data from these test are maintained by the Crew Escape Technologies office at Wright-Patterson AFB, Ohio (Plagha, 1995).

Within the ATB model, mock-ups of the F-16 aircraft cockpit and ACES II ejection seat are developed. This is the same cockpit type and ejection seat used by the MASE sled track. Acceleration and velocity data recorded during the ADAM/MASE Integration Tests are used to prescribe the motion of the ejection seat vehicle developed in the ATB model. ADAM's joint angular displacements as calculated by the ATB are graphically compared to the joint angular displacements recorded during the two ADAM/MASE Integration Tests. These comparisons determine the validity of the current ADAM data set.

## Organization

The remainder of this thesis is structured as follows. Chapter II describes the development of the ATB input file required to simulate the AMIT 79E-G2A test. Chapter III presents the results of the first ATB simulation of AMIT 79E-G2A as well as justification for ADAM data set modifications. Chapter IV describes the tests performed on the ADAM in order to acquire data necessary to accomplish the modifications described in Chapter III. Chapter V presents the results of the second ATB simulation of AMIT 79E-G2A. Chapter VI describes modifications made to the ATB input file in order to simulate AMIT 79E-F1. Chapter VII presents the results of the ATB simulation of AMIT 79E-F1. Chapter VIII presents an overall evaluation of the current ADAM data set's validity stating both conclusions and offering recommendations for further efforts necessary to enhance the data set's ability to accurately model the ADAM.

## II. Articulated Total Body Input File Development For AMIT 79E-G2A

The ATB input file is the primary tool used to build an ATB simulation. The input file is subdivided into “cards”. Each card serves a different purpose in building the model. Each of these cards is briefly described in Appendix A (Input Description for the Articulated Total Body Model ATB-IV.5, 1994: 4). The ADAM data set being validated is contained in the B and E cards.

This chapter first begins with a description of AMIT 79E-G2A, the first test to which the ADAM data set is compared. Second, the development of the aircraft cockpit and ejection seat in the ATB model using contact planes is discussed. Third, a description is given as to when and how wind forces on the body are calculated. Fourth, modifications to the ADAM data set in order to account for a flight helmet and flight boots are described. Fifth, placement and balancing of the ADAM in the ATB modeled ACES II ejection seat are described. Sixth, approved segment/segment contacts and plane/segment contacts are given. Seventh, force-deflection used in this simulation are defined. Finally, a description of the procedure used to condition the data from the AMIT 79E-G2A test in order to define the trajectory of the ACES II ejection seat in the ATB model is presented. A picture of the resulting ATB modeled ADAM, ACES II ejection seat, and F-16 cockpit is presented in Appendix Y.

### AMIT 79E-G2A Test Description

The AMIT 79E-G2A test data is maintained by the Crew Escape Technologies (CREST) program office located at Wright Patterson AFB, OH (Plagha, 1995). The following information describes the time and conditions under which AMIT 79E-G2A was conducted.

Launch Date	23 April 1993
Launch Time	1100 MDT
Ambient Temperature	22.78 °C
Barometric Pressure	87000 N/m
Sled Track Velocity	320 m/s
Sled Track Orientation	Straight and Level
Sled Track Angular Rates	All Zero

Observation of the video taken of AMIT 79E-G2A displays a less than completely controlled ejection. Specifically, the ACES II ejection seat exhibits a high roll rate upon clearing the ejection seat rails. As the seat rolls right, a significant yaw and pitch rate are also observed. The result is a tumbling motion followed by the ejection seat stabilizing inverted just prior to *Seat-ADAM Separation*.

The only portion of this test which is simulated using the ATB model is the time period between *Seat First Motion* and *Seat-ADAM Separation*. This is approximately a 1.0 second time period.

### Ejection Seat and Cockpit

As described in Chapter I, the environment in which the ATB modeled ADAM exists is constructed primarily of planar surfaces. These planes are used to describe the

elements of the ACES II ejection seat and F-16 cockpit with which the ADAM interacts during the simulation. Dimensions for the ACES II ejection seat are measured from an actual seat provided by the Air Crew Protection Branch of the USAF Wright Laboratory (Meyer, 3 May 1995). Scaled drawings of the ACES II furnished by this same office are also used to develop the ejection seat model. Only the basic structure of the seat, composed of the seat back, sides, leg guards, lower front, and head rest, is modeled for this simulation. These components of the seat are the main surfaces with which the ADAM interacts during an ejection.

Due to the possibility of the ADAM interacting with both the inside and outside of the ejection seat leg guards as well as the lower right and left sides of the seat, each of these portions of the ACES II seat are modeled as two coincident planes with opposing positive surfaces. There are also two seat back planes. These two planes are oriented such that both positive surfaces are in the same direction. This duplication is necessitated by an ATB limitation which allows only five possible contacts (body segments contacting the seat back) per positive planar surface. The seat back has the possibility of more than five contacts in this simulation. Consequently, a second plane is collocated with the first seat back. Appendix B displays a listing of the planes describing the ejection seat and the corresponding X, Y, and Z coordinates (in the inertial reference frame) of the vectors defining these planes.

The F-16 cockpit is similarly modeled using planar surfaces. The only cockpit plane capable of exerting force on the body is defined to be the cockpit floor which contacts the ADAM's feet. All other cockpit planes are only modeled to ensure proper

placement of the body prior to ejection. Contact with these planes is not considered for two reasons. First, it is assumed that the ADAM manikin is properly placed in the ejection seat for an ideal exit which would minimize the possibility of contact with any portion of the cockpit other than the floor. Observation of the AMIT 79E-G2A video supports this assumption. Second, the real time required to run each ATB simulation is on the order of a half hour for the one second simulated time. Increasing possible contacts with the numerous planes defining the cockpit would prohibitively increase the real time required to run the simulation. A listing of X, Y, and Z coordinates defining the vectors describing the planes of the F-16 cockpit is displayed in Appendix C.

#### Wind Plane

Along with defining planes to describe the ejection seat and cockpit, a separate plane, termed the *wind plane*, is defined. The ATB simulation only calculates wind forces on the ADAM once the manikin has passed through this wind plane. This affords accurate modeling of the wind protection provided by the cockpit. Note that contact between the ADAM and the wind plane should not be allowed. In other words, unlike the planes defining the cockpit and ejection seat, the wind plane should not exert a reactive force on the ADAM when the manikin passes through the wind plane. For this particular simulation, the wind plane is defined as being horizontal (parallel with the inertial X-Y plane) with the surface touching the top of the Heads-Up Display (HUD).

### Wind Force Calculation

Two types of wind force calculations can be made within the ATB model. The wind force can be either time dependent or velocity dependent. For this validation, the velocity dependent wind force calculation is used. In order to make this calculation, the ATB model requires the definition of two segments. The relative velocity of these two segments is then used as the independent variable in the wind force calculation. Normally, as is true for this validation, one of these segments is chosen to be the ground. The other segment is normally chosen as either the ejection seat, the lower torso, or the upper torso (Obergefell, 1995). As will be described in Chapter III, altering the definition of the second segment has significant effects on the ATB's ability to model the complete test period between *Seat-First Motion* to *Seat-ADAM Separation*. Initially, the second segment is chosen as the ejection seat.

### Addition of Flight Helmet and Boots to the ADAM Data Set

In order to accurately describe the state of the ADAM during the ADAM/MASE Integration Tests, certain modifications are made to the ADAM data set. The properties defining ADAM data set such as mass, moments of inertia, and joint resistive torques, were originally measured when the ADAM was not wearing a flight suit, G-suit, flight helmet, or flight boots, as the manikin is during the ejection seat sled tests (Rizer and others, 1994). The flight suit and G-suit are assumed to have a negligible effect on ADAM's motion during an ejection. The flight helmet and boots, on the other hand, are considered massive enough to warrant consideration.

In order to account for the flight helmet (HGU-55/P helmet with MBU-12/P mask), the weight and size of the head ellipsoid is increased so that this segment includes both the head and helmet. The measurements necessary to modify the ADAM model to account for a flight helmet are presented in Appendix D. This modification is accomplished by first shifting the ADAM head CG to account for the flight helmet. To do so, the location of the new head, with helmet, CG is measured relative to the mechanical axis of the ADAM head. This location is then added to the location of the mechanical axis system relative to the geometric center of the head ellipsoid resulting in the location of the head ellipsoid's CG relative to its geometric center. Following the shifting of the head's CG, the weight of the head ellipsoid is increased to account for the helmet weight. Finally, the new principal axis orientation and principal moments of inertia of the head and helmet are measured. These four new ADAM head measurements, CG location, mass, moments of inertia, and principal axis orientation, are then entered into the input file.

The flight boots are accounted for by increasing the weight of the feet ellipsoids. It is assumed that the CG of each foot will not significantly shift since the weight of the boot is distributed evenly about the foot. Consequently, neither the CG shift nor changes in moments of inertia are considered. The mass per flight boot is presented in Appendix D.

### Placement and Balancing of the Body in the Ejection Seat

The placement of the body in the ejection seat is accomplished using two pieces of information from AMIT 79E-G2A. First, the initial joint angular measurements prior to the start of the test are examined in an attempt to discern the initial position of the ADAM. Unfortunately, individuals conducting AMIT 79E-G2A made no record of the ADAM's physical joint position which corresponds to each joint's zero angle. Best estimates are made as to the joint zero angle position of the ADAM during AMIT 79E-G2A. These estimates are based on the experience of those individuals who currently prepare the ADAM for test (Thompson, 1995).

The second and more useful piece of information used to accurately position the ADAM are photographs taken of the ADAM prior to the beginning of the test. These photographs provide a much better estimate of the ADAM's initial position. The combination of these two pieces of information facilitates the proper initial placement of the body in the ejection seat.

Following initial placement of the ADAM, the ATB model is run for one incremental time step. This gives an output of the initial linear and angular accelerations on the modeled ADAM. SRL recommends that the angular accelerations should be less than 171.9 degrees per second squared and the linear acceleration should be less than 2.943 meters per second squared (Rizer, 1995). Minor modifications are made to the placement of the body to ensure adherence to these limitations. This initial placement of the body is termed a balanced state.

### Approved Segment/Segment and Segment/Plane Contacts

The ATB software will only calculate a force resulting from segment/segment or segment/plane contact if those contacts are predefined in the ATB input data file. If such a contact between one segment and another or a segment and a plane is not predefined, the segment will pass through the other segment or plane, an obviously unrealistic condition. Recall that the ATB model was originally designed to simulate automobile crashes. Due to limited computing power at the time, it was determined that limiting the number of segment/segment contacts to 40 was sufficient for its intended application. In an ejection scenario, in which the range of possible motion is much greater than in an automobile crash, the number of possible segment/segment contacts is greater than 40. Consequently, modifications are made to the ATB software to allow up to 80 segment/segment contacts (Cheng, 1995). The table in Appendix E defines each segment number and the corresponding approved segment for which the ATB model will calculate a resultant force upon contact.

Similarly, Appendix F defines each plane number and the corresponding approved segment for which the ATB model will calculate a resultant force upon contact. Note that the segment numbers in Appendix E correspond to the segments in Appendix F.

### Force Deflection Functions

As described in Chapter I, force deflection functions define how a segment will react when it comes in contact with a plane or another segment. Current methods for developing force deflection functions are strictly empirical. Those functions currently

used by the Vulnerability Branch of AL, the organization which maintains the ATB model, have been developed through a continuous improvement process of modifying the functions as more experimental data become available. Based on the numerous enhancements to these force deflection functions and the confidence that the Vulnerability Branch has with them, these force deflection functions are used for this validation.

#### Filtering and Conditioning Ejection Seat Accelerometer Data

During AMIT 79E-G2A and AMIT 79E-F1 tests, accelerometers and rate gyros were affixed to the ACES II ejection seat. Four linear accelerometers, designated accelerometers A, B, C, and D, were located in the seat pan section of the ejection seat during the tests. Each separately measured accelerations in the X (forward), Y (lateral), and Z (vertical) directions in the ejection seat's local reference frame. During the test, linear acceleration and angular velocity data were taken from the instant the sled started down the track until the ejection seat hit the ground. As stated earlier in this chapter, the only time period of this test which is modeled using the ATB is the time period from *Seat First Motion to Seat-ADAM Separation*, approximately a 1.0 second period of time.

Removal of Acceleration and Velocity Biases. Prior to examining this 1.0 second period of acceleration and velocity data, the linear acceleration and angular velocity data prior to *Seat First Motion* is analyzed in order to determine if any of the data are biased. Figure 2.1 displays sample plots of raw linear acceleration and angular velocity data for this time period.

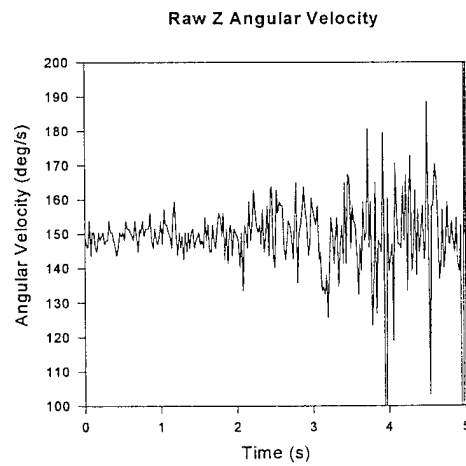
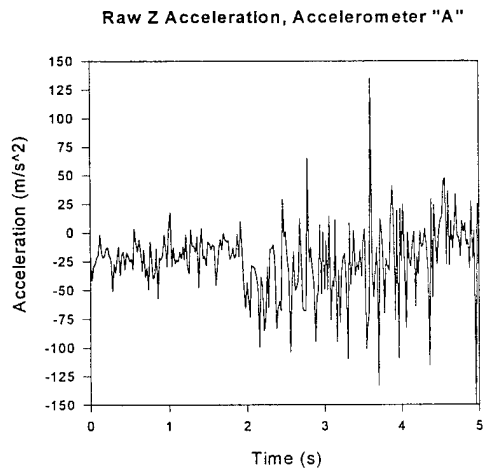
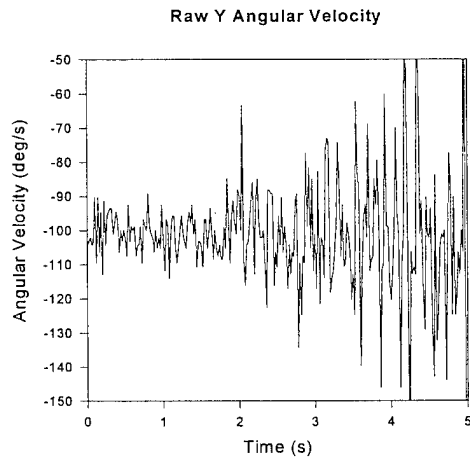
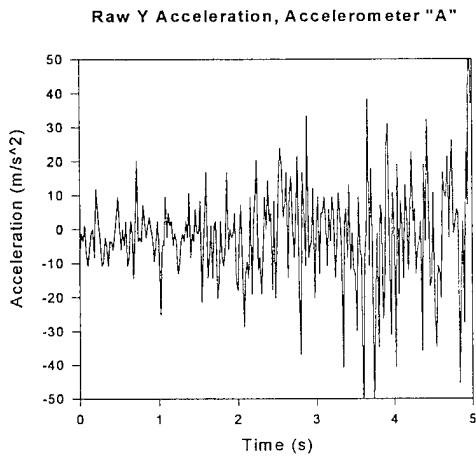
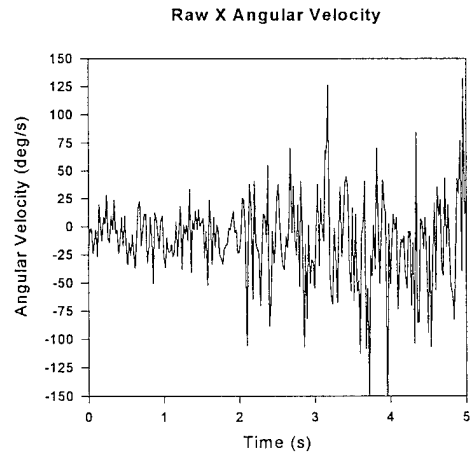
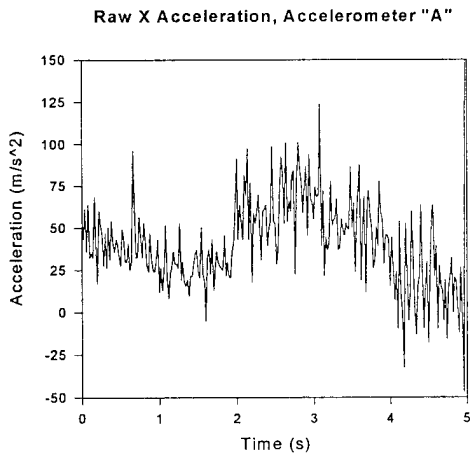


FIGURE 2.1 Raw Acceleration and Velocity Data Prior to *Seat First Motion*

Plots similar to those presented in Figure 2.1 showing all linear acceleration and angular velocity data prior to *Seat First Motion* are displayed in Appendix G.

Although these data are noisy, it is possible to determine if there exists a bias on the linear acceleration data in the Y and Z directions as well as a bias on the angular velocity data in all three directions. Ideally, these data should be zero until *Seat First Motion*. The only exception to this is the linear Z acceleration which should be 9.81 meters per second squared. No attempt is made to determine if a bias exists on the linear acceleration data in the X direction since the true acceleration in that direction is not known. The average linear accelerations and angular velocities in the X, Y, and Z directions plus or minus a confidence interval based on a 99% confidence level are calculated. The results are presented in Table 2.1. Note that all average accelerations are in meters per second squared and all average angular velocities are in degrees per second.

TABLE 2.1 Biases in Raw Linear Acceleration and Angular Velocity Data

Accelerometer	Bias
	X = 44.64 ± 0.353
<u>Accelerometer A</u>	Y = -2.97 ± 0.245
	Z = -26.00 ± 0.598
	X = 36.89 ± 0.618
<u>Accelerometer B</u>	Y = -1.46 ± 0.314
	Z = 18.64 ± 0.648
	X = 41.40 ± 0.559
<u>Accelerometer C</u>	Y = -1.99 ± 0.245
	Z = -13.73 ± 0.637
	X = 39.53 ± 0.706
<u>Accelerometer D</u>	Y = -2.25 ± 0.363
	Z = -19.62 ± 0.681
	X = -9.890 ± 0.774
<u>Angular Velocity</u>	Y = -101.8 ± 0.300
	Z = 149.75 ± 0.150

After studying the data in Table 2.1, it is clear that there is no significant bias on the linear acceleration data in the Y direction. It is possible that a bias on linear acceleration in the Z direction may exist. Three out of the four average Z accelerations exceed the nominal value of 9.81 meters per second by less than 9.81 meters per second squared (1 g). Since the average Z acceleration values do not clearly define a bias and without further evidence that a bias exists, it is determined that a bias does not exist on the Z acceleration data. In contrast, there are clear biases on the angular velocity data in the Y and Z directions. These data exceed their nominal values by approximately 100 degrees per second and 150 degrees per second respectively. The existence of a bias on the X

angular velocity is debatable. In light of the ATB's sensitivity to excessive angular accelerations, this borderline bias is considered significant enough to warrant consideration.

Filtering Acceleration and Velocity Data Prior to *Seat First Motion*. It is possible that the large amount of noise in the linear acceleration and angular velocity data could contribute to the biases defined in the previous section. In an attempt to remove noise and correctly define the amount of data bias, the raw linear acceleration and raw angular velocity data are filtered. Filtering is accomplished via an ideal low pass filter by converting the raw data from the time domain into the frequency domain using a Fast Fourier Transform and cutting off frequencies above a certain threshold (Peterson, 1995). Based on recommendations from AL, the data are filtered (cut off) at a frequency of 15 Hz (Obergefell, 1995). The filtered data are then converted back to the time domain using an Inverse Fast Fourier Transform. The code to filter this data is written in MATHCAD® and displayed in Appendix H. Sample plots of the unfiltered linear acceleration and angular velocity data and the corresponding filtered data are displayed in Figures 2.2 and 2.3 respectively. Similar plots for all acceleration and velocity data are presented in Appendix G.

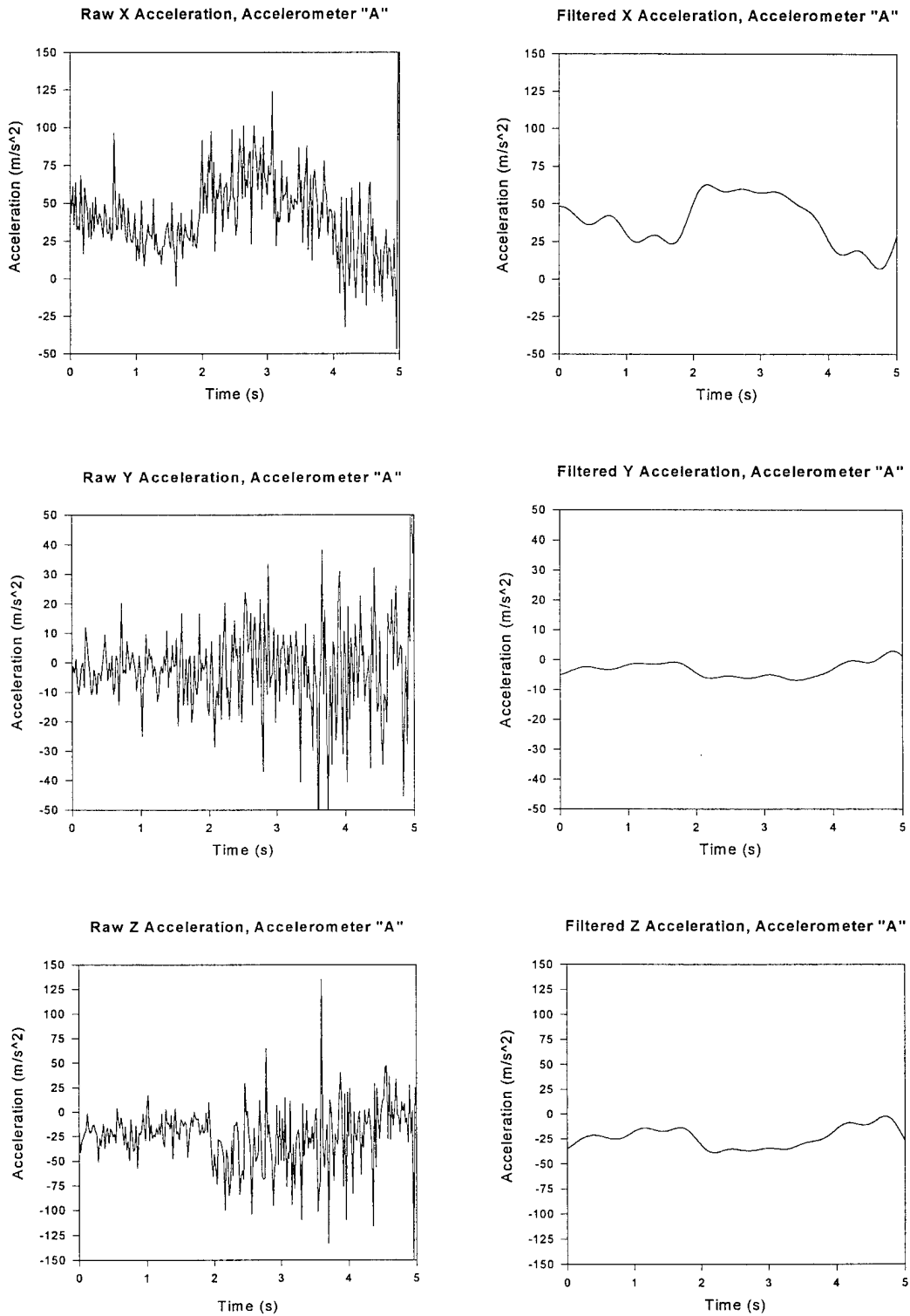


FIGURE 2.2 Raw and Filtered Linear Acceleration Data Prior to *Seat First Motion*

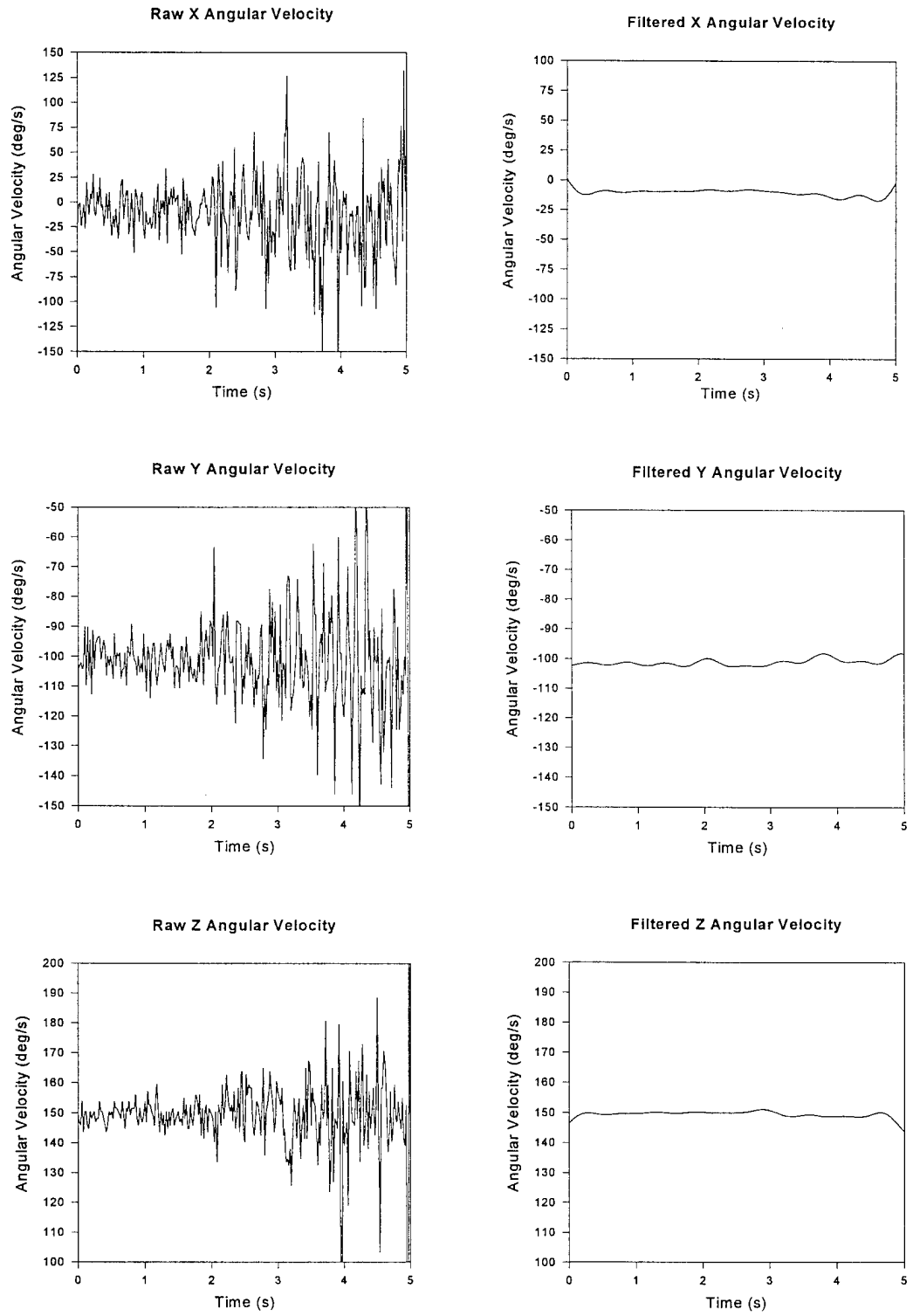


FIGURE 2.3 Raw and Filtered Angular Velocity Data Prior to *Seat First Motion*

Similar to the unfiltered data, there are possible biases in both the linear acceleration data and the angular velocity data. The average of the linear acceleration data and angular velocity data are calculated for all three directions (X, Y, and Z) plus or minus a confidence interval based on a 99% confidence level. The results of these calculations are displayed in Table 2.2. Note that all average linear accelerations are in meters per second squared and all average angular velocities are in degrees per second.

TABLE 2.2 Biases in Filtered Linear Acceleration and Angular Velocity Data

Accelerometer	Bias
	X = $38.75 \pm 0.589$
<u>Accelerometer A</u>	Y = $-3.83 \pm 0.088$
	Z = $-23.15 \pm 0.372$
	X = $33.65 \pm 0.540$
<u>Accelerometer B</u>	Y = $-2.77 \pm 0.029$
	Z = $16.95 \pm 0.216$
	X = $35.81 \pm 0.549$
<u>Accelerometer C</u>	Y = $-2.83 \pm 0.029$
	Z = $-17.66 \pm 0.275$
	X = $35.81 \pm 0.549$
<u>Accelerometer D</u>	Y = $-2.83 \pm 0.029$
	Z = $-17.66 \pm 0.275$
	X = $-10.43 \pm 0.115$
<u>Angular Velocity</u>	Y = $-101.2 \pm 0.041$
	Z = $149.5 \pm 0.035$

As is characteristic of the unfiltered data, there does not appear to be a bias on the linear acceleration in the Y direction, and there is a negligible bias on the linear

acceleration in the Z direction. In contrast, the X, Y, and Z angular velocity data are all biased. These conclusions result from the same logic on which the existence of biases in the unfiltered linear acceleration and angular velocity data are based. As a result of this discovery, an average of the filtered and unfiltered angular velocity data biases displayed in Tables 2.1 and 2.2 are subtracted from the angular velocity data recorded during AMIT 79E-G2A in the time frame between *Seat First Motion* and *Seat-ADAM Separation*.

Ejection Seat Trajectory Simulation Data. Having removed biases from the angular velocity data, the linear acceleration and angular velocity data measured during the period between *Seat First Motion* and *Seat-ADAM Separation* is examined. This is the data used to describe the trajectory of the ejection seat in the ATB simulation. Examples of raw linear acceleration and angular velocity data for this time period are displayed in Figure 2.4. Similar data for all accelerometers are presented in Appendix I.

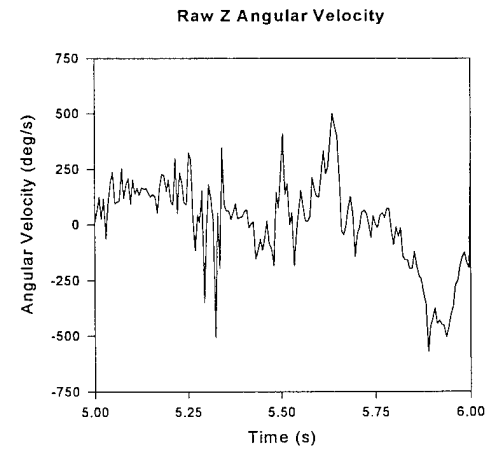
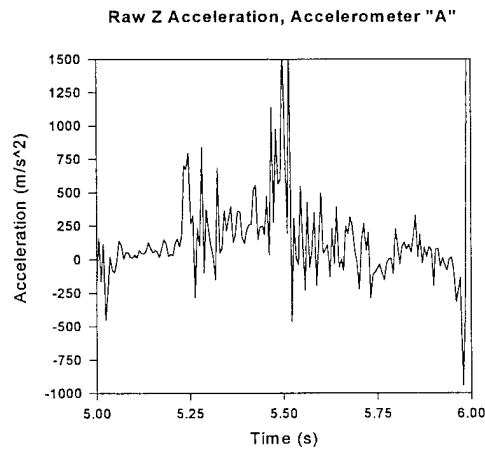
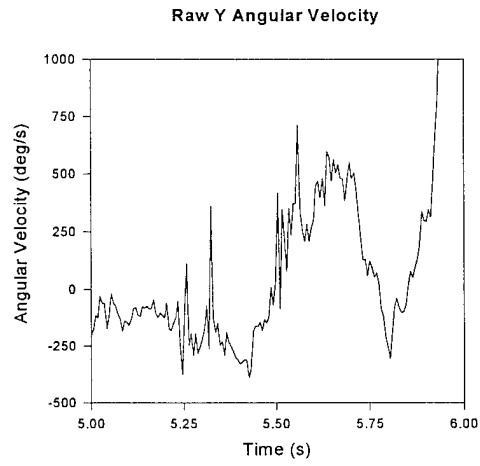
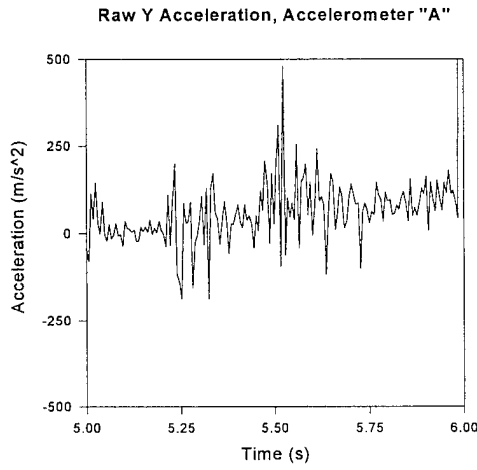
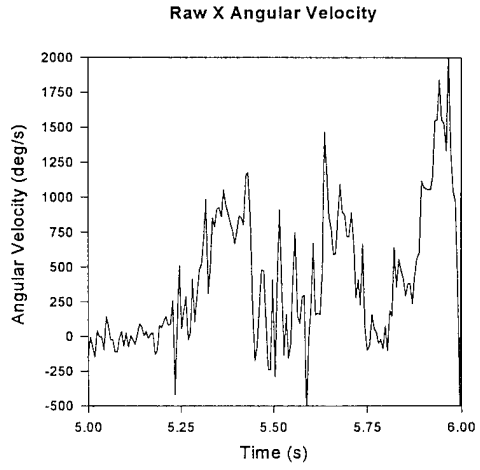
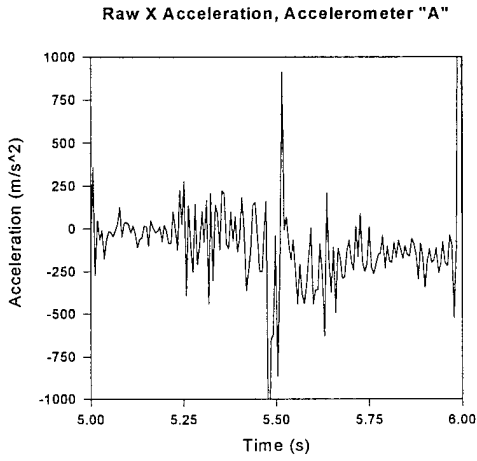


FIGURE 2.4 Raw Ejection Seat Trajectory Simulation Data

Observation of the data indicates a significant amount of noise which is considered excessive in terms of accurately describing the trajectory of the ejection seat in the ATB simulation. Attempts are made to remove as much of the noise as possible.

Filtering Ejection Seat Trajectory Simulation Data. The data used to describe the trajectory of the ejection seat are filtered using the same procedure described earlier in this chapter. Recall, the filtering procedure involves converting noisy data from the time domain to the frequency domain via the Fast Fourier Transform, cutting off high frequency, white noise, and reconvertng the data back to the time domain. The MATHCAD® code written to perform this filtering is presented in Appendix H.

When only filtering a one second time period of data (the time period during AMIT 79E-G2A which the ATB is simulating), it is noted that the filtered data do not follow the same general path as the noisy data for the first 0.2 seconds and the last 0.2 seconds of this 1.0 second time period. Instead, the filtered data are either several orders of magnitude greater or less than the noisy data. This inaccuracy results from difficulty encountered in combining continuous sinusoidal functions to model discrete data (Peterson, 1995). In order to ensure accurate filtering of the entire 1.0 second data set, raw data for a 1.5 second time period is filtered. This 1.5 second period encompasses the 1.0 second of data used to define the trajectory of the ejection seat plus 0.25 seconds prior to and 0.25 seconds after the 1.0 second time period. After filtering this 1.5 second data set, only the data in the original 1.0 second time period is used to define the trajectory of the ejection seat.

Unlike the acceleration and velocity data prior to *Seat First Motion*, the linear acceleration and angular velocity data used to describe the trajectory of the ejection seat are not all filtered at the same frequency of 15 Hz. The specific frequency at which particular acceleration or velocity data are filtered is based on two factors. The first factor is the structure of the frequency pattern for that data. The cut-off frequency is chosen according to where it appears the frequency spectrum maintains a constant power spectral density. It is assumed that frequencies beyond this point result primarily from white noise. The second factor used to determine the frequency at which particular data are filtered is the time domain plot of the resulting filtered data. This plot is examined to ensure that the acceleration and/or velocity does not change too quickly. This is clearly a subjective determination but one that must be addressed due to the sensitivity of the ATB model to acceleration and velocity rates. Appendix J contains a table showing the specific cut-off frequencies at which each acceleration and velocity data set are filtered. Sample plots of the filtered and unfiltered linear acceleration and angular velocity data prior to *Seat First Motion* are displayed in Figures 2.5 and 2.6. A complete set of similar plots for all accelerometers is presented in Appendix I.

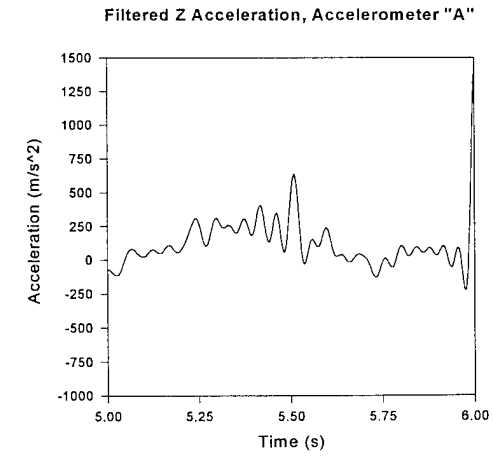
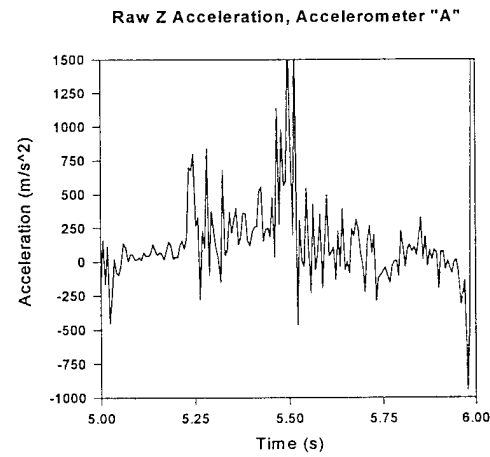
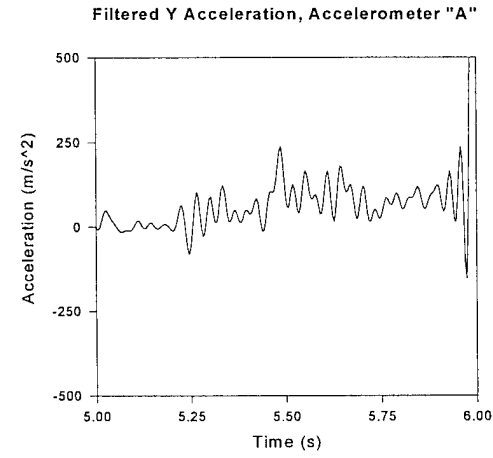
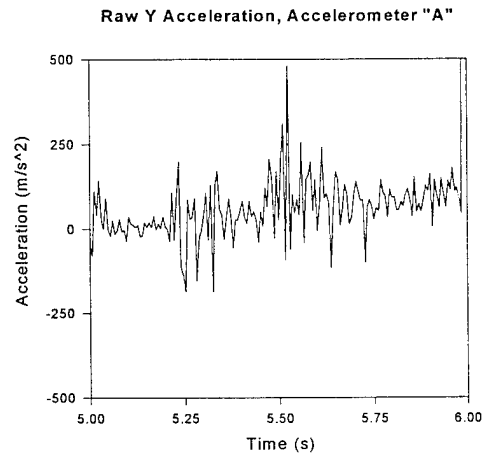
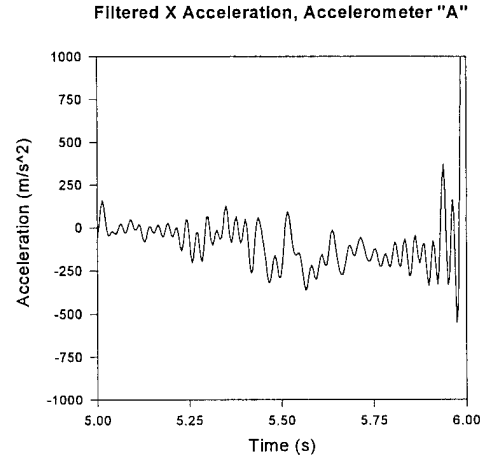
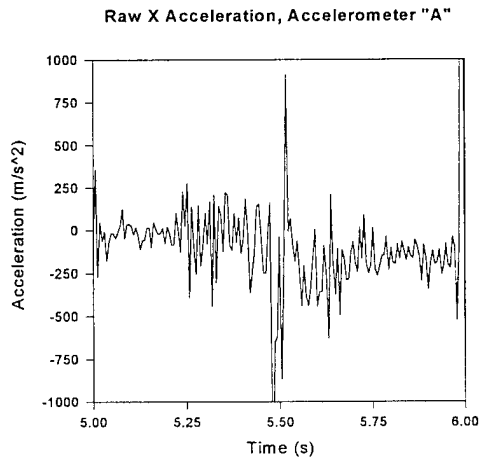


FIGURE 2.5 Raw and Filtered Linear Acceleration Ejection Seat Trajectory Simulation Data

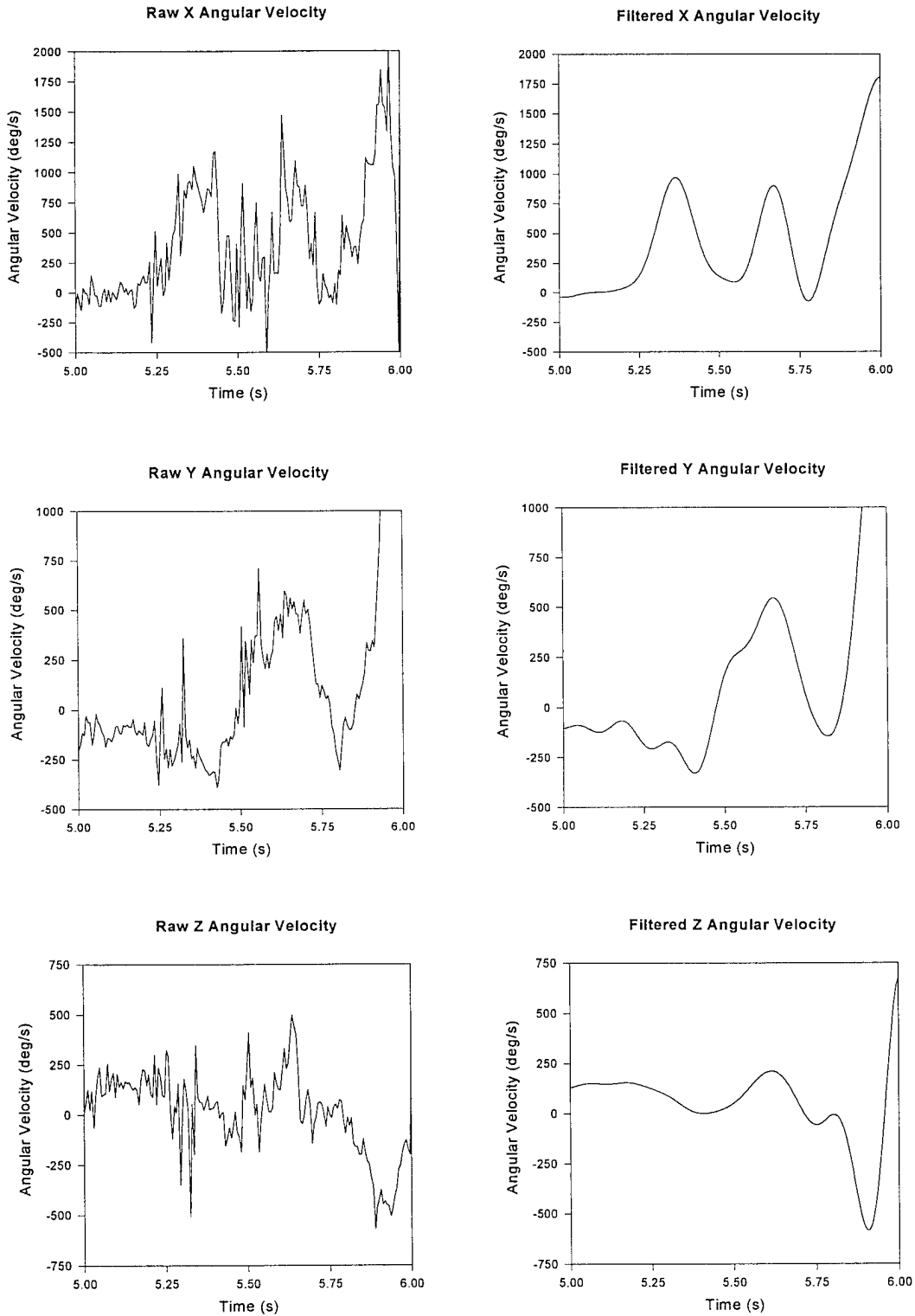


FIGURE 2.6 Raw and Filtered Angular Velocity Ejection Seat Trajectory Simulation Data

Integrating Linear Acceleration Data. Ejection seat data from AMIT 79E-G2A are a combination of linear acceleration data and angular velocity data. The ATB model can accept acceleration, velocity, or position data to define the trajectory of the ejection seat, but not a combination thereof. Therefore, in order to define the ejection seat's trajectory, either the acceleration or velocity data needs to be modified. Differentiating the already noisy angular velocity data would amplify the noise. Differentiation calculates the slope at a particular point on a curve. With data that are noisy, the slopes are large. As a result, differentiating even a moderately noisy signal would make it significantly noisier. Consequently, the linear acceleration data are integrated to obtain linear velocity data. The integration is performed using the SIMULINK™ block diagram presented in Appendix K. At this same time, the polarity of the Z acceleration from accelerometer B is reversed. As can be seen in Appendix I, the original Z acceleration from accelerometer B appears to be a mirror image of the Z accelerations measured by the other three accelerometers. It is assumed that this particular channel of the accelerometer was wired improperly prior to the test. Sample plots of the integrated accelerations are displayed in Figure 2.7. Plots of integrated accelerations for all four accelerometers are presented in Appendix L.

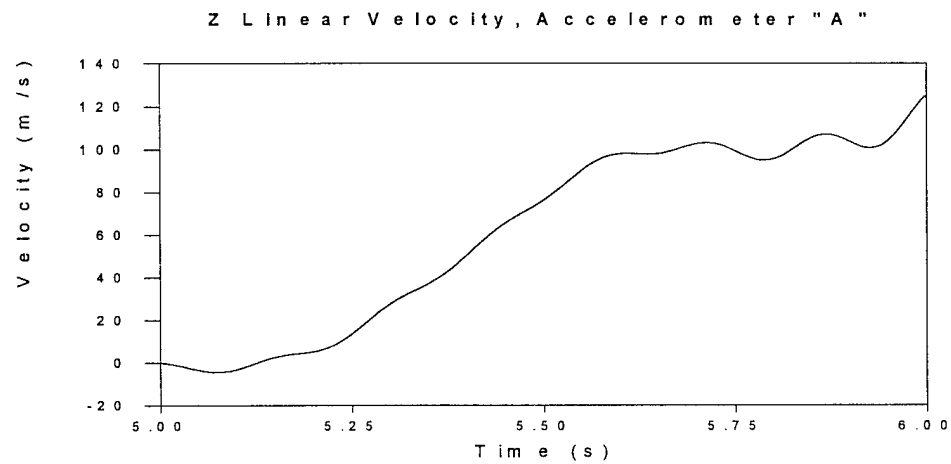
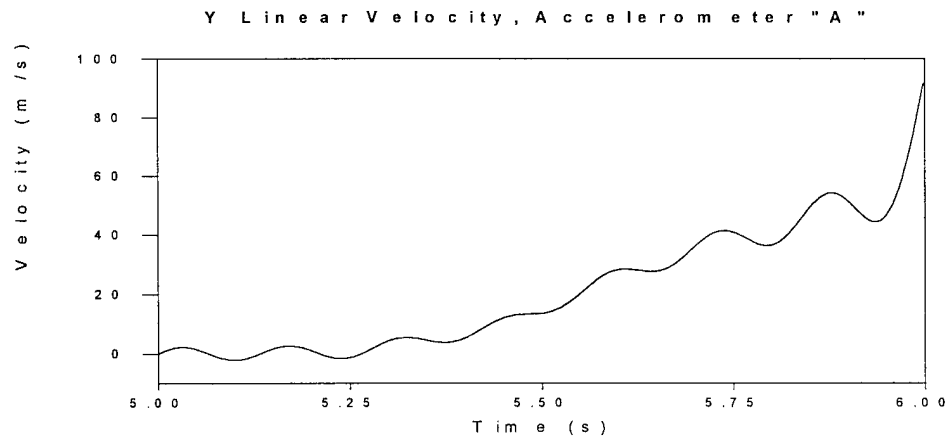
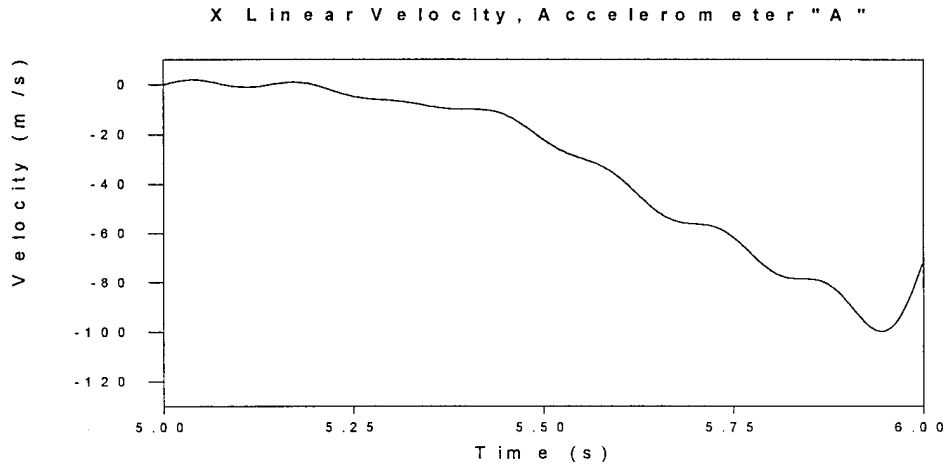


FIGURE 2.7 Integrated Linear Acceleration Data

Calculating Velocity at the Seat Reference Point. The linear velocity of the ejection seat in the ATB model must be defined with respect to the ejection seat's vehicle axis system, located at the seat reference point. The linear velocity data currently calculated define the velocity of the ejection seat at the seat pan, the location of the accelerometers. Consequently, in order to properly define the trajectory of the ejection seat, the linear velocity data currently calculated along with the measured angular velocity, are used to calculate the linear velocity of the ejection seat at the SRP (Greenwood, 1988:45).

At the same time this calculation of the SRP linear velocity is made, two other modifications are made to the angular velocity data. First, the angular velocity biases defined earlier in this chapter are subtracted from the filtered angular velocity data. Second, all angular velocity data are set to zero for the first 0.14 seconds. The filtered data show angular velocities for the first 0.14 seconds which is the time it takes the ACES II ejection seat to ride up the seat rails (Meyer, 1995). Obviously, there can be no rotation of the seat during this time. The fact that the filtered data show angular velocities at this time is attributed to noisy data. For the same 0.14 seconds, the linear velocity data in the Y direction is also set to zero as it would be impossible to attain a lateral velocity while the ejection seat is riding up the rails.

The code written to calculate the linear velocity of ejection seat's SRP, subtract biases from the angular velocity data, and zero all angular velocity and lateral velocity data for the first 0.14 seconds is written in MATLAB© as a script M-file. This M-file is presented in Appendix M. Sample plots of the resulting linear velocity at the SRP are

displayed in Figure 2.8. Plots of the resulting linear velocity at the SRP for all four accelerometers are presented in Appendix N.

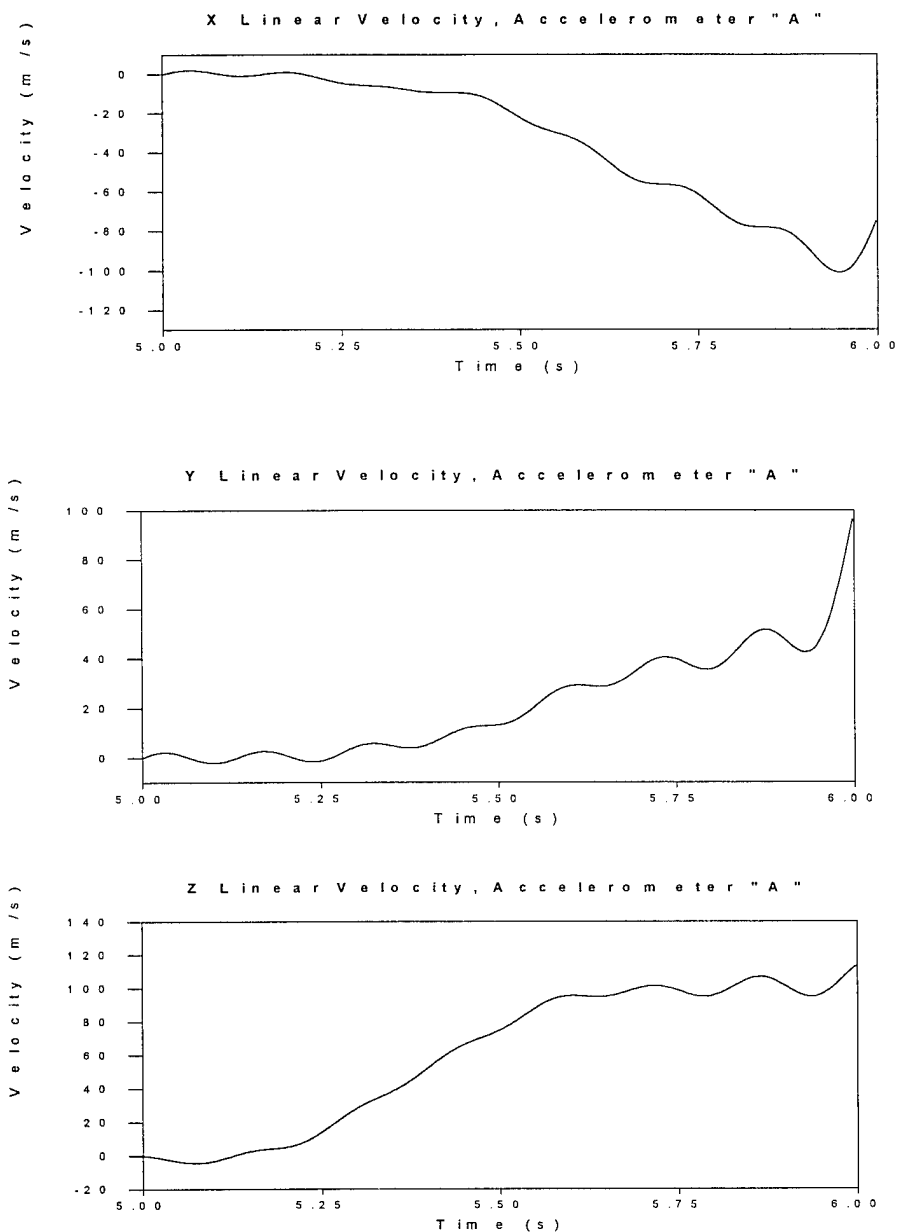


FIGURE 2.8 Velocity at Seat Reference Point

Employing Mean of All Accelerometers in ATB Model. Finally, the linear velocity data at the SRP calculated from the data measured by the four accelerometers are

averaged in order to obtain the linear velocity which defines the trajectory of the ejection seat in the ATB model. Plots of the linear and angular velocity data which are entered in to the ATB input file describing the trajectory of the ejection seat are displayed in Figures 2.9 and 2.10 respectively.

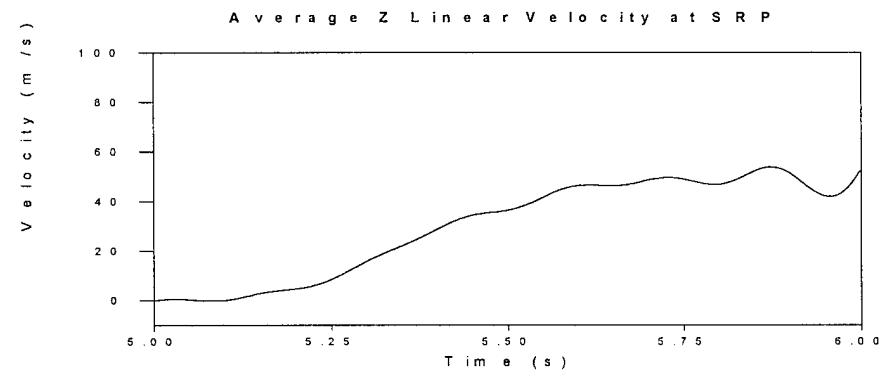
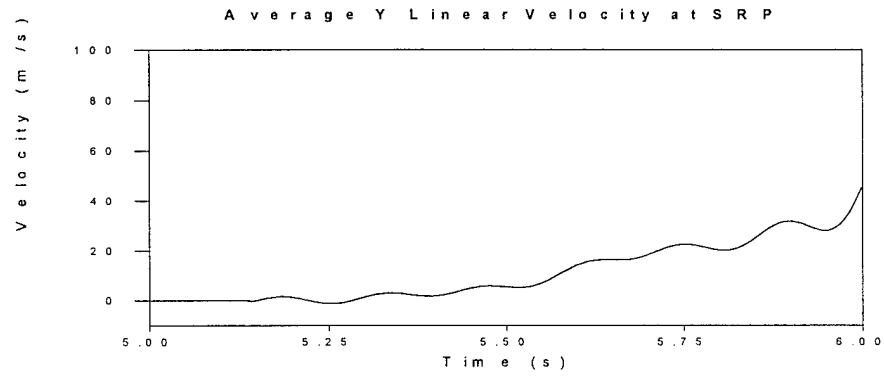
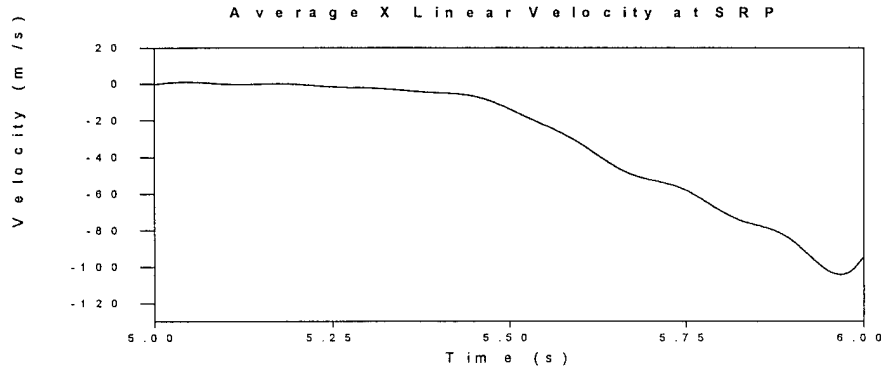


FIGURE 2.9 Average Linear Velocity At Seat Reference Point

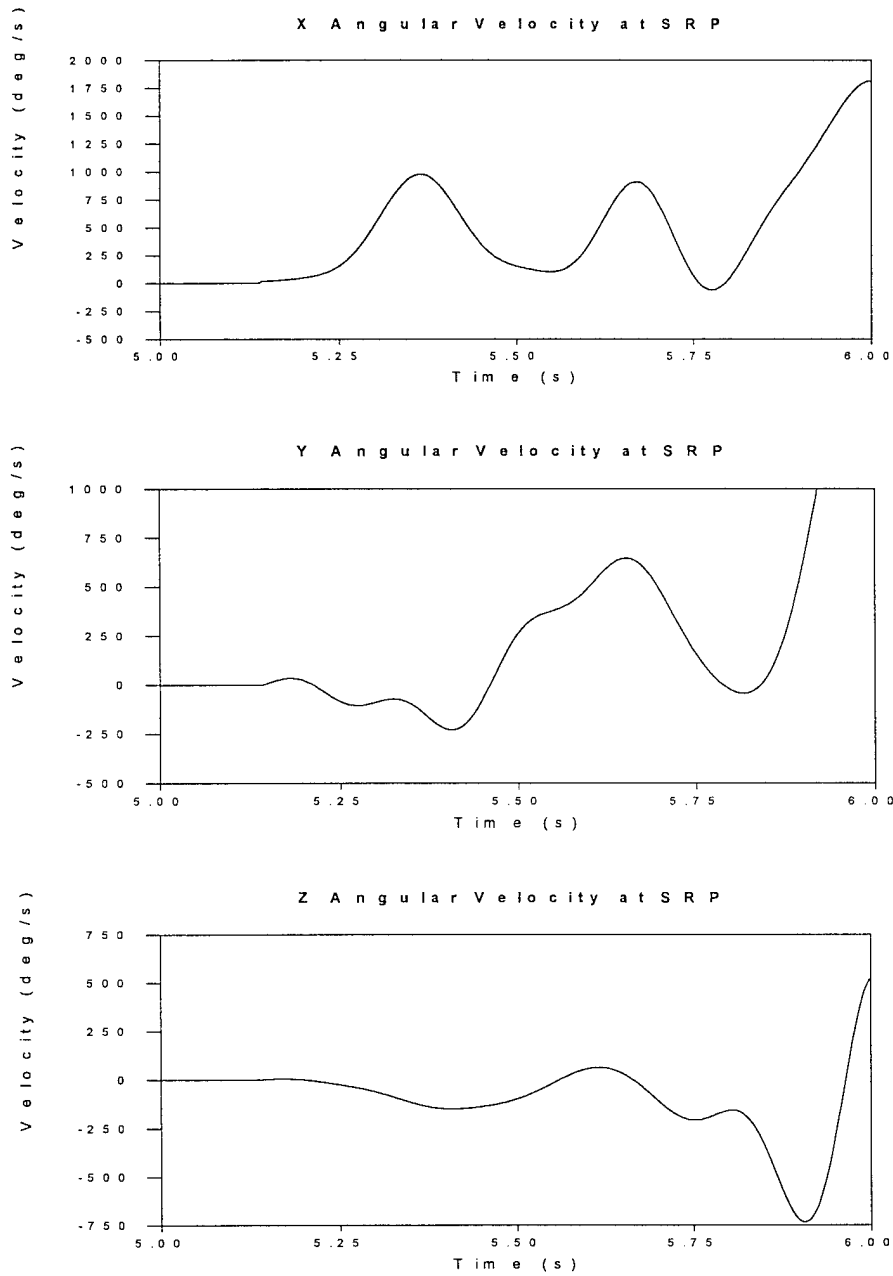


FIGURE 2.10 Angular Velocity at Seat Reference Point

From these linear and angular velocities, the ATB code calculates the linear and angular accelerations of the ejection seat. These accelerations are then used by the ATB model to define the ejection seat trajectory.

### III. Results of the First ATB Simulation of AMIT 79E-G2A

This chapter describes the results of the ATB model's first simulation of AMIT 79E-G2A. Difficulties in modeling the full 1.0 second portion of AMIT 79E-G2A are discussed. Comparisons between joint angular displacements modeled by the ATB and those measured during AMIT 79E-G2A are presented. At this same time, an explanation regarding the required shifting and reverse polarization of certain measured joint angular displacement data is given. Perceived problems concerning excessive joint oscillations are explained. Finally possible solutions to these joint oscillations problems are presented.

#### Incomplete Simulation

Instead of the ATB model simulating the full 1.0 second portion of AMIT 79E-G2A as expected, the ATB model reaches a point at 0.26 seconds into the simulation where its Runge-Kutta integration routine is not able to converge due to excessive head accelerations which results in the termination of the simulation. Three modifications are made to the input file in an attempt to rectify this situation. First, the minimum integration step size is decreased to the smallest possible value of  $1.0 \times 10^{-7}$  seconds. This modification improves the duration of the ATB simulation to 0.395 seconds. Second, the integration tolerances are both increased and decreased. Both variations have worsening effects. As a result, the ATB model is unable to simulate more than 0.395 seconds of AMIT 79E-G2A. Finally, the segment used to calculate the velocity of the

wind is altered. Recall that the velocity of the wind is calculated as being the relative velocity between the inertial reference frame and the local reference frame of either the ejection seat, lower torso, or upper torso. Attempts are made to complete the full 1.0 second ATB simulation using each of these three local reference frames. The best results are obtained when the upper torso is chosen. Even with this improvement, the ATB is still only able to simulate 0.5 seconds of the full 1.0 second simulation due to excessive head accelerations.

#### Joint Angular Displacement Comparisons

In order to better understand the dynamics of the ADAM during the 0.5 second simulation, the joint angular displacement of the knee, hip, elbow, and shoulder are plotted. Sample plots are displayed in Figure 3.1. Plots for all joints are presented in Appendix O. As an aid in interpreting these plots, graphical explanations of the terms flexion, abduction/adduction, supination/pronation, and medial/lateral are given in Appendix P (Plagha, 1995).

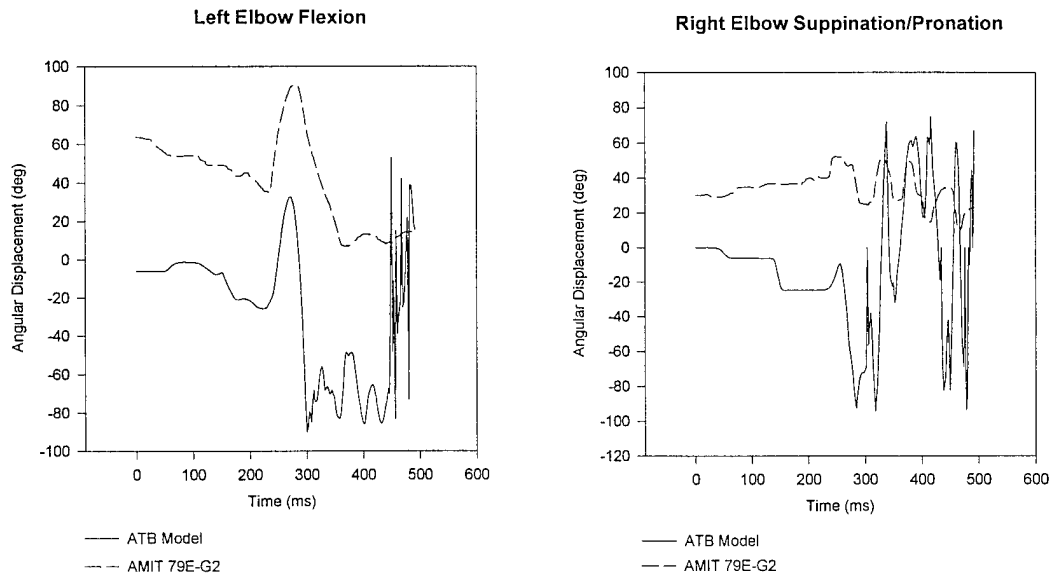


FIGURE 3.1 ADAM Right and Left Elbow Flexion

Since the two plots on each graph do not begin at the same angle, it is clear that the zero angle of each joint defined by the operators of the AMIT 79E-G2A test is not the same zero angle defined by the ATB model. In order to account for this discrepancy, the ATB angular displacement data are shifted by a value equal to the difference between the zero angle defined during the AMIT 79E-G2A test and the zero angle defined by the ATB model.

In Appendix O, graphs similar to those presented in Figure 3.1 indicate that the polarity of certain data channels recording the ADAM's joint angular displacements during AMIT 79E-G2A test are reversed. This reverse polarity condition is a subjective determination based on the precision with which the ATB modeled joint angular displacements parallel the corresponding joint angular displacements measured during AMIT 79E-G2A. If it appears that the joint angular displacements modeled by ATB are a mirror images of the measured joint angular displacements, it is assumed that the polarity

of the test signal is reversed. This assumption is justified due to the low probability that such a mirrored state would exist without the polarity of the test data being reversed.

SRL employees who currently maintain the ADAM manikins and prepare them for test agree that such a reversal in polarity could have happened during AMIT 79E-G2A (Thompson, 1995). This reversed polarity condition is assumed for the following joint motions.

1. Left Shoulder Coronal Plane Abduction/Adduction
2. Right Elbow Flexion
3. Right Elbow Supination/Pronation
4. Right Hip Abduction/Adduction
5. Right Hip Medial/Lateral

In order to account for this reversed polarity condition, the original polarity of the data describing the five motions listed is reversed. A sample of the joint angular displacement data, originally displayed in Figure 3.1, after being shifted and reverse polarized is presented in Figure 3.2. Plots of all ATB modeled joint angular displacements, after the data have been shifted and, where necessary, reverse polarized, are presented in Appendix Q.

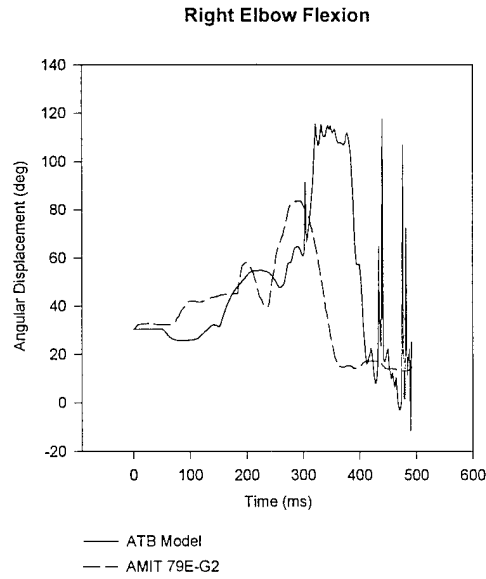


FIGURE 3.2 ADAM Right Elbow Flexion After Shifting and Polarization

Overall Similarity Between ATB Modeled and Measured Joint Motions

For approximately the first 300 milliseconds of the ATB simulation of AMIT79E-G2A, the joint angular displacements modeled by the ATB simulation and the joint angular displacements measured during AMIT 79E-G2A parallel each other relatively closely. Beyond this time, certain ATB modeled joint angular displacements such as *Elbow Flexion*, *Knee Flexion*, and *Hip Medial/Lateral* continue to follow the same basic trend of the corresponding test data.

Based on the assumption that left and right hip test data are labeled incorrectly (reversed), the ATB modeled data defining *Hip Abduction/Adduction* also closely match the corresponding test data. In other words, it appears that the ATB modeled data defining *Right Hip Abduction/Adduction* closely match the *Left Hip Abduction/Adduction* test data and visa versa. SRL personnel who currently prepare the ADAM for tests agree

that this mislabeling of the data could have occurred during AMIT 79E-G2A (Thompson, 1995).

The single characteristic most prevalent in a majority of these plots is the high rate of joint oscillation that occurs at approximately 300 milliseconds into the ATB simulation. Joint angular displacement plots indicate that the rotation of segments about their respective joints appears to start out in a controlled manner, but after a certain time, the controlled rotation degenerates into an erratic oscillatory mode.

#### Excessive Joint Oscillation

The erratic joint oscillations are a result of assumptions made when the ADAM joint resistive torques, torque resisting the motion of each of the ADAM's joints, were originally measured. As described in Development of a Simulation Database for the Advanced Dynamic Anthropomorphic Manikin (ADAM), the resistances in the ADAM joints were measured when the ADAM was disassembled. At this time, the skin of the ADAM was not attached, and the ADAM was not wearing a flight suit or a G-suit (Rizer and others, 1994). Joint resistances were measured with the ADAM in this state in an attempt to simplify the difficult task of taking these measurements when the ADAM was fully assembled. As a result of the absence of the skin, flight suit, and G-suit, the constant coulomb friction torque measured for each ADAM joint, between joint soft stops, only accounts for the resistance due to the friction plates in each joint.

This simplified procedure for measuring the resistance in each of the ADAM joints results in the corresponding ATB modeled joints encountering a lower than normal

resistance to motion in the range between joint soft stops. Once a segment impacts a joint soft stop, the segment is repelled with a torque many times greater than the coulomb friction torque (as described in Figure 1.9). Subsequently, the segment rotates through the joint motion, impacts the opposing soft stop, and is similarly repelled in the opposite direction. Once entering this mode, the segment continues to rotate quickly back and forth between soft stops with little coulomb friction resistance (1 N•m - 7 N•m) to slow the segment motion. This condition results in the erratic joint oscillations depicted in the plots displayed in Figure 3.2 and in Appendix Q.

#### Solutions To Joint Oscillation Problem

A possible solution to this joint oscillation problem is to alter the joint resistive torque functions by increasing the constant coulomb friction torque. The increase would model the resistive torque resulting from the ADAM skin, flight suit and G-suit. This theory is tested by arbitrarily increasing the coulomb friction torque in all of the joints by a factor of 10. Plots displayed in Figure 3.3 and Appendix R compare joint angular displacements before and after the coulomb friction is increased. These plots indicate a significant decrease the segment oscillations due to increasing the coulomb friction torque.

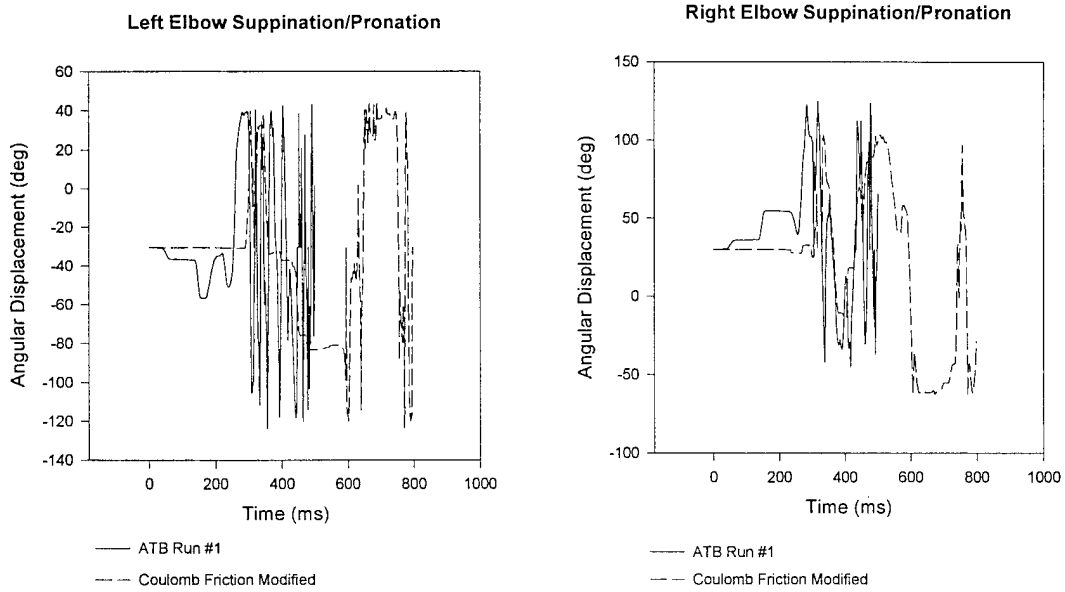


FIGURE 3.3 Left and Right Elbow Supination/Pronation With Coulomb Friction Multiplied By a Factor of 10

Based on the results observed by artificially increasing the coulomb friction torque in the ADAM joints, it is clear that the ADAM skin, flight suit, and G-suit need to be taken into account when calculating the joint resistive torque functions. In order to account for these previously absent components, new constant coulomb friction torque values are measured while the ADAM is fully assembled, and is wearing a flight suit and G-suit. The next chapter describes how these measurements are taken and the subsequent results.

#### IV. Modifications to the Advanced Dynamic Anthropomorphic Manikin Data Set

This chapter describes modifications to the joint resistive torque functions in the ADAM data set (B.5 and E.7 cards). The purpose of these modifications is to define more accurate joint resistive torque functions. The chapter begins with a description of the procedure used to measure the resistive torques in the ADAM joints. This is followed by a presentation of results indicating that not only does the coulomb friction torque need to be increased in certain joints, but a certain portion of the constant segment of the joint resistive torque function needs to be modified to an increasing function as well. Results of measurements necessary to define this new increasing function are presented in this same section. Finally, the method of implementing these results in the data set is described.

##### Joint Resistive Torque Measurement Procedure

In order to measure the same joint resistive torques in which the ADAM would encounter during an ejection seat sled track test, the number 8 prototype ADAM is fitted with skin, flight suit, and a G-suit. The measurement of a particular joint's resistive torque is accomplished by orienting the two segments of the ADAM attached by said joint in such a way that the motion of the proximal segment, while the distal segment is held motionless, is in a plane parallel to the ground. In doing so, the effect of gravity on the motion of the proximal segment can be neglected.

One end of a cable is attached to the proximal segment while the other end is attached to a load cell. The load cell is displaced resulting in the movement of the proximal segment. The force required to move the segment multiplied by the distance from the cable to the joint center results in the joint's resistive torque.

Prior to initiating the movement of the load cell, the segment to be moved is positioned in such a way that the cable is not perpendicular to the segment. Movement of the load cell eventually results in a state where the cable is perpendicular to the segment. It is only at this time that the load reading is taken. This procedure is accomplished several times per segment to ensure a consistent load reading.

#### Joint Resistive Torque Function Modifications

As stated in the previous chapter, it is believed that increasing the coulomb friction torque,  $\tau$ , will damp the erratic oscillatory motion currently experienced in the ATB model. In order to accomplish this task, the measurement procedure defined in the previous section is performed on the ADAM hip, knee, shoulder, and elbow joints. Measurements taken for one joint such as the right knee are assumed to be the same for the corresponding joint, left knee.

Constant Torque Addition. While taking these measurements, it is discovered that only when the skin of one segment rubs against the skin of an adjoining segment is there a constant friction torque which can be added directly to the existing coulomb friction torque. Joint motions which exhibit this characteristic and the corresponding torque increases are displayed in Table 4.1.

TABLE 4.1 Joints Functions Modified By a Constant Torque Increase

Joint Motion	Constant Torque Increase (N·m)
Elbow Flexion / Extension	4.83
Shoulder Coronal Plane Abduction / Adduction	11.87

Torque Function Addition. In contrast, when the skin of one segment is deformed by the skin of an adjoining segment due to joint motion or when the joint motion is impeded by the flight suit or G-suit, the resulting increase in torque is not constant. Instead it is described by an increasing function. Consequently, for those joints in which the skin of one segment does not simply rub against the skin of an adjoining segment, it is determined that modifications to the joint torque functions can not be made by simply adding a constant value to the existing coulomb friction torque.

The exact joint torque function resulting from skin segment, flight suit, and G-suit interaction is difficult to determine. There is still a certain range of joint motion in which the resistive torque is constant. Similarly, the joint resistance will still rapidly increase when the soft stop is impacted. It is the region between these two regimes that requires clearer definition. At this point, a simplification is made by assuming this new region is a linearly increasing function. Figure 4.2 presents a graphical description of this modification to the joint resistive torque functions.

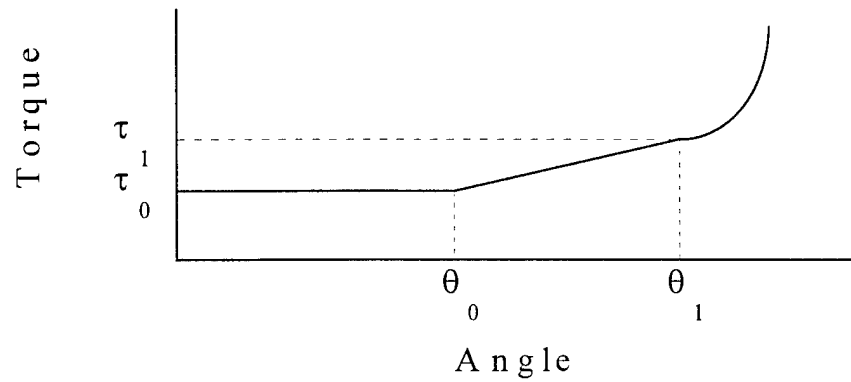


FIGURE 4.1 Modified Joint Resistive Torque Function

This modified joint resistive torque function initially models a constant resistive torque from the joint zero angle until some angle,  $\theta_0$ .  $\theta_0$  is the angle at which joint motion is impeded due to the deformation of the skin, the flight suit and/or the G-suit. The newly added function then models a linearly increasing resistive torque from  $\theta_0$  to  $\theta_1$ , the joint soft stop angle. The resistive torque encountered by a particular joint just prior to impacting the soft stop is defined as  $\tau_1$ . Finally, the third portion of this new function models the rapidly increasing resistive torque resulting from the joint impacting the soft stop.

In order to define this new linear function, the angles  $\theta_0$ ,  $\theta_1$ ,  $\tau_0$ , and,  $\tau_1$  are measured for the joint motions presented in Table 4.2.

TABLE 4.2 Joint Functions Modified By a Linearly Increasing Function

Joint Motion	$\tau_0$ (N m)	$\tau_1$ (N m)	$\theta_0$ (°)	$\theta_1$ (°)
Elbow Flexion	4.83	19.55	0	38
Knee Flexion	3.62	24.97	0	22.5
Shoulder Adduction	6.55	10.51	105	130
Shoulder Flexion	4.63	9.15	45	160
Shoulder Extension	4.45	9.15	0	40.7
Shoulder Coronal Abduction	11.87	17.80	90	117
Hip Flexion	12.66	40.17	-15	2

Because the joint angle at which skin deformation impedes hip flexion is negative, a new zero angle is redefined for the hip so that at this new angle, the joint resistive torque is only the constant coulomb friction torque.

The following joint motions are unaffected by the skin, flight suit, or G-suit.

1. Shoulder Abduction
2. Knee Extension
3. Hip Extension

The joint resistive torque functions characterizing the following joint motions are not modified due to lack of test equipment necessary to measure  $\theta_0$ ,  $\theta_1$ ,  $\tau_0$ , and  $\tau_1$ .

1. Elbow Supination / Pronation
2. Shoulder Medial / Lateral
3. Hip Abduction / Adduction
4. Knee Medial / Lateral
5. Hip Medial / Lateral
6. Lumbar Pitch
7. Lumbar Roll

Implementation. Using the linear functions developed along with the existing nonlinear function, resistive torques for each joint are calculated from  $0^\circ$  to  $180^\circ$  by  $10^\circ$  increments. These values are then entered into the E.7 cards defining the joint resistive

torques for the appropriate joint motion. Constant coulomb friction torques calculated are entered into the B.5 cards for the appropriate joint motions.

## V. Results of the Second ATB Simulation of AMIT 79E-G2A

Comparisons between the ADAM's joint angular displacements modeled by the second ATB simulation of AMIT 79E-G2A and those joint angular displacements measured during AMIT 79E-G2A are presented in this chapter in three different formats. First, angular displacements in terms of Euler angles are presented. Second, the Euler angles are converted to a quaternion, and the four elements of the quaternion are compared. Third, the rotation of certain joints are compared in three dimensional form. Finally, a discussion regarding the overall similarity between the ADAM's joint angular displacements modeled by the ATB and the joint angular displacements measured during AMIT 79E-G2A is presented.

### Euler Angle Comparison

The second ATB simulation of AMIT 79E-G2A results in a noticeable damping of the joint oscillation phenomena described in Chapter III. Sample joint angular displacement comparisons for this second ATB simulation of AMIT 79E-G2A are presented in Figure 5.1. Similar plots for all joints under consideration are presented in Appendix S.

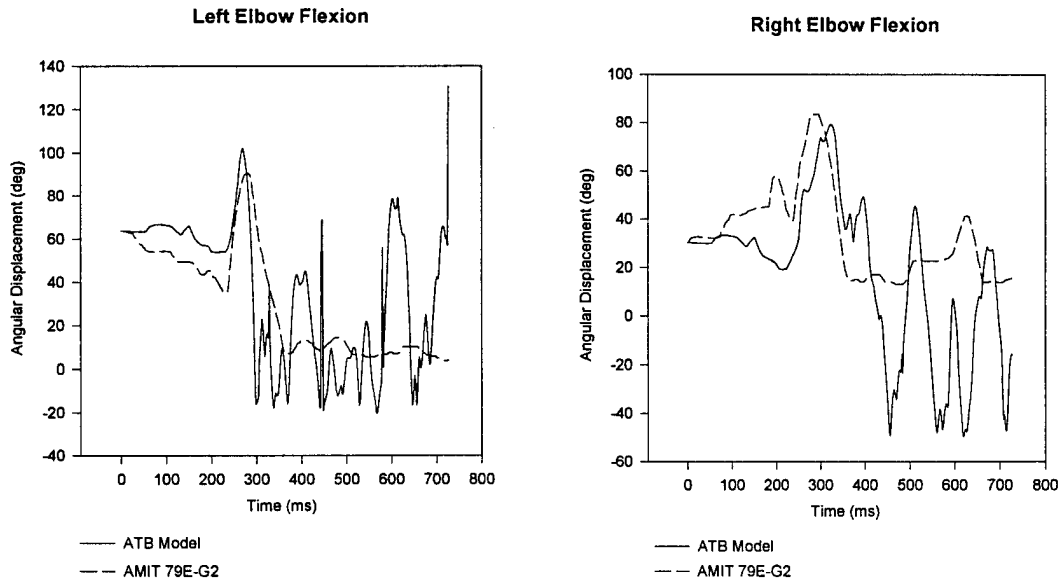


FIGURE 5.1 ADAM Left and Right Elbow Flexion

Comparisons of joint angular displacement for the second ATB simulation of AMIT 79E-G2A indicate a majority of the ATB modeled joint motions parallel the test measured joint motions for the first 300 milliseconds to 400 milliseconds. Motions such as *Knee Flexion* and *Hip Medial/Lateral*, for example, match very closely. Beyond this time, joint motions such as *Right Elbow Flexion*, *Right Knee Flexion*, and *Lumbar Pitch* all display improvements in modeling accuracy. Unfortunately, there are also certain motions such as *Shoulder Abduction/Adduction* which do not seem to parallel the test data very well even from the beginning of the simulation. Nonetheless, the modifications to the joint resistive torque functions do have the desired effect damping the excessive joint oscillations experience during the first ATB simulation of AMIT 79E-G2A. This damping is displayed in a sample comparison between the ADAM's joint angular displacements calculated during the first and second ATB simulations of AMIT 79E-G2A

which is presented in Figure 5.2. Only the time frame after 300 milliseconds is plotted in order to provide greater resolution. Similar plots for all joints are displayed in Appendix T.

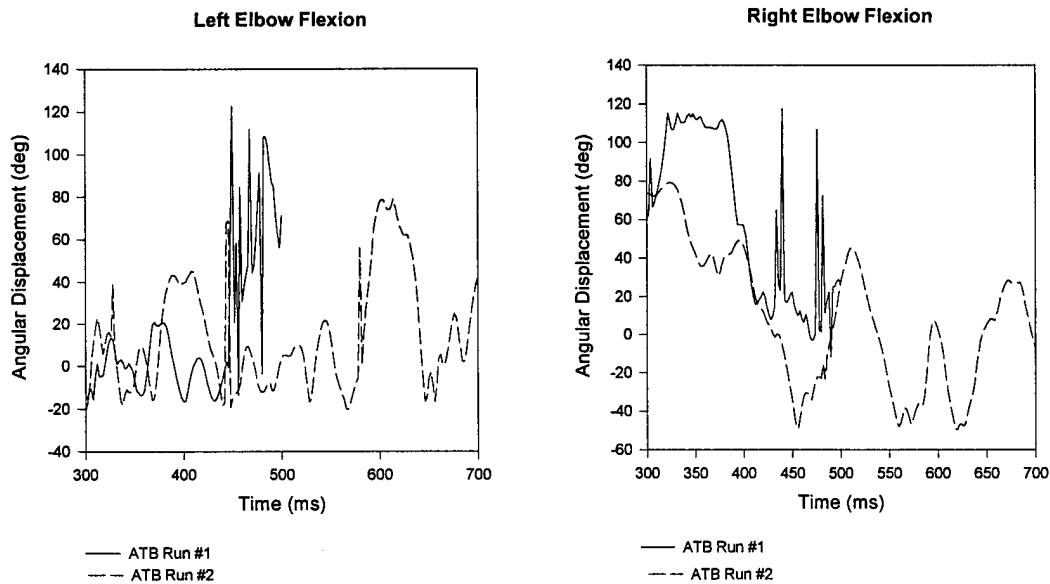


FIGURE 5.2 Comparison of ADAM Left and Right Elbow Flexion For Runs 1 and 2

### Quaternion Comparison.

Realizing the possibility that singularity problems associated with Euler angles may be causing the appearance of erratic joint oscillations which in fact do not exist, the Euler angle data compared in the previous section are converted to quaternions. The elements of the quaternion are then compared. Figure 5.3 presents an example of this comparison. Similar comparisons for all joints under consideration are displayed in Appendix U.

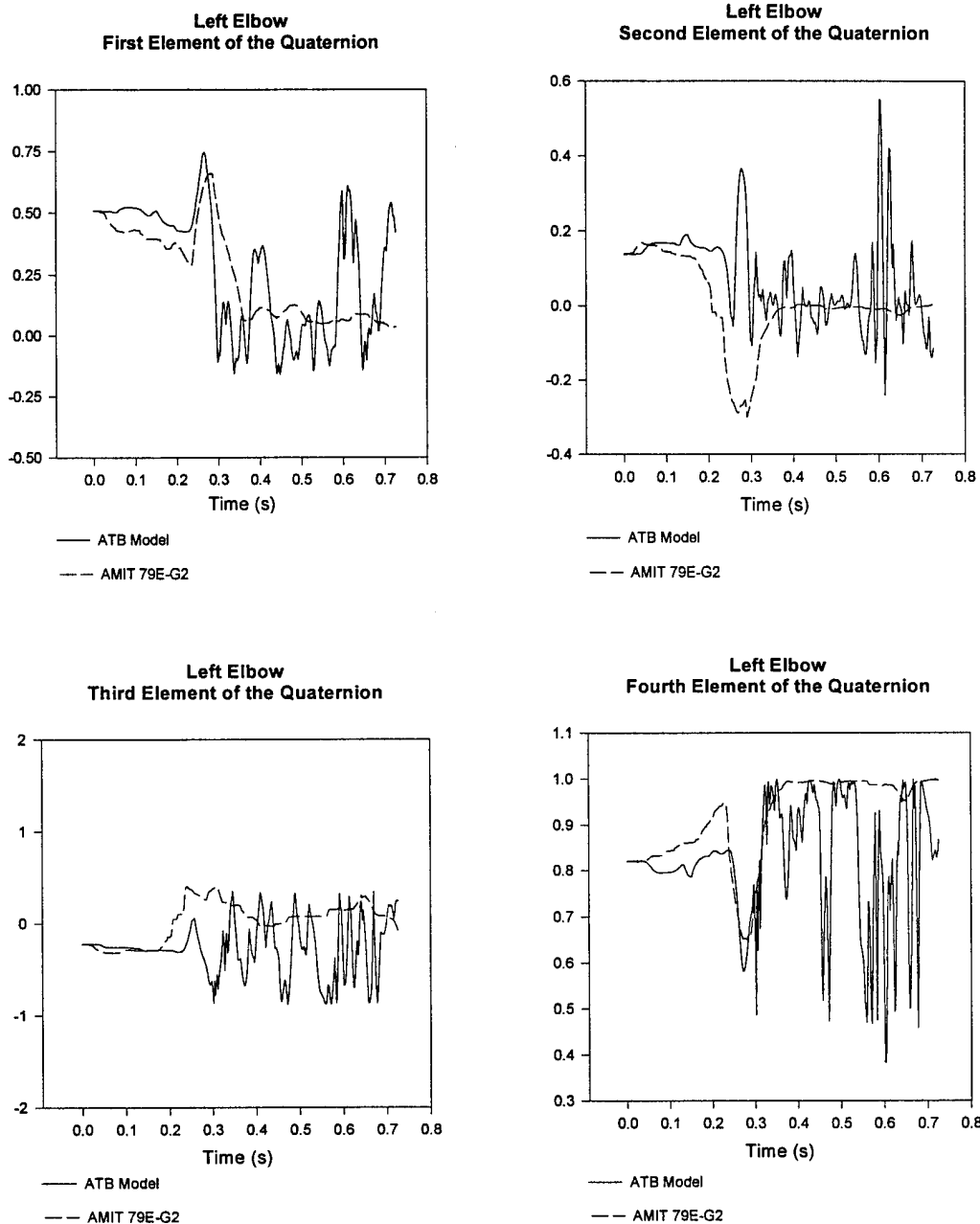


FIGURE 5.3 Quaternion Elements of the Left Elbow

The quaternion element comparison presents results similar to the Euler angle comparison. The ATB is able to accurately simulate a majority of the ADAM's joint angular displacements for the first 300 milliseconds to 400 milliseconds. After this time,

the ATB continues to model certain joints well, but a majority of the joints begin to display the erratic oscillations described in Chapter III.

### Three Dimensional Comparison.

In order to move a segment such as the lower arm from one point in space to another, there are several possible combinations of Euler angles which will result in the desired displacement. For example, assume the ATB model calculates a set of Euler Angles at one instant in time which places a particular segment at point *A* in space. At the following instant in time, the ATB calculates an entirely different set of Euler angles in order to move the segment to point *B* in space. Although the resulting motion may only move the segment a short distance, when comparing the first set of Euler angles to the second, it can appear that a significant rotation in all three Euler angles occurs. In other words it may not be possible to compare the Euler angles or the elements of the quaternion separately. Only via a three dimensional comparison can the accuracy of the ATB model be determined.

This comparison is accomplished by developing a graphical, three dimensional representation of each joint axis system. The code which generates this three dimensional representation is written as a MATLAB® script M-file and presented in Appendix V. In order to create the three dimensional representation of a particular joint, the rotation matrix for that joint is calculated at each instant in time. The rows of the rotation matrix define the projection of the joint axis onto the inertial axis. As a result, the joint axis can then be plotted with respect to an inertial reference frame. Rotation matrices using both

ATB modeled and AMIT 79E-G2A measured joint angular displacement data are calculated and plotted simultaneously for a particular instant in time. A sample of this comparison is presented in Figures 5.4 and 5.5.

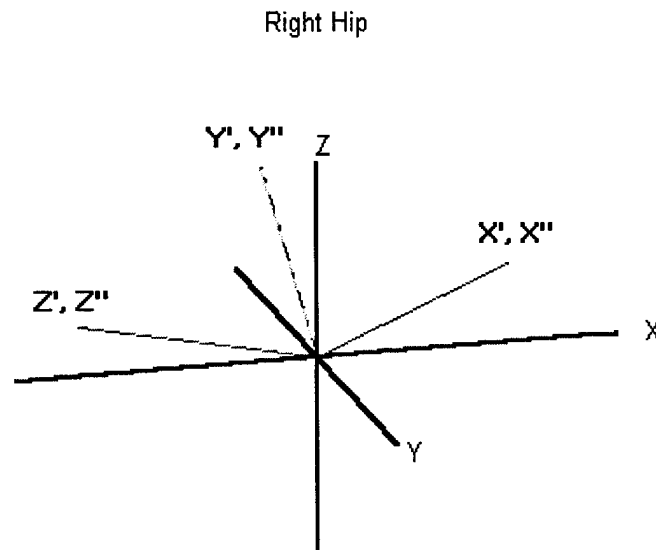


FIGURE 5.4 Initial State of 3-D Comparison

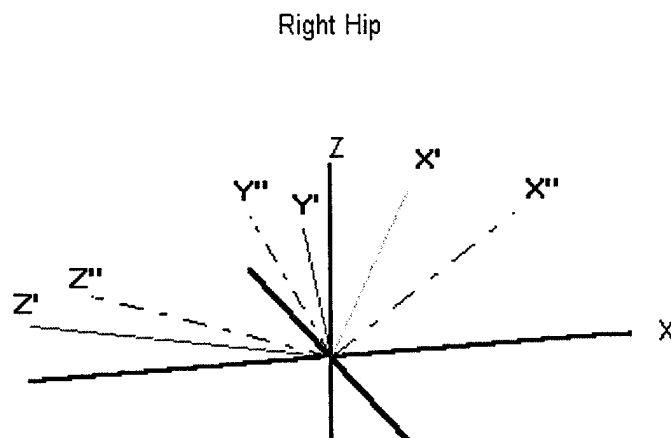


FIGURE 5.5 3-D Comparison During Joint Motion

Figure 5.4 depicts the initial state of the three dimensional comparison. The X, Y, and Z inertial axes remain stationary throughout the comparison. Initially, the X', Y',

and Z' axes representing the joint axis system modeled by the ATB simulation and the X'', Y'', and Z'' representing the joint axis motion measured during AMIT 79E-G2A are coincident. Once the comparison begins, as shown in figure 5.5, the position of the *prime* axis system deviates from the *double prime* axis system. The amount of deviation defines the degree to which the joint motion modeled by the ATB varies from the joint motion measured during the AMIT 79E-G2A test.

Clearly it is difficult to present a three dimensional comparison, which is also a function of time, in a two dimensional thesis. Nonetheless, the results of this comparison present results similar to those discovered when comparing the Euler angles and quaternion elements of each joint. At approximate 300 milliseconds to 400 milliseconds, a significant deviation between the ATB modeled and AMIT 79E-G2A joint motions begins to occur.

#### Overall Similarity Between ATB Modeled and Measured Joint Motions

The duration of the ATB simulation of AMIT 79E-G2A is increased from 0.5 seconds to 0.75 seconds. For the same reason as the first ATB simulation of AMIT 79E-G2A, the Runge-Kutta integration routine is unable to converge during this run due to excessive head accelerations. All three methods of comparing ATB modeled to AMIT 79E-G2A measured joint angular displacements appear to present the same basic results. The modifications to the joint resistive torque functions clearly improve the ability of the ATB to accurately model the ADAM. The ATB model is able to progress further along

in the simulation (closer to a full 1.0 second), and the degree of excessive joint oscillation is decreased.

A majority of the joint angular displacement data modeled by the ATB closely parallel the AMIT 79E-G2A measured joint angular displacement data for the first 300 milliseconds to 400 milliseconds of the simulation. Beyond this time, certain joint angular displacements continue to match closely such as *Knee Flexion*, *Left Knee Medial/Lateral*, and *Lumbar Pitch*. Based on the same logic defined in Chapter III, ATB modeled *Hip Abduction/Adduction* could also be considered to parallel the test data relatively well, assuming the right and left hip test data is improperly marked (reversed). Other ATB modeled angular displacements such as *Right Shoulder Coronal Plane Abduction/Adduction*, *Right Elbow Supination/Pronation*, and *Left Elbow Flexion* follow the same basic shape as those joint angular displacements measured during AMIT 79E-G2A, but do not match well in magnitude. There are also those joint angular displacement data that do not seem to match well either in shape or magnitude such as *Hip Flexion* and *Right Knee Medial/Lateral*.

## VI. Articulated Total Body Input File Development For the AMIT 79E-F1 Test

In order to more accurately define the validity of the large ADAM data set, a second ADAM/MASE Integration Test, AMIT 79E-F1, is modeled using the ATB simulation. This chapter begins with a short description of the differences between AMIT 79E-G2A and AMIT 79E-F1. It then proceeds to describe modifications made to the AMIT 79E-G2A input file in order to model AMIT 79E-F1.

### AMIT 79E-F1 Test Description

The AMIT 79E-F1 test data is maintained by the Crew Escape Technologies (CREST) office located at Wright-Patterson AFB, OH (Plagha, 1995). The following information describes the time and conditions under which AMIT 79E-F1 was conducted.

Launch Date	24 Nov 1992
Launch Time	1157 MST
Ambient Temperature	6.67 °C
Barometric Pressure	87700 N/m
Sled Track Velocity	237 m/s
Sled Track Orientation	Straight and Level
Sled Track Angular Rates	All Zero

Note that this test is conducted at a significantly slower airspeed, 83 m/s slower, than AMIT 79E-G2A. Comparisons of video taken of AMIT 79E-G2A and AMIT 79E-F1 denote a smoother ejection during latter test. Specifically, the ACES II ejection seat does not exhibit the same high rate of yaw, pitch and roll during AMIT 79E-F1 as it does

during AMIT 79E-G2A. During AMIT 79E-F1, the ejection seat leaves the rails cleanly and rolls slightly to the right.

#### Modifications to AMIT 79E-G2A Input File

Excluding the C cards which describe the motion of the ejection seat, the input file for the ATB model to simulate AMIT 79E-F1 remains the same as the input file used to model AMIT 79E-G2A. Using the same procedure as described in the Chapter II section titled "Filtering and Conditioning Ejection Seat Accelerometer Data", ejection seat acceleration and velocity data are converted to an acceptable format for the ATB input file C.2 cards. Unlike AMIT 79E-G2A in which four accelerometers recorded data throughout the test, all accelerometers except accelerometer *A* lost either the X, Y, or Z signal at some point during the AMIT 79E-F1 sled track run. Consequently, only accelerometer *A* data is used to define the ejection seat linear velocity during this simulation.

Removal of Acceleration and Velocity Biases. Linear acceleration and angular velocity data prior to *Seat First Motion* are analyzed to determine if any of the data are biased. Based on experience from analyzing similar AMIT 79E-G2A data, the filtered and unfiltered average linear acceleration and angular velocity data in the time period prior to *seat first motion* are assumed to be effectively the same. The average filtered linear acceleration and angular velocity data in the X, Y, and Z directions plus or minus a confidence interval based on a 99% confidence level are calculated and displayed in

Table 6.1. All linear acceleration data are in meters per second squared and all angular velocity data are in degrees per second.

TABLE 6.1 Biases in Raw Linear Acceleration and Angular Velocity Data

Accelerometer	Bias
<u>Accelerometer A</u>	X = $15.32 \pm 0.384$
	Y = $0.54 \pm 0.14$
	Z = $9.53 \pm 0.35$
<u>Angular Velocity</u>	X = $-213.1 \pm 0.44$
	Y = $-91.88 \pm .38$
	Z = $-65.97 \pm .59$

No attempt is made to determine a bias on the linear acceleration data in the X direction since the true acceleration in this direction is not known. It is known that the true acceleration in the Y direction should be 0 meters per second squared and in the Z direction should be 9.81 meters per second squared. The average values for the measured accelerations are considered close enough to the expected accelerations to conclude that a bias does not exist in Y or Z linear acceleration data. It is expected that the angular velocity in all three directions, X, Y, and Z, should be zero prior to ejection. Based on the excessive deviation of the average measured X, Y, and Z angular velocity data relative to the expected value of zero, it is determined that the angular velocity data in the X, Y, and Z directions are biased by the amounts defined in Table 6.1. These biases are subtracted from the measured angular velocity data in the time period between *Seat First Motion* and *Seat-ADAM Separation*, the time frame during the ejection which is being modeled.

Filtering Ejection Seat Trajectory Simulation Data. Similar to the data used to describe the trajectory of the ejection seat when simulating AMIT 79E-G2A, the ejection seat's linear acceleration and angular velocity measurements taken during AMIT 79E-F1 are noisy. Consequently, in order to accurately describe the trajectory of the ejection seat, the noise is removed from this data using the same ideal, low-pass filter described in Chapter II. Recall, the filtering procedure involves converting noisy data from the time domain to the frequency domain via the Fast Fourier Transform, cutting off high frequency noise, and reconvertng the data back to the time domain. The MATHCAD® code written to perform this filtering is presented in Appendix H. The linear acceleration and angular velocity data are filtered at the frequencies displayed in Appendix X.

Calculating Linear and Angular Velocities at SRP. In order to describe the trajectory of the ejection seat in terms of velocity, the filtered linear acceleration data are integrated using the SIMULINK™ code displayed in Appendix K. Using the linear and angular velocity data, the linear velocity at the SRP is calculated using the MATLAB® code displayed in Appendix M (Greenwood, 1988). These calculated linear velocity data, displayed in Figure 6.1, and measured angular velocity data, displayed in Figure 6.2, are entered into the C cards of the ATB simulation to define the trajectory of the ejection seat.

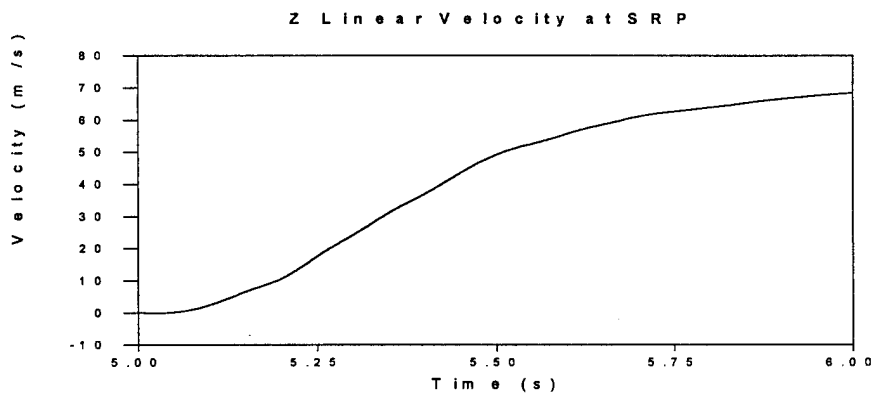
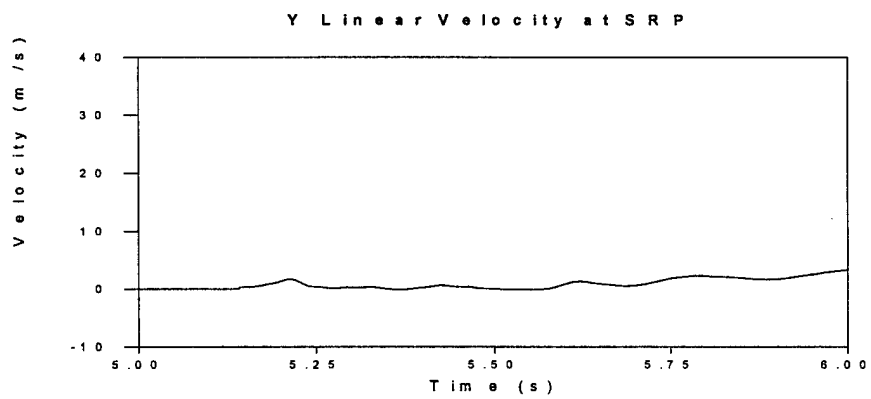
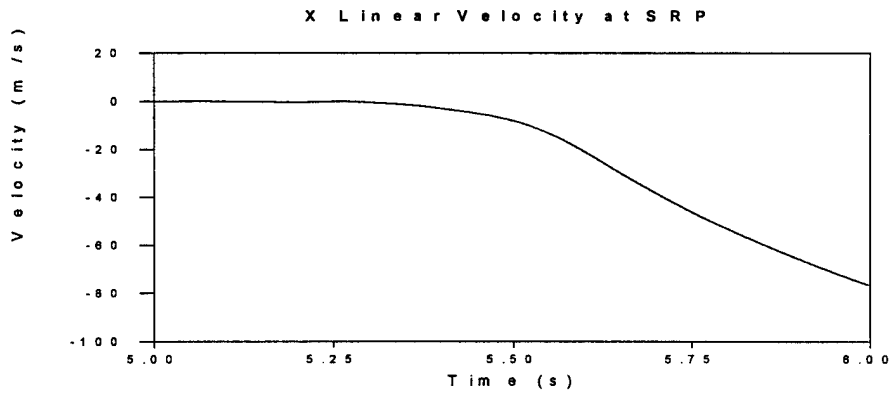


**FIGURE 6.1 Linear Velocity at Seat Reference Point**

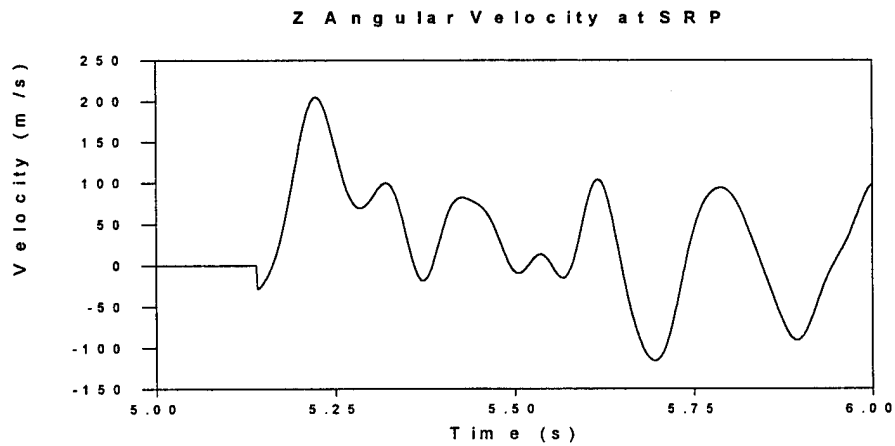
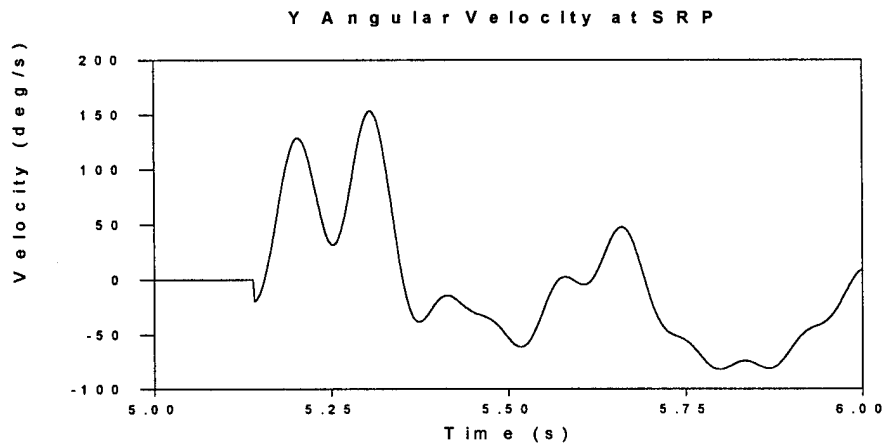
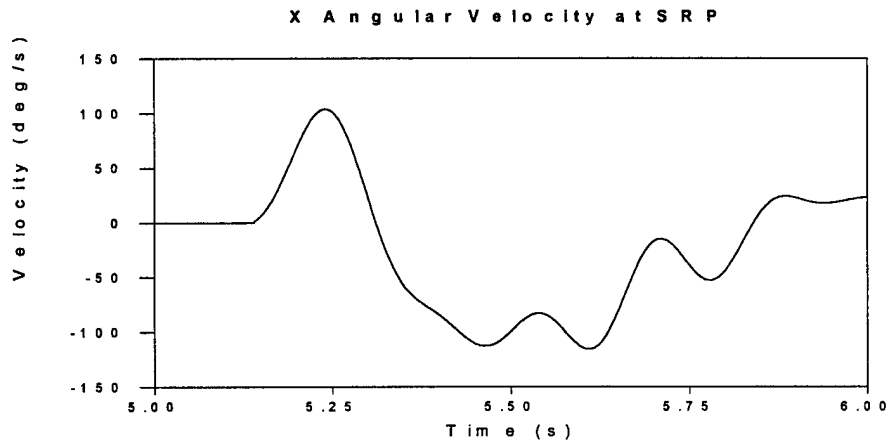


**FIGURE 6.2 Angular Velocity at Seat Reference Point**

### Modifications To Ejection Seat Trajectory Data

As depicted in Figure 6.2, artificially setting the ejection seat's X, Y, and Z angular velocity data to zero for the first 0.14 seconds results in sharp changes in angular velocity at the 0.14 second instant in time. Although not as readily apparent in Figure 6.1, this situation also exists for the Y linear velocity data as well. As a result, the ATB model calculates excessively high accelerations at 0.14 seconds. This situation does not present itself during the ATB simulation of AMIT 79E-G2A because the X, Y, and Z angular velocity data and Y linear velocity data describing the trajectory of the ejection seat are close to zero at the 0.14 second instant in time.

In order to rectify this problem, the velocity data entered into the ATB model just prior to the 0.14 second time are artificially altered to create a smooth transition from zero velocity prior to 0.14 seconds to what ever the velocity actually is at 0.14 seconds. The rate of smoothing the data is subjective. For this simulation, Y linear velocity data are smoothed at a rate of 12.7 meters per second squared and the angular velocities at a rate of between 250 and 500 degrees per second squared.

## VII. Results of the ATB Modeling of AMIT 79E-F1

This chapter presents the results of the ATB modeling of AMIT 79E-F1.

Presented first are comparisons of the ADAM joint angular displacements defined by the ATB simulation and those measured during AMIT 79E-F1 . Contained within this section is a short discussion regarding the shifting and reverse polarization of certain joint motions modeled by the ATB. Following this section is a discussion regarding the overall similarity between the ADAM's joint angular displacements modeled by the ATB and those measured during AMIT 79E-F1. A graphical display of the ATB simulation of AMIT 79E-F1 is presented in Appendix Z.

### Joint Angular Displacement Comparison

Based on the same logic defined in Chapter III of this thesis, all of the ATB angular displacement data are shifted so that the ADAM joint zero angles defined during the AMIT 79E-F1 test coincide with the ATB defined zero angles. Also based on the same logic defined in Chapter III of this thesis, the polarities of two of the data channels are reversed. This results in a mirroring of the following two joint motions.

1. Right Elbow Flexion
2. Right Hip Medial/Lateral

Figures 7.1 and 7.2 respectively display these joint motions before and after polarity reversal. Plots depicting all joints angular displacement comparisons are presented in Appendix W.

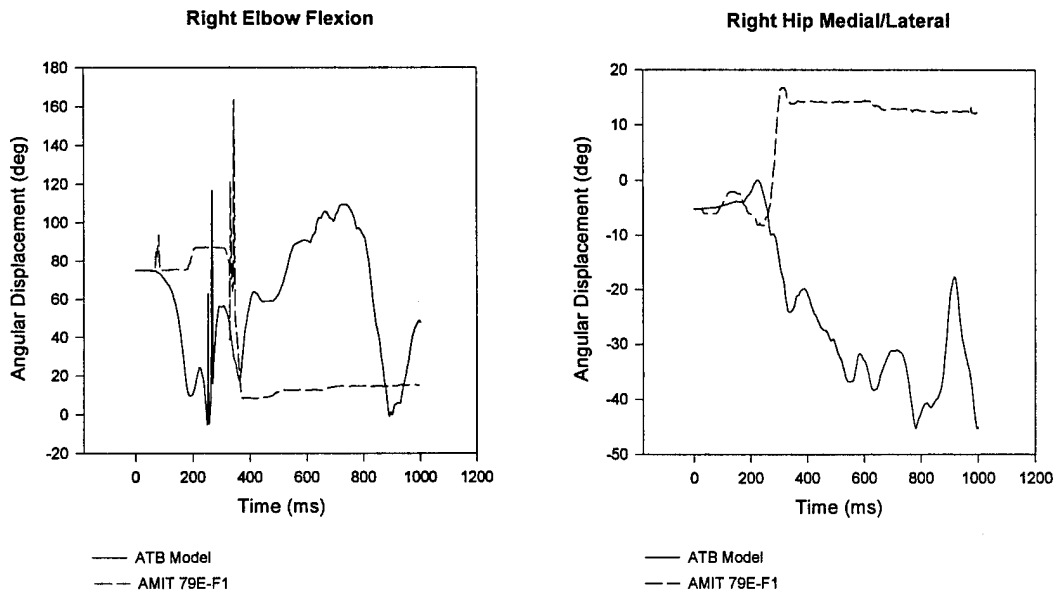


FIGURE 7.1 AMIT 79E-F1 Joint Motions Prior to Polarity Reversal

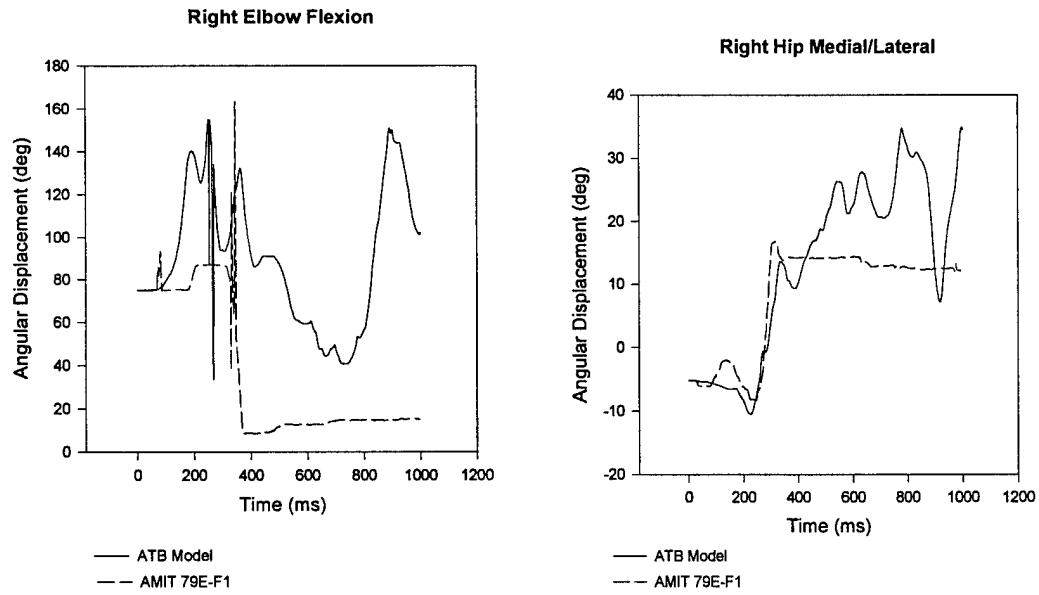


FIGURE 7.2 AMIT 79E-F1 Joint Motions After Polarity Reversal

### Overall Similarity Between ATB Modeled and Measured Joint Motions

Unlike the ATB simulation of AMIT 79E-G2A, the ATB is able to simulate the full 1.0 second portion of AMIT 79E-F1. It is believed this is primarily due to the fact that the AMIT 79E-F1 ejection is much smoother. During the AMIT 79E-F1 ejection, the ADAM experiences lower angular accelerations than during the AMIT 79E-G2A ejection.

In general, the ATB model is able to simulate the ADAM's joint angular displacements during AMIT 79E-F1 more closely than during AMIT 79E-G2A. Excluding *Right Elbow Flexion* and *Left Shoulder Flexion*, all other flexion motions, left and right, modeled by the ATB coincide with the AMIT 79E-F1 measured flexion motions plus or minus approximately 15° throughout the entire 1.0 second simulation. Similarly, both *Hip Abduction/Adduction* and *Hip Medial/Lateral* motions modeled by the ATB simulations parallel the same measured motions plus or minus 15° to 20°.

The ATB modeled *Lumbar Pitch* never deviates more than 10° to 15° from the AMIT 79E-F1 measured *Lumbar Pitch*. Similarly, the ATB modeled *Lumbar Roll* never deviates more than approximately 15°. Although it can be argued that both the ATB modeled *Lumbar Pitch* and *Lumbar Roll* motions closely match the corresponding measured motions, it is believed that these apparent correlations are primarily due to the small ranges of motion allowed by the Lumbar joint, 7° in pitch and 2° in roll, prior to impacting the soft stops.

Similar to the ATB modeling of AMIT 79E-G2A, certain ADAM joint motions modeled by the ATB simulation parallel the corresponding AMIT 79E-F1 measured joint motions in shape but not in magnitude. The *Left Shoulder Coronal Plane Abduction/Adduction* motion displays these characteristics. There are also ATB modeled joint motions that continue to oscillate erratically such as *Elbow Supination/Pronation*, *Shoulder Abduction/Adduction*, and *Shoulder Medial Lateral*.

Neither the *Left Knee Medial/Lateral* nor *Right Knee Medial/Lateral* motions are compared beyond the first 300 milliseconds. Beyond this time, it appears that the data channels recording these motions during AMIT 79E-F1 ceased to function.

## VIII. Conclusions and Recommendations

The following chapter presents conclusions regarding the accuracy of the Articulated Total Body (ATB) model in simulating the elbow, shoulder, knee, hip, and lumbar joints of the Advanced Dynamic Anthropomorphic Manikin (ADAM) during ADAM/MASE Integration Tests (AMIT) 79E-G2A and 79E-F1. From these conclusions, the overall validity of the current ADAM data set is defined. Following these conclusions are recommendations for further improvements to the current ADAM data set.

### Conclusions

The ATB is clearly able to model AMIT 79E-F1 better than AMIT 79E-G2A. This is due to the lower angular accelerations experienced by the ADAM during the AMIT 79E-F1 test. The comparisons presented in this thesis indicate that the current ADAM data set more accurately models the ADAM's dynamics during lower versus higher airspeed ejections. A correlation to this conclusion is that the current ADAM data set models the dynamics of the ADAM more accurately during a controlled ejection (one absent of high angular accelerations, above 250 degrees per second) versus an uncontrolled ejection. Discussions with Wright Laboratory personnel who use computer models of the ACES II and are familiar with the ejection seat indicate that at 320 meters per second (600 KEAS), the airspeed at which AMIT 79E-G2A was conducted, the aerodynamic flow around the ejection seat is very unpredictable. Consequently, the seat design does not necessarily guarantee stability at this high an airspeed (Meyer, 1995).

The difficulty of modeling the ADAM during AMIT 79E-G2A directly correlates with similar difficulty encountered in modeling the ACES II at high airspeeds. Consequently, the inability of the ADAM data set to accurately characterize the ADAM during a 320 meter per second (600 KEAS) airspeed ejection is not unexpected.

The ATB model is able to simulate AMIT 79E-G2A for a greater period of time and with greater accuracy after modifications are made to the joint resistive torque functions. The modifications to the joint resistive torque functions are helpful in damping the erratic joint oscillations observed during the first ATB simulation of AMIT 79E-G2A. The following discussion supports this conclusion. The resistances in the ADAM's joints to *flexion* motion are the easiest to measure, and, as a result, the modifications made to the *flexion* joint resistive torque functions are the most accurate. This relative ease of measurement and ensuing accuracy account for the ATB's ability to most accurately model the ADAM's *flexion* motions. In contrast, it is very difficult, with the equipment available at the time of conducting this research, to accurately measure the resistances in the ADAM's joints to *Medial/Lateral* and *Supination/Pronation* motions. As a result, modifications are not made to the joint resistive torque functions defining *Medial/Lateral* and *Supination/Pronation* motions. This lack of modifications accounts for the continued joint oscillations observed during the ATB simulations.

Although it is concluded that the modifications to the joint resistive torque functions (when it is possible to make the modifications) are a step in the right direction, the ADAM data set is not completely valid. This conclusion is based on two reasons. First, those joint motions in which the corresponding joint resistive torque functions are

not modified due to the difficulty of measuring the resistance in the joints are currently not accurately modeled by the ATB. Second, the assumption that the joint resistive torque function characterizing the resistance in the joints due to skin compression is linear may not be accurate for certain joints. For example, although measurements of the parameters required to modify the joint resistive torque functions characterizing the motion of the ADAM's shoulder joints are considered relatively accurate, the ATB is not able to closely model the ADAM's shoulder motion.

In summary, the ADAM data set better characterizes the ADAM at lower airspeeds than higher airspeeds. The modifications made to the joint resistive torque functions improve the accuracy of the ADAM data set but not sufficiently to warrant the complete validation of the ADAM data set.

### Recommendations

Based on the conclusions presented in the previous section, two recommendations are offered. The first recommendation is to conduct more comparisons, such as those described in this thesis, between the ADAM's joint angular displacements modeled by the ATB and the ADAM's joint angular displacements measured during full scale ejection seat sled tests. Joint angular displacements measured during ADAM/MASE Integration Tests are good to use for comparison purposes. Joint angular displacements measured during recent tests conducted with the ADAM on the Horizontal Impact Accelerator (HIA) in the fall of 1995 are even better to use. The tests conducted on the HIA are more highly recommended based on the fact that these tests were conducted

specifically for the purpose of validating the ADAM data set. Along with comparing joint angular displacements, head, chest, and pelvic accelerations should also be compared. These accelerations are often used as indicators of the extent to which an aviator will be injured during an ejection, and, consequently, must be accurately modeled by the ADAM data set.

It is further recommended that these comparisons should concentrate on tests conducted at lower airspeeds (100 meters per second to 200 meters per second). This recommendation is based on the fact that the ejection airspeeds considered in this validation are higher than a majority of ejections that occur during normal Air Force and Navy flight operations. Based on information from the Air Force Safety Office at Kirtland AFB, NM, ejections from Air Force aircraft in the past five years have occurred at an average airspeed of 107 meters per second (208 KIAS) with a confidence interval of 8.4 meters per second (16.4 KIAS) based on a 99% confidence level (Clark, 1995). Similarly, Figure 8.1 indicates that 81% of U.S. Naval ejections between 1976-1989 occurred at airspeeds less than 153 meters per second (299 KIAS) (Karner, 1993).

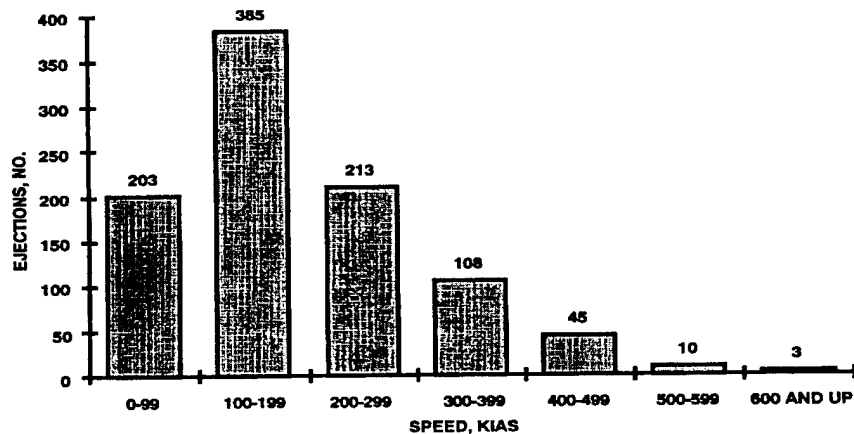


FIGURE 8.1 U.S. Naval Aircraft Ejections (Karner, 1993)

Although a majority of these Air Force and Navy ejections occurred during peace time (peace time ejections normally occur at lower airspeeds relative to war time ejection air speeds), if one considers a life lost during peace time as valuable as one lost during war time, the accuracy of the ADAM data set is just as important at airspeeds between 102 meters per second (200 KIAS) and 154 meters per second (300 KIAS) as it is between 257 meters per second (500 KIAS) and 309 meters per second (600 KIAS).

The second recommendation is to perform more accurate tests on the ADAM, with skin attached and fully suited for test, to measure the true resistance in each of the ADAM's joints. This would help to define accurate joint resistive torque functions. Although the modifications to the joint resistive torque functions described in this thesis produce the desired results of decreasing excessive joint oscillations and improving the accuracy of the ADAM data set, the modifications are not accurate enough. It is only through the correct definition of these joint resistive torques that a true validation of the ADAM data set can be achieved.

## Appendix A: ATB Input File Card Definitions

- Cards A - Date and run description, units of input and output, control of restart, integrator and optional output.
- Cards B - Physical characteristics of the segments and joints.
- Cards C - Description of vehicle motion.
- Cards D - Contact planes, belts, air bags, contact (hyper)ellipsoids, constraints, symmetry options, spring dampers, and prescribed forces and torques.
- Cards E - Functions defining force-deflections, stress-strains, inertial spikes, energy absorption factor, and friction coefficients.
- Cards F - Allowed contacts among segments, planes, belts, airbags, contact (hyper)ellipsoids and harnesses.
- Cards G - Initial orientations and velocities of the segments.
- Cards H - Control of output of time history of selected segment motions, joint parameters, wind forces, joint forces and torques, total body properties, and injury criteria.
- Cards I - Control information for plotter output.

Appendix B: Planes Describing the ACESII Ejection Seat in the Articulated Total Body Model

<u>Seat Bottom</u>			<u>Seat Back #1</u>		
0.85	-9.10	-0.85	0.85	-9.10	-37.93
0.85	9.10	-0.85	0.85	9.10	-37.93
18.67	-9.10	-0.85	0.85	-9.10	-0.85
<u>Seat Back #2</u>			<u>Left Side Seat Back</u>		
0.85	-9.10	-37.93	-10.42	-9.10	-37.93
0.85	9.10	-37.93	0.85	-9.10	-37.93
0.85	-9.10	-0.85	-10.42	-9.10	-0.85
<u>Right Side Seat Back</u>			<u>Left Side Lower Seat / Out</u>		
10.42	9.10	-37.93	-9.67	-9.10	-5.12
-10.42	9.10	-0.85	21.43	-9.10	2.28
0.85	9.10	-37.93	-9.67	-9.10	2.75
<u>Left Side Lower Seat / In</u>			<u>Right Side Lower Seat/Out</u>		
-9.67	-9.10	-5.12	-9.67	-9.10	-5.12
-9.67	-9.10	2.75	-9.67	9.10	2.75
21.43	-9.10	2.28	21.43	9.10	2.28
<u>Right Side Lower Seat / In</u>			<u>Lower Front Seat</u>		
-9.67	-9.10	-5.12	17.07	-9.10	0.00
21.43	9.10	2.28	17.07	9.10	0.00
-9.67	9.10	2.75	14.03	-9.10	8.72
<u>Left Leg Guard / In</u>			<u>Left Leg Guard / Out</u>		
17.82	-9.10	1.52	17.82	-9.10	1.52
17.82	9.10	-2.65	21.43	9.10	2.28
21.43	9.10	2.28	17.82	9.10	-2.65
<u>Right Leg Guard / In</u>			<u>Right Leg Guard / Out</u>		
17.82	9.10	1.52	17.82	9.10	1.52
17.82	9.10	-2.65	21.43	9.10	2.28
21.43	9.10	2.28	17.82	9.10	-2.65
<u>Left Head Rest</u>			<u>Right Head Rest</u>		
0.85	-1.50	-2.92	0.85	1.50	-29.20
2.65	-4.36	-29.20	0.85	1.50	-36.78
0.85	-1.50	-36.78	2.65	4.36	-2.92

Appendix C: Planes Describing the F-16A Cockpit in the Articulated Total Body Model

	<u>Floor</u>		<u>Angled Floor of Seat Well</u>		
22.39	-13.50	2.55	22.39	-13.50	2.55
50.68	-13.50	2.55	8.84	-13.50	13.16
22.39	13.50	2.55	22.39	13.50	2.55
	<u>Horizontal Floor of Seat Well</u>		<u>Aft Cockpit Pressure Bulkhead</u>		
8.84	-13.50	13.16	-19.25	-13.50	11.79
8.84	13.50	13.16	-19.25	-13.50	-14.34
19.25	-13.50	11.79	-19.25	13.50	11.79
	<u>Fire Wall</u>		<u>Upper Center Console Panel #1</u>		
50.68	-13.50	2.55	24.94	-3.75	-12.57
50.68	13.50	2.55	24.94	3.75	-12.57
50.68	-13.50	-10.8	22.09	-3.75	-12.57
	<u>Upper Center Console Panel #2</u>		<u>Upper Center Console Panel #3</u>		
22.09	-3.75	-12.57	22.79	-3.75	-17.68
22.09	3.75	-12.57	22.79	3.75	-17.68
22.79	-3.75	-17.68	20.63	-3.75	-20.82
	<u>Upper Center Console Panel #4</u>		<u>Upper Center Console Panel #5</u>		
20.63	-3.75	-20.82	20.53	-3.75	-24.16
20.63	3.75	-20.82	20.53	3.75	-24.16
20.53	-3.75	-24.16	27.89	-3.75	-22.39
	<u>Lower Center Console Panel #1</u>		<u>Lower Center Console Panel #2</u>		
24.94	3.75	-12.57	17.48	3.75	-6.68
24.94	-3.75	-12.57	17.48	-3.75	-6.68
17.48	3.75	-6.68	22.39	3.75	2.55
	<u>Heads Up Display (HUD)</u>				
28.09	-3.84	-23.77			
28.09	3.84	-23.77			
21.51	-3.84	-29.86			

Appendix D: Measurements Required to Modify the ADAM Model to Account For a Flight Helmet

Mass of Helmet: 5.70 kg

Center of Gravity Relative to Mechanical Axis System

X = 0.0139 m

Y = 0.0000 m

Z = 0.0503 m

Geometric Center Relative to Mechanical Axis System

X = 0.0032 m

Y = 0.0000 m

Z = 0.0062 m

Orientation of the Principal Axis With Respect to the ATB Axis

Yaw = 0 deg

Pitch = 42.10 deg

Roll = 180 deg

Principal Moments of Intertia

X = 94.41 N cm<sup>2</sup>

Y = 92.5 N cm<sup>2</sup>

Z = 66.97 N cm<sup>2</sup>

Mass Per Boot: 2.4 Kg

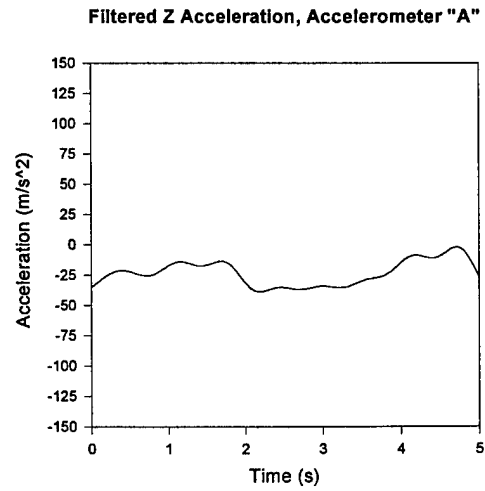
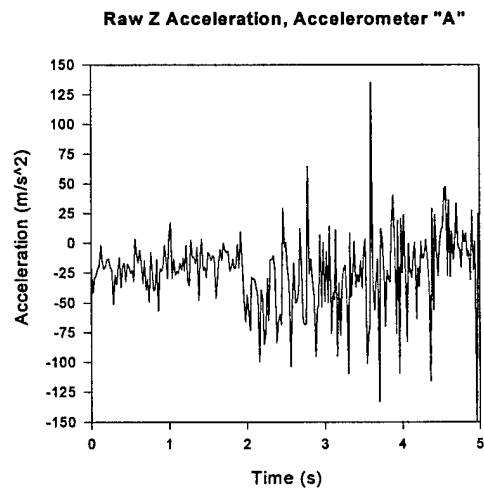
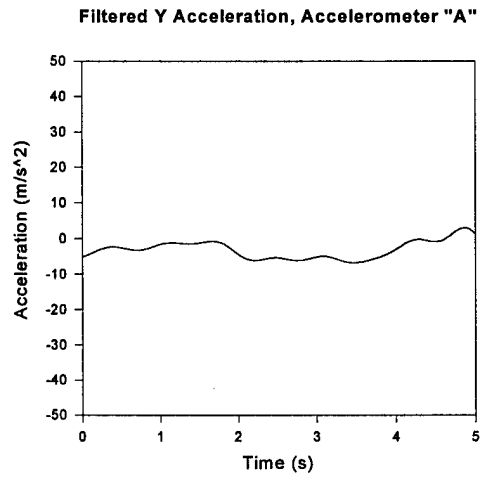
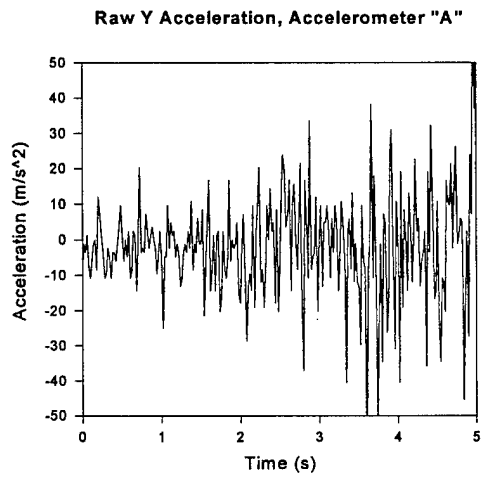
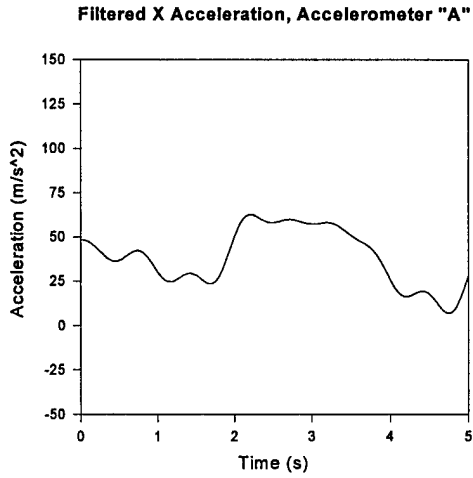
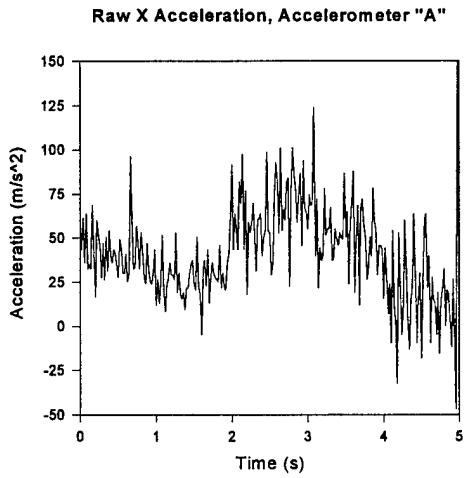
Appendix E: Segment / Segment Contacts

Segment	Contact Segments
1. Lower Torso	13, 14, 17, 18
2. Upper Torso	12, 13, 14, 16, 17
3. Neck	12, 13, 14, 16, 17
4. Head	2, 12, 13, 14, 16
5. Right Upper Leg	8, 9, 13, 14, 17
6. Right Lower Leg	8, 9, 10, 13, 18
7. Right Foot	9, 10, 13, 14, 18
8. Left Upper Leg	13, 17, 18
9. Left Lower Leg	17, 18
10. Left Foot	14, 17, 18
11. Right Shoulder	4, 13, 14, 17, 18
12. Right Upper Arm	17, 18
13. Right Lower Arm	9, 10, 17, 18
14. Right Hand	6, 8, 9, 17, 18
15. Left Shoulder	4, 13, 14, 17, 18
16. Left Upper Arm	13, 14
17. Left Lower Arm	4, 6, 7
18. Left Hand	2, 3, 4, 5

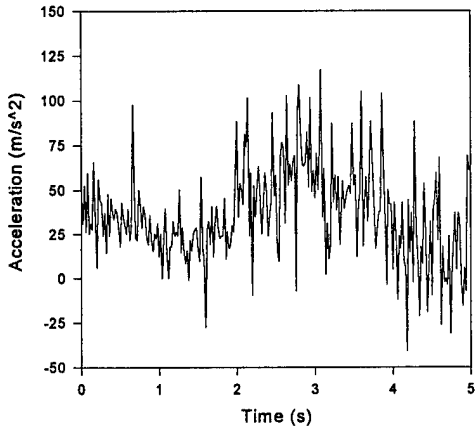
Appendix F: Plane / Segment Contacts

Plane	Contact Segments
1. Seat Bottom	1, 5, 8, 17, 18
2. Seat Back #1	1, 2, 4, 13, 17
3. Left Side Seat Back	16, 17, 18
4. Right Side Seat Back	12, 13, 14
5. Seat Back #2	11, 12, 14, 15, 16
6. Right Side Lower Seat / Out	13, 14
7. Left Side Lower Seat / Out	17, 18
8. Left Side Lower Seat / In	1, 8, 9
9. Right Side Lower Seat / In	1, 5, 6
10. Lower Front Seat	6, 7, 9, 10
11. Left Leg Guard / In	8, 9
12. Right Leg Guard / In	5, 6
13. Left Leg Guard / Out	17, 18
14. Right Leg Guard / Out	13, 14
15. Left Head Rest	4
16. Right Head Rest	4
17. Floor	7, 10

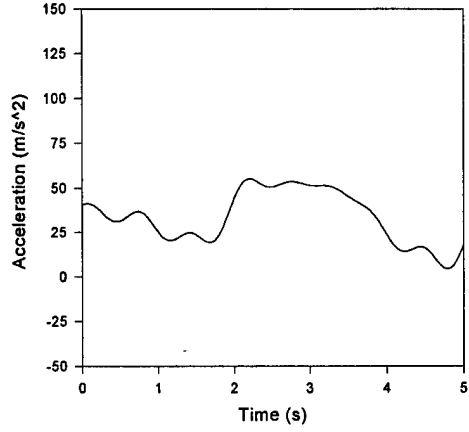
Appendix G: Raw and Filtered Linear Acceleration and Angular Velocity Data Prior to Seat First Motion



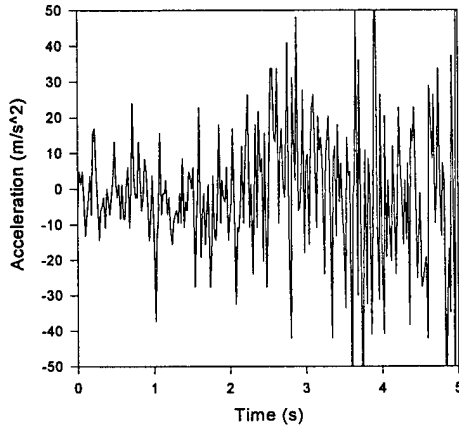
Raw X Acceleration, Accelerometer "B"



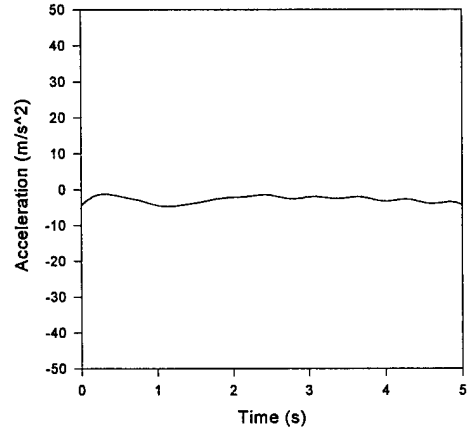
Filtered X Acceleration, Accelerometer "B"



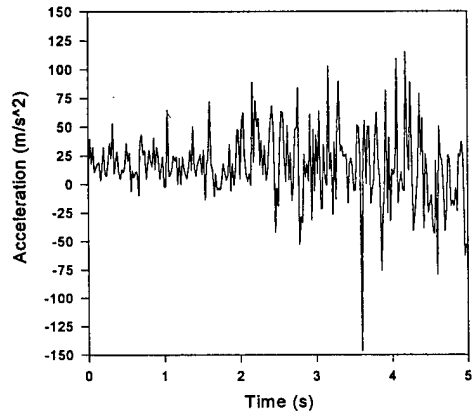
Raw Y Acceleration, Accelerometer "B"



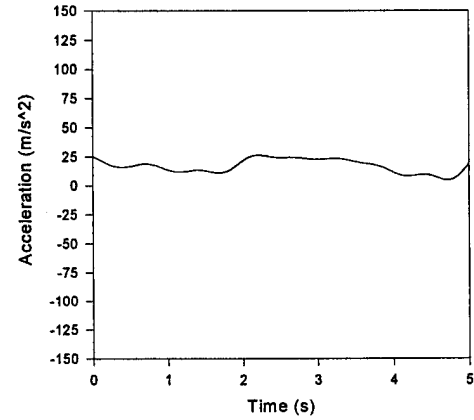
Filtered Y Acceleration, Accelerometer "B"



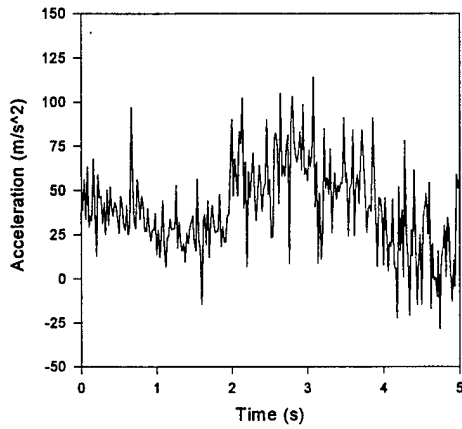
Raw Z Acceleration, Accelerometer "B"



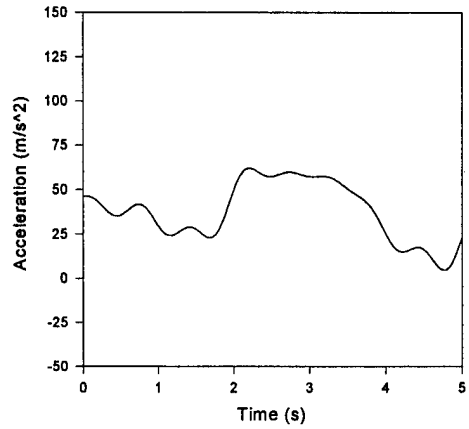
Filtered Z Acceleration, Accelerometer "B"



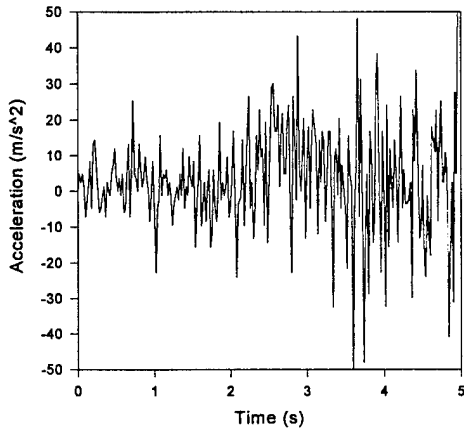
Raw X Acceleration, Accelerometer "C"



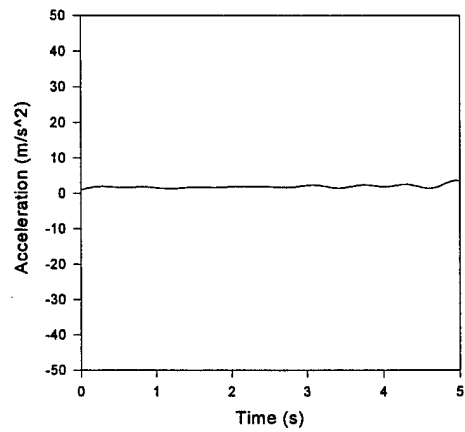
Filtered X Acceleration, Accelerometer "C"



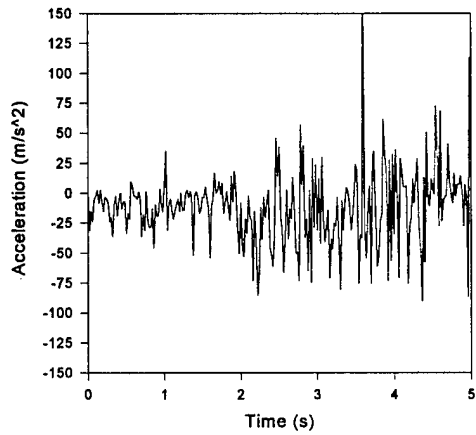
Raw Y Acceleration, Accelerometer "C"



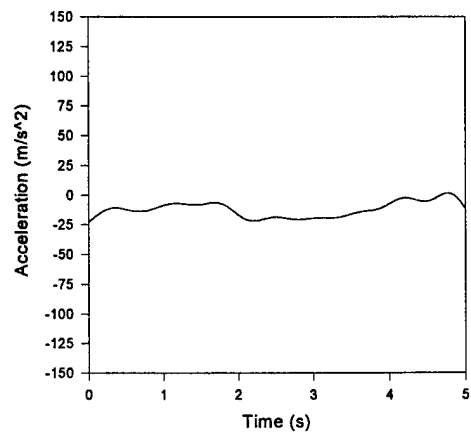
Filtered Y Acceleration, Accelerometer "C"



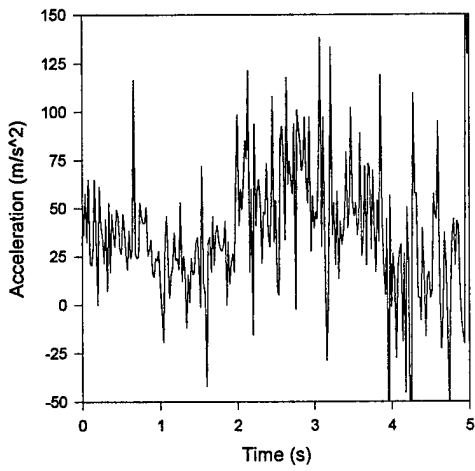
Raw Z Acceleration, Accelerometer "C"



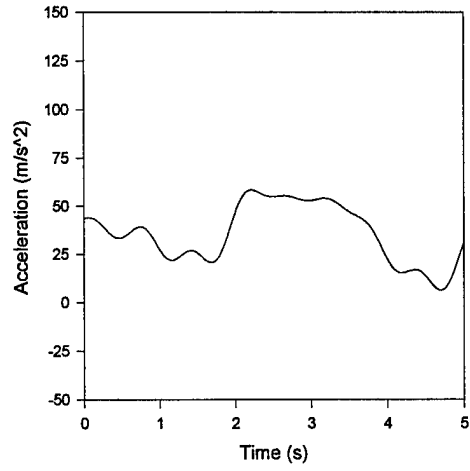
Filtered Z Acceleration, Accelerometer "C"



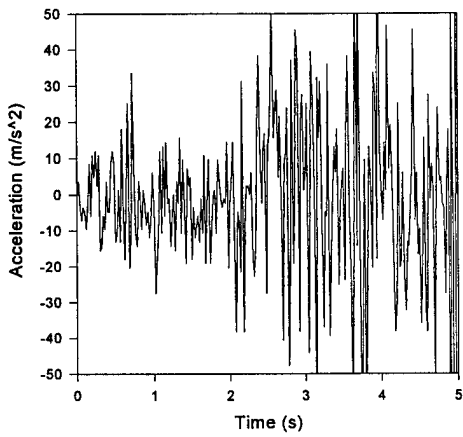
Raw X Acceleration, Accelerometer "D"



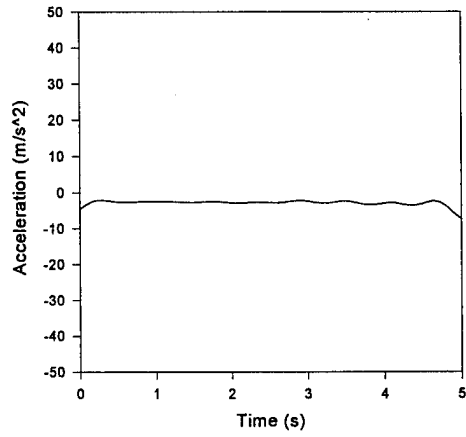
Filtered X Acceleration, Accelerometer "D"



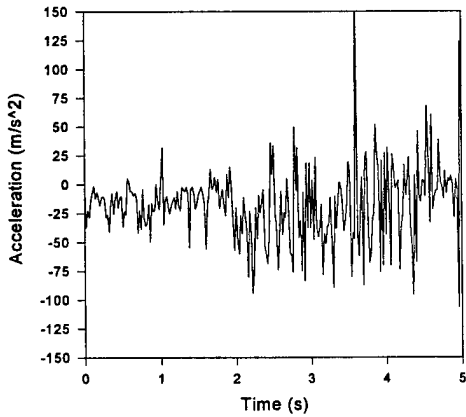
Raw Y Acceleration, Accelerometer "D"



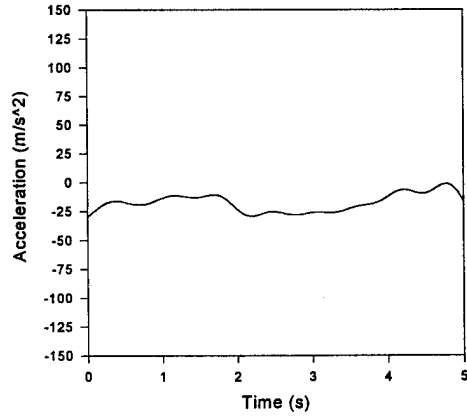
Filtered Y Acceleration, Accelerometer "D"



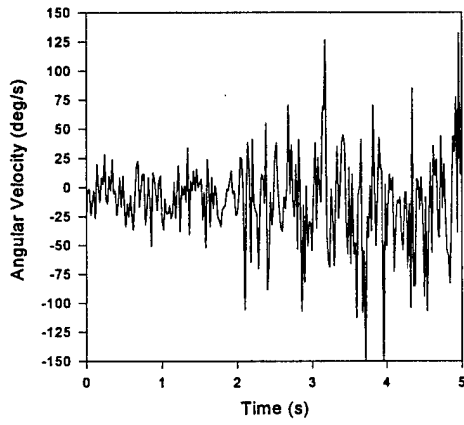
Raw Z Acceleration, Accelerometer "D"



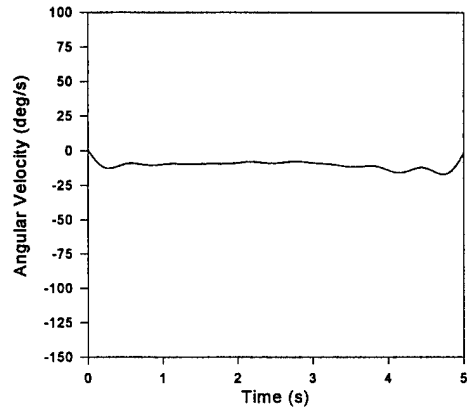
Filtered Z Acceleration, Accelerometer "D"



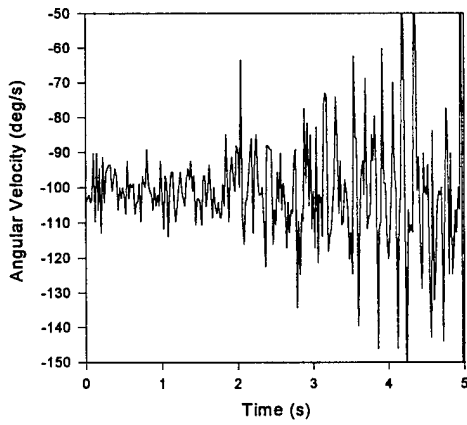
**Raw X Angular Velocity**



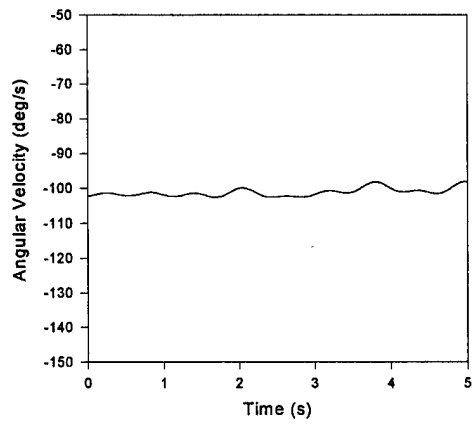
**Filtered X Angular Velocity**



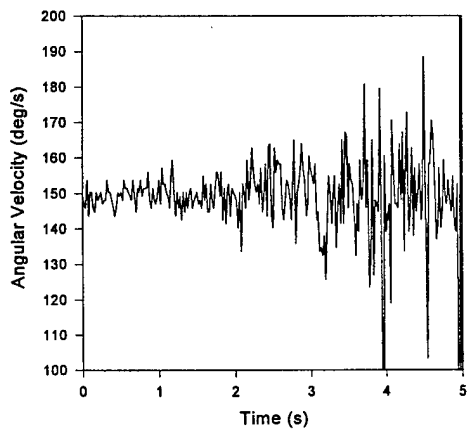
**Raw Y Angular Velocity**



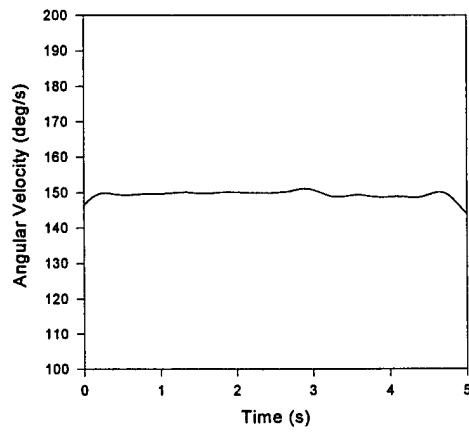
**Filtered Y Angular Velocity**



**Raw Z Angular Velocity**



**Filtered Z Angular Velocity**



## Appendix H: MATHCAD® Code to Filter Ejection Seat Data

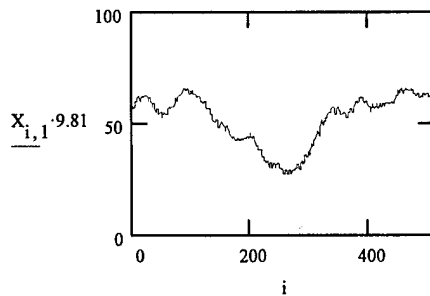
$X := \text{READPRN}(y)$

Read unfiltered data into this file

$i := 0..8192 \quad k := 5000..8192$

Increase number of unfiltered data points so that its size is a power of 2. This is necessary in order to perform a Fast Fourier Transform. In order to accomplish this, the last true unfiltered data point is repeated the number of times required to attain a data set size which is a power of 2.

$X_{k,1} := X_{750,1}$



Original time history

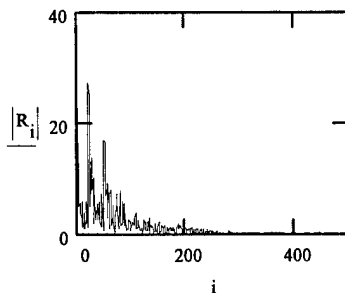
$V := \text{submatrix}(X, 0, 8191, 1, 1)$

Consider all rows in column number 1 of the input data set. The zero column only contains time data points which do not need to be filtered

$R := \text{fft}(V)$

Perform a Fast Fourier Transform on the raw data

$i := 1..4096$

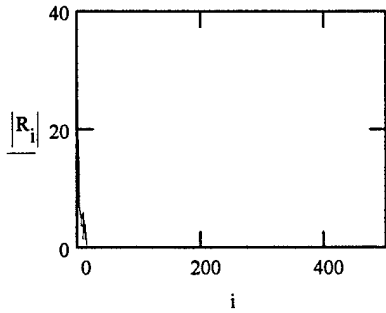


Original frequency spectrum

$k := 15..4096$

Cut off frequencies below 15 Hz by setting them equal to zero

$R_k := 0$



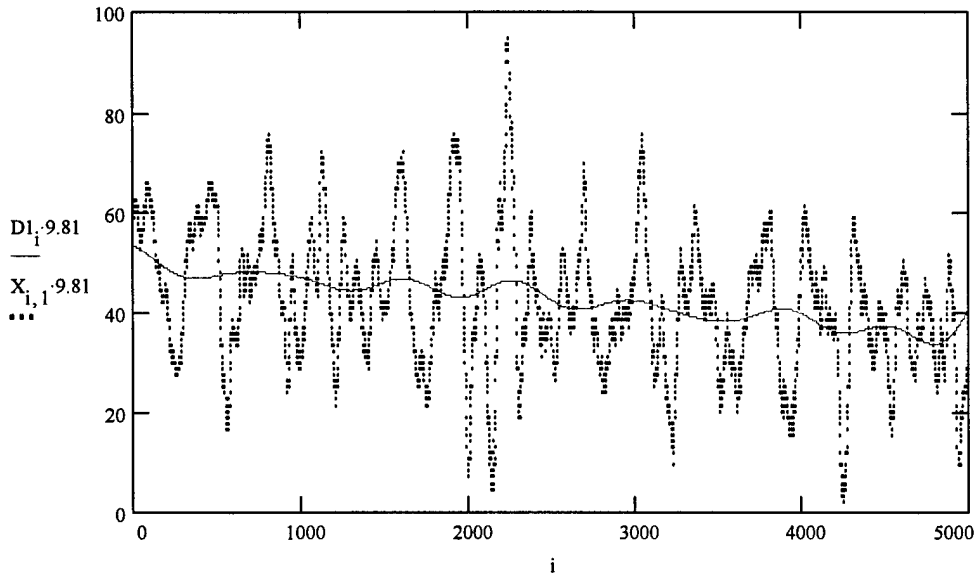
Resulting filtered frequency spectrum

$D1 := \text{ifft}(R)$

Perform an Inverse Fast Fourier Transform on the filtered data to bring it back into the time domain

Filtered time history data overlay on unfiltered time history data

$i := 0..4999$



Calculate mean, standard deviation, and confidence interval and 99% confidence level

$$\text{AVERAGE} := \frac{\sum_{i=0}^{4999} D1_i}{5000} \quad \text{STDV} := \sqrt{\frac{1}{5000} \sum_{i=0}^{4999} (D1_i - \text{AVERAGE})^2} \quad \text{CI} := \frac{2.576 \text{STDV}}{\sqrt{5000}}$$

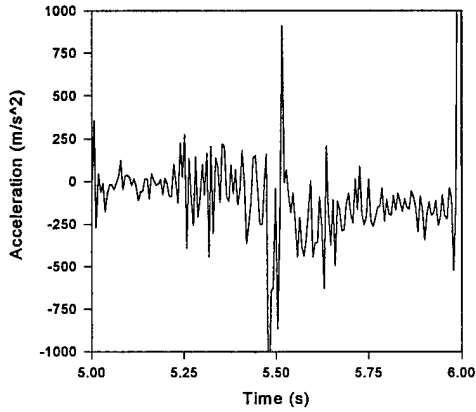
AVERAGE = 4.335

STDV = 0.447

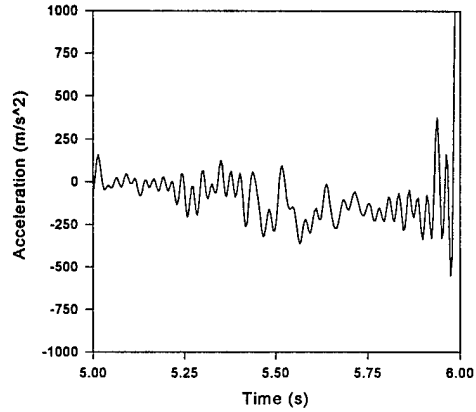
CI = 0.016

Appendix I: Raw and Filtered Linear Acceleration and Angular Velocity Data Between  
Seat-First Motion and Seat-Adam Separation

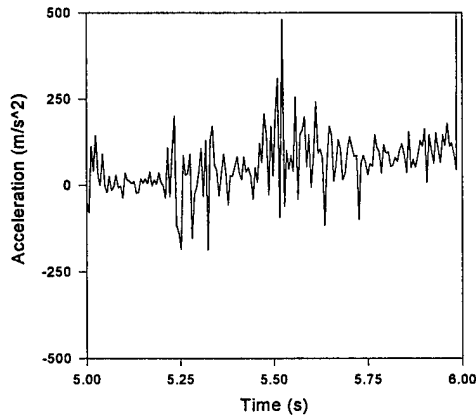
**Raw X Acceleration, Accelerometer "A"**



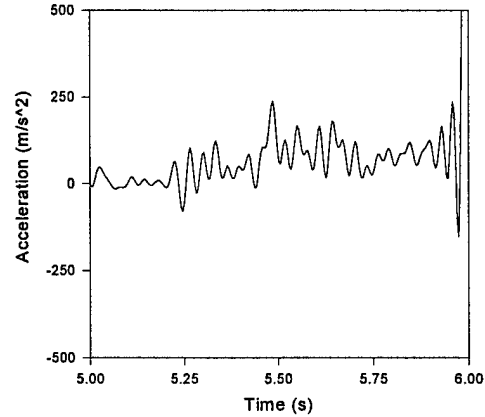
**Filtered X Acceleration, Accelerometer "A"**



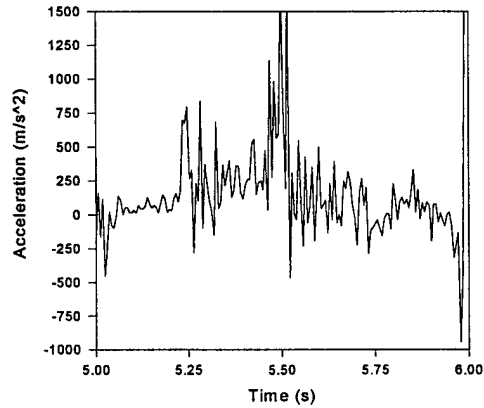
**Raw Y Acceleration, Accelerometer "A"**



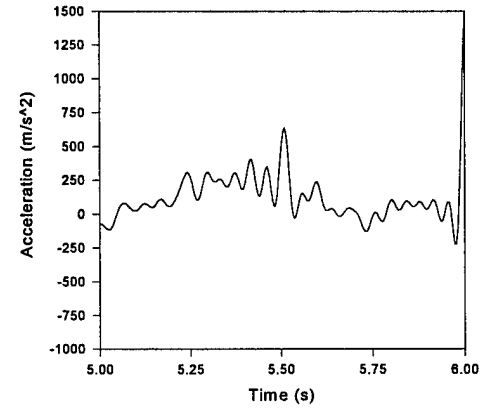
**Filtered Y Acceleration, Accelerometer "A"**



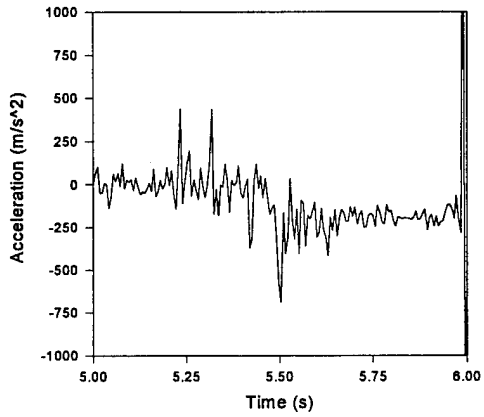
**Raw Z Acceleration, Accelerometer "A"**



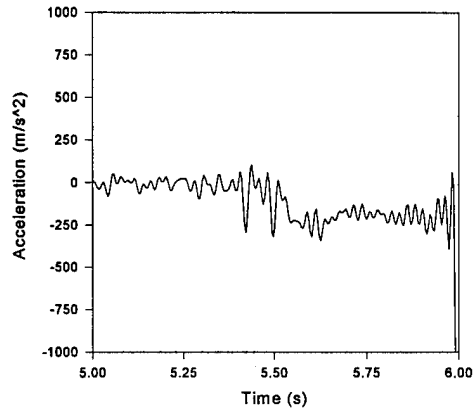
**Filtered Z Acceleration, Accelerometer "A"**



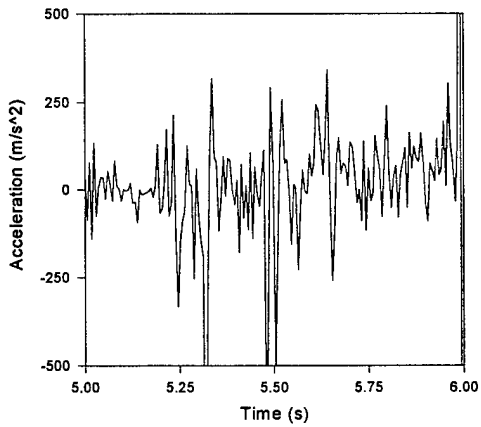
Raw X Acceleration, Accelerometer "B"



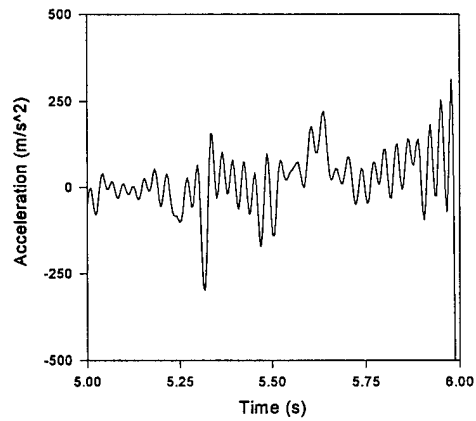
Filtered X Acceleration, Accelerometer "B"



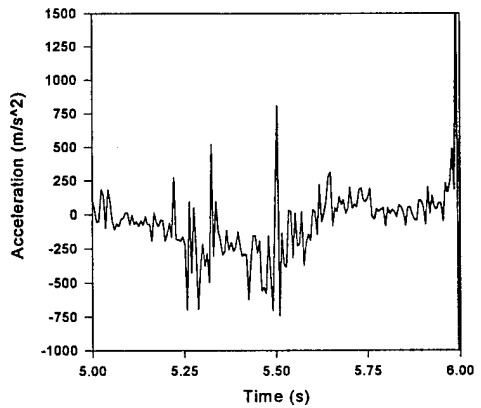
Raw Y Acceleration, Accelerometer "B"



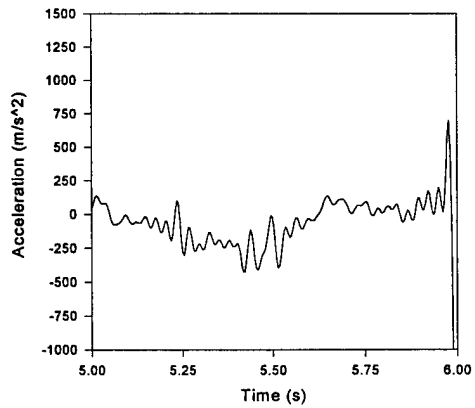
Filtered Y Acceleration, Accelerometer "B"



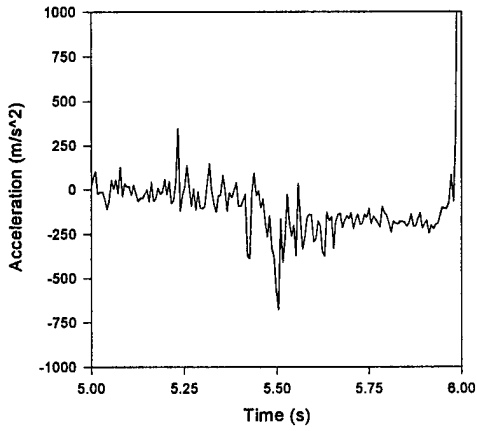
Raw Z Acceleration, Accelerometer "B"



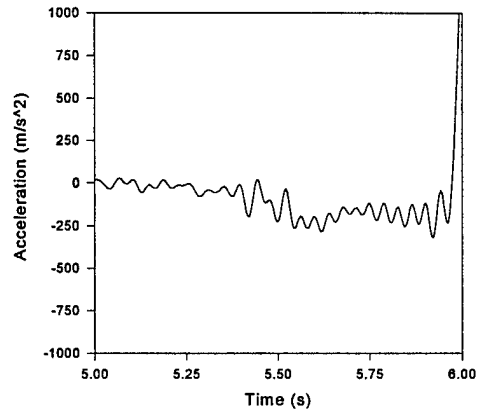
Filtered Z Acceleration, Accelerometer "B"



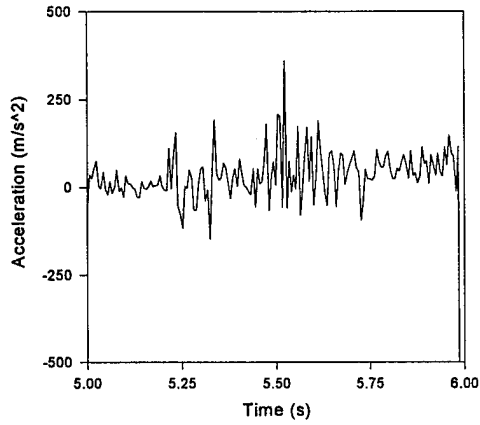
Raw X Acceleration, Accelerometer "C"



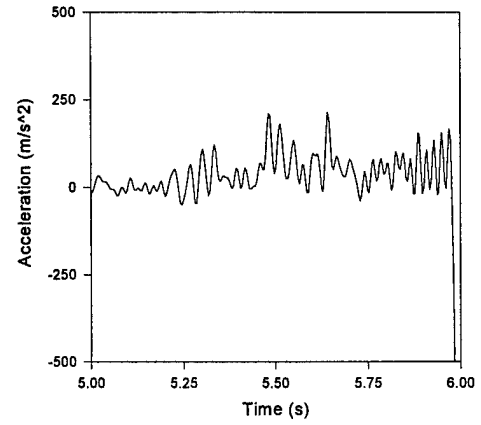
Filtered X Acceleration, Accelerometer "C"



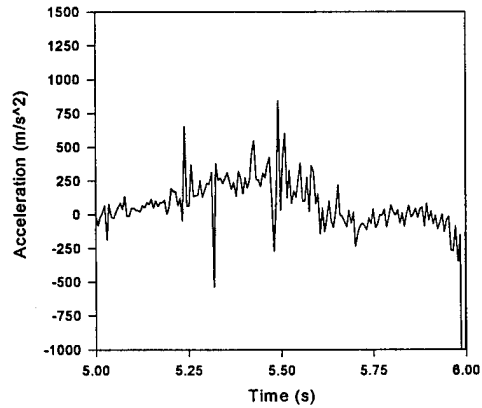
Raw Y Acceleration, Accelerometer "C"



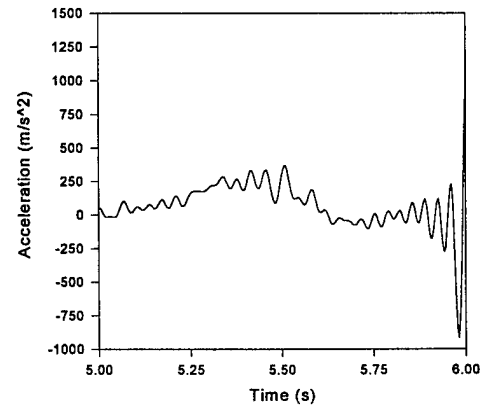
Filtered Y Acceleration, Accelerometer "C"



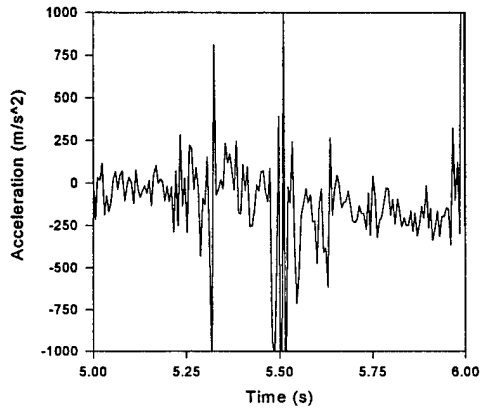
Raw Z Acceleration, Accelerometer "C"



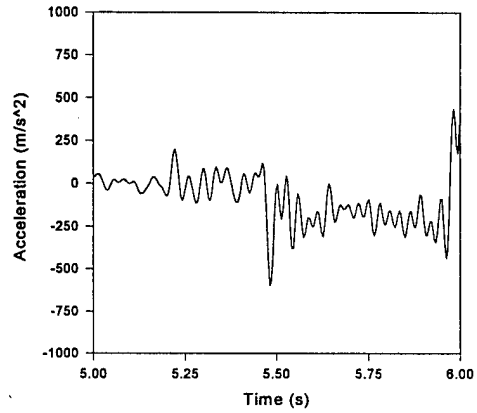
Filtered Z Acceleration, Accelerometer "C"



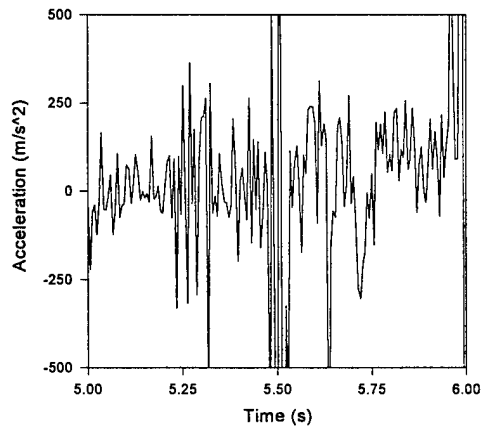
Raw X Acceleration, Accelerometer "D"



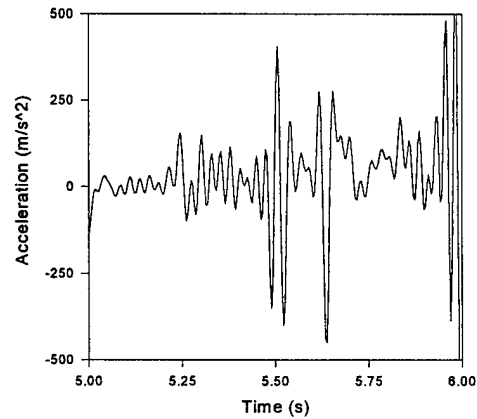
Filtered X Acceleration, Accelerometer "D"



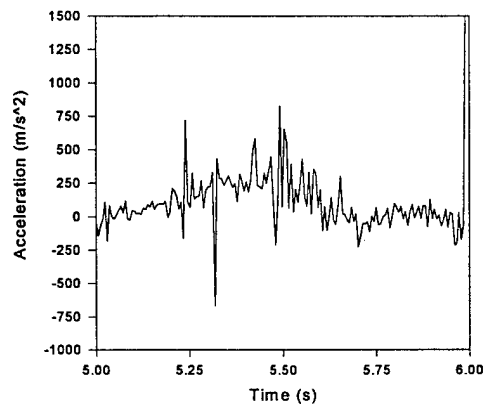
Raw Y Acceleration, Accelerometer "D"



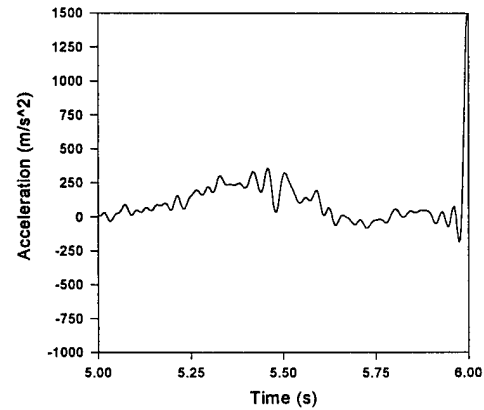
Filtered Y Acceleration, Accelerometer "D"



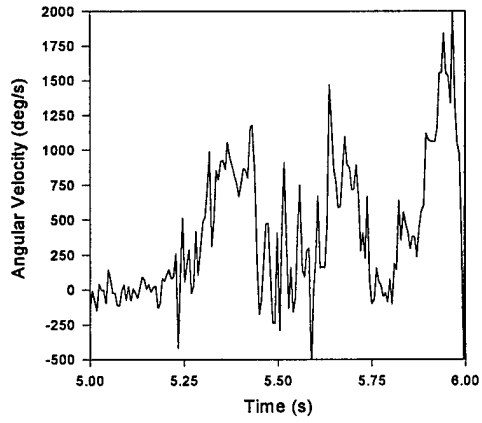
Raw Z Acceleration, Accelerometer "D"



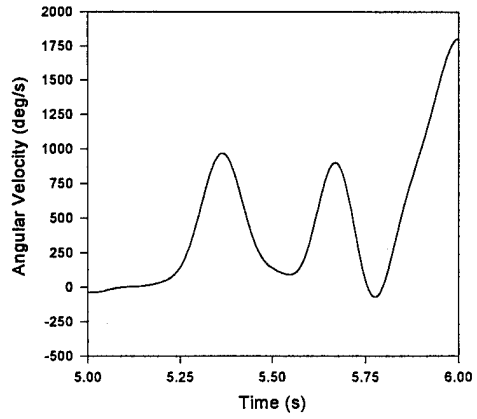
Filtered Z Acceleration, Accelerometer "D"



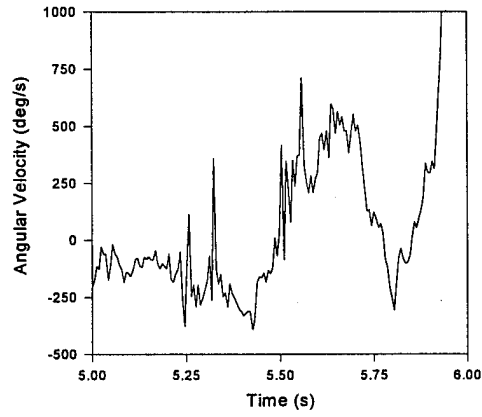
**Raw X Angular Velocity**



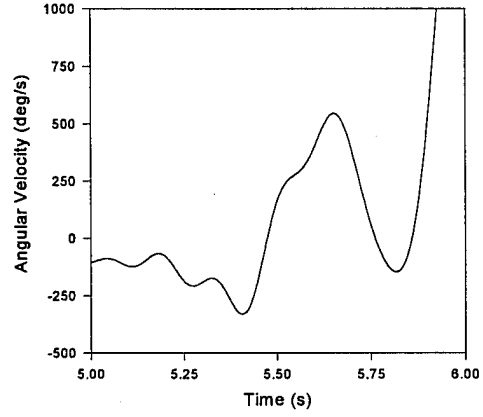
**Filtered X Angular Velocity**



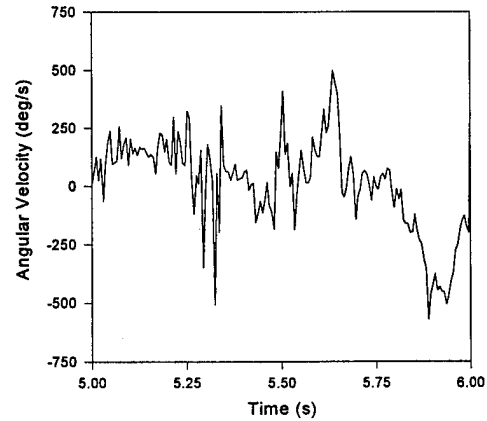
**Raw Y Angular Velocity**



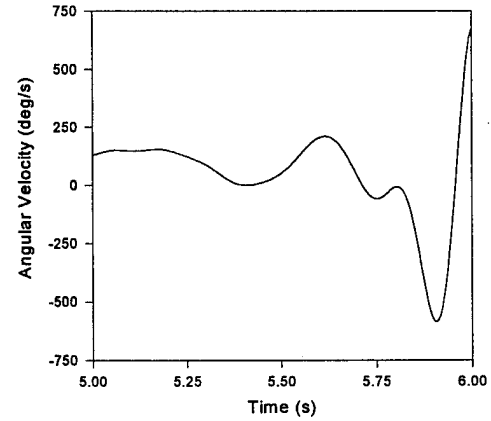
**Filtered Y Angular Velocity**



**Raw Z Angular Velocity**



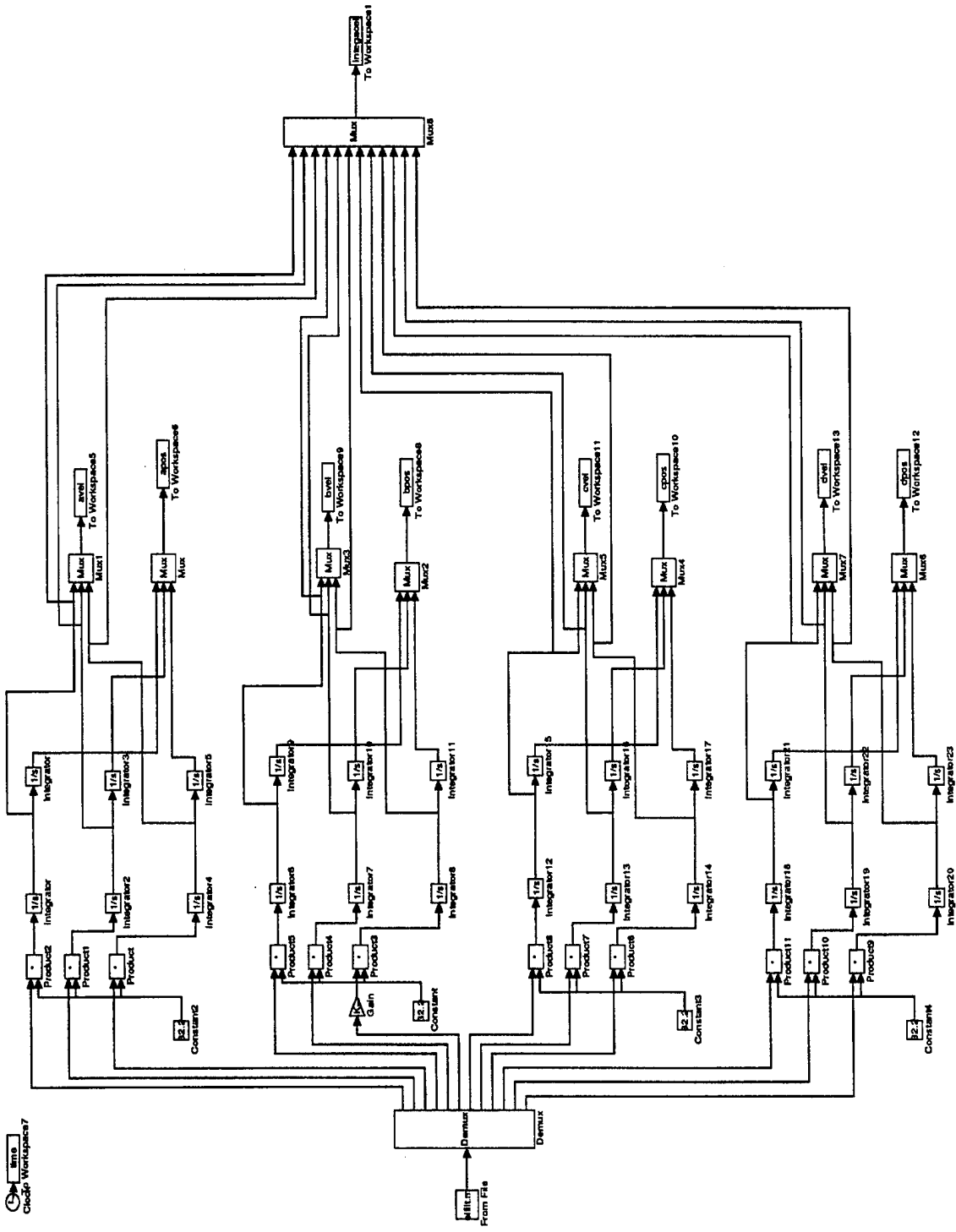
**Filtered Z Angular Velocity**



Appendix J: AMIT 79E-G2A Cut-off Frequencies

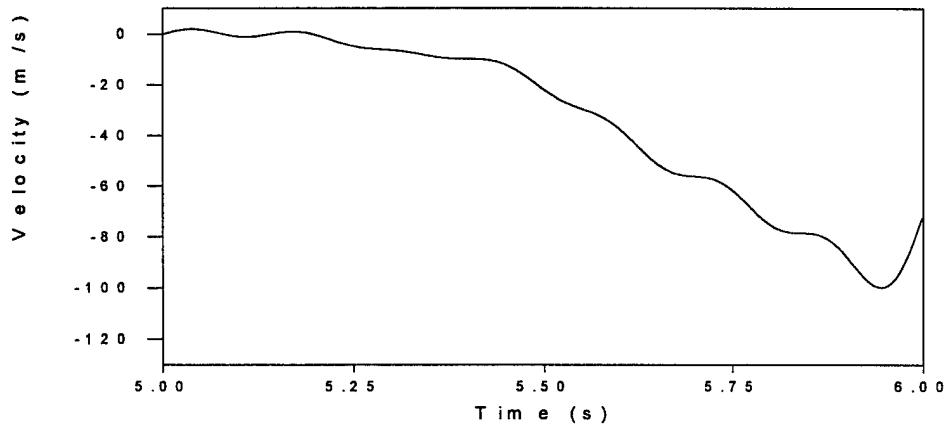
Signal	Cut-off Frequency (Hz)
X Acceleration, Accelerometer "A"	80
Y Acceleration, Accelerometer "A"	70
Z Acceleration, Accelerometer "A"	50
X Acceleration, Accelerometer "B"	100
Y Acceleration, Accelerometer "B"	70
Z Acceleration, Accelerometer "B"	75
X Acceleration, Accelerometer "C"	55
Y Acceleration, Accelerometer "C"	100
Z Acceleration, Accelerometer "C"	60
X Acceleration, Accelerometer "D"	75
Y Acceleration, Accelerometer "D"	85
Z Acceleration, Accelerometer "D"	75
X Angular Velocity	15
Y Angular Velocity	15
Z Angular Velocity	15

# Appendix K: SIMULINK™ Block Diagram Used to Integrate Linear Acceleration Data

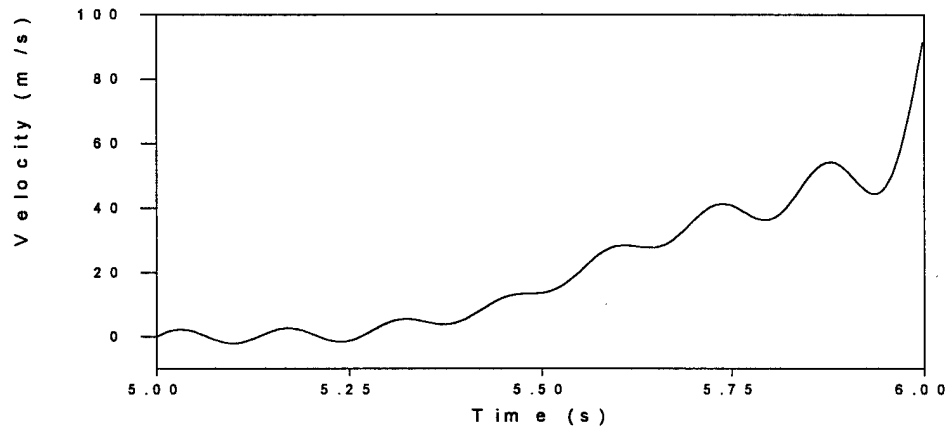


## Appendix L: Integrated Linear Accelerations

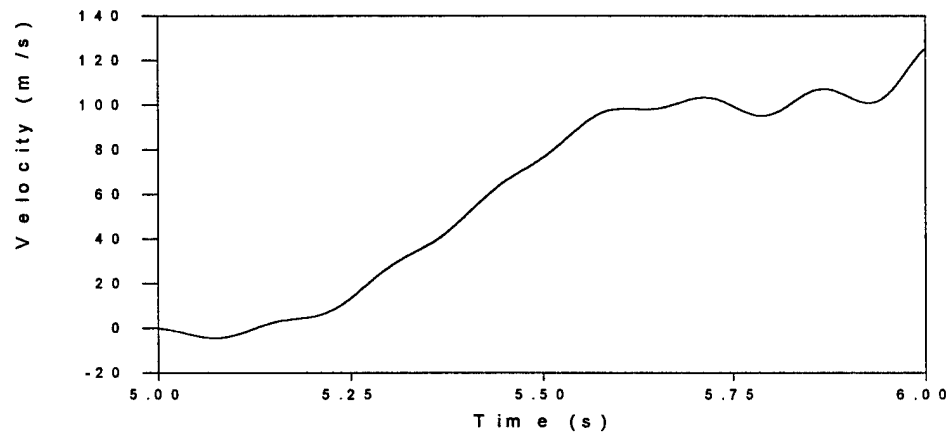
**X Linear Velocity, Accelerometer "A"**



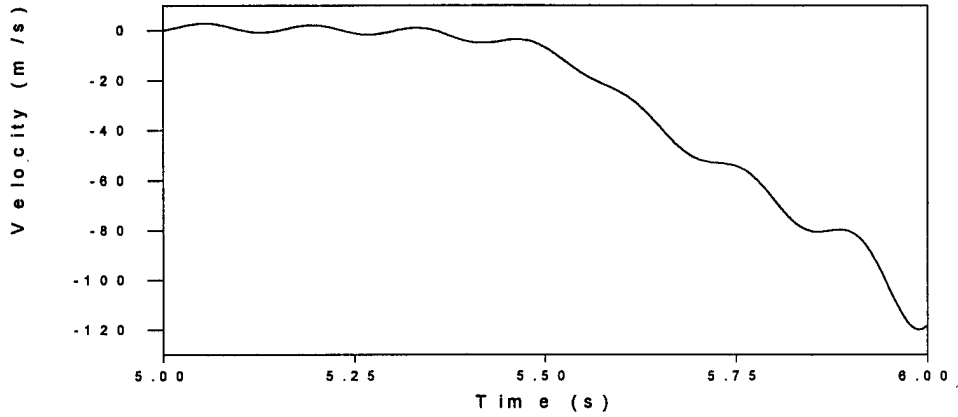
**Y Linear Velocity, Accelerometer "A"**



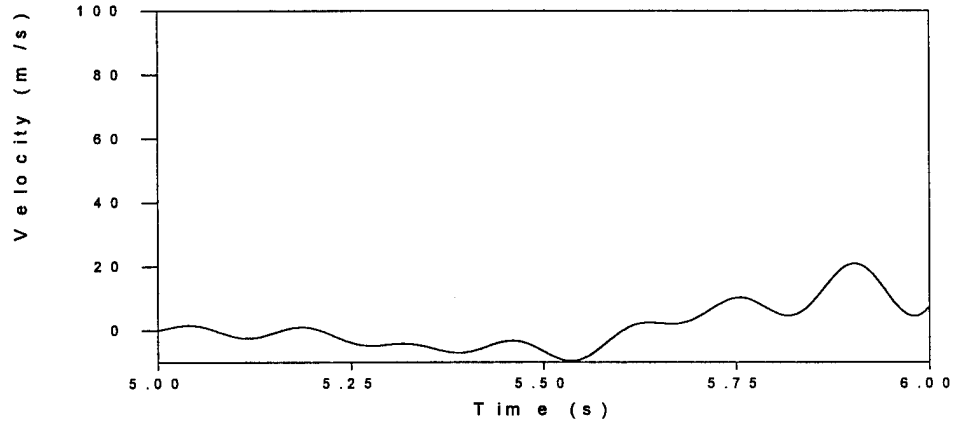
**Z Linear Velocity, Accelerometer "A"**



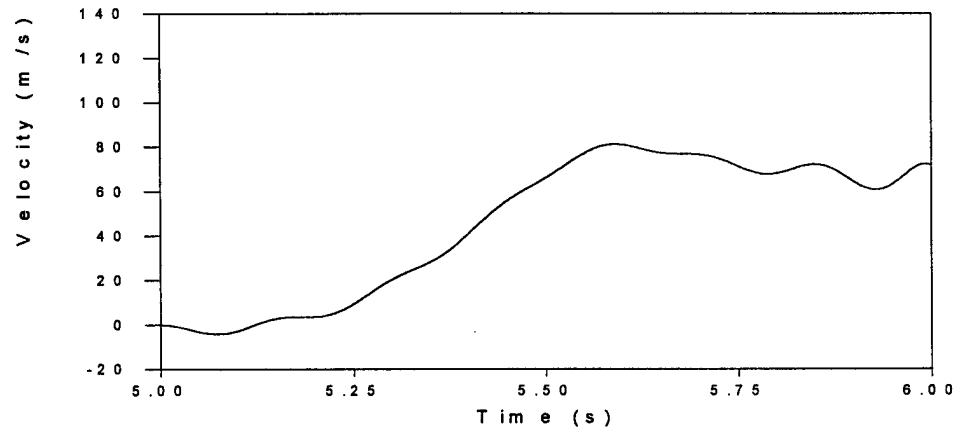
X Linear Velocity, Accelerometer "B"



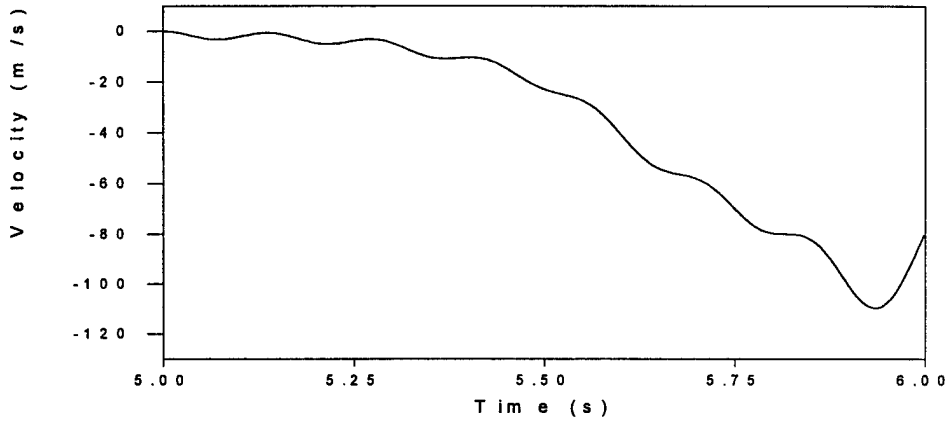
Y Linear Velocity, Accelerometer "B"



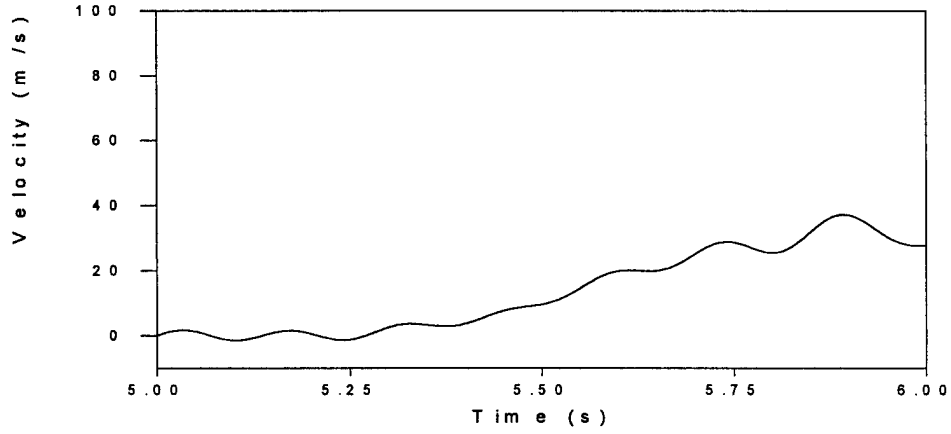
Z Linear Velocity, Accelerometer "B"



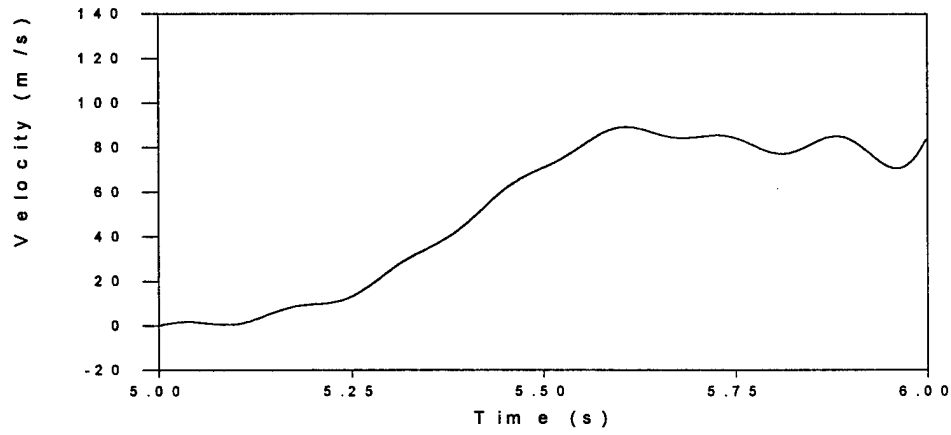
X Linear Velocity, Accelerometer "C"



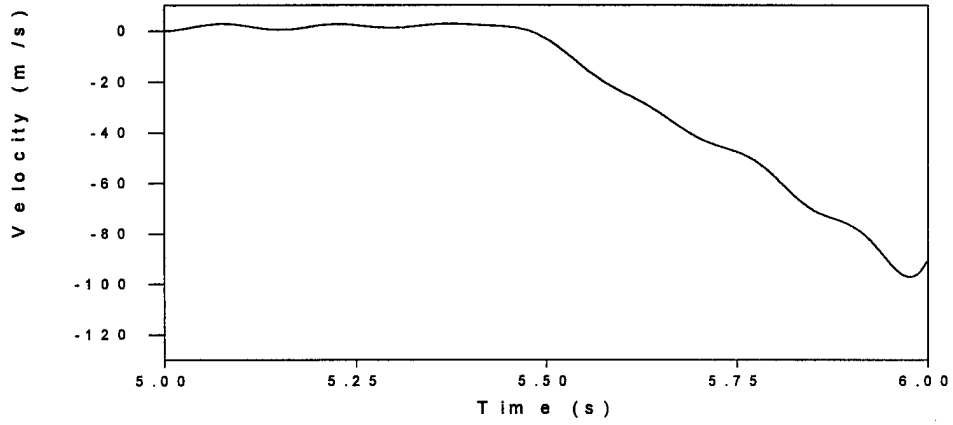
Y Linear Velocity, Accelerometer "C"



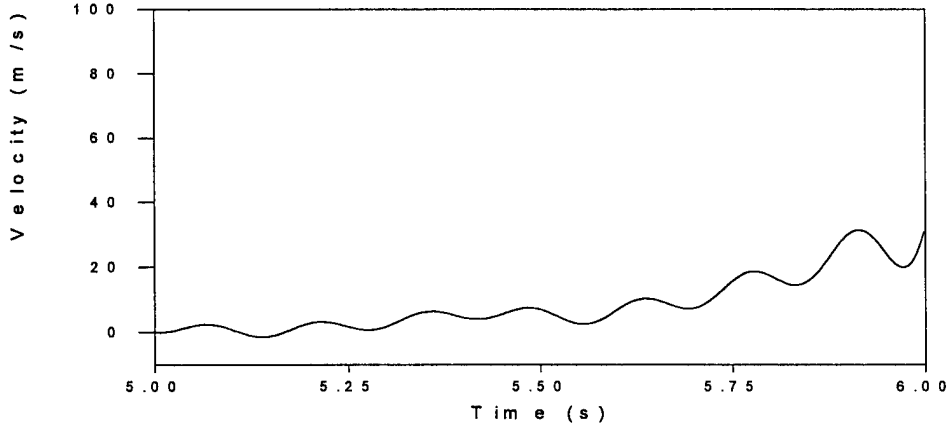
Z Linear Velocity, Accelerometer "C"



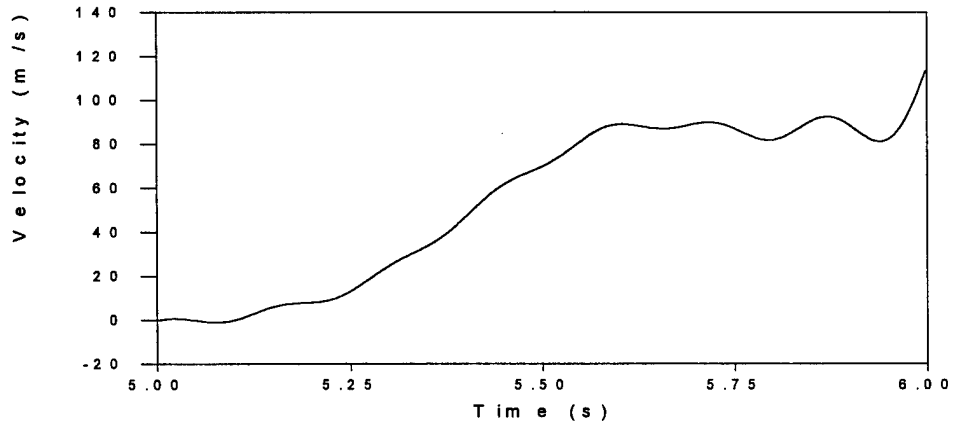
X Linear Velocity, Accelerometer "D"



Y Linear Velocity, Accelerometer "D"



Z Linear Velocity, Accelerometer "D"



Appendix M: MATLAB® Code to Transform Ejection Seat Linear Velocities From the Location of the Accelerometers to the Seat Reference Point

```
%Define biases for X,Y,Z directions of angular velocities in
%RAD/SEC
ANGbias=[-.1745 -1.77 2.61];

%Runs simulink file acel2vel to convert linear accelerations
%to linear velocities (by integration)
[t,x,y]=linsim('acel2vel',[0 .998],[],[.002,.002,.001]);

load ch61filt.prn;
load ch62filt.prn;
load ch63filt.prn;

ww=[ch61filt,ch62filt,ch63filt];

%Subtract off bias
sizeang=size(ch61filt);
for biasang=1:sizeang(1)
    w(biasang,:)=ww(biasang,:)-ANGbias;
end

%Zero out angular velocity data from time=0 to time=.14 sec when
%the ACESII seat leaves the rails. This is at index 71

zerolevel=71;

for i=1:zerolevel
    w(i,1)=0;
end
for j=1:zerolevel
    w(j,2)=0;
end
for k=1:zerolevel
    w(k,3)=0;
end

%%A ACCELEROMETER
%Read in linear velocity matrix in ft/sec
alinvel=avel;

%Define displacement between linear accelerometers and seat
```

```

%reference point (SRP) in ft.
xdis=1.092;
ydis=.1833;
zdis=-.1833;

%Define rho vector
rho=[xdis,ydis,zdis];

%Calculate linear velocity of Seat Reference Point (SRP)
sizew=size(w);

for i=1:sizew(1)
    term1(i,:)=cross(w(i,:),rho);
end

%Add term1 to linear velocity to get acceleration at SRP
avsrp=alinvel+term1;

%%B ACCELEROMETER
%Read in linear velocity matrix in ft/sec
blinvel=[bvel(:,1),bvel(:,2),bvel(:,3)];

%Define displacement between linear accelerometers and seat
%reference point (SRP) in ft.
xdis=1.425;
ydis=.51666;
zdis=-.2083;

%Define rho vector
rho=[xdis,ydis,zdis];

%Calculate linear velocity of Seat Reference Point (SRP)
sizew=size(w);

for i=1:sizew(1)
    term2(i,:)=cross(w(i,:),rho);
end

%Add term2 to linear velocity to get acceleration at SRP
bvsrp=blinvel+term2;

%%C ACCELEROMETER
%Read in linear velocity matrix in ft/sec
clinvel=cvel;

```

```

%Define displacement between linear accelerometers and seat
%reference point (SRP) in ft.
xdis=1.083;
ydis=.51667;
zdis=-.191667;

%Define rho vector
rho=[xdis,ydis,zdis];

%Calculate linear velocity of Seat Reference Point (SRP)
sizew=size(w);

for i=1:sizew(1)
    term3(i,:)=cross(w(i,:),rho);
end

%Add term3 to linear velocity to get acceleration at SRP
cvsrp=clinvel+term3;

%%D ACCELEROMETER
%Read in linear velocity matrix in ft/sec
dlinvel=dvel;

%Define displacement between linear accelerometers and seat
%reference point (SRP) in ft.
xdis=1.058;
ydis=.5083;
zdis=-.525;

%Define rho vector
rho=[xdis,ydis,zdis];

%Calculate linear velocity of Seat Reference Point (SRP)
sizew=size(w);

for i=1:sizew(1)
    term4(i,:)=cross(w(i,:),rho);
end

%Add term4 to linear velocity to get acceleration at SRP
dvsrp=dlinvel+term4;

%%Average the 4 linear accelerations at SRP {which are in FT/SEC}
srplinvel=[avsrp+bvsrp+cvsrp+dvsrp]/4;

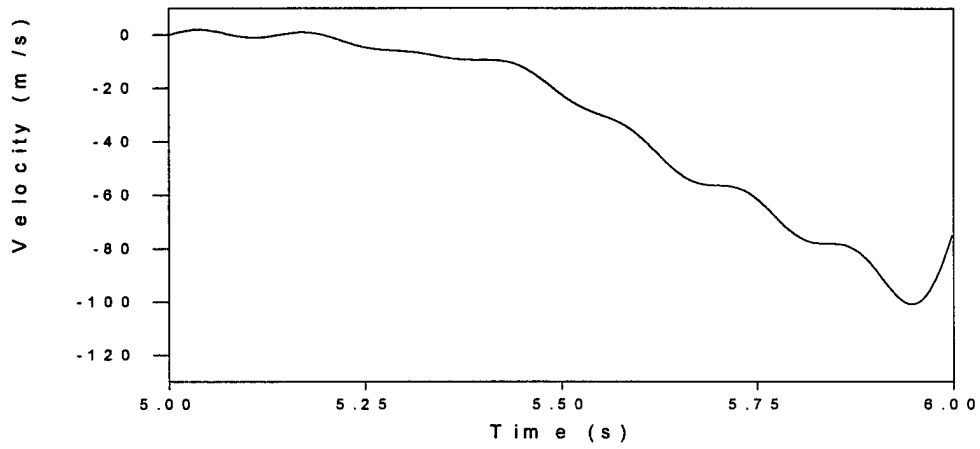
```

```
%Set y linear velocity=0 for the first .14 sec as the seat moves  
%up the rails  
for j=1:zerolevel  
    srplinel(j,2)=0;  
end
```

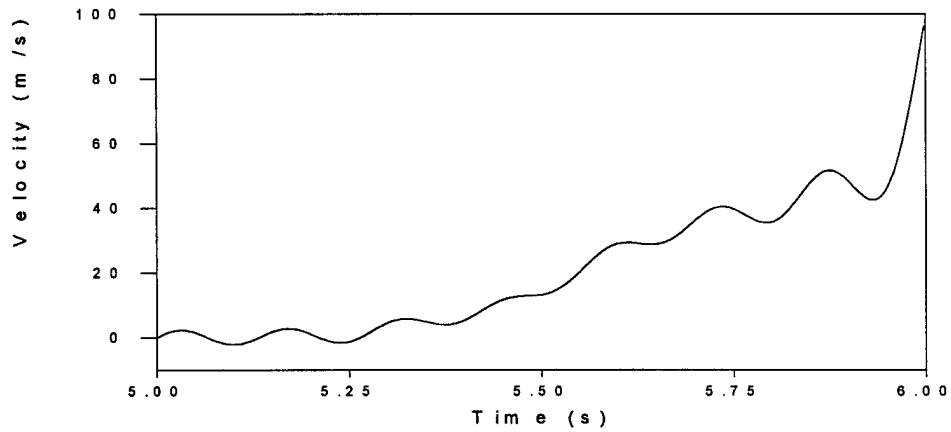
```
%%Define angular accleration at SRP {which are in RAD/SEC}  
srpangvel=w;
```

Appendix N: Linear Velocities at Seat Reference Point

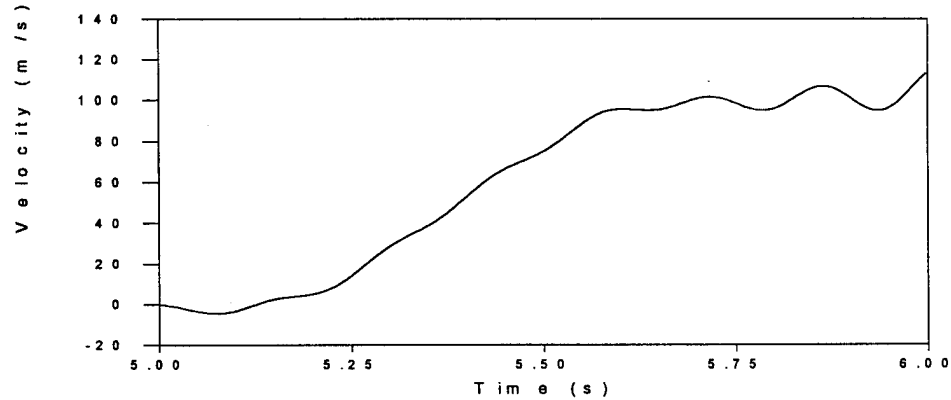
**X Linear Velocity, Accelerometer "A"**



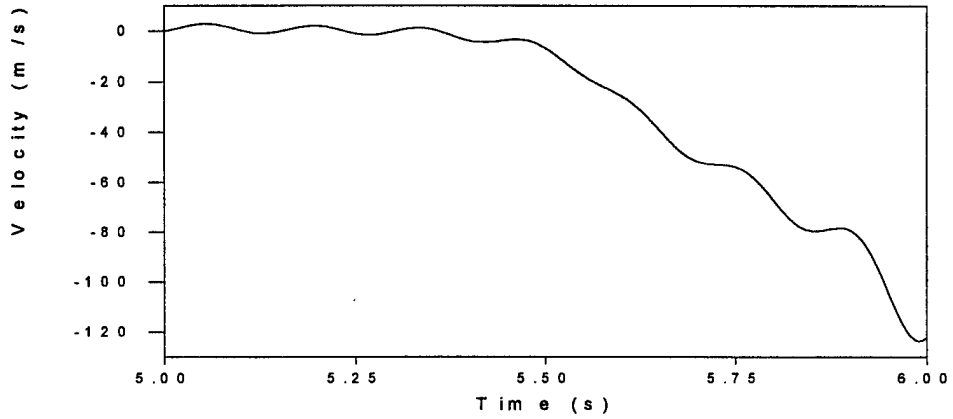
**Y Linear Velocity, Accelerometer "A"**



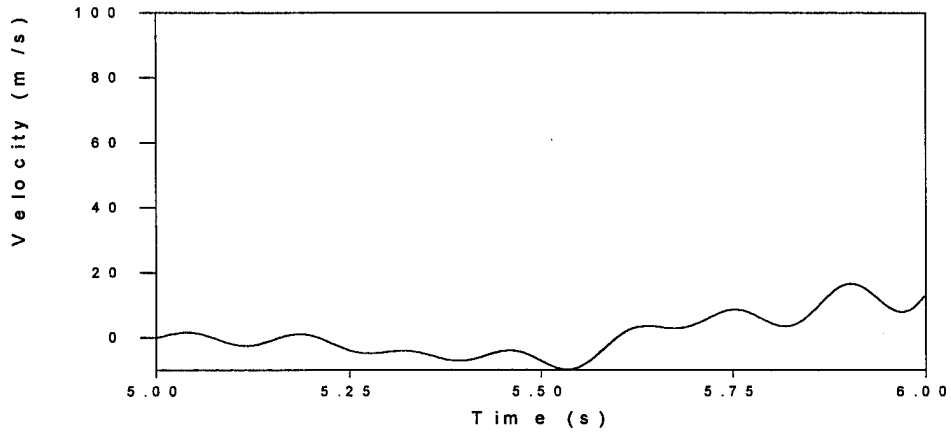
**Z Linear Velocity, Accelerometer "A"**



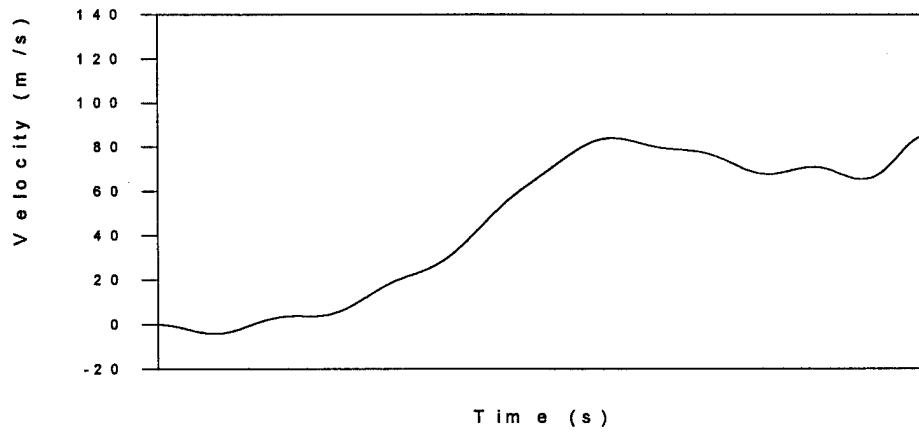
X Linear Velocity, Accelerometer "B"



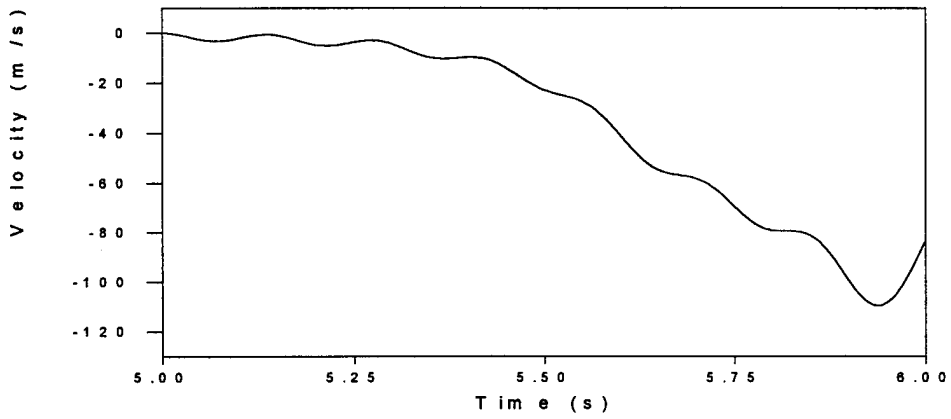
Y Linear Velocity, Accelerometer "B"



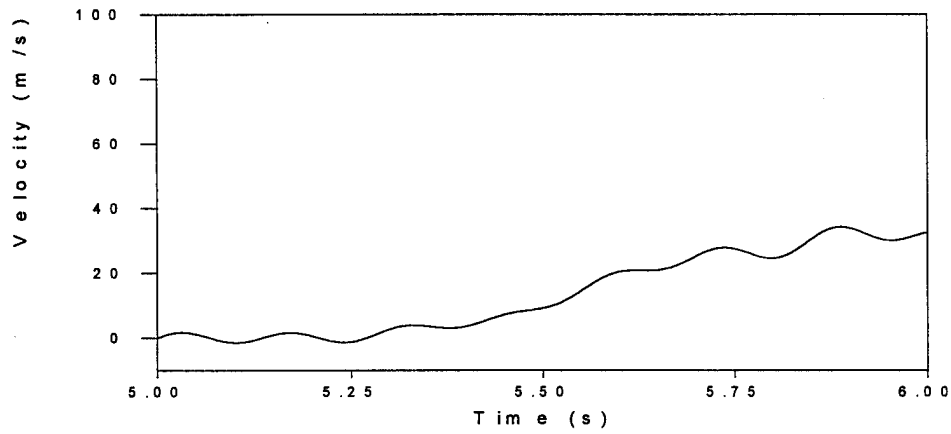
Z Linear Velocity, Accelerometer "B"



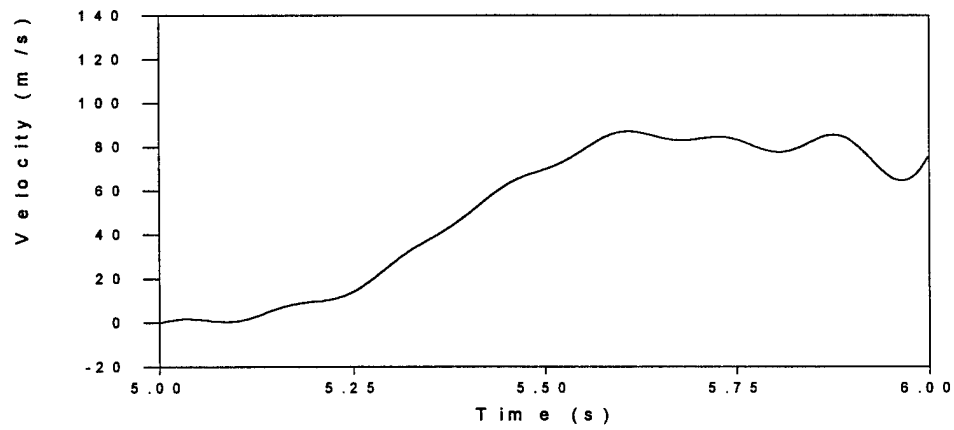
X Linear Velocity, Accelerometer "C"



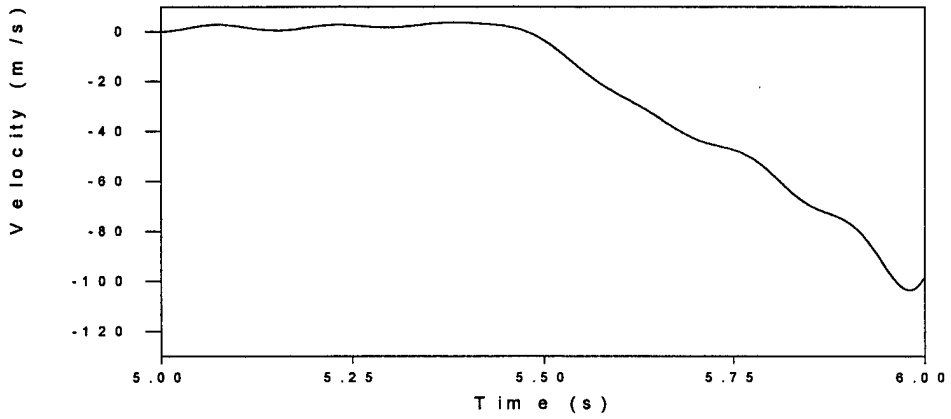
Y Linear Velocity, Accelerometer "C"



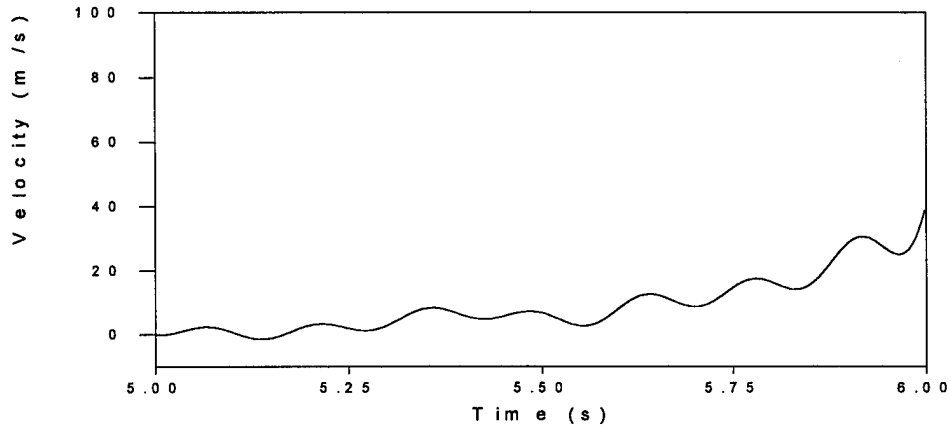
Z Linear Velocity, Accelerometer "C"



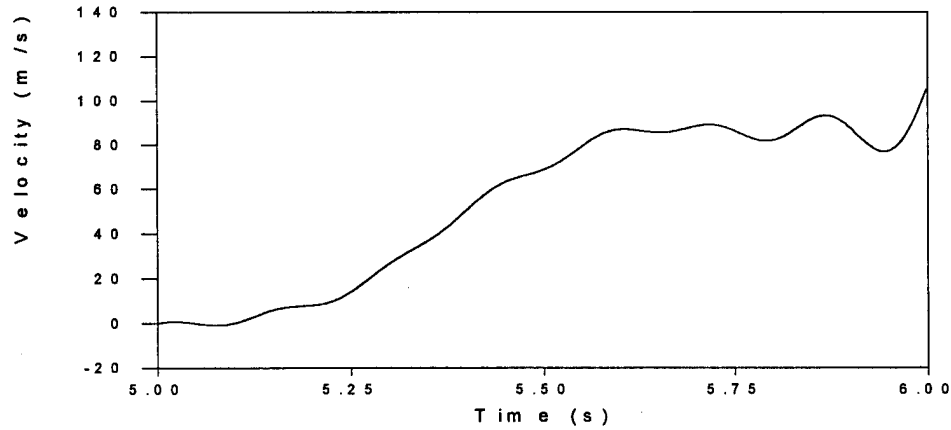
X Linear Velocity, Accelerometer "D"



Y Linear Velocity, Accelerometer "D"

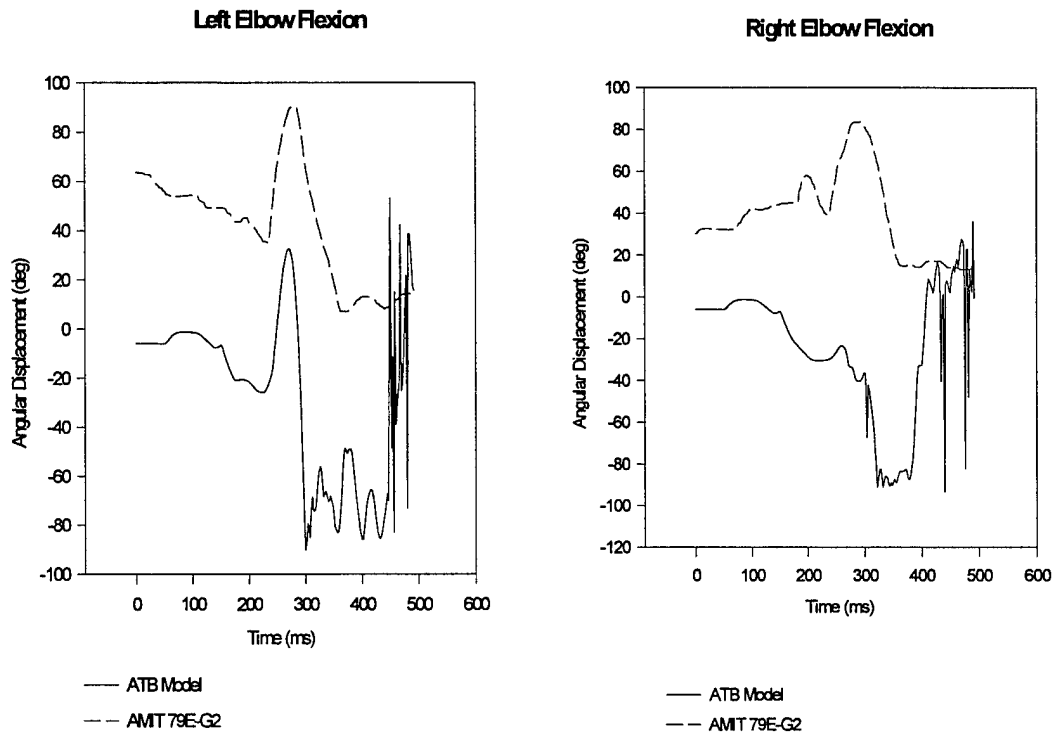


Z Linear Velocity, Accelerometer "D"

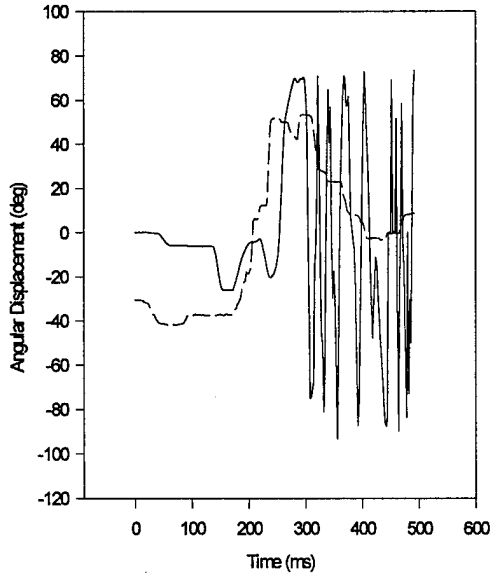


Appendix O: ADAM Joint Angular Displacement Comparisons For the First ATB Simulation of AMIT 79E-G2A (Raw Data)

The following plots are comparisons between the actual motion of the ADAM during the AMIT 79E-G2A test and the motion of the ADAM modeled by the ATB simulation of the AMIT 79E-G2A test. The data presented here are termed *raw* data due to the fact that neither the AMIT 79E-G2A data nor the ATB data have been modified. This is in contrast to similar plots presented in Appendix Q which compare the motion of the ADAM for run number 1 after the data have been shifted and where necessary, reverse polarized.

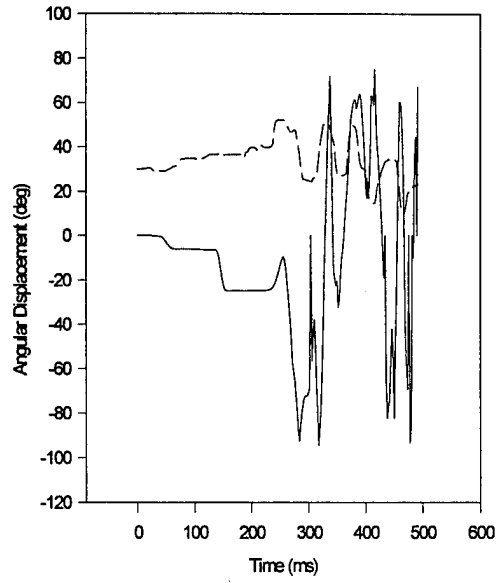


Left Elbow Supination/Pronation



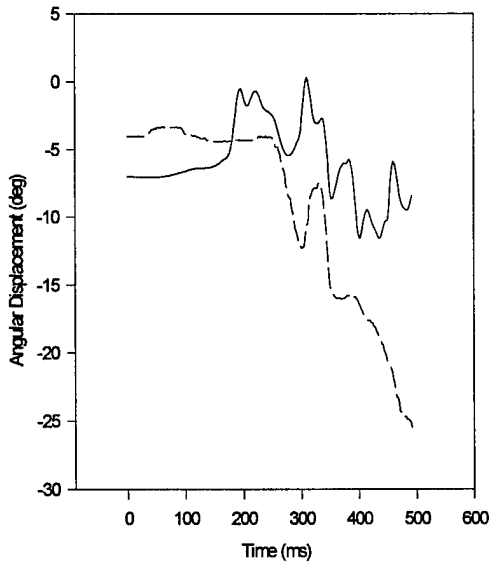
— ATB Model  
-- AMIT 79E-G2

Right Elbow Supination/Pronation



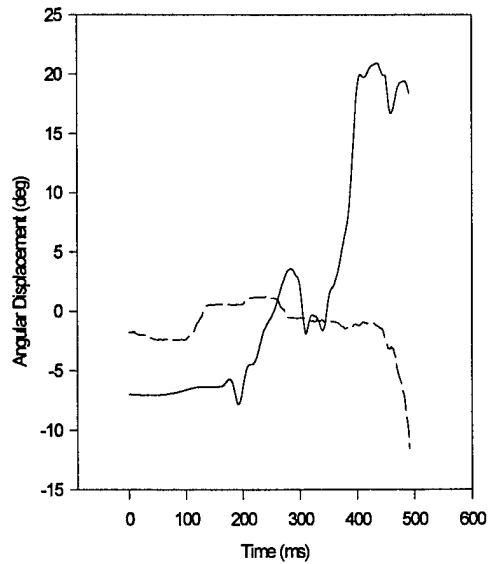
— ATB Model  
-- AMIT 79E-G2

Left Hip Abduction/Adduction



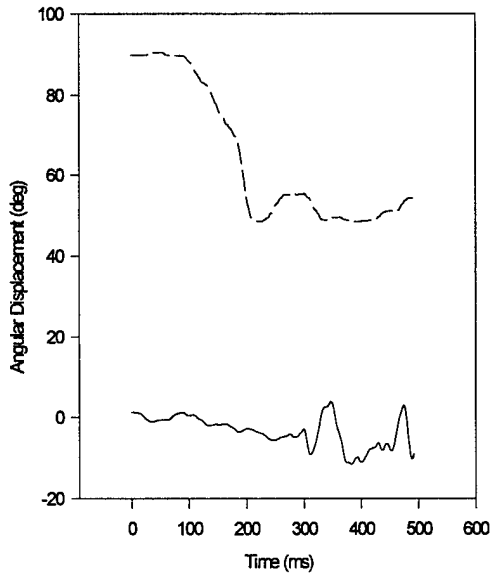
— ATB Model  
-- AMIT 79E-G2

Right Hip Abduction/Adduction



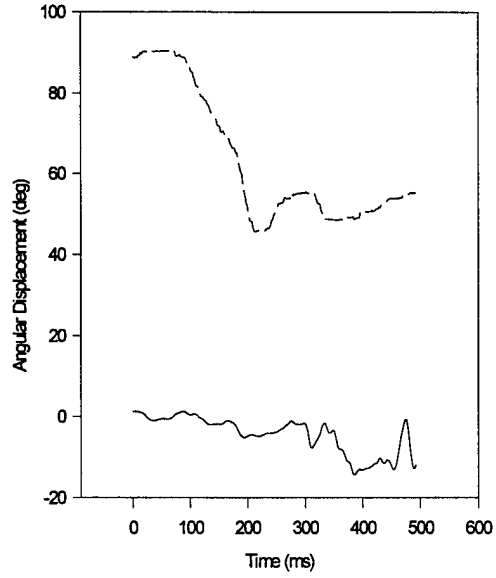
— ATB Model  
-- AMIT 79E-G2

**Left Hip Flexion**



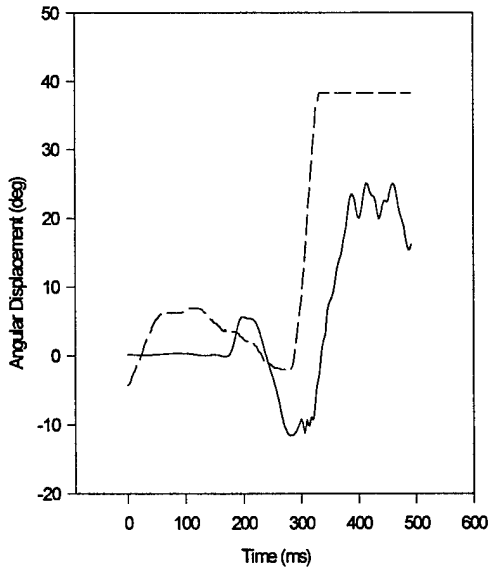
ATB Model  
AMIT 79E-G2

**Right Hip Flexion**



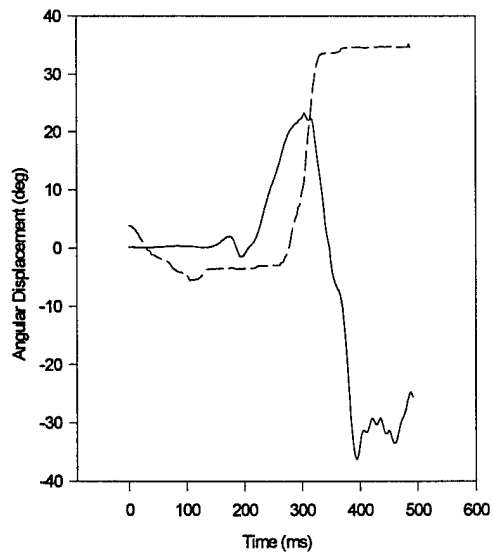
— ATB Model  
- - AMIT 79E-G2

**Left Hip Medial/Lateral**



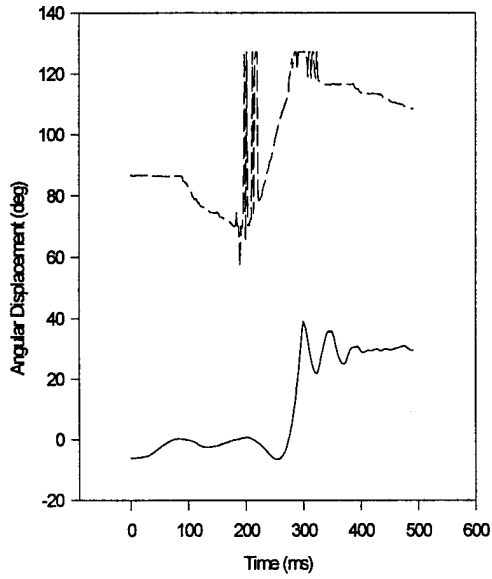
ATB Model  
AMIT 79E-G2

**Right Hip Medial/Lateral**



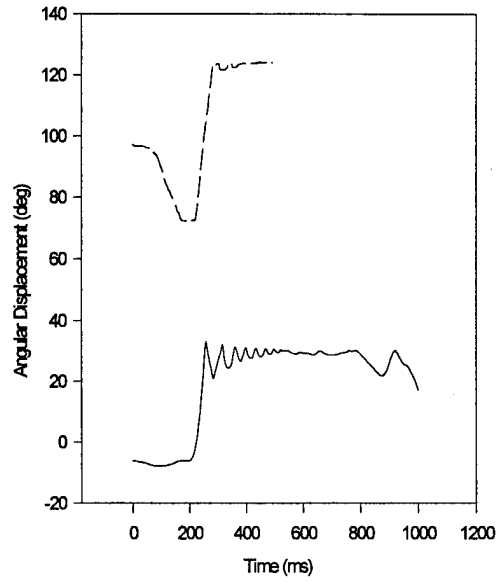
— ATB Model  
- - AMIT 79E-G2

**Left Knee Flexion**



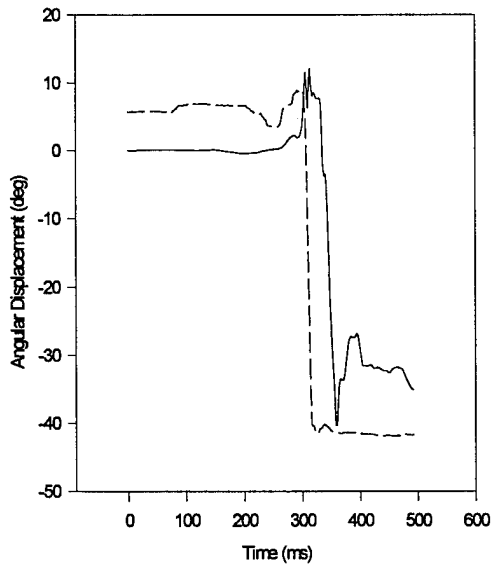
— ATB Model  
-- AMIT 79E-G2

**Right Knee Flexion**



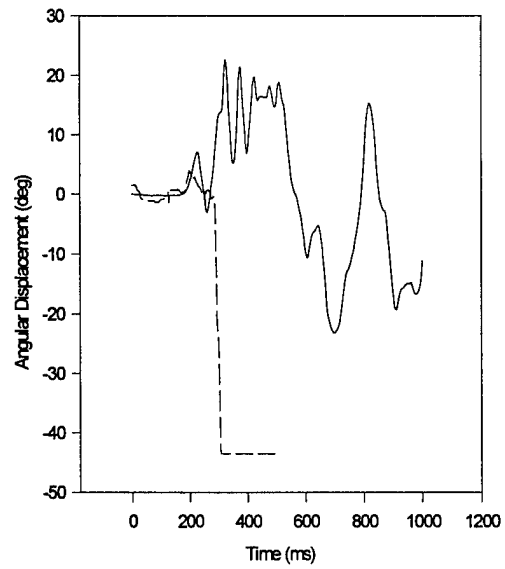
— ATB Model  
-- AMIT 79E-G2

**Left Knee Medial/Lateral**



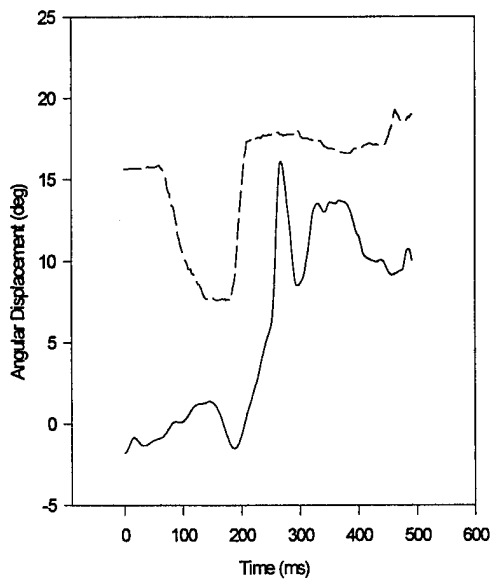
— ATB Model  
-- AMIT 79E-G2

**Right Knee Medial/Lateral**



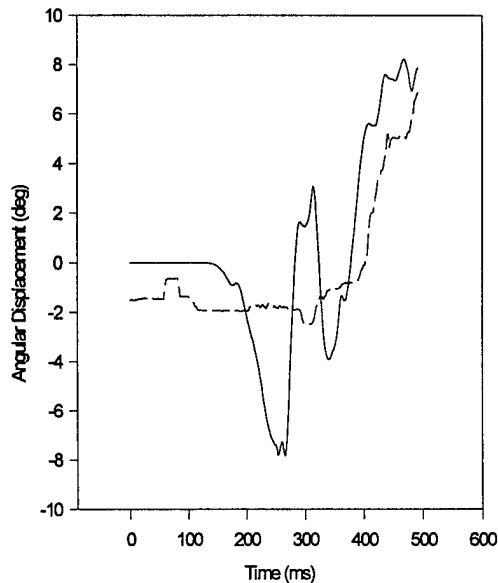
— ATB Model  
-- AMIT 79E-G2

Lumbar Pitch



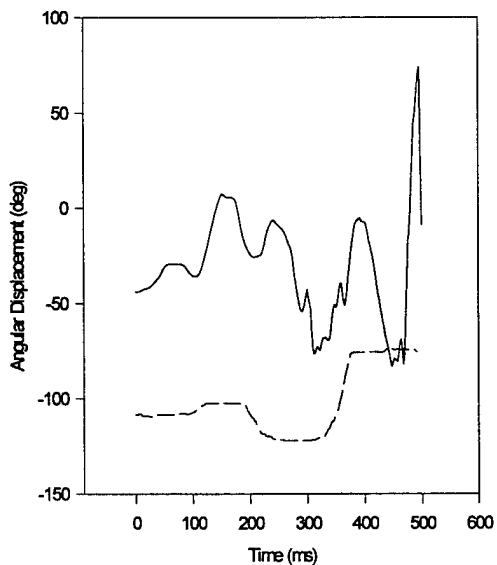
— ATB Model  
-- AMIT 79E-G2

Lumbar Roll



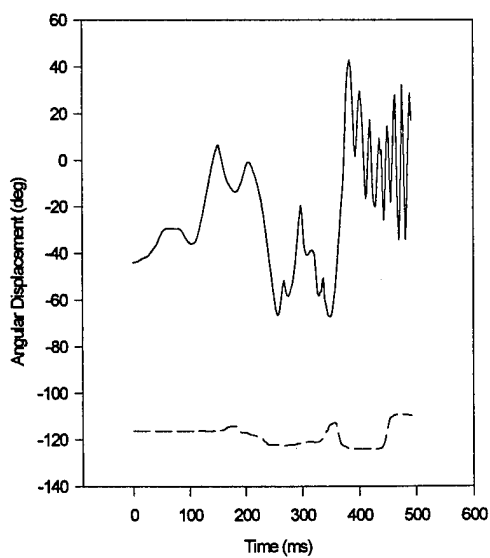
— ATB Model  
-- AMIT 79E-G2

Left Shoulder Abduction/Adduction



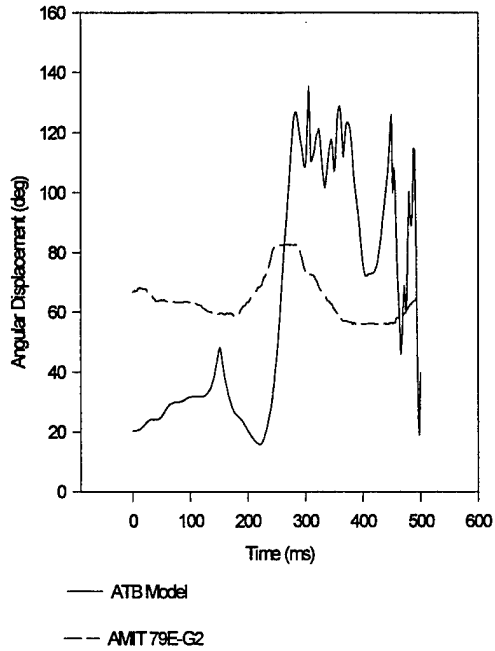
— ATB Model  
-- AMIT 79E-G2

Right Shoulder Abduction/Adduction

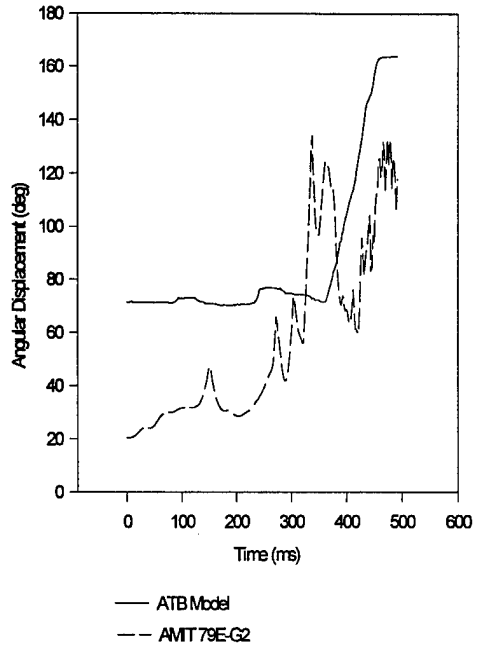


— ATB Model  
-- AMIT 79E-G2

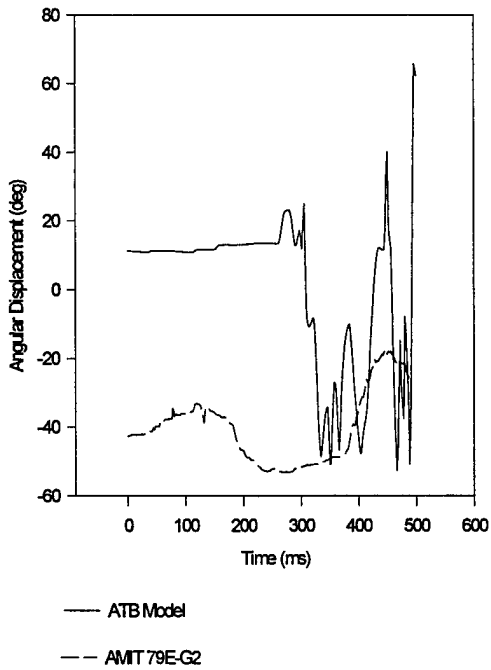
Left Shoulder Coronal Plane Abduction/Adduction



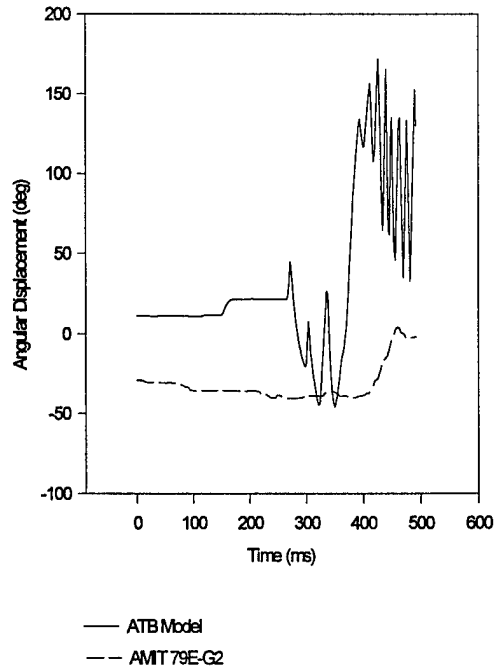
Right Shoulder Coronal Plane Abduction/Adduction



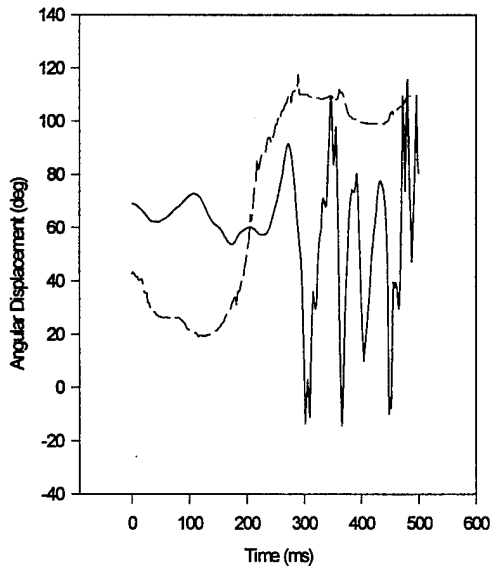
Left Shoulder Flexion



Right Shoulder Flexion

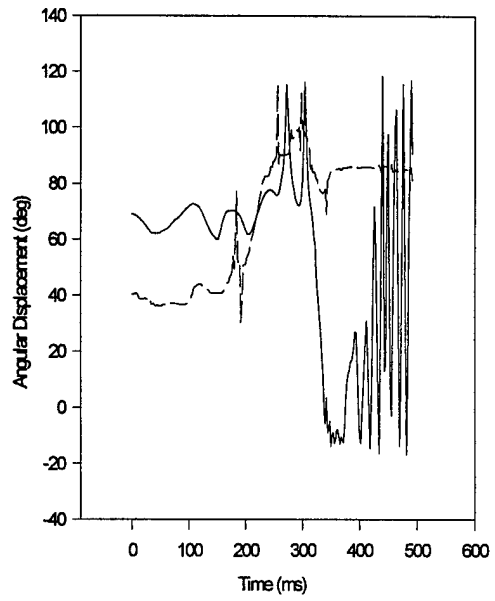


Left Shoulder Medial/Lateral



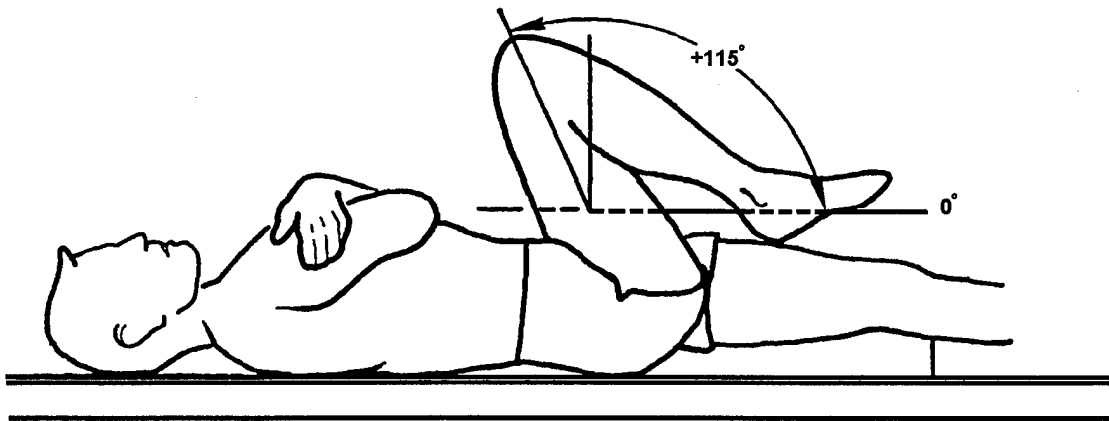
— ATB Model  
-- AMIT 79E-G2

Right Shoulder Medial/Lateral

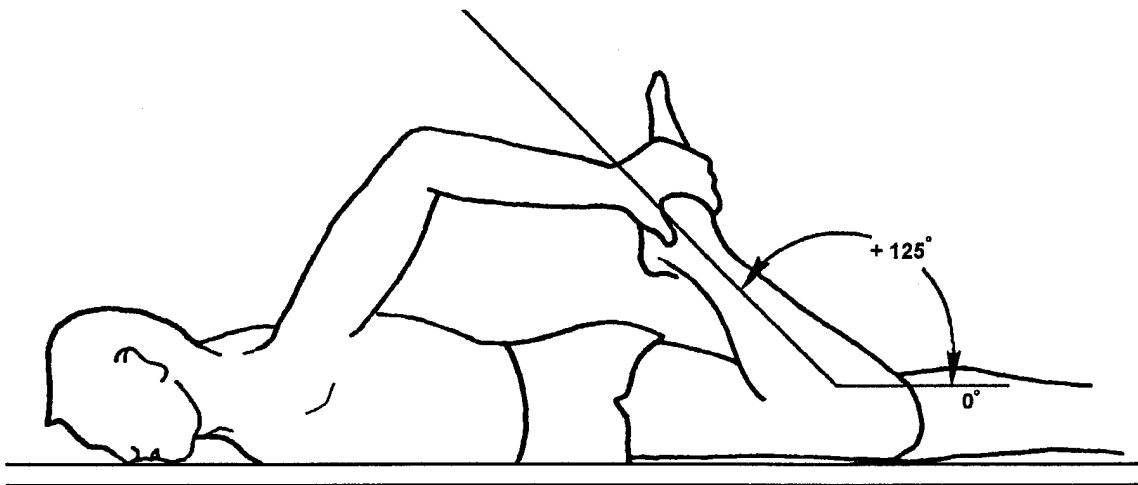


— ATB Model  
-- AMIT 79E-G2

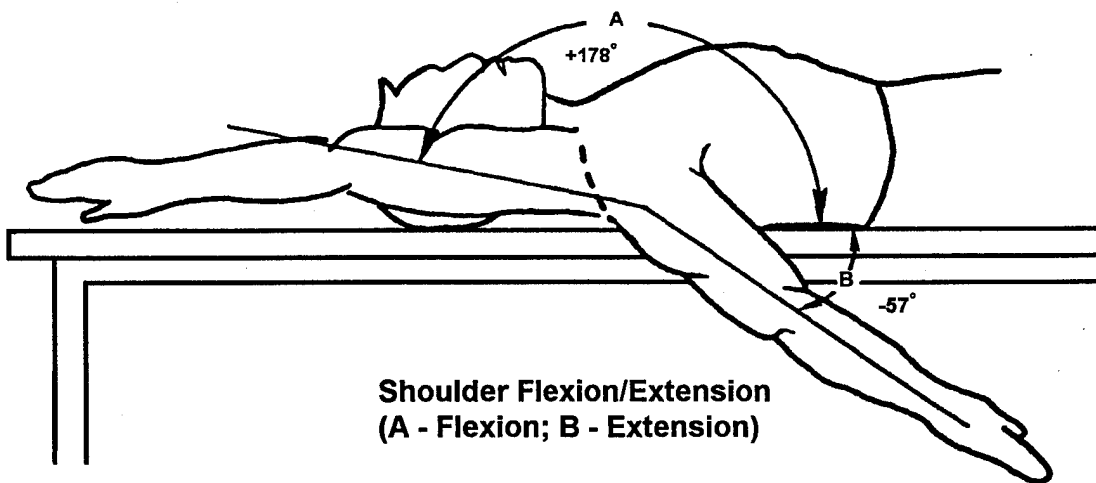
Appendix P: Explanation of the Terms - Flexion/Extension, Abduction/Adduction, Medial/Lateral and Supination/Pronation



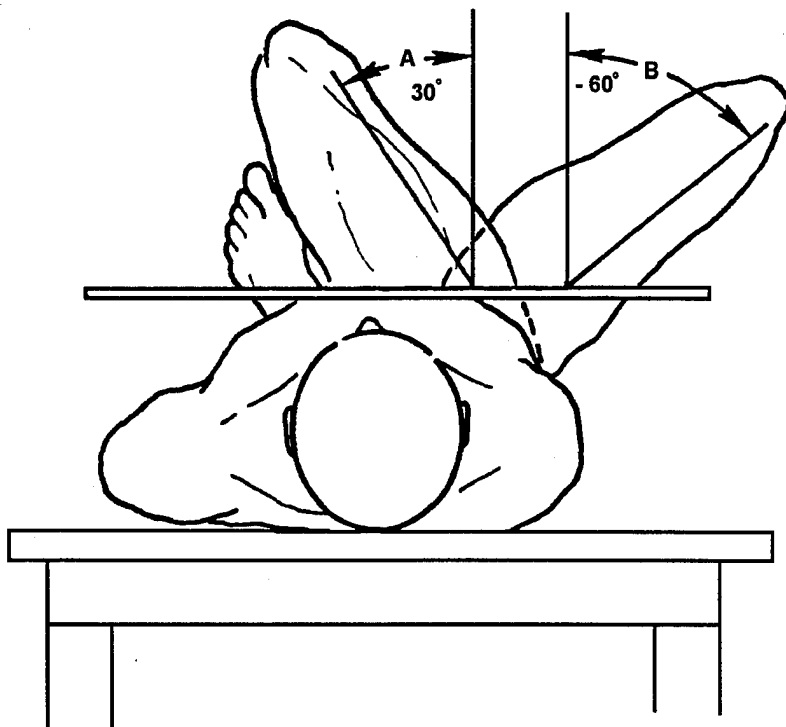
**Hip Flexion**



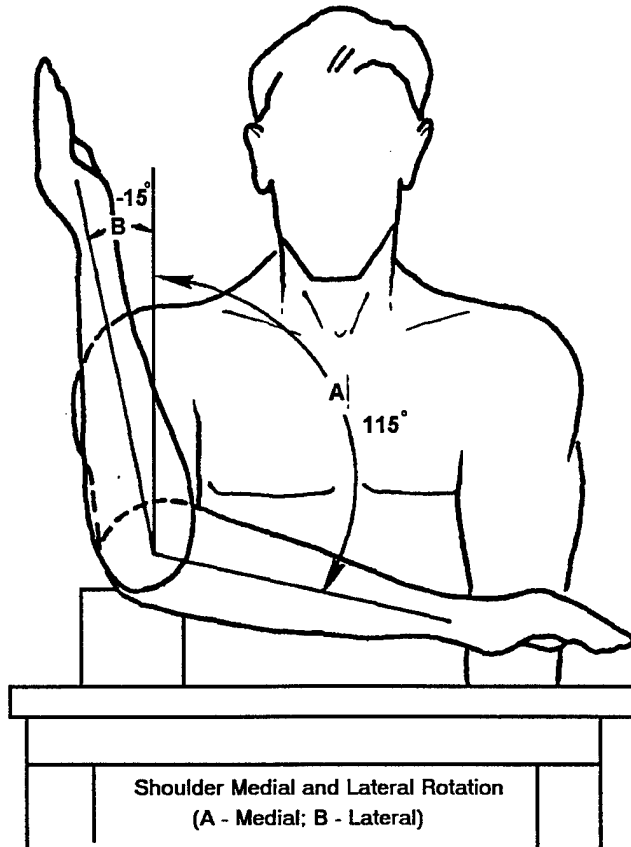
**Knee Flexion**



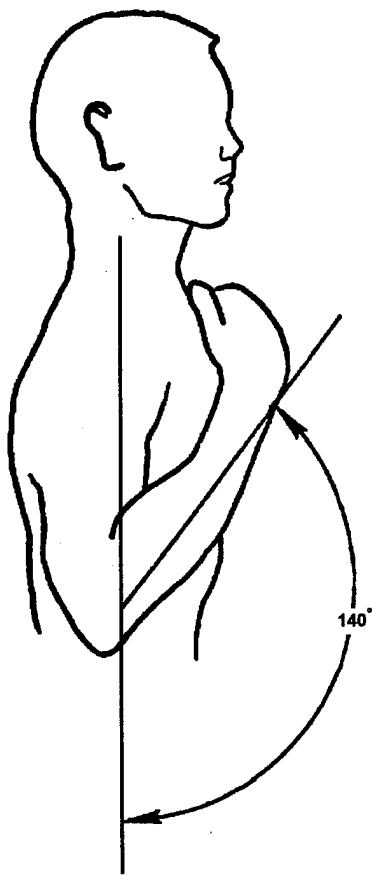
**Shoulder Flexion/Extension  
(A - Flexion; B - Extension)**



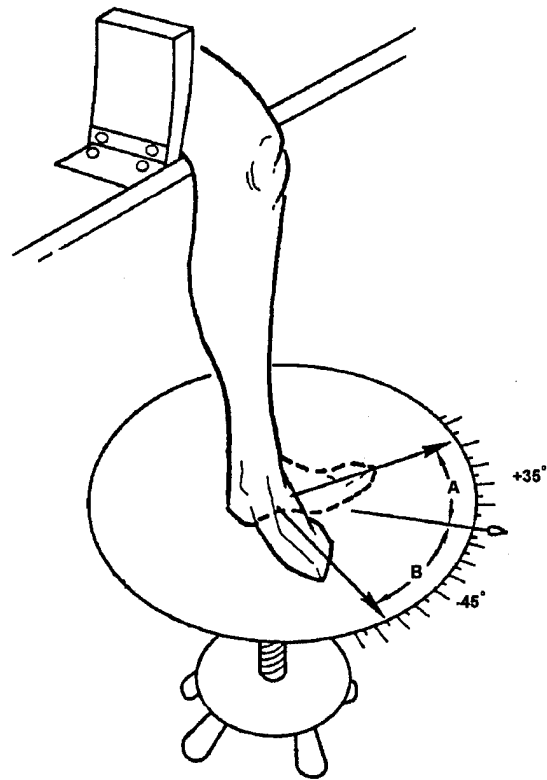
Hip Adduction and Abduction  
(A - Adduction; B - Abduction)



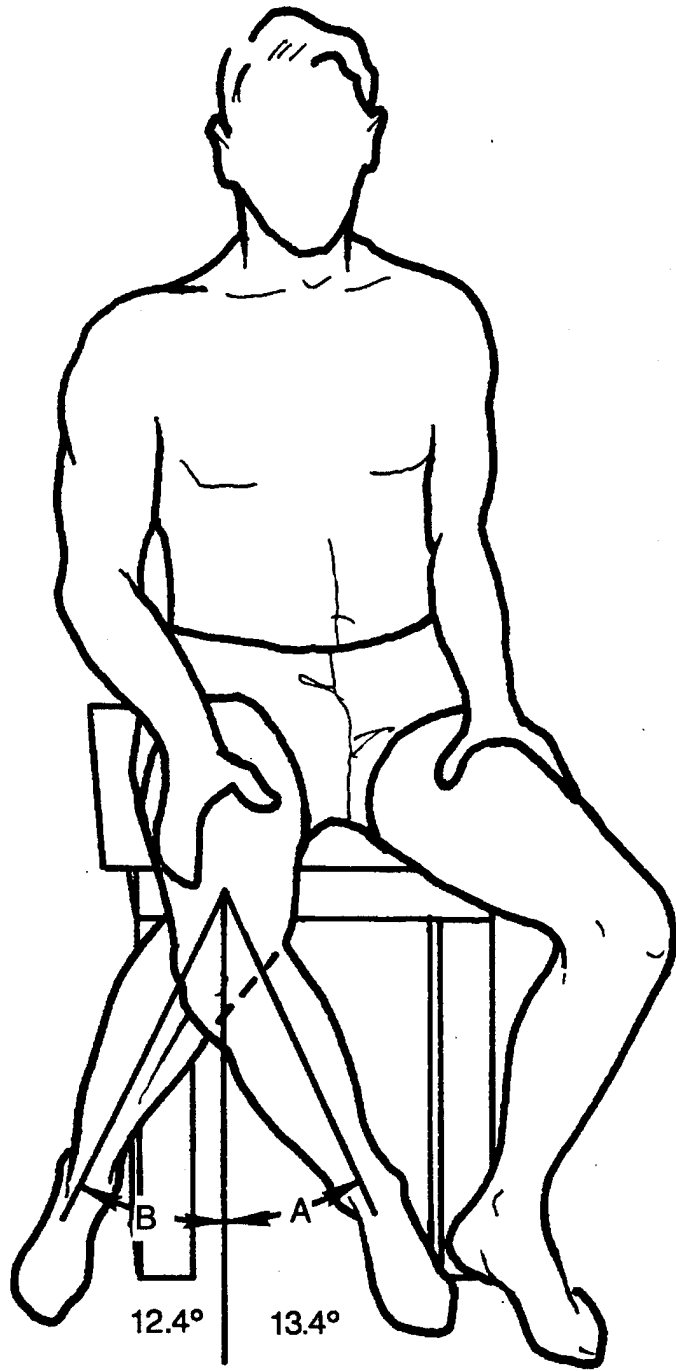
Shoulder Medial and Lateral Rotation  
(A - Medial; B - Lateral)



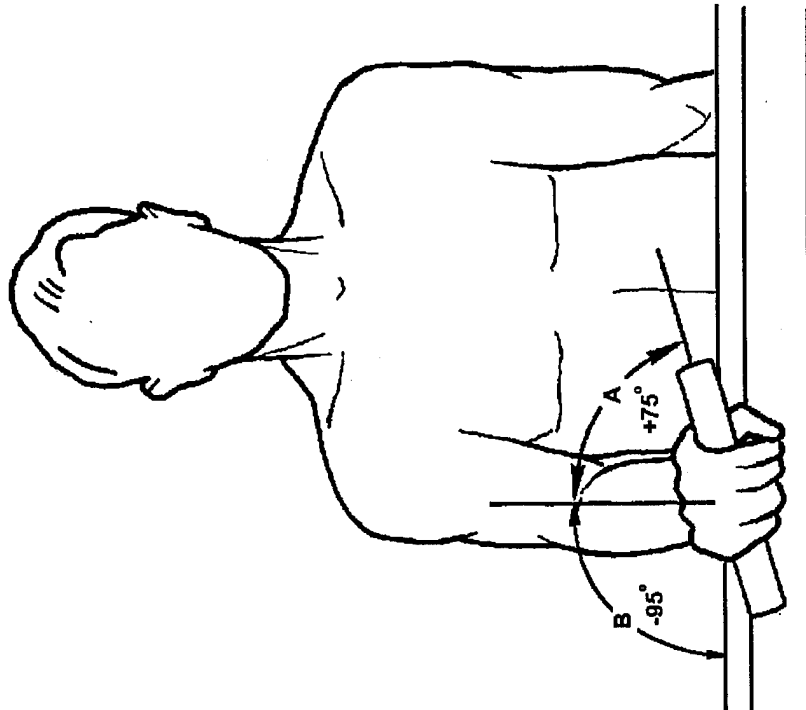
**Elbow Flexion**



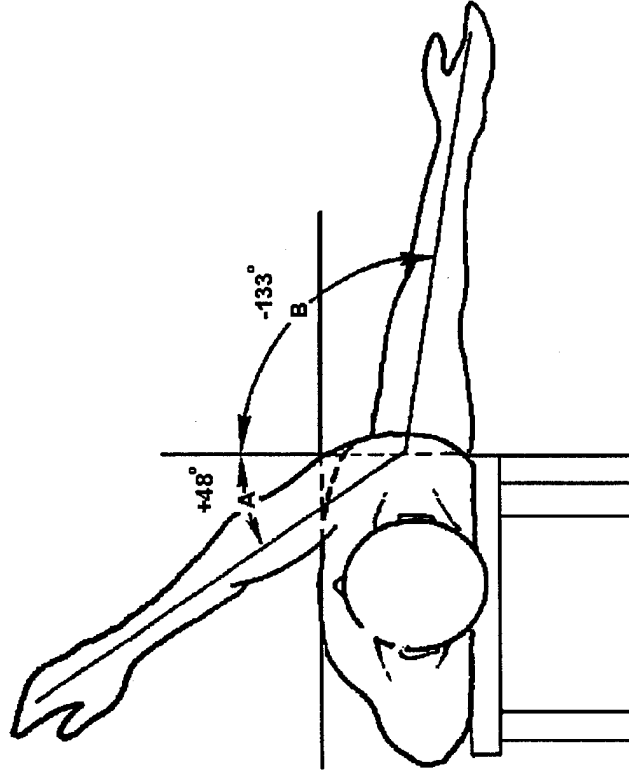
**Knee Medial/Lateral Rotation  
(A - Medial; B - Lateral)**



**Hip Medial and Lateral Rotation  
(A - Medial; B - Lateral)**



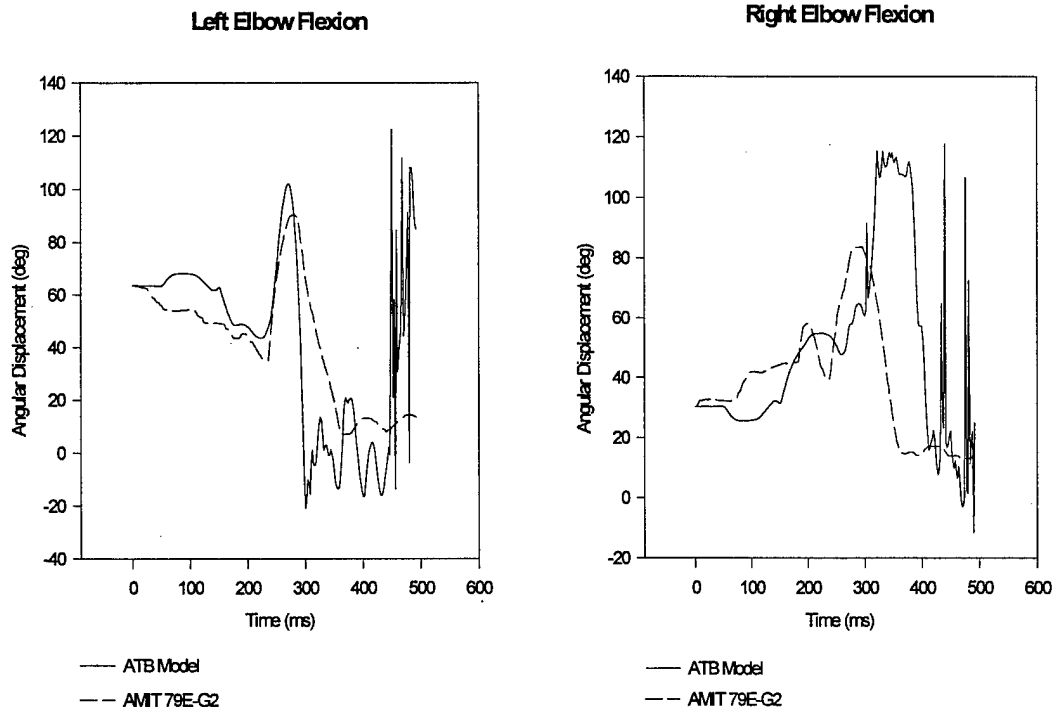
**Forearm Pronation/Supination**  
(A - Pronation; B - Supination)



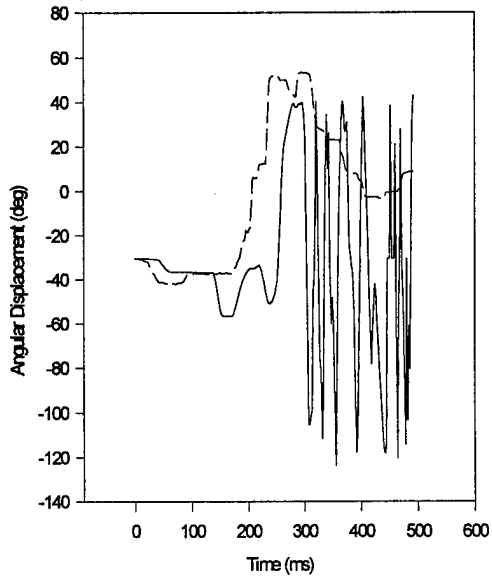
**Shoulder Adduction/Abduction**  
(A - Adduction; B - Abduction)

Appendix Q: ADAM Joint Angular Displacement Comparisons For the First ATB Simulation of AMIT 79E-G2A (Shifted and Polarized Data)

The following plots are comparisons between the actual motion of the ADAM during the AMIT 79E-G2A test and the motion of the ADAM modeled by the ATB simulation of the AMIT 79E-G2A test. The data from the ATB model presented here are shifted so that the zero angle for each joint defined by the ATB model corresponds to the zero angle defined during the AMIT 79E-G2A test. The polarity of certain plots are also reversed. This polarity reversal is explained in Chapter III of this thesis.

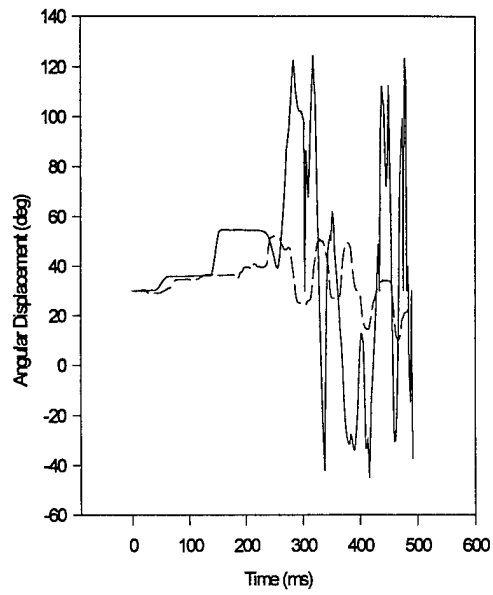


Left Elbow Supination/Pronation



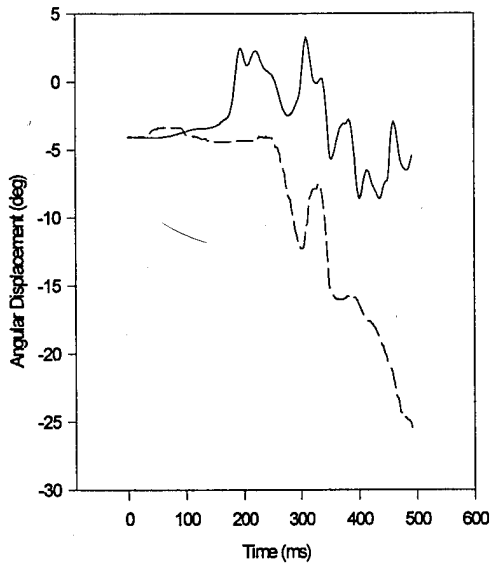
— ATB Model  
-- AMIT 79E-G2

Right Elbow Supination/Pronation



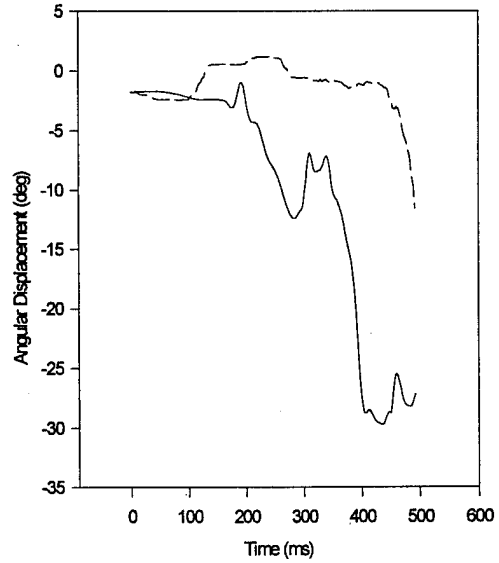
— ATB Model  
-- AMIT 79E-G2

Left Hip Abduction/Adduction



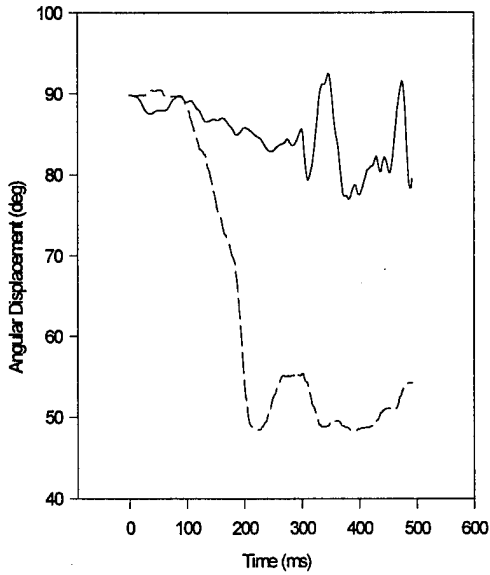
— ATB Model  
-- AMIT 79E-G2

Right Hip Abduction/Adduction



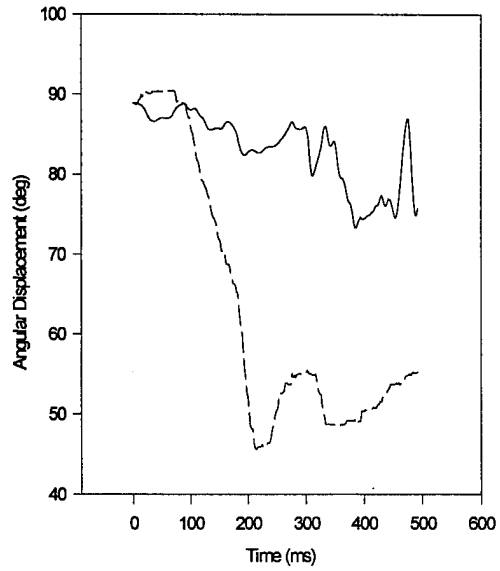
— ATB Model  
-- AMIT 79E-G2

**Left Hip Flexion**



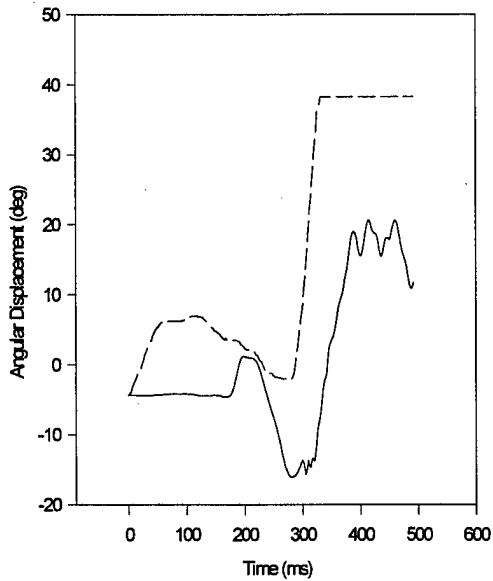
— ATB Model  
- - - AMIT 79E-G2

**Right Hip Flexion**



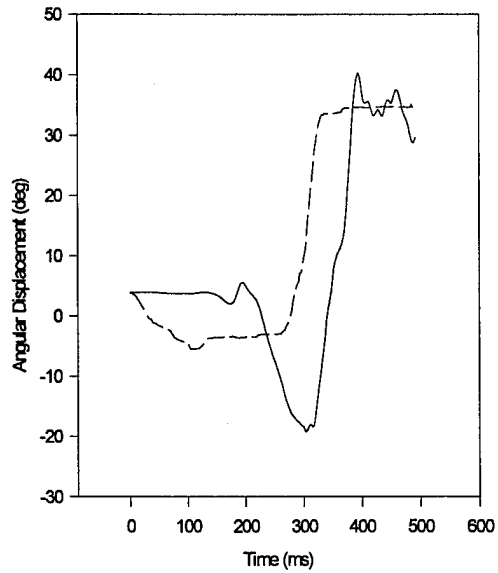
— ATB Model  
- - - AMIT 79E-G2

**Left Hip Medial/Lateral**



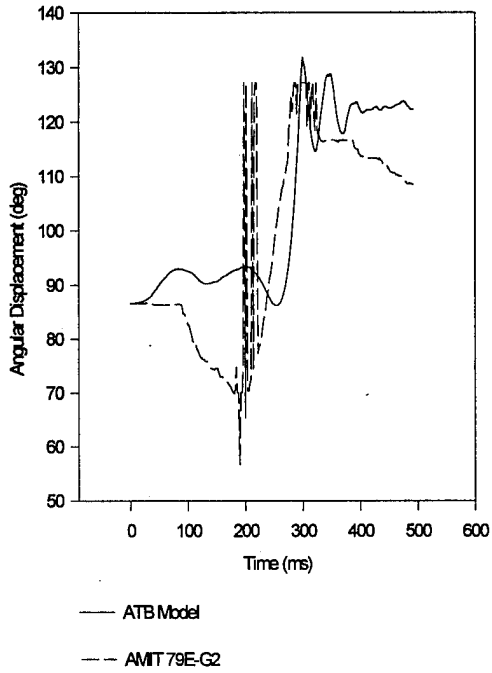
— ATB Model  
- - - AMIT 79E-G2

**Right Hip Medial/Lateral**

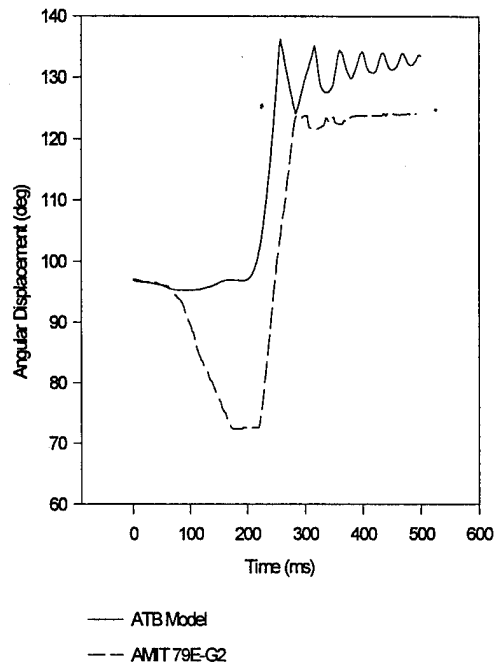


— ATB Model  
- - - AMIT 79E-G2

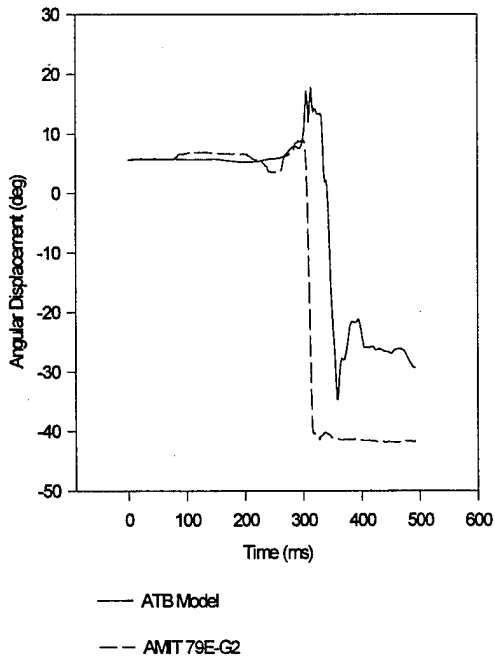
Left Knee Flexion



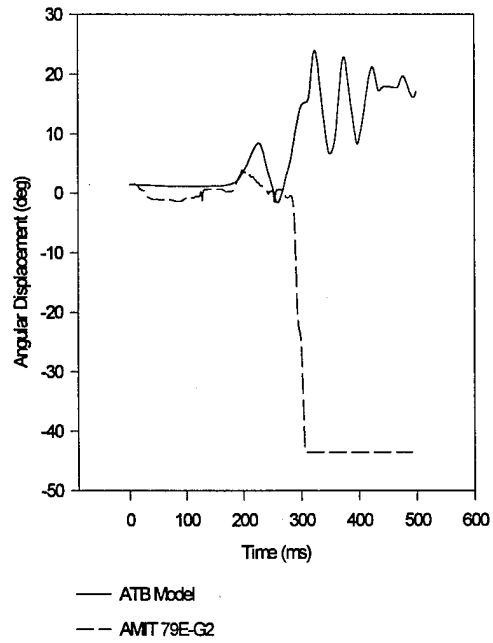
Right Knee Flexion



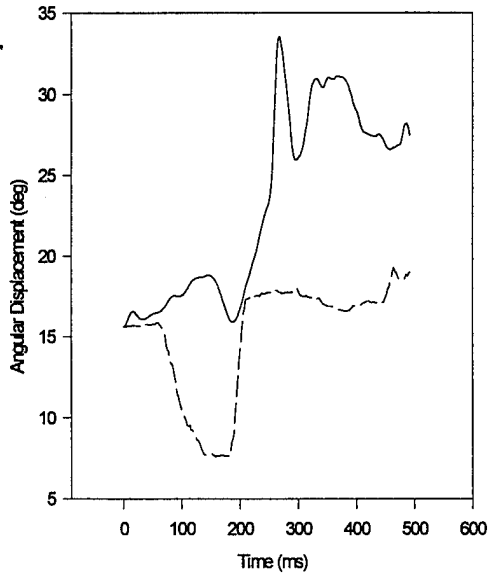
Left Knee Medial/Lateral



Right Knee Medial/Lateral

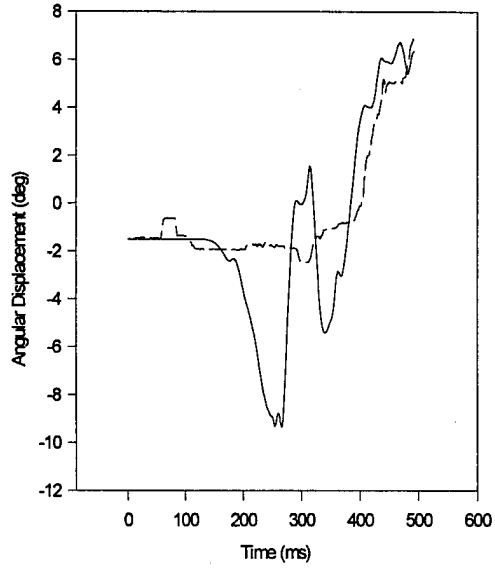


Lumbar Pitch



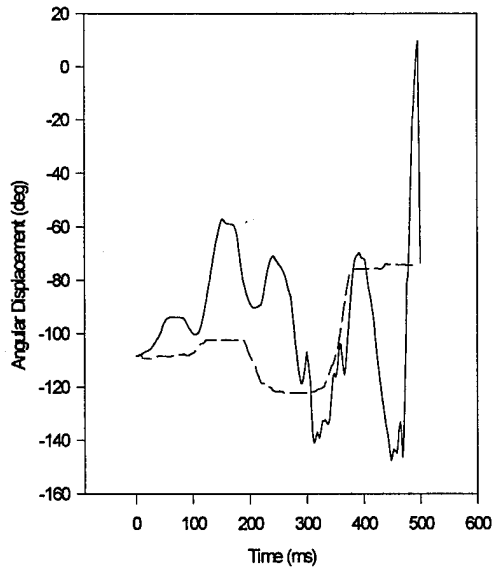
— ATB Model  
-- AMIT 79E-G2

Lumbar Roll



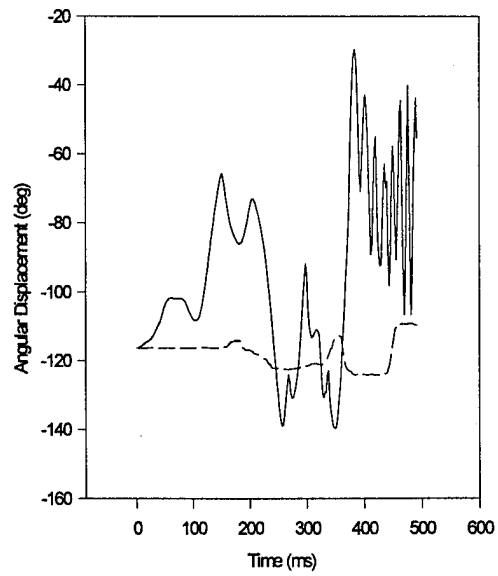
— ATB Model  
-- AMIT 79E-G2

Left Shoulder Abduction/Adduction



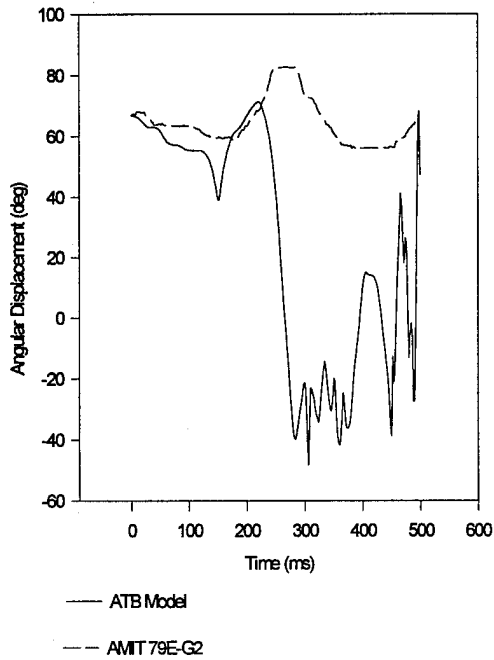
— ATB Model  
-- AMIT 79E-G2

Right Shoulder Abduction/Adduction

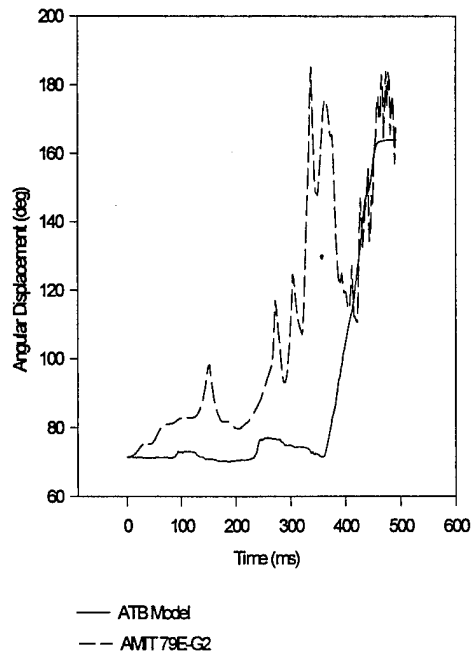


— ATB Model  
-- AMIT 79E-G2

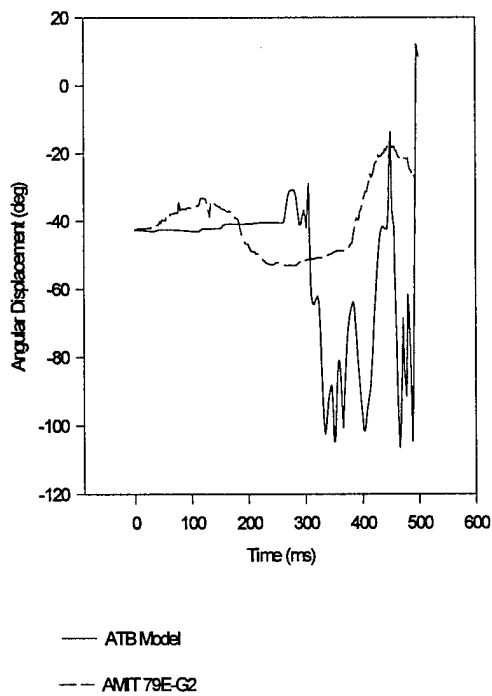
Left Shoulder Coronal Plane Abduction/Adduction



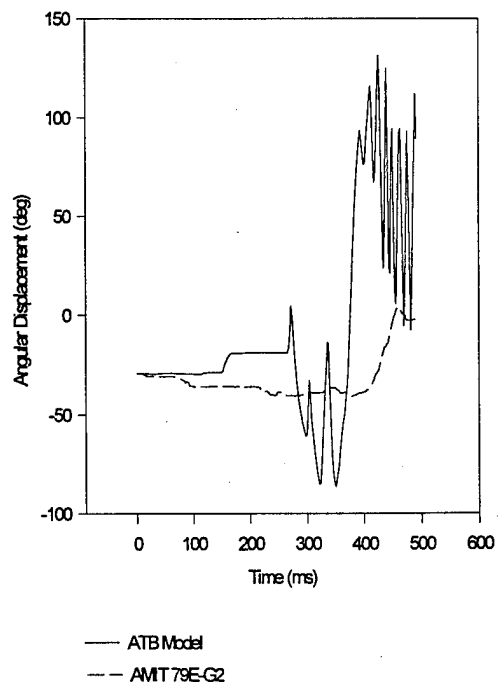
Right Shoulder Coronal Plane Abduction/Adduction



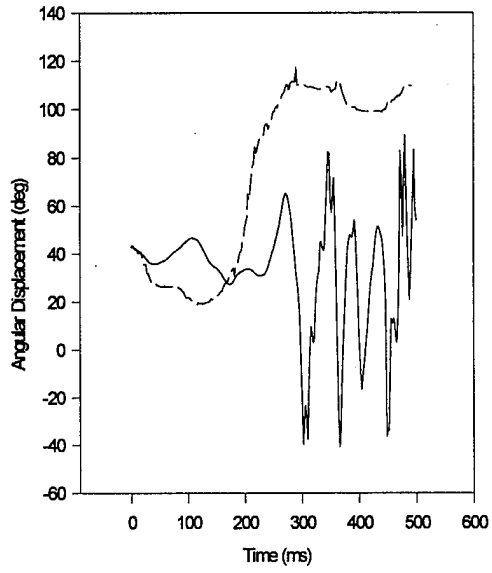
Left Shoulder Flexion



Right Shoulder Flexion

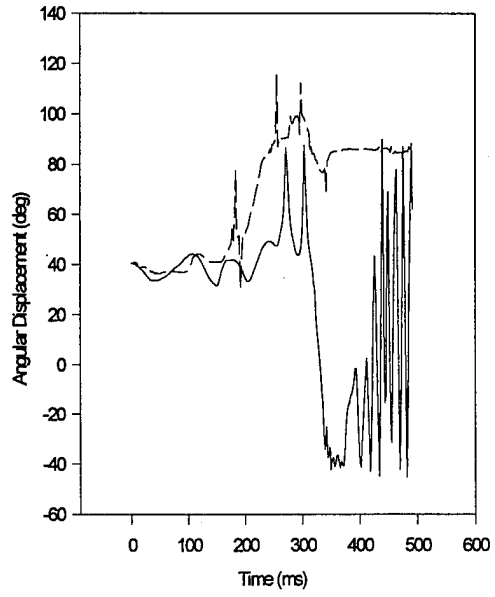


Left Shoulder Medial/Lateral



— ATB Model  
-- AMIT 79E-G2

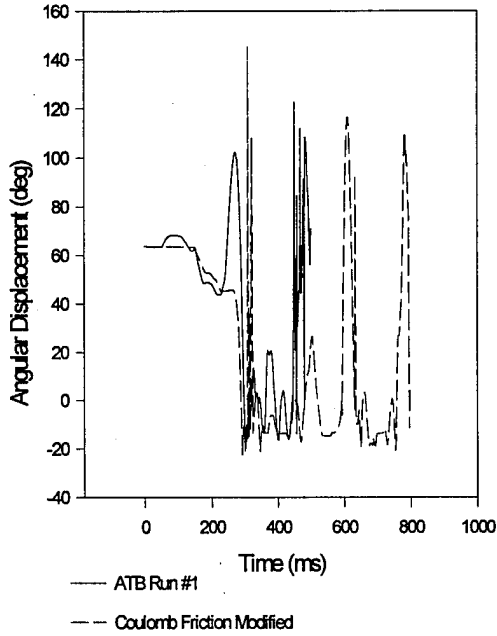
Right Shoulder Medial/Lateral



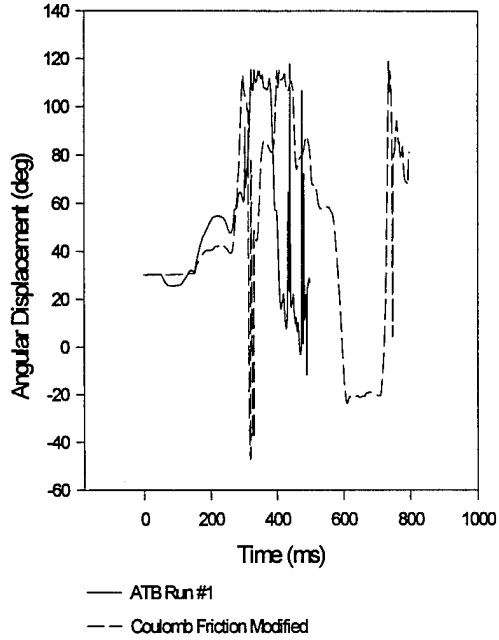
— ATB Model  
-- AMIT 79E-G2

Appendix R: ADAM Joint Angular Displacement Comparison With Joint Coulomb Friction Multiplied By 10

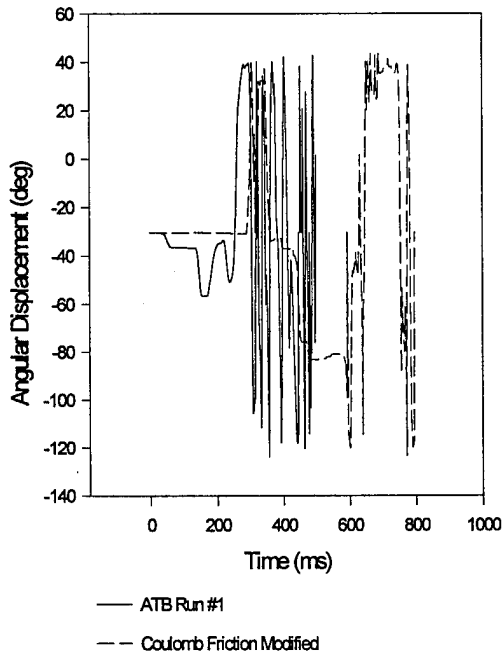
**Left Elbow Flexion**



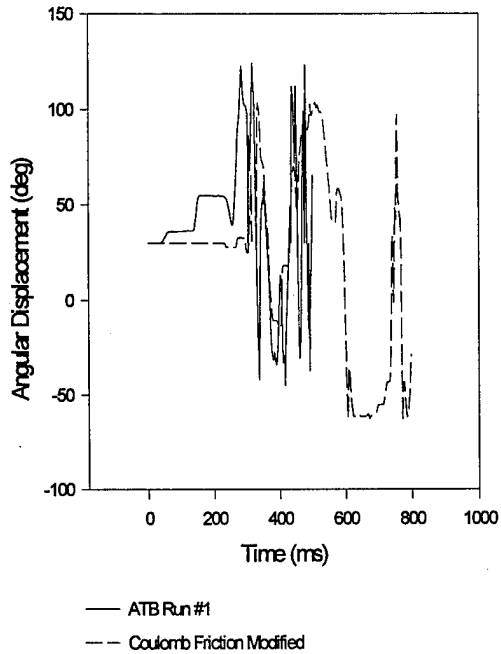
**Right Elbow Flexion**



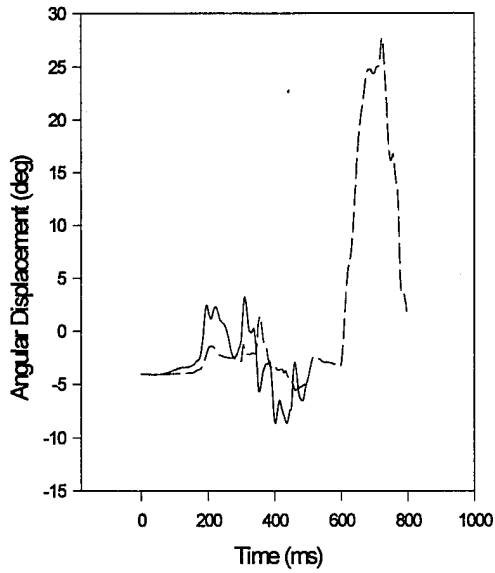
**Left Elbow Supination/Pronation**



**Right Elbow Supination/Pronation**

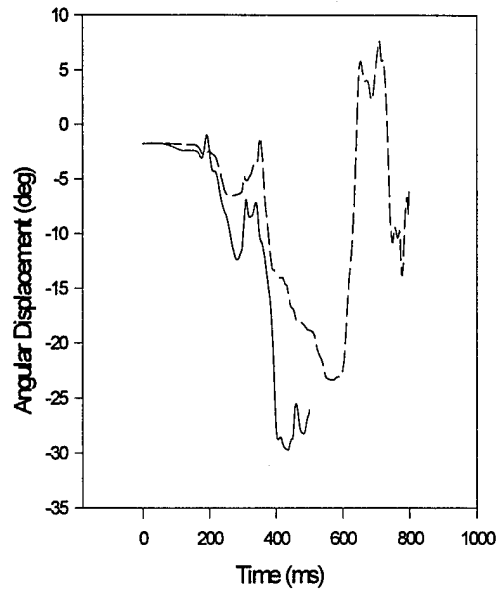


Left Hip Abduction/Adduction



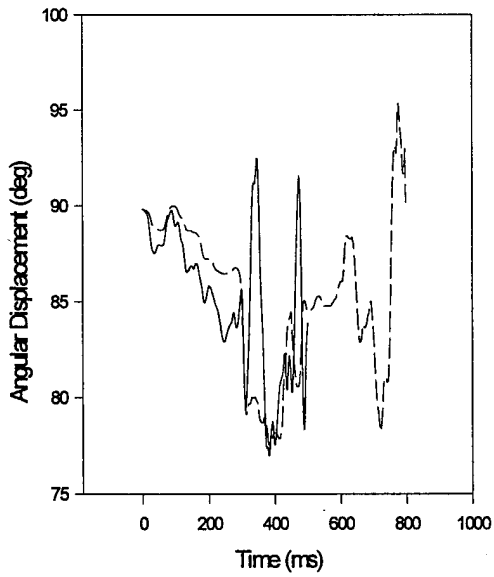
— ATB Run #1  
-- Coulomb Friction Modified

Right Hip Abduction/Adduction



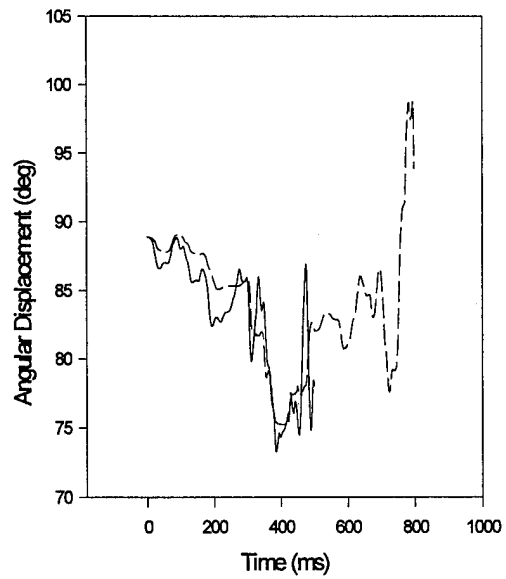
— ATB Run #1  
-- Coulomb Friction Modified

Left Hip Flexion



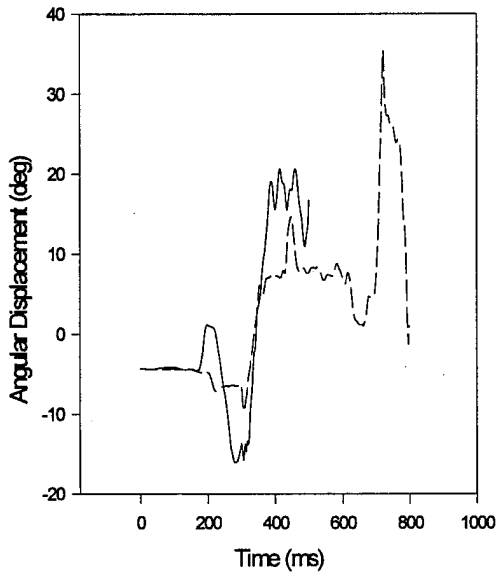
— ATB Run #1  
-- Coulomb Friction Modified

Right Hip Flexion



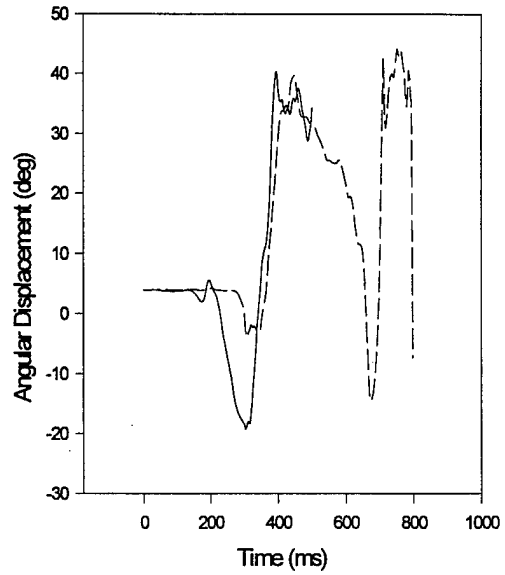
— ATB Run #1  
-- Coulomb Friction Modified

Left Hip Medial/Lateral



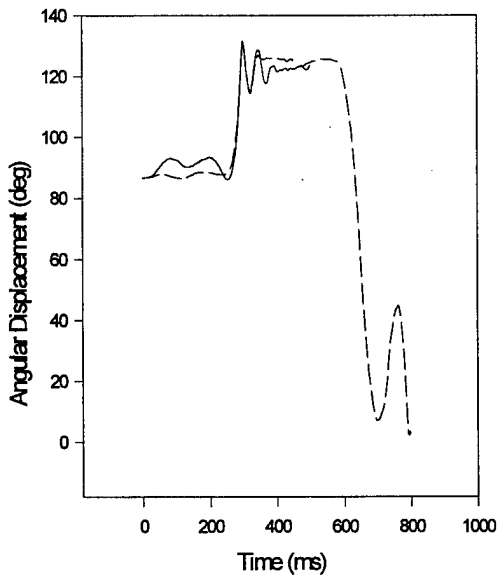
— ATB Run #1  
-- Coulomb Friction Modified

Right Hip Medial/Lateral



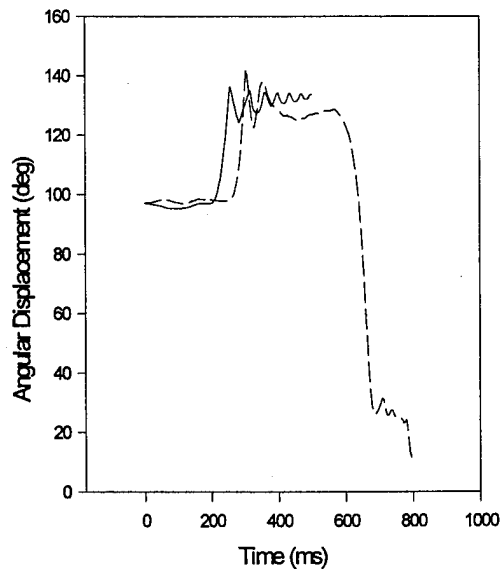
— ATB Run #1  
-- Coulomb Friction Modified

Left Knee Flexion



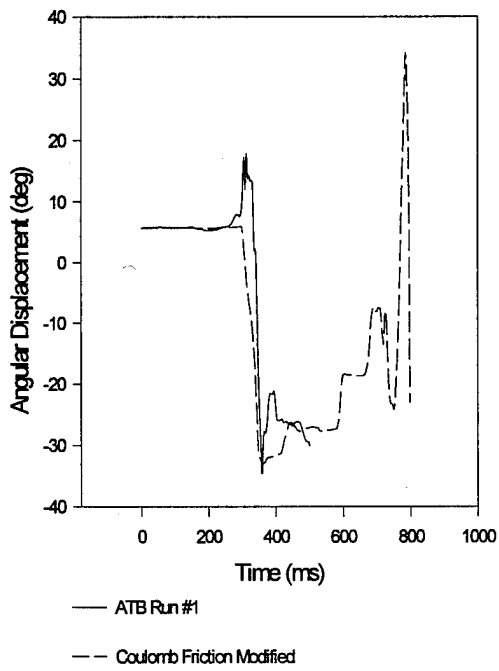
— ATB Run #1  
-- Coulomb Friction Modified

Right Knee Flexion

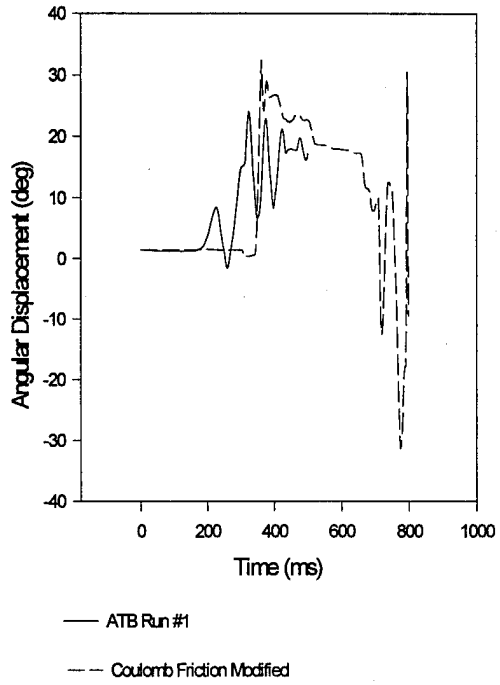


— ATB Run #1  
-- Coulomb Friction Modified

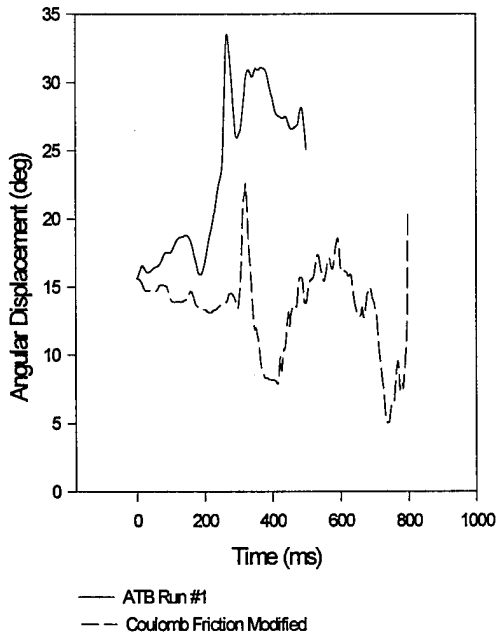
Left Knee Medial/Lateral



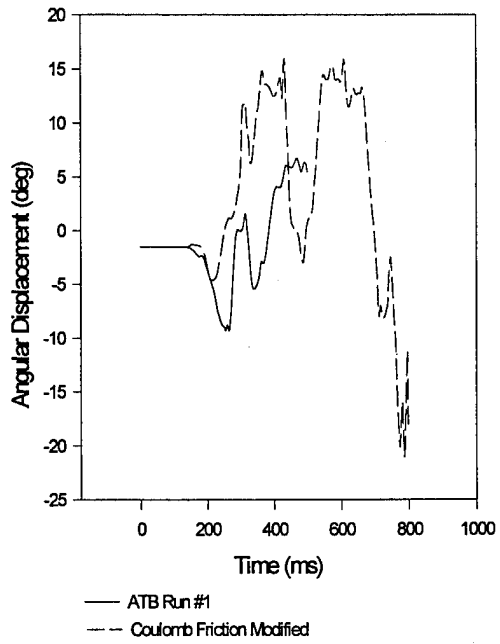
Right Knee Medial/Lateral



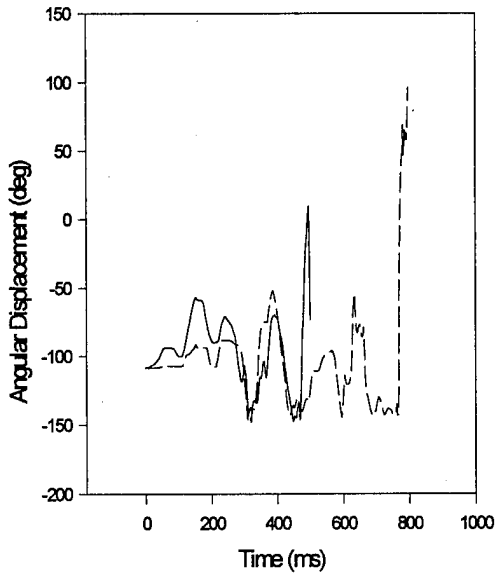
Lumbar Pitch



Lumbar Roll

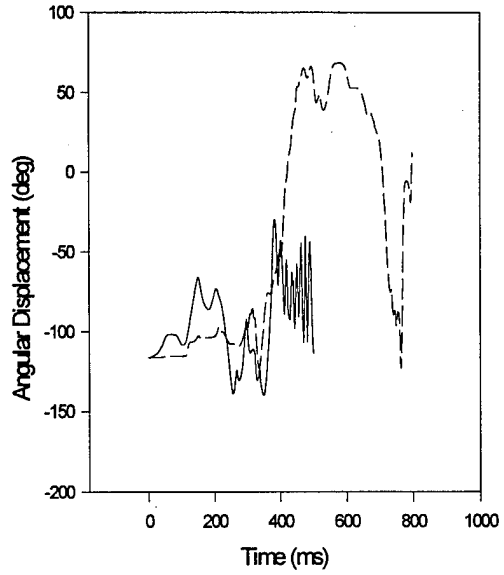


Left Shoulder Abduction/Adduction



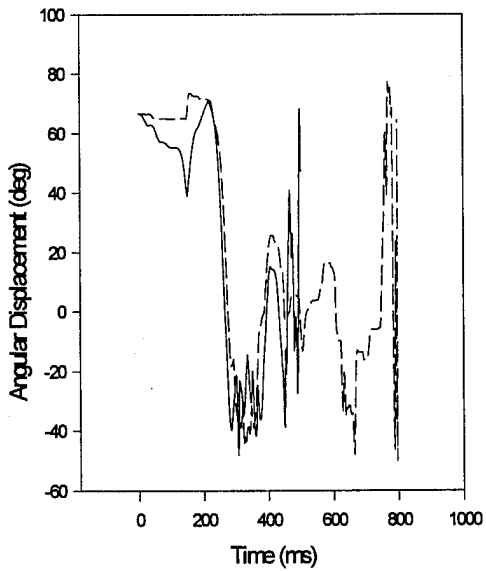
— ATB Run #1  
- - Coulomb Friction Modified

Right Shoulder Abduction/Adduction



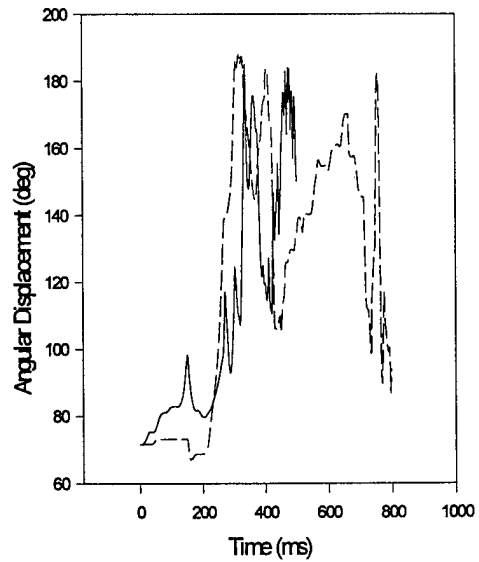
— ATB Run #1  
- - Coulomb Friction Modified

Left Shoulder Coronal Plane Abduction/Adduction



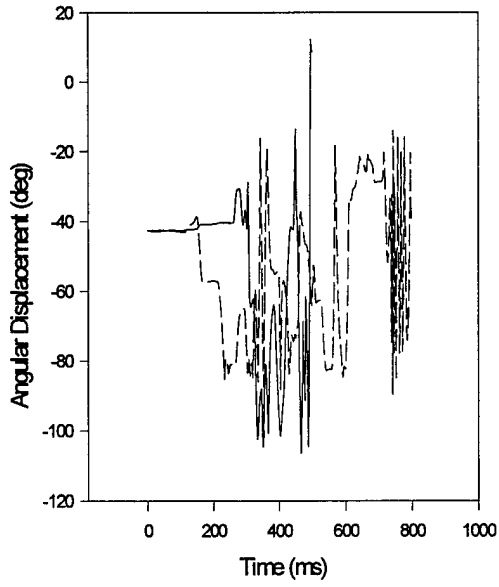
— ATB Run #1  
- - Coulomb Friction Modified

Right Shoulder Coronal Plane Abduction/Adduction



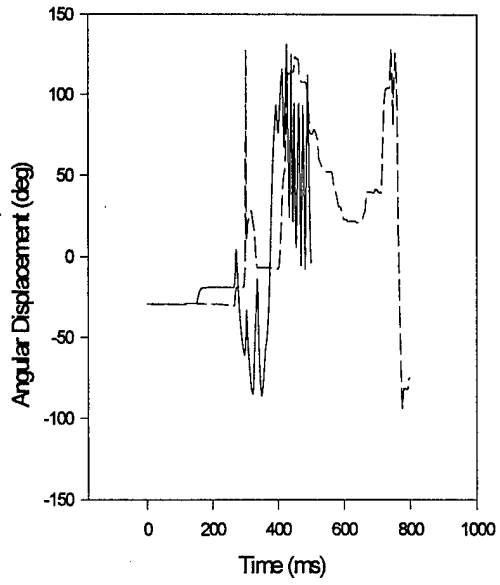
— ATB Run #1  
- - Coulomb Friction Modified

Left Shoulder Flexion



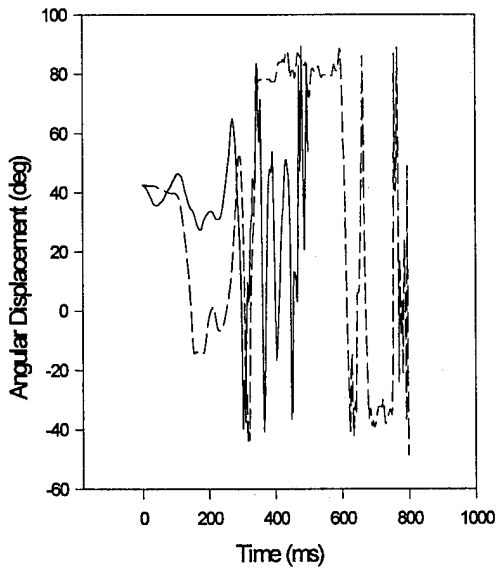
— ATB Run #1  
- - Coulomb Friction Modified

Right Shoulder Flexion



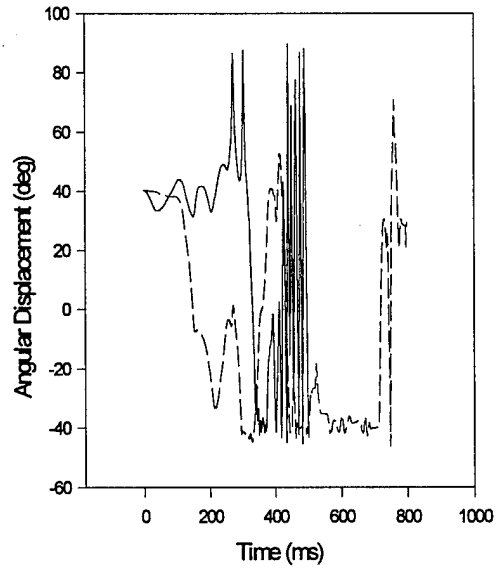
— ATB Run #1  
- - Coulomb Friction Modified

Left Shoulder Medial/Lateral



— ATB Run #1  
- - Coulomb Friction Modified

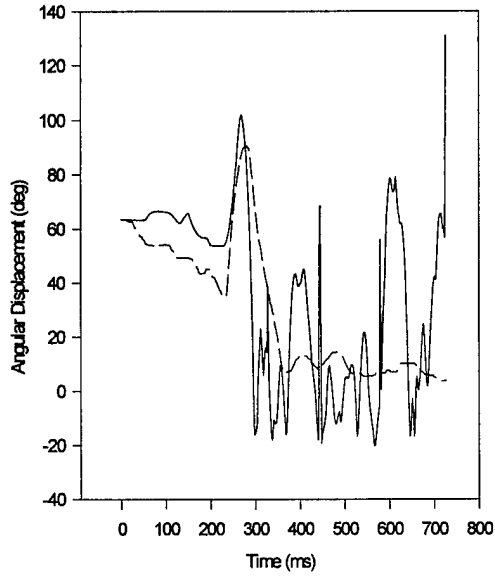
Right Shoulder Medial/Lateral



— ATB Run #1  
- - Coulomb Friction Modified

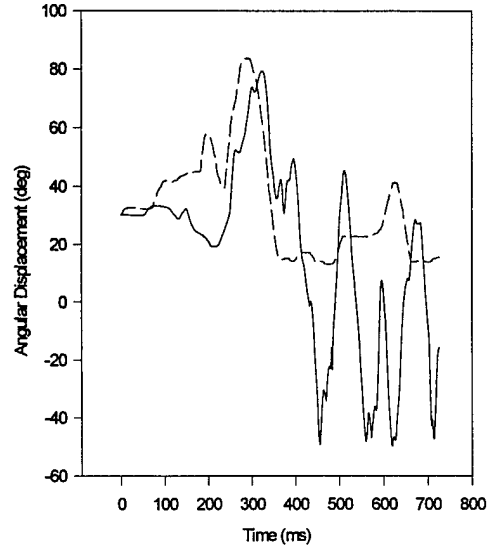
Appendix S: ADAM Joint Angular Displacement Comparisons For the Second ATB Simulation of AMIT 79E-G2A (Shifted and Polarized Data)

**Left Elbow Flexion**



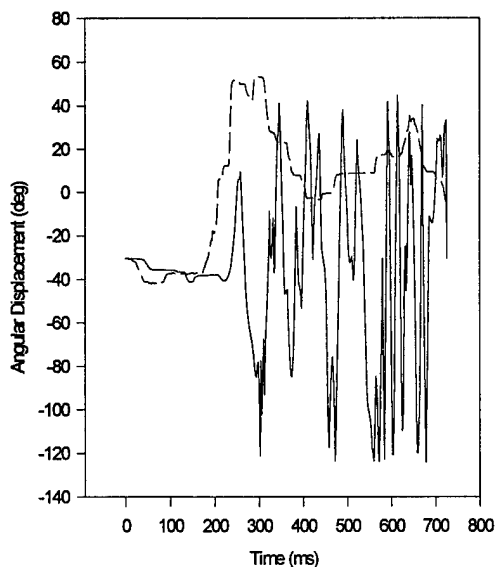
— ATB Model  
- - AMIT 79E-G2

**Right Elbow Flexion**



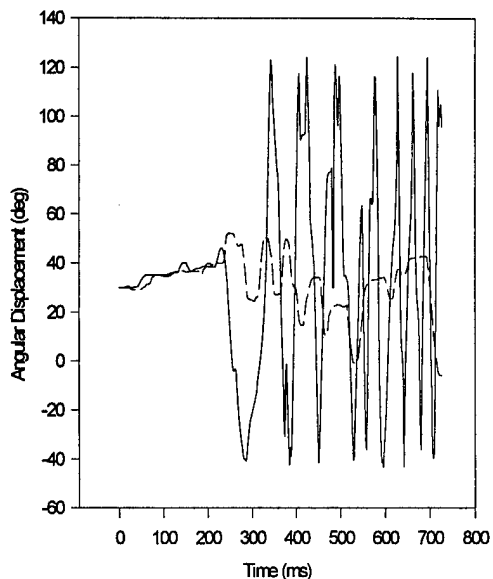
— ATB Model  
- - AMIT 79E-G2

Left Elbow Supination/Pronation



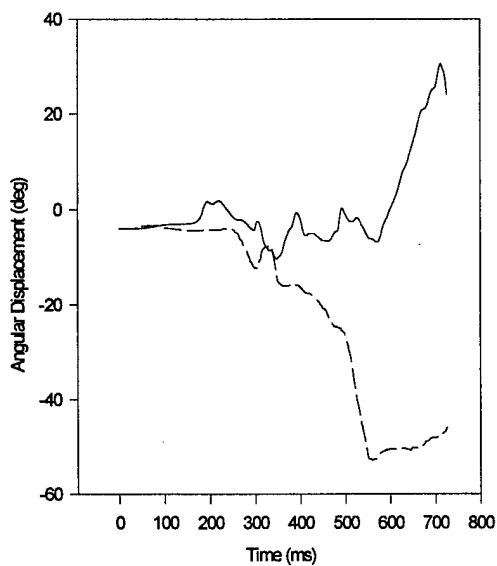
— ATB Model  
-- AMIT 79E-G2

Right Elbow Supination/Pronation



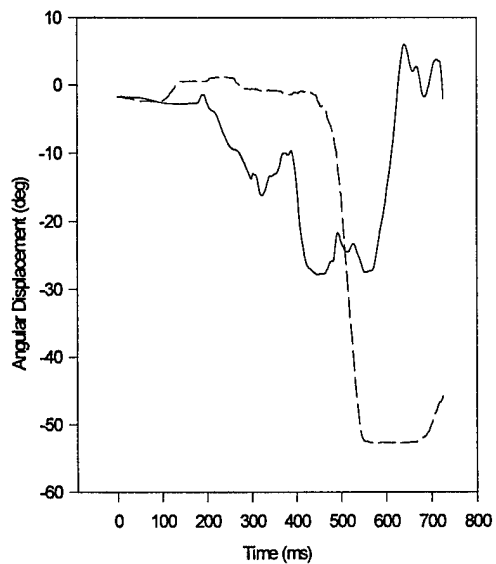
— ATB Model  
-- AMIT 79E-G2

Left Hip Abduction/Adduction



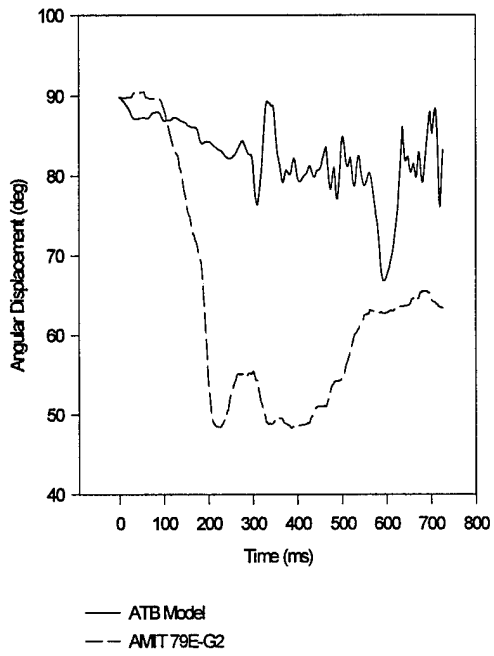
— ATB Model  
-- AMIT 79E-G2

Right Hip Abduction/Adduction

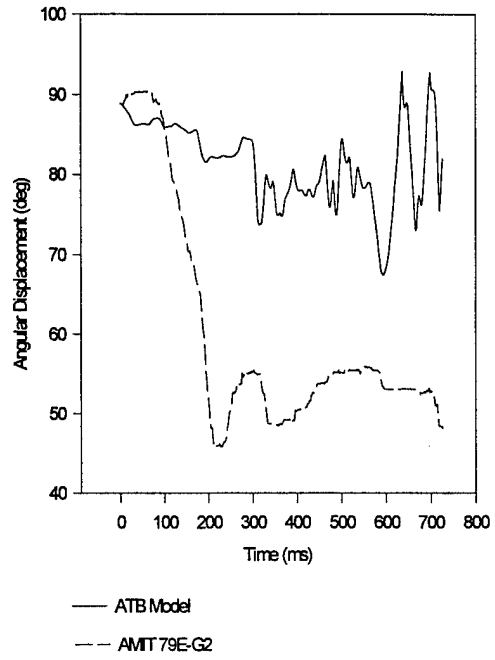


— ATB Model  
-- AMIT 79E-G2

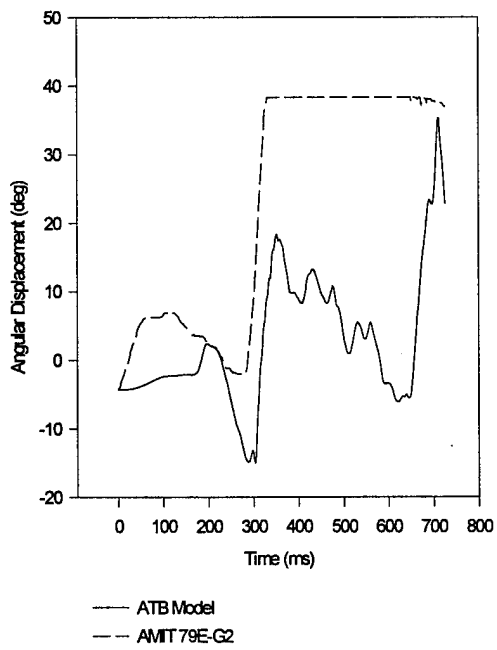
**Left Hip Flexion**



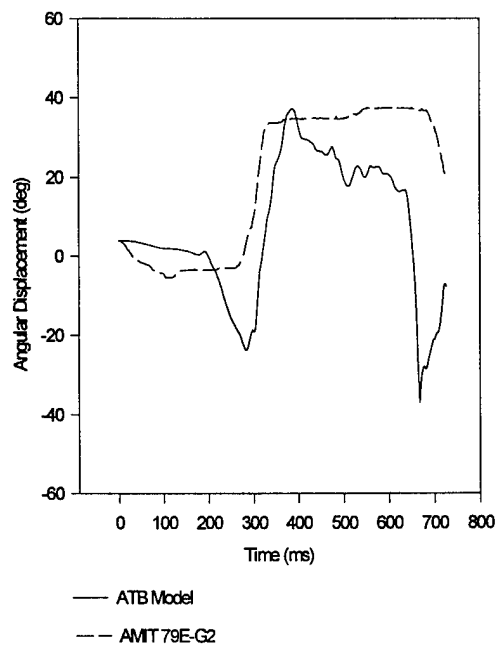
**Right Hip Flexion**



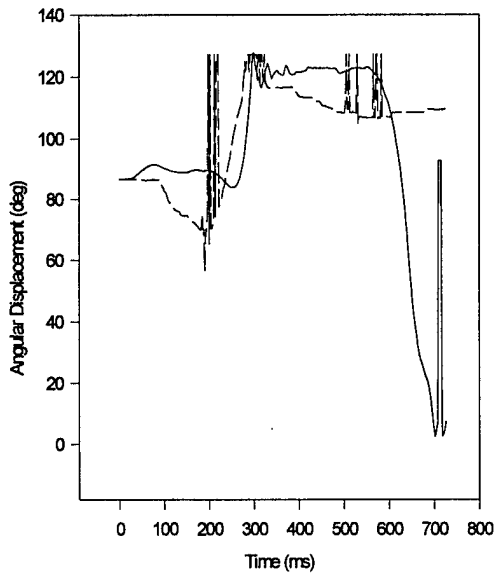
**Left Hip Medial/Lateral**



**Right Hip Medial/Lateral**

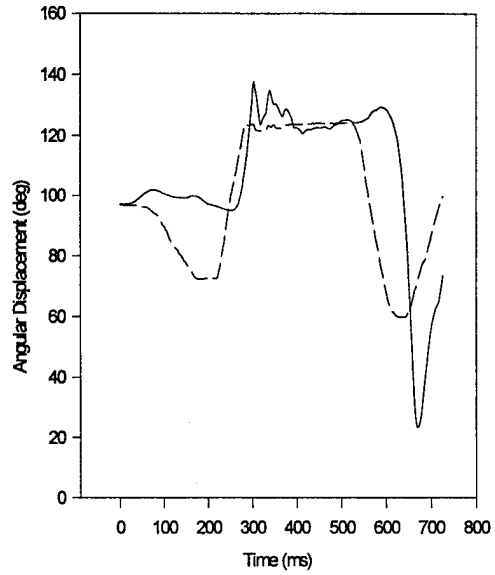


Left Knee Flexion



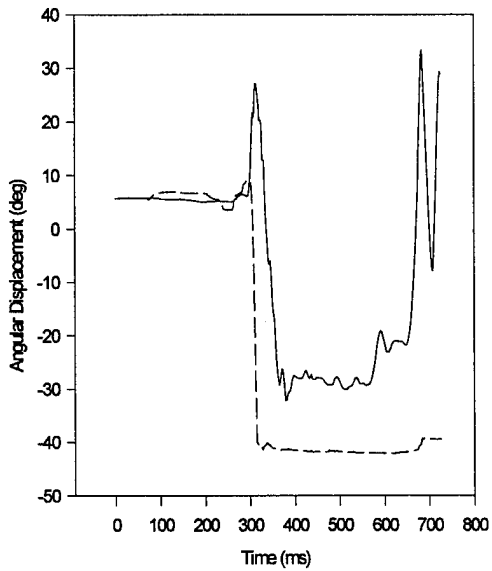
— ATB Model  
-- AMIT 79E-G2

Right Knee Flexion



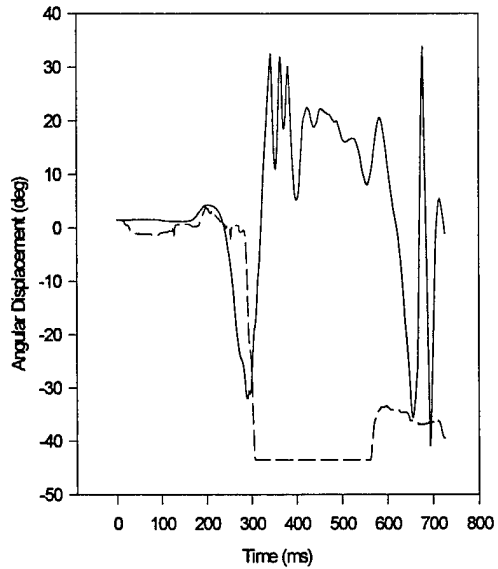
— ATB Model  
-- AMIT 79E-G2

Left Knee Medial/Lateral



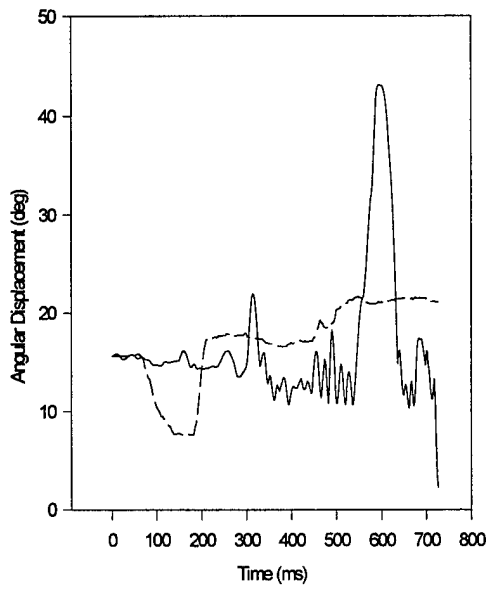
— ATB Model  
-- AMIT 79E-G2

Right Knee Medial/Lateral



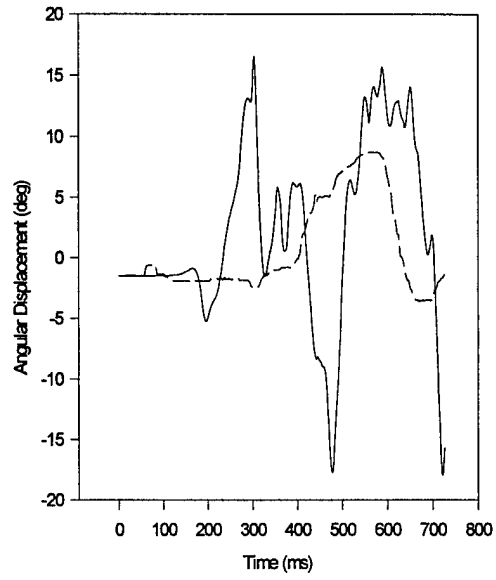
— ATB Model  
-- AMIT 79E-G2

Lumbar Pitch



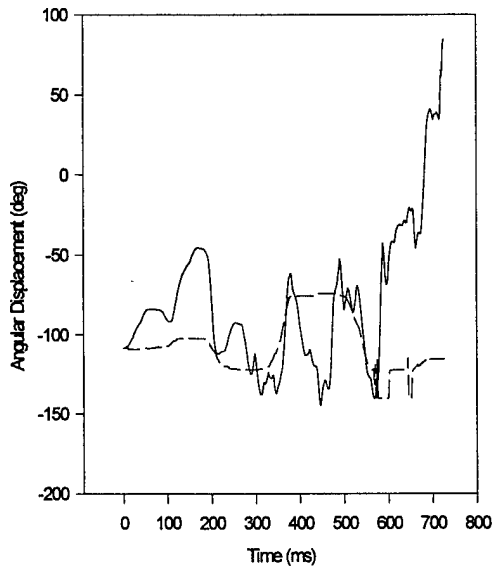
— ATB Model  
-- AMIT 79E-G2

Lumbar Roll



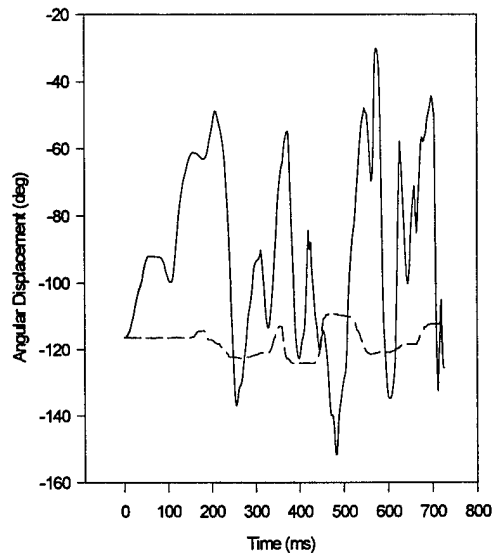
— ATB Model  
-- AMIT 79E-G2

Left Shoulder Abduction/Adduction



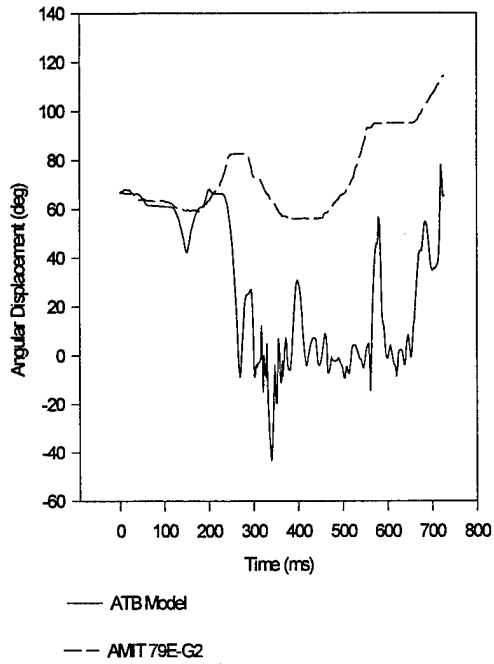
— ATB Model  
-- AMIT 79E-G2

Right Shoulder Abduction/Adduction

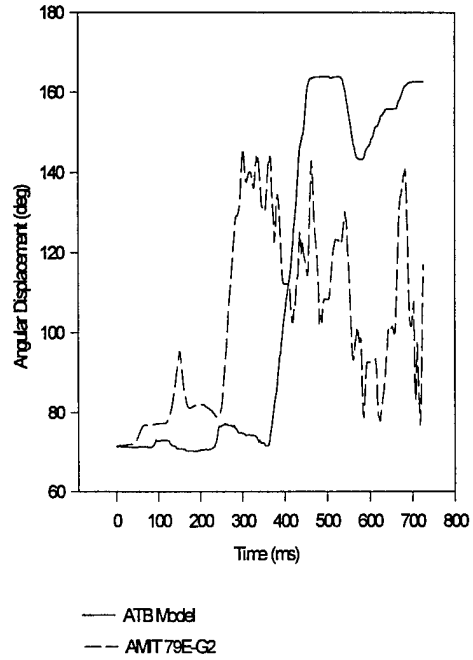


— ATB Model  
-- AMIT 79E-G2

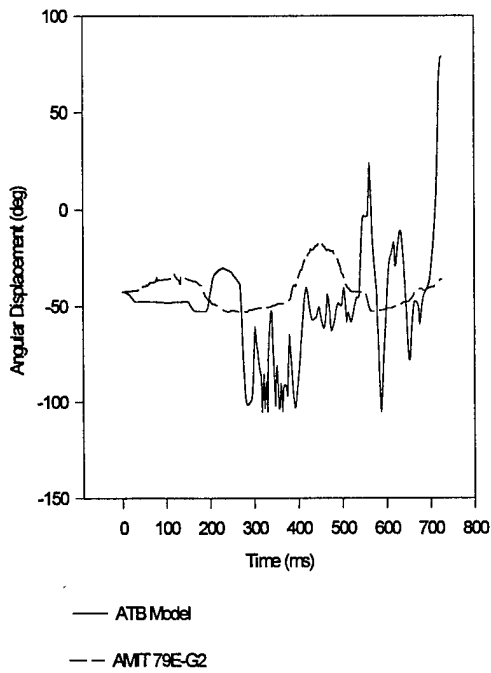
Left Shoulder Coronal Plane Abduction/Adduction



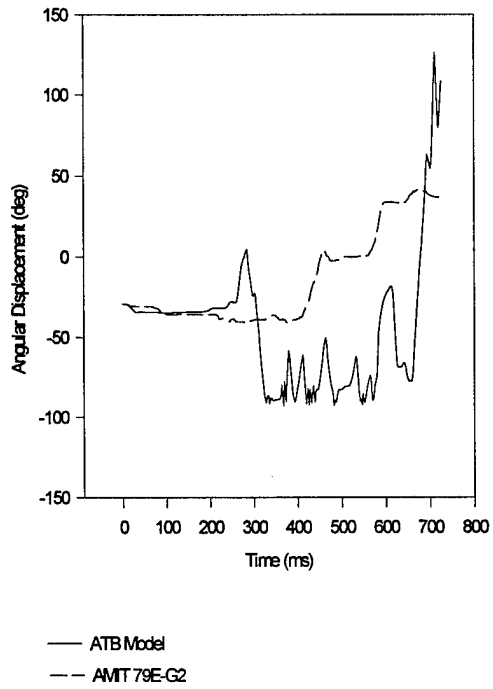
Right Shoulder Coronal Plane Abduction/Adduction



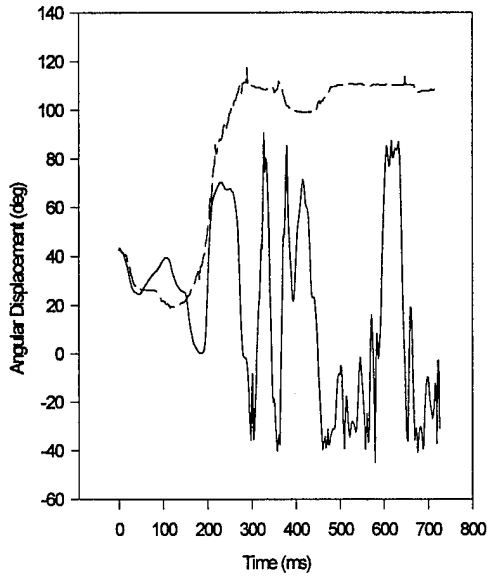
Left Shoulder Flexion



Right Shoulder Flexion

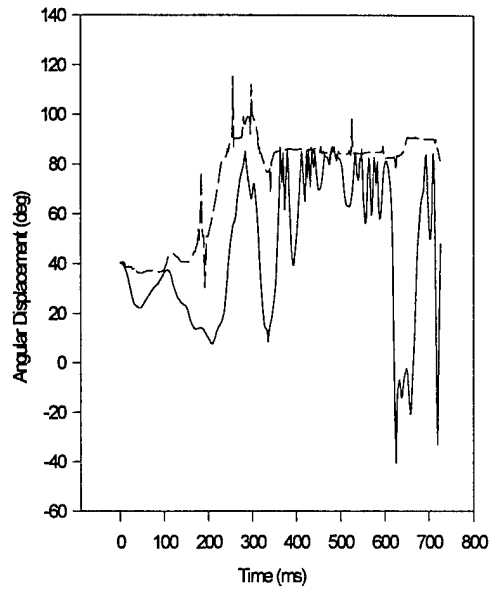


Left Shoulder Medial/Lateral



— ATB Model  
-- AMIT 79E-G2

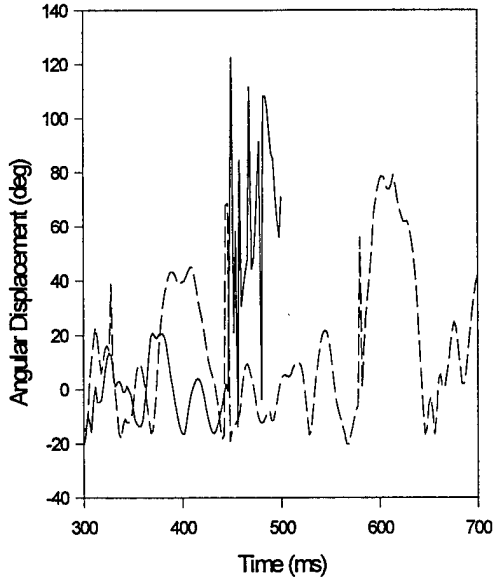
Right Shoulder Medial/Lateral



— ATB Model  
-- AMIT 79E-G2

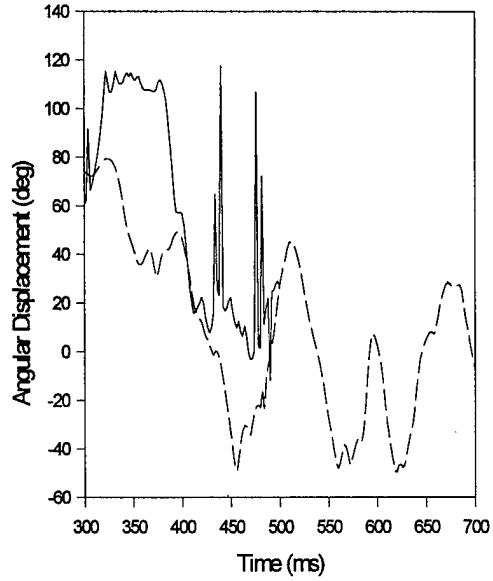
Appendix T: Comparison of ADAM Joint Angular Displacements For the First and Second ATB Simulations of AMIT 79E-G2A

**Left Elbow Flexion**



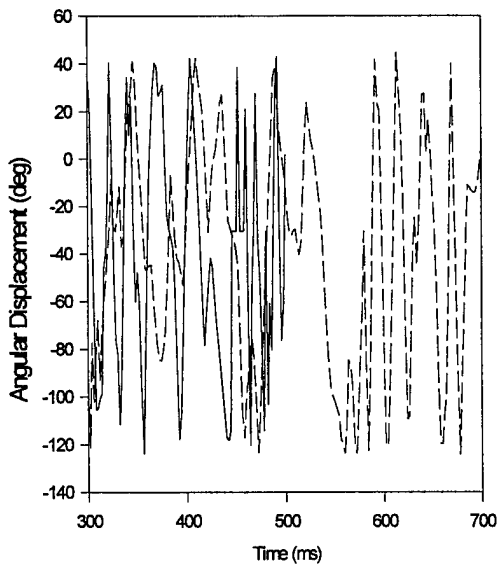
— ATB Run #1  
- - - ATB Run #2

**Right Elbow Flexion**



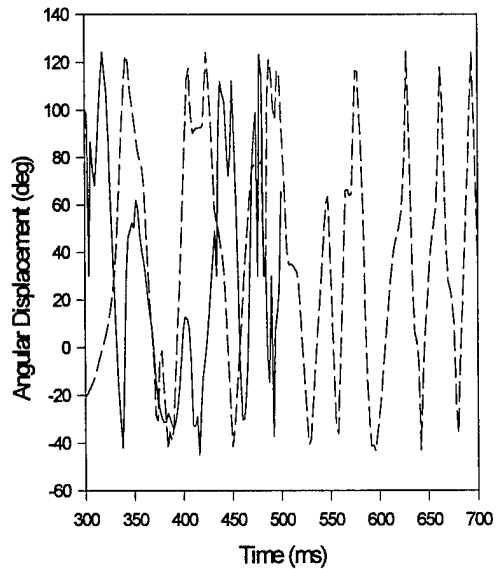
— ATB Run #1  
- - - ATB Run #2

**Left Elbow Supination/Pronation**



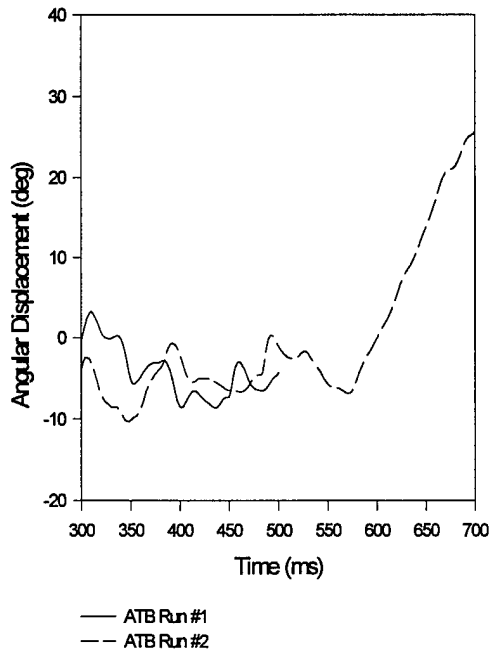
— ATB Run #1  
- - - ATB Run #2

**Right Elbow Supination/Pronation**

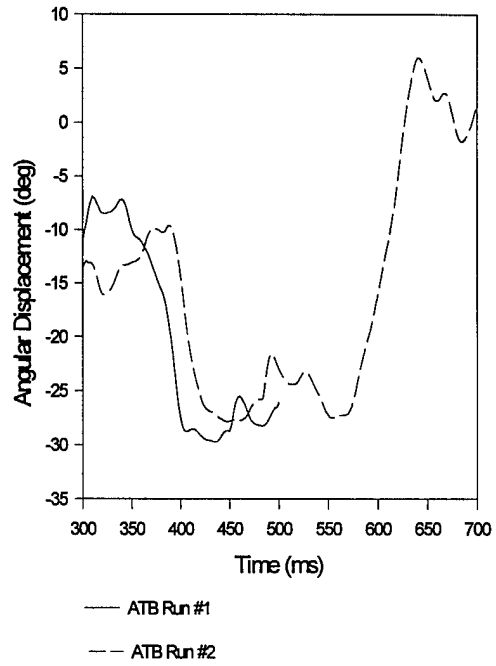


— ATB Run #1  
- - - ATB Run #2

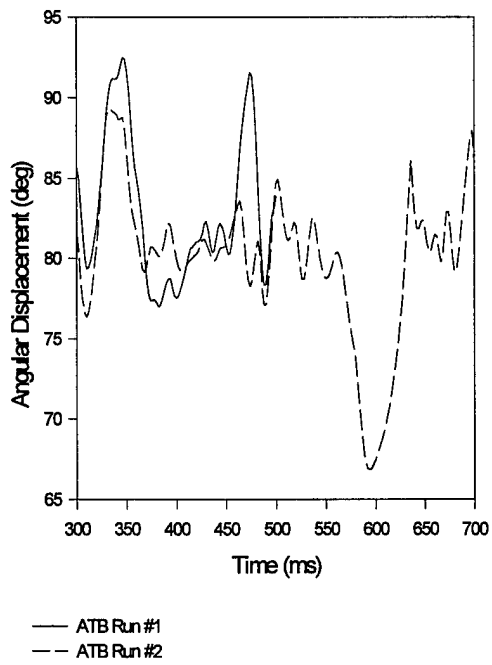
Left Hip Abduction/Adduction



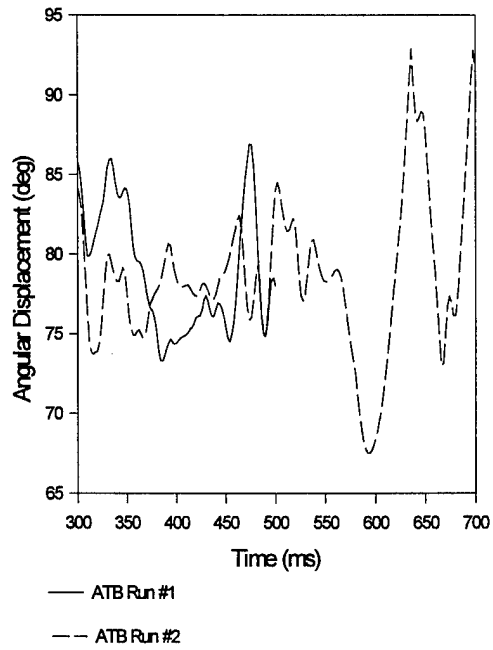
Right Hip Abduction/Adduction



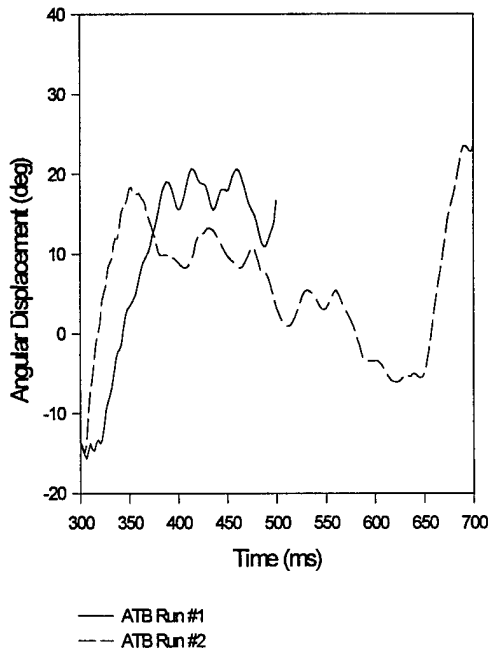
Left Hip Flexion



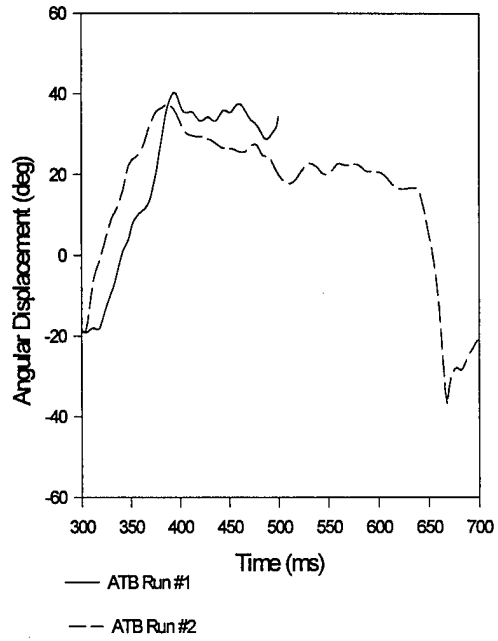
Right Hip Flexion



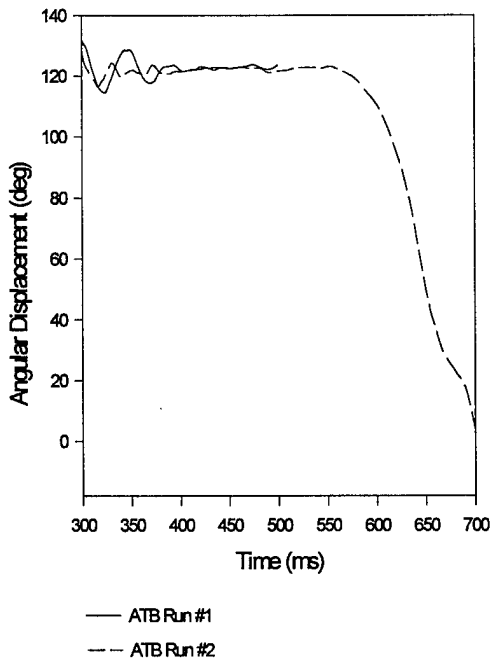
Left Hip Medial/Lateral



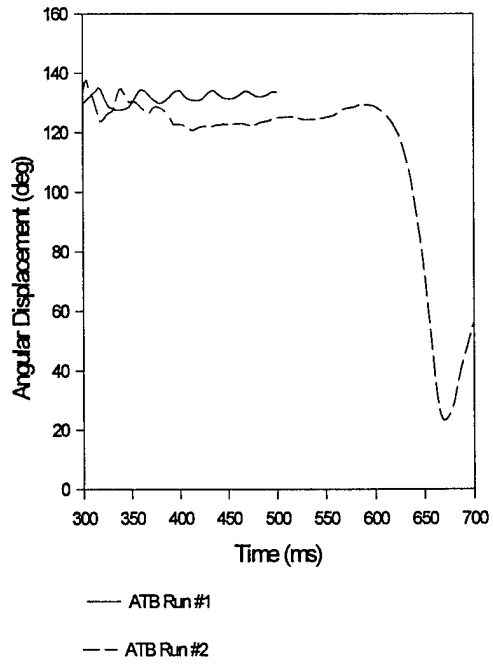
Right Hip Medial/Lateral



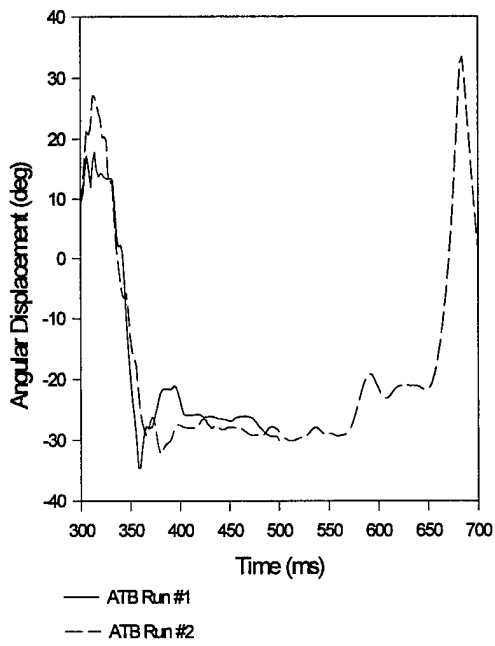
Left Knee Flexion



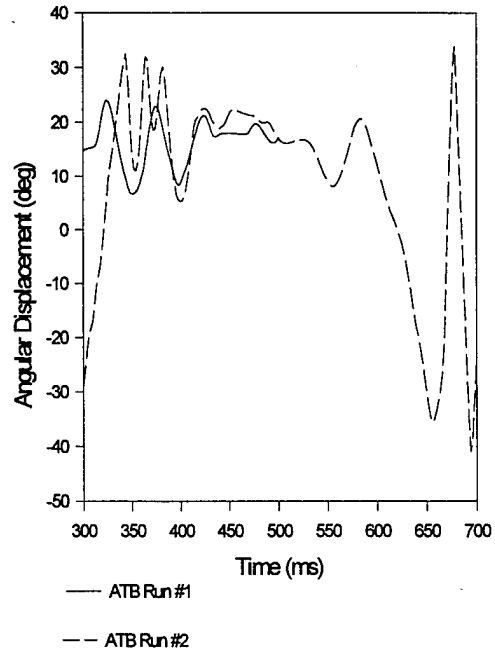
Right Knee Flexion



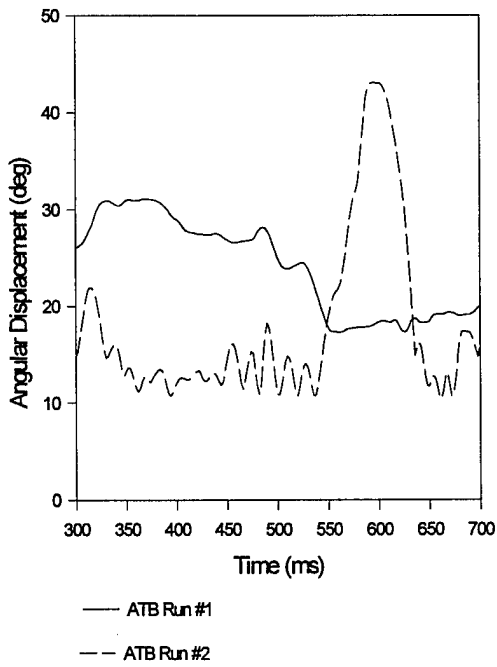
Left Knee Medial/Lateral



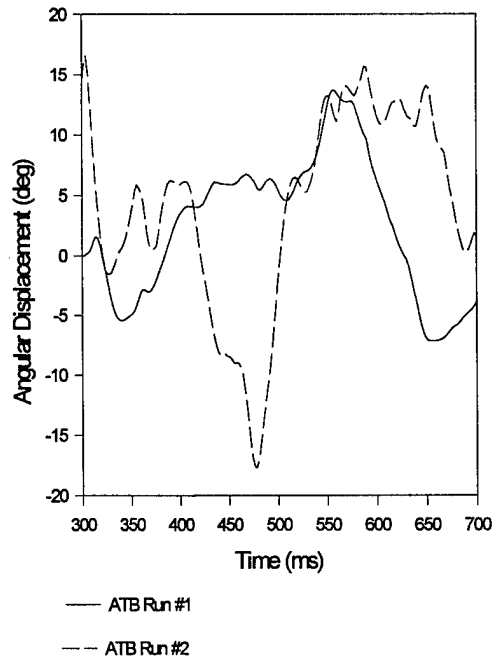
Right Knee Medial/Lateral



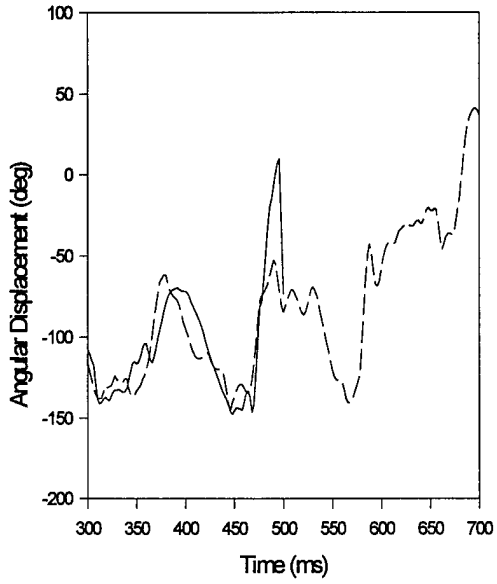
Lumbar Pitch



Lumbar Roll

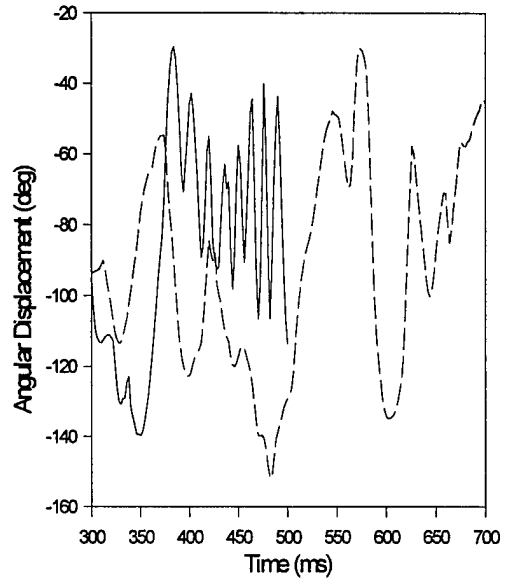


Left Shoulder Abduction/Adduction



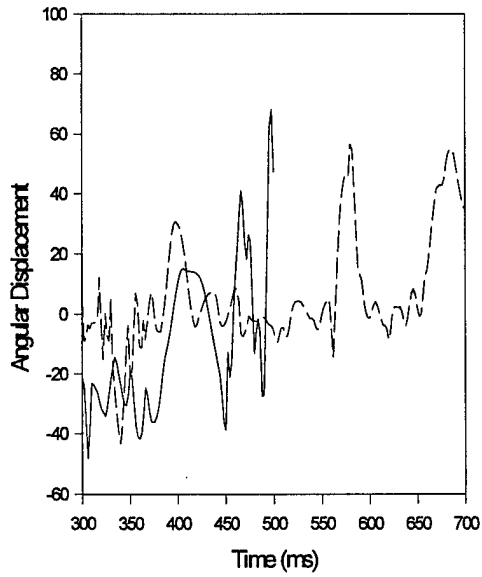
— ATB Run #1  
- - - ATB Run #2

Right Shoulder Abduction/Adduction



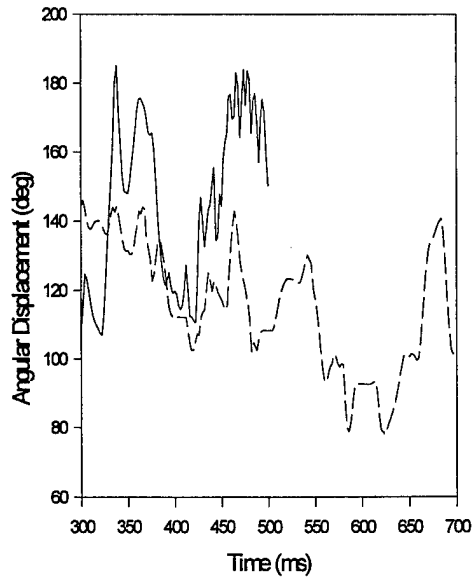
— ATB Run #1  
- - - ATB Run #2

Left Shoulder Coronal Plane Abduction/Adduction



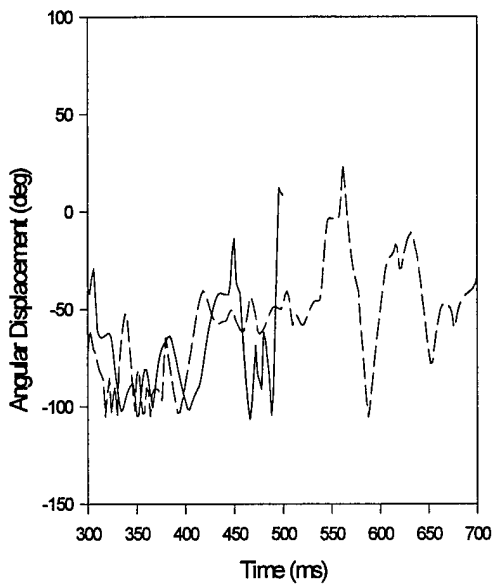
— ATB Run #1  
- - - ATB Run #2

Right Shoulder Coronal Plane Abduction/Adduction



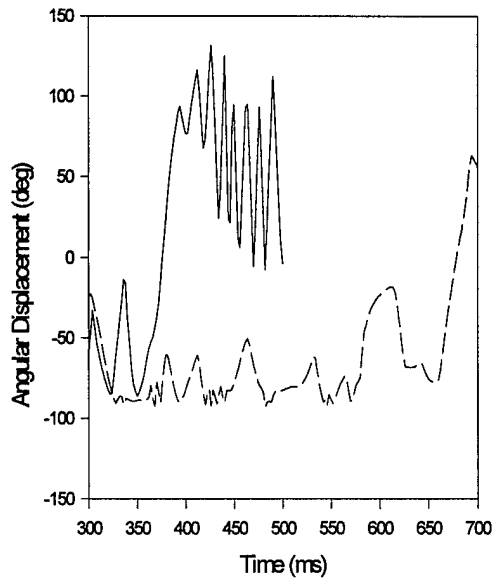
— ATB Run #1  
- - - ATB Run #2

Left Shoulder Flexion



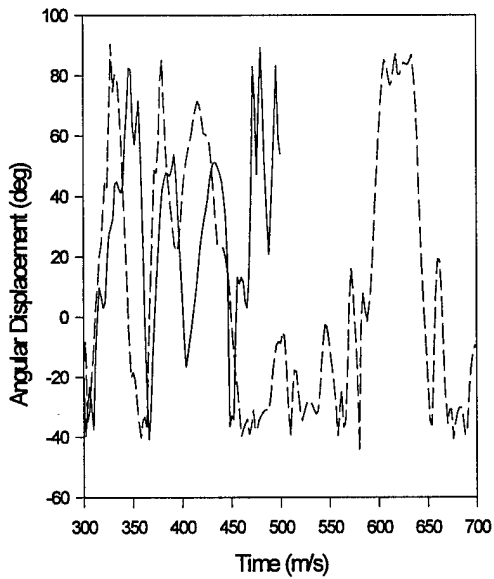
— ATB Run #1  
-- ATB Run #2

Right Shoulder Flexion



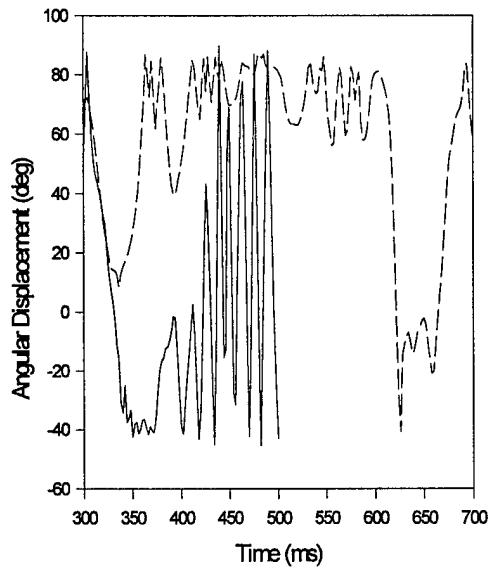
— ATB Run #1  
-- ATB Run #2

Left Shoulder Medial/Lateral



— ATB Run #1  
-- ATB Run #2

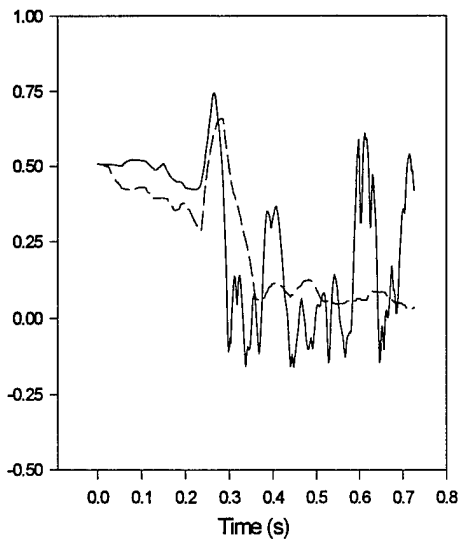
Right Shoulder Medial/Lateral



— ATB Run #1  
-- ATB Run #2

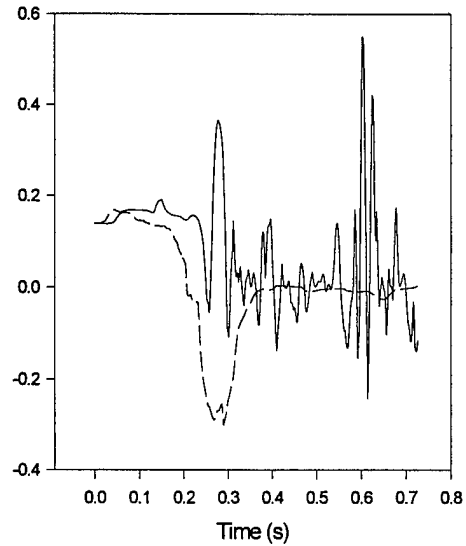
Appendix U: ADAM Joint Angular Displacements For the Second ATB Simulation of AMIT 79E-G2A Described in Terms of Quaternion Elements

**Left Elbow  
First Element of the Quaternion**



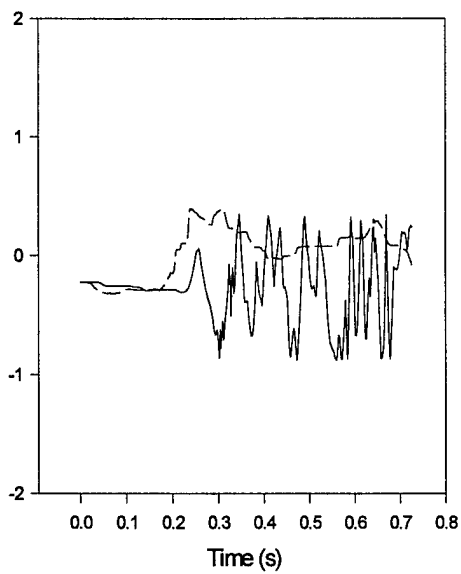
— ATB Model  
-- AMIT 79E-G2

**Left Elbow  
Second Element of the Quaternion**



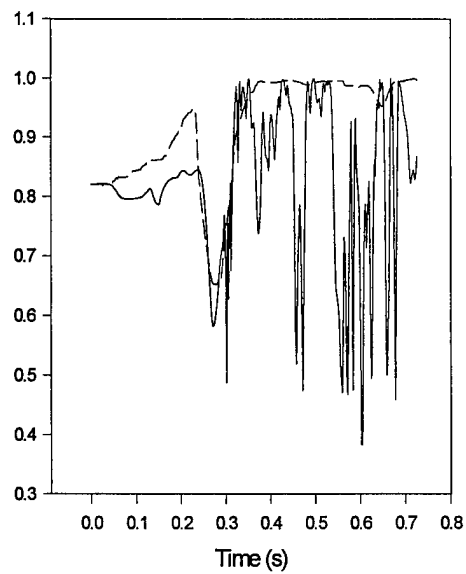
— ATB Model  
-- AMIT 79E-G2

**Left Elbow  
Third Element of the Quaternion**



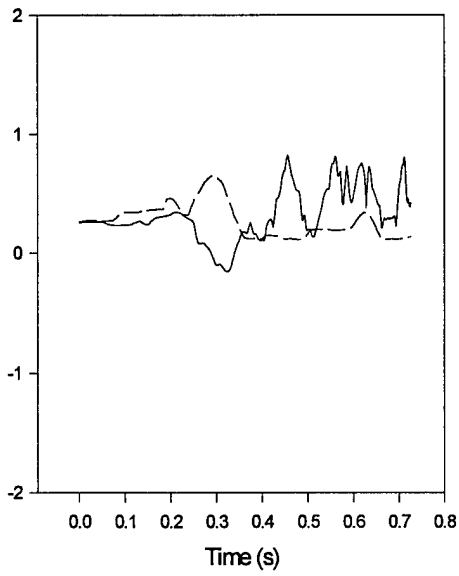
— ATB Model  
-- AMIT 79E-G2

**Left Elbow  
Fourth Element of the Quaternion**



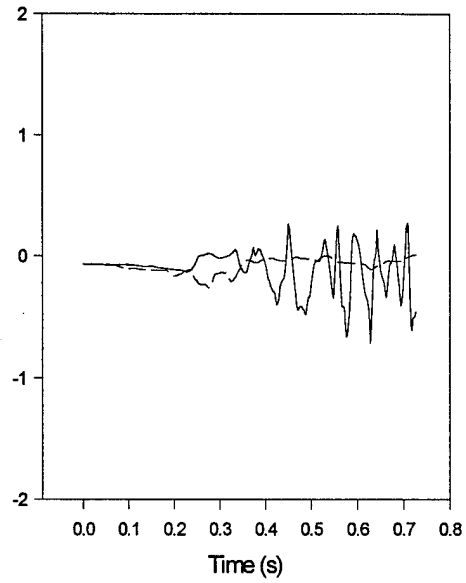
— ATB Model  
-- AMIT 79E-G2

Right Elbow  
First Element of the Quaternion



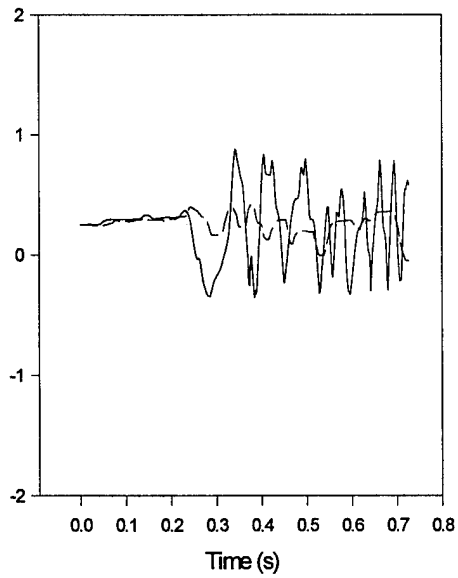
— ATB Model  
-- AMIT 79E-G2

Right Elbow  
Second Element of the Quaternion



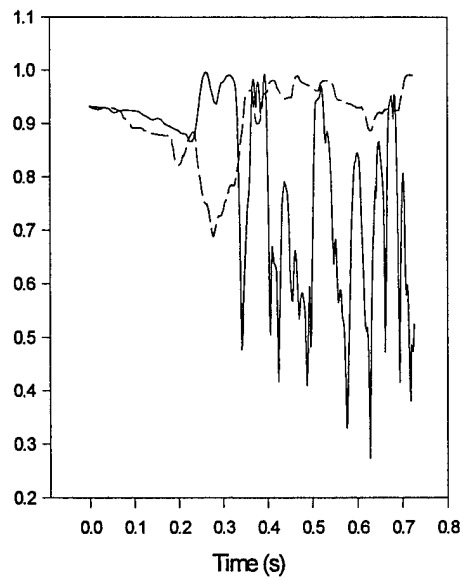
— ATB Model  
-- AMIT 79E-G2

Right Elbow  
Third Element of the Quaternion



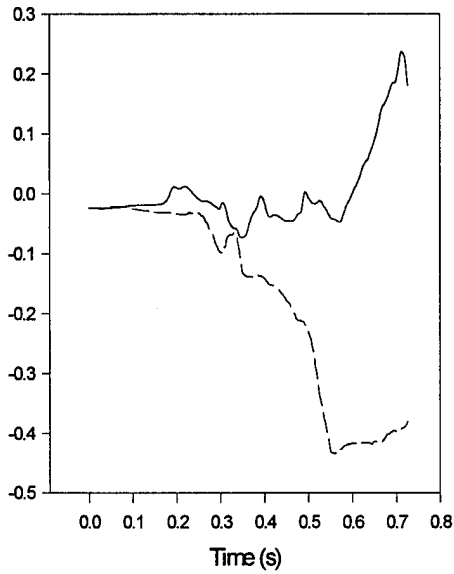
— ATB Model  
-- AMIT 79E-G2

Right Elbow  
Fourth Element of the Quaternion



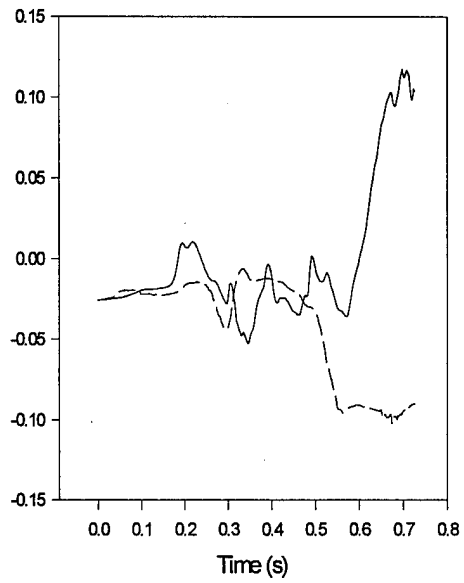
— ATB Model  
-- AMIT 79E-G2

Left Hip  
First Element of the Quaternion



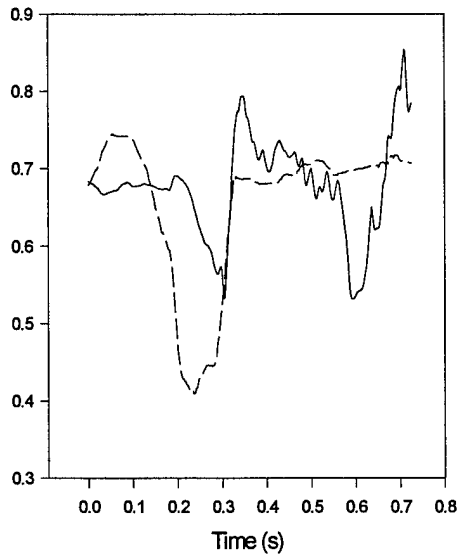
— ATB Model  
-- AMIT 79E-G2

Left Hip  
Second Element of the Quaternion



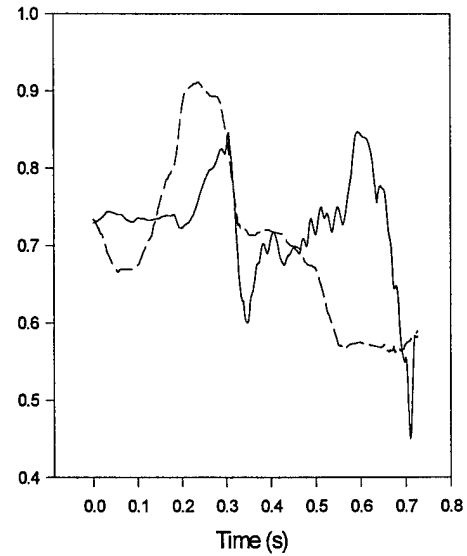
— ATB Model  
-- AMIT 79E-G2

Left Hip  
Third Element of the Quaternion



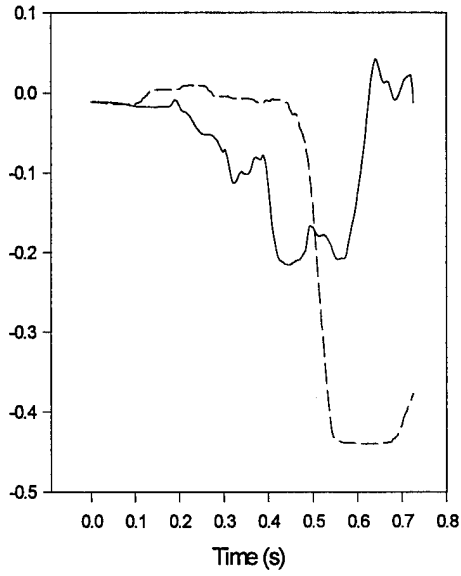
— ATB Model  
-- AMIT 79E-G2

Left Hip  
Fourth Element of the Quaternion



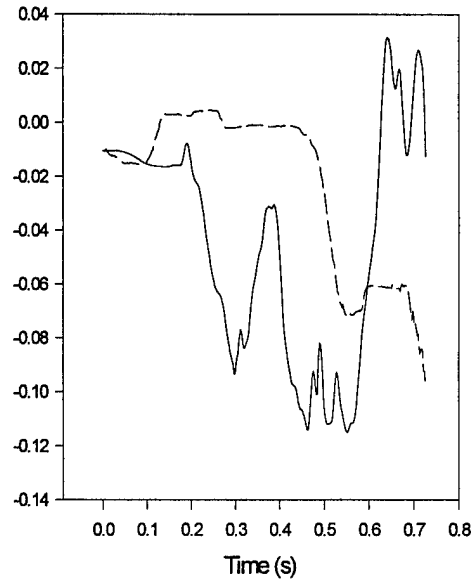
— ATB Model  
-- AMIT 79E-G2

Right Hip  
First Element of the Quaternion



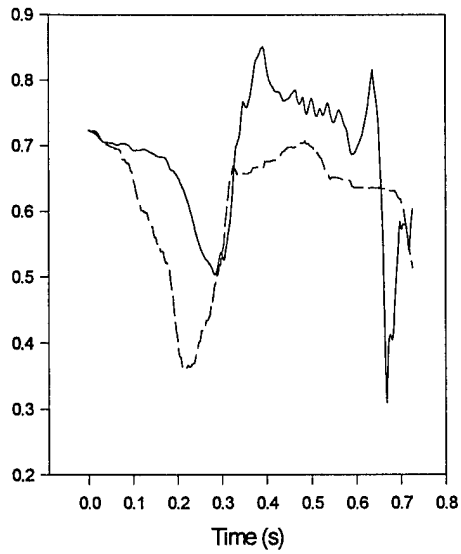
— ATB Model  
-- AMIT 79E-G2

Right Hip  
Second Element of the Quaternion



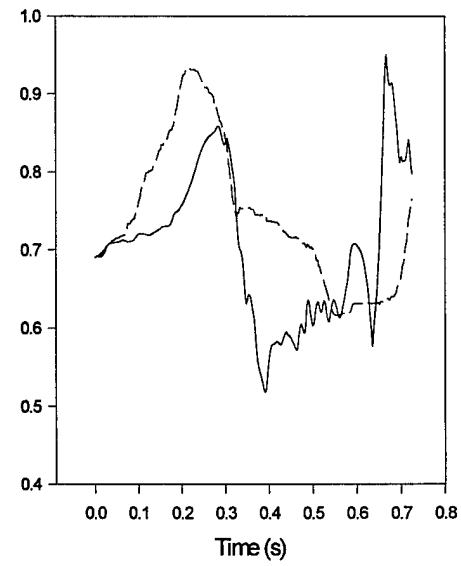
— ATB Model  
-- AMIT 79E-G2

Right Hip  
Third Element of the Quaternion



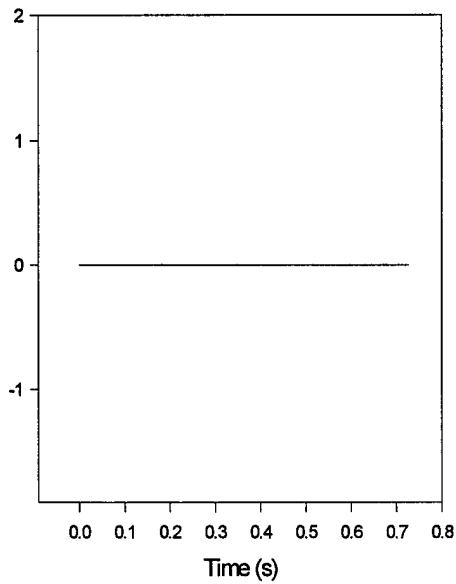
— ATB Model  
-- AMIT 79E-G2

Right Hip  
Fourth Element of the Quaternion



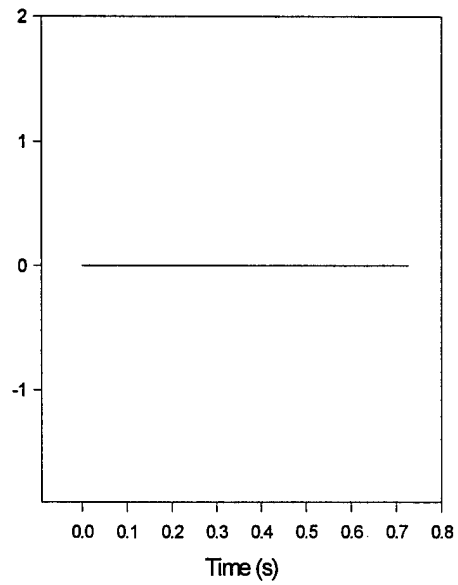
— ATB Model  
-- AMIT 79E-G2

Left Knee  
First Element of the Quaternion



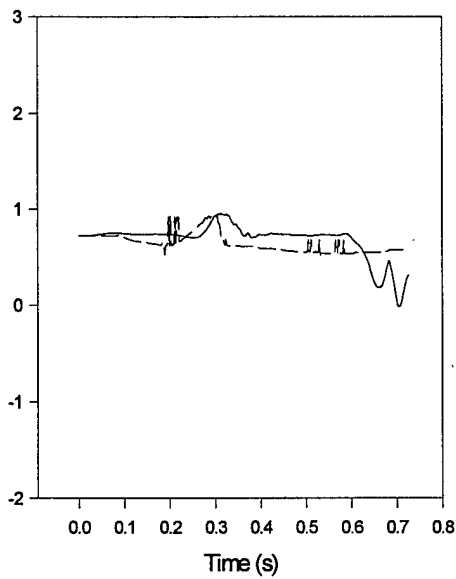
— ATB Model  
-- AMIT 79E-G2

Left Knee  
Second Element of the Quaternion



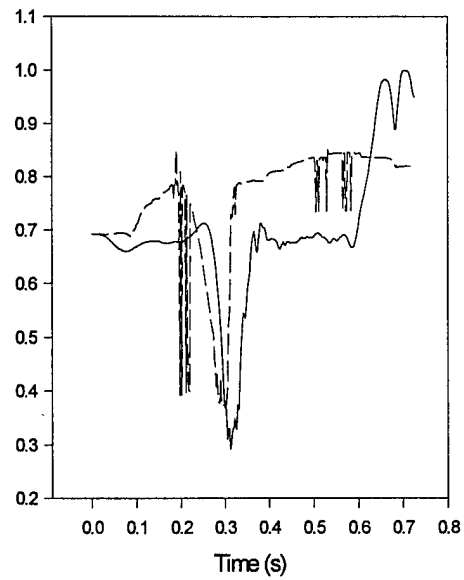
— ATB Model  
-- AMIT 79E-G2

Left Knee  
Third Element of the Quaternion



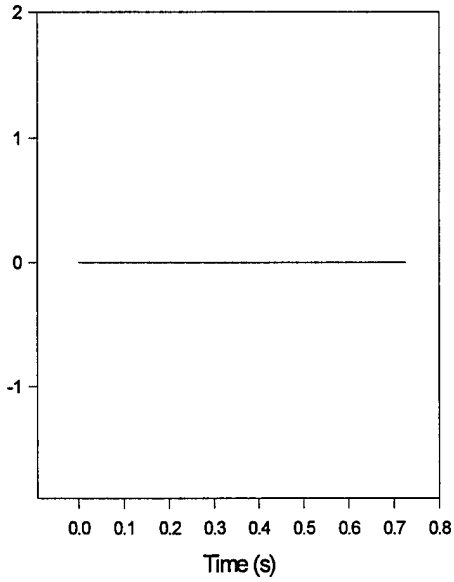
— ATB Model  
-- AMIT 79E-G2

Left Knee  
Fourth Element of the Quaternion



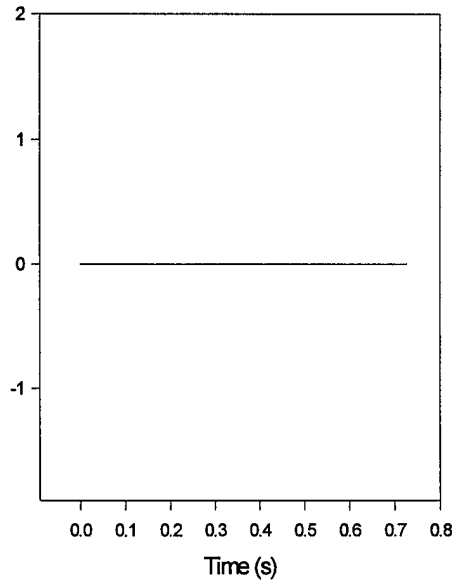
— ATB Model  
-- AMIT 79E-G2

Right Knee  
First Element of the Quaternion



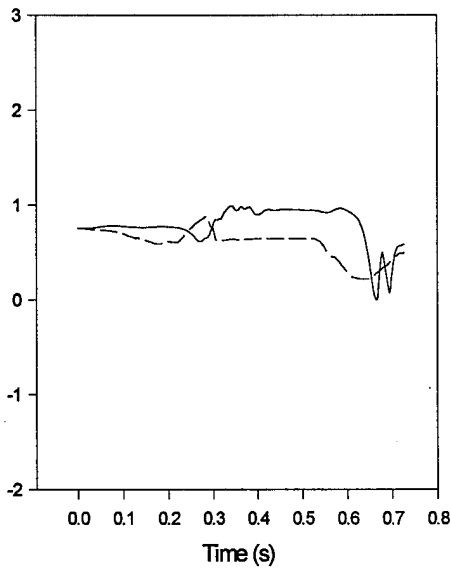
— ATB Model  
-- AMIT 79E-G2

Right Hip  
Second Element of the Quaternion



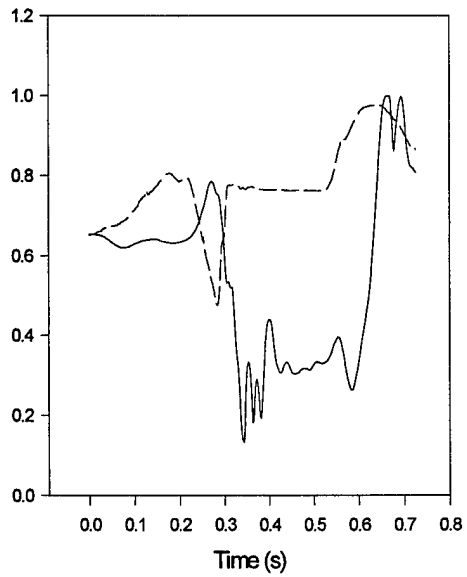
— ATB Model  
-- AMIT 79E-G2

Right Hip  
Third Element of the Quaternion



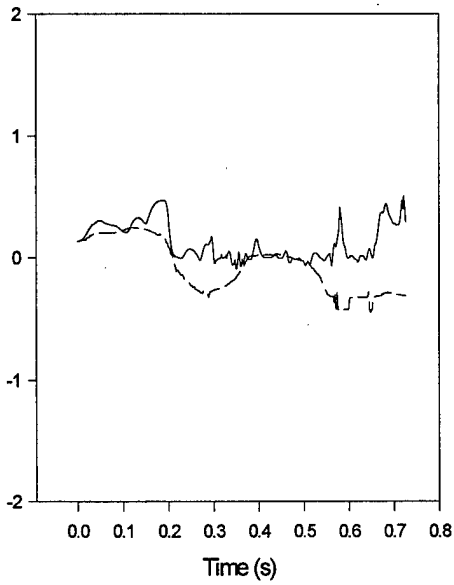
— ATB Model  
-- AMIT 79E-G2

Right Hip  
Fourth Element of the Quaternion



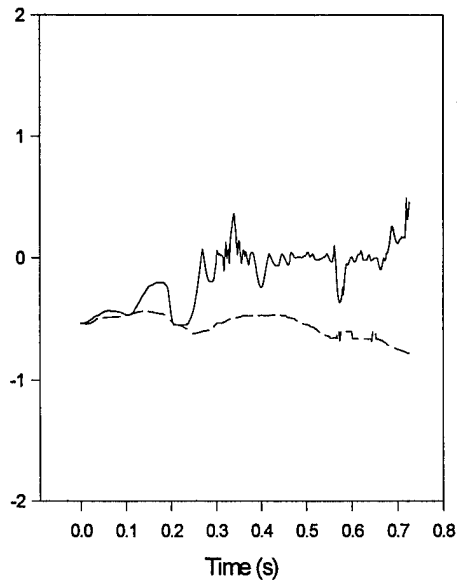
— ATB Model  
-- AMIT 79E-G2

Left Shoulder  
First Element of the Quaternion



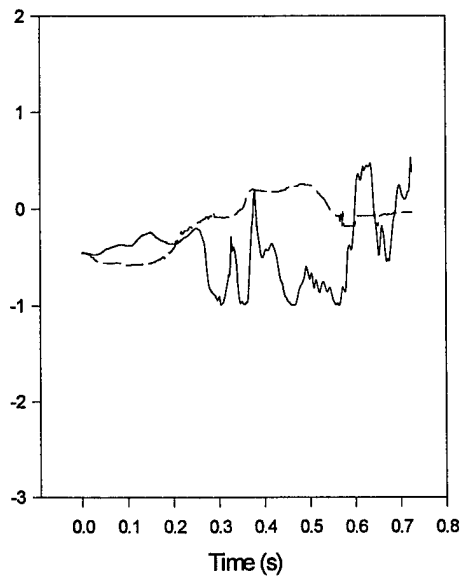
— ATB Model  
-- AMIT 79E-G2

Left Shoulder  
Second Element of the Quaternion



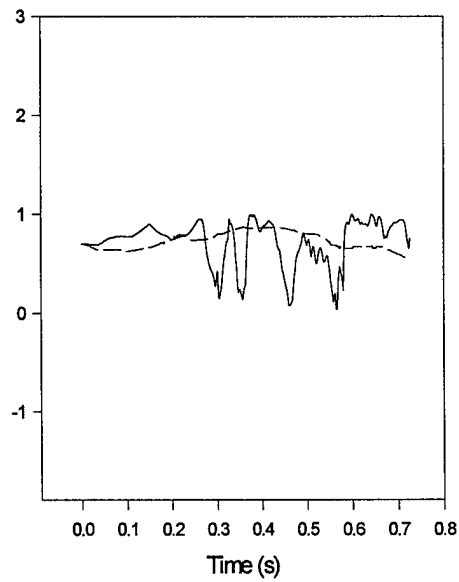
— ATB Model  
-- AMIT 79E-G2

Left Shoulder  
Third Element of the Quaternion



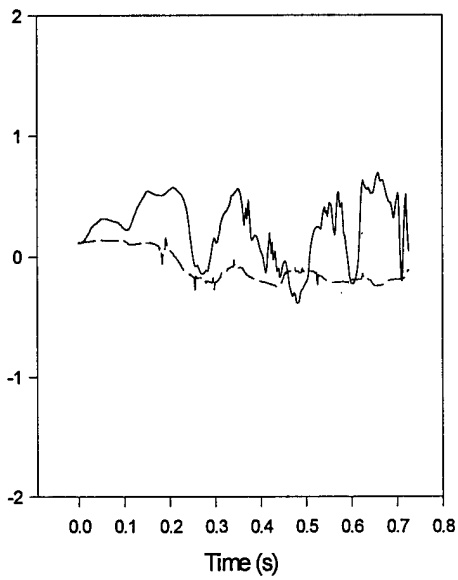
— ATB Model  
-- AMIT 79E-G2

Left Shoulder  
Fourth Element of the Quaternion

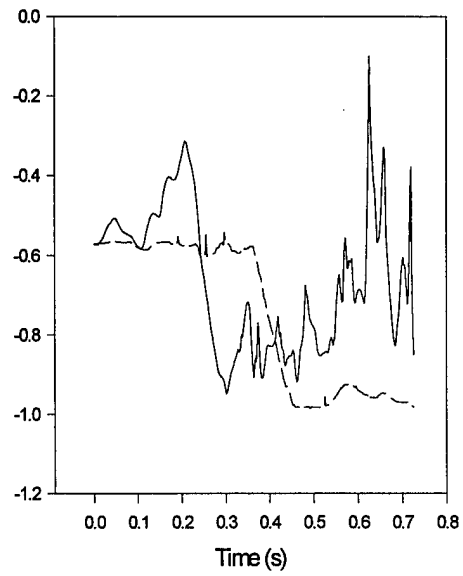


— ATB Model  
-- AMIT 79E-G2

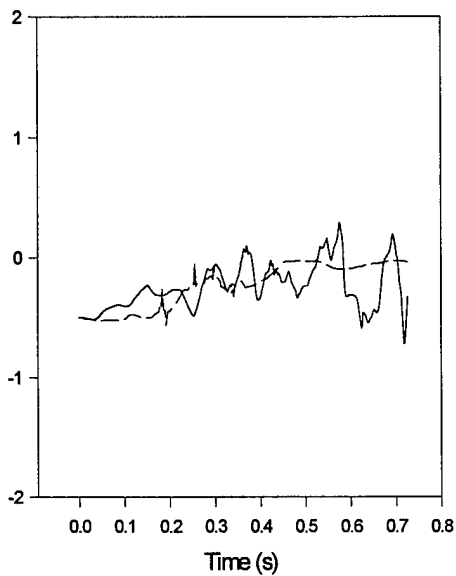
Right Shoulder  
First Element of the Quaternion



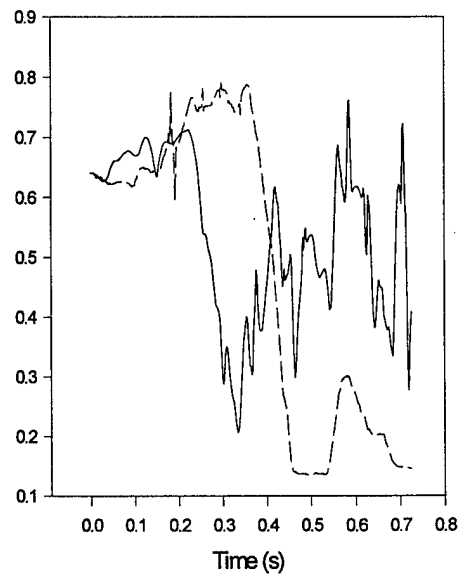
Right Shoulder  
Second Element of the Quaternion



Right Shoulder  
Third Element of the Quaternion



Right Shoulder  
Fourth Element of the Quaternion



Appendix V: Code Written In Order To Describe ADAM Joint Angular Displacements  
in Three Dimensions

```
%Clear work space
clear

%Channel 1 always loaded for time calculation purposes
load ch1.asc;

%Load precession, nutation, and spin angles from ATB simulation

load mod.t28;
lshoulder_atb=mod(:,3:5);

%Load ADAM angular measurements from AMIT 79E-G2A test

load ch43.asc;
load ch45.asc;
load ch46.asc;
lshoulder_test=[ch43(1:174,2),ch46(1:174,2),ch45(1:174,2)];

%Remove offset between what ATB considers a "0" position
%and what the "0" position of the test ADAM was defined to be.

dif_lshoulder=lshoulder_atb(1:5,:)-lshoulder_test(1:5,:);
avg_dif_lshoulder=mean(dif_lshoulder);
size_lshoulder_atb=size(lshoulder_atb);
for x=1:size_lshoulder_atb(1,1)
lshoulder_atb(x,:)=lshoulder_atb(x,:)-avg_dif_lshoulder;
end

%%%%%%%%%%%%%%%%%%%%%%%%%%%%%%%%%%%%%%%%%%%%%%%%%%%%%%%%%%%%%%%%%%%%%%%%
atb_angles=lshoulder_atb;
test_angles=lshoulder_test;
%%%%%%%%%%%%%%%%%%%%%%%%%%%%%%%%%%%%%%%%%%%%%%%%%%%%%%%%%%%%%%%%%%%%%%%%

size_atb_angles=size(atb_angles);
for index=1:size_atb_angles(1,1);

%Define angles in radian
phi_atb=atb_angles(index,1)./57.3;
theta_atb=atb_angles(index,2)./57.3;
psi_atb=atb_angles(index,3)./57.3;

%Define elements in rotation matrix
```

```

    r_atb11(index)=cos(psi_atb)*cos(phi_atb)-
cos(theta_atb)*sin(phi_atb)*sin(psi_atb);
    r_atb21(index)=-sin(psi_atb)*cos(phi_atb)-
cos(theta_atb)*sin(phi_atb)*cos(psi_atb);
    r_atb31(index)=sin(theta_atb)*sin(phi_atb);
    r_atb12(index)=cos(psi_atb)*sin(phi_atb)+cos(theta_atb)*cos(phi_atb)*sin(psi_at
b);
    r_atb22(index)=-
sin(psi_atb)*sin(phi_atb)+cos(theta_atb)*cos(phi_atb)*cos(psi_atb);
    r_atb32(index)=-sin(theta_atb)*cos(phi_atb);
    r_atb13(index)=sin(psi_atb)*sin(theta_atb);
    r_atb23(index)=cos(psi_atb)*sin(theta_atb);
    r_atb33(index)=cos(theta_atb);

```

```

%Define angles in radian
phi_test=test_angles(index,1)/57.3;
theta_test=test_angles(index,2)/57.3;
psi_test=test_angles(index,3)/57.3;

```

```

%Define elements in rotation matrix
    r_test11(index)=cos(psi_test)*cos(phi_test)-
cos(theta_test)*sin(phi_test)*sin(psi_test);
    r_test21(index)=-sin(psi_test)*cos(phi_test)-
cos(theta_test)*sin(phi_test)*cos(psi_test);
    r_test31(index)=sin(theta_test)*sin(phi_test);
    r_test12(index)=cos(psi_test)*sin(phi_test)+cos(theta_test)*cos(phi_test)*sin(psi_
test);
    r_test22(index)=-
sin(psi_test)*sin(phi_test)+cos(theta_test)*cos(phi_test)*cos(psi_test);
    r_test32(index)=-sin(theta_test)*cos(phi_test);
    r_test13(index)=sin(psi_test)*sin(theta_test);
    r_test23(index)=cos(psi_test)*sin(theta_test);
    r_test33(index)=cos(theta_test);

```

```

%Calculate angles between x atb axis and x test axis, y atb axis and y test
%axis and z atb axis and z test axis

```

```

d1x=(r_atb11(index)^2+r_atb12(index)^2+r_atb13(index)^2)^.5;
d2x=(r_test11(index)^2+r_test12(index)^2+r_test13(index)^2)^.5;
xatbtest_angle(index)=57.3*acos((r_atb11(index)*r_test11(index)+r_atb12(index)*r_test
12(index)+r_atb13(index)*r_test13(index))/(d1x*d2x));

d1y=(r_atb21(index)^2+r_atb22(index)^2+r_atb23(index)^2)^.5;
d2y=(r_test21(index)^2+r_test22(index)^2+r_test23(index)^2)^.5;

```

```
yatbtest_angle(index)=57.3*acos((r_atb21(index)*r_test21(index)+r_atb22(index)*r_test22(index)+r_atb23(index)*r_test23(index))/(d1y*d2y));
```

```
d1z=(r_atb31(index)^2+r_atb32(index)^2+r_atb33(index)^2)^.5;  
d2z=(r_test31(index)^2+r_test32(index)^2+r_test33(index)^2)^.5;  
zabtest_angle(index)=57.3*acos((r_atb31(index)*r_test31(index)+r_atb32(index)*r_test32(index)+r_atb33(index)*r_test33(index))/(d1z*d2z));
```

```
end;
```

```
%Plot angles between x atb line and x test line, y atb line and y test line, and z atb  
%line and z test line  
time=ch1(1:174,1);  
figure  
title('Left Shoulder');  
plot(time,zabtest_angle,time,xatbtest_angle,time,yatbtest_angle);
```

```
%Draw x, y, & z labels  
figure  
title('Left Shoulder');  
text(1.1,0,0,'X');  
hold;  
text(0,1.1,0,'Y');  
text(0,0,1.1,'Z');  
axis('off');
```

```
%Draw Inertial axes  
xi1=[-1;1];  
xi2=[0;0];  
xi3=[0;0];  
hix=line(xi1,xi2,xi3);  
set(hix,'linewidth',2);  
%RED  
set(hix,'color',[1 0 0]);  
drawnow;
```

```
yi1=[0;0];  
yi2=[-1;1];  
yi3=[0;0];  
hiy=line(yi1,yi2,yi3);  
set(hiy,'linewidth',2);  
%BLACK  
set(hiy,'color',[0 0 0]);  
drawnow;
```

```

zi1=[0;0];
zi2=[0;0];
zi3=[-1;1];
hiz=line(zi1,zi2,zi3);
set(hiz,'linewidth',2);
%BLUE
set(hiz,'color',[0 0 1]);
drawnow;

for index=1:sizeatb_angles(1,1);

%Draw x y z atb axes
x1_atb=[0;r_atb11(index)];
x2_atb=[0;r_atb12(index)];
x3_atb=[0;r_atb13(index)];
h1(index)=line(x1_atb,x2_atb,x3_atb);
%YELLOW
set(h1,'color',[1 1 .0625]);
%drawnow

azimuth=15;
elevation=-25;
view(azimuth,elevation);

%legend(h1,'x atb')

y1_atb=[0;r_atb21(index)];
y2_atb=[0;r_atb22(index)];
y3_atb=[0;r_atb23(index)];
h2(index)=line(y1_atb,y2_atb,y3_atb);
%GREEN
set(h2,'color',[0 1 0]);
%drawnow

z1_atb=[0;r_atb31(index)];
z2_atb=[0;r_atb32(index)];
z3_atb=[0;r_atb33(index)];
h3(index)=line(z1_atb,z2_atb,z3_atb);
%LIGHT BLUE
set(h3,'color',[0 1 1]);
%drawnow

%Draw x y z test axes
x1_test=[0;r_test11(index)];
x2_test=[0;r_test12(index)];

```

```

x3_test=[0;r_test13(index)];
h4(index)=line(x1_test,x2_test,x3_test);
%PEACH
set(h4,'color',[1 .3 .3]);
set(h4,'linestyle','-');
%drawnow
view(azimuth,elevation);

y1_test=[0;r_test21(index)];
y2_test=[0;r_test22(index)];
y3_test=[0;r_test23(index)];
h5(index)=line(y1_test,y2_test,y3_test);
%PURPLE
set(h5,'color',[1 .2 1]);
set(h5,'linestyle','-');
%drawnow

z1_test=[0;r_test31(index)];
z2_test=[0;r_test32(index)];
z3_test=[0;r_test33(index)];
h6(index)=line(z1_test,z2_test,z3_test);
%ORANGE
set(h6,'color',[1 .5 .0625]);
set(h6,'linestyle','-');
drawnow

if index==1
pause
elseif Simulation_time>=5.144 & Simulation_time<=5.1445
pause
end

lines_off=1;
Simulation_time=ch1(index,1)

if lines_off==1 & index>0
%Turn atb lines off
set(h1(index-0),'visible','off');
set(h2(index-0),'visible','off');
set(h3(index-0),'visible','off');

%Turn test lines off
set(h4(index-0),'visible','off');
set(h5(index-0),'visible','off');
set(h6(index-0),'visible','off');

```

drawnow  
end

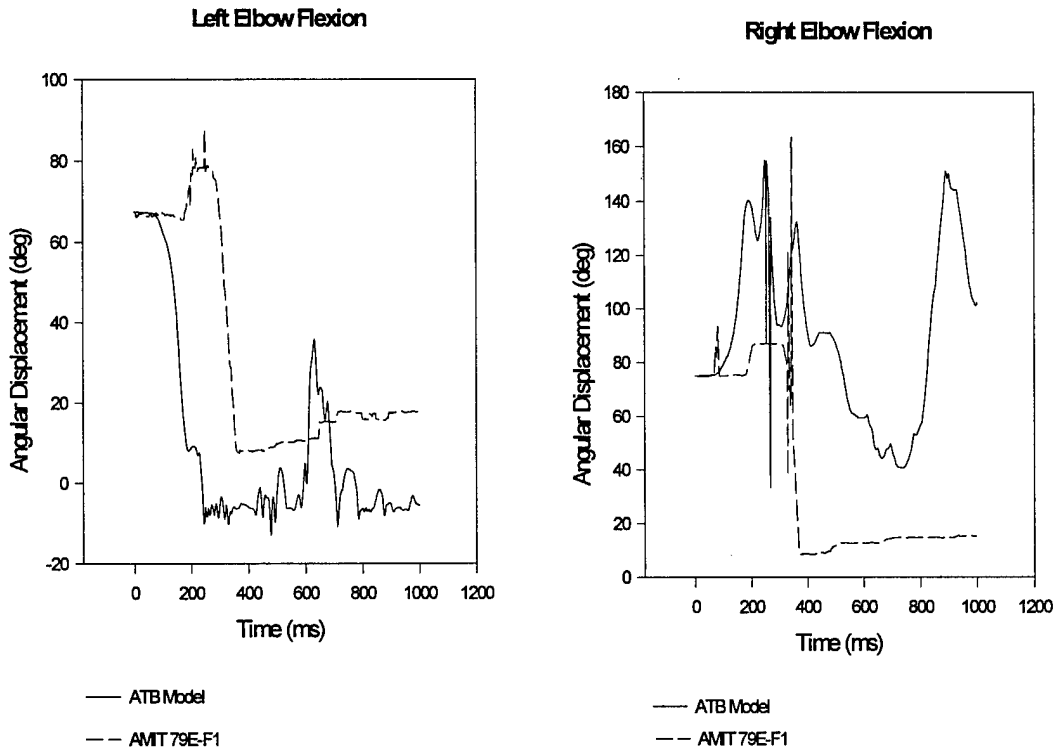
end

Appendix W: AMIT 79E-F1 Cut-off Frequencies

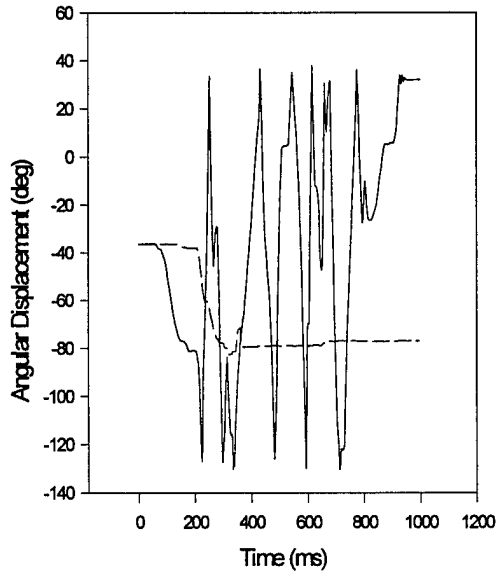
Signal	Cut-off Frequency (Hz)
X Acceleration Accelerometer "A"	10
Y Acceleration Accelerometer "A"	70
Z Acceleration Accelerometer "A"	15
X Angular Velocity	15
Y Angular Velocity	25
Z Angular Velocity	35

Appendix X: ADAM Joint Angular Displacement Comparisons For the First ATB Simulation of AMIT 79E-F1

The following plots are comparisons between the actual motion of the ADAM during the AMIT 79E-F1 test and the motion of the ADAM modeled by the ATB simulation of the AMIT 79E-F1 test. The data from the ATB model presented are shifted so that the zero angle for each joint defined by the ATB model is the same as the zero angle defined during the AMIT 79E-F1 test. The polarity of certain plots are also reversed. This polarity reversal is explained in Chapter III of this thesis.

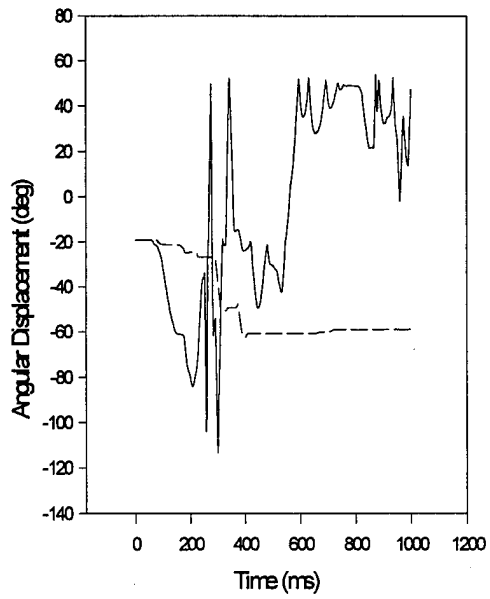


Left Elbow Supination/Pronation



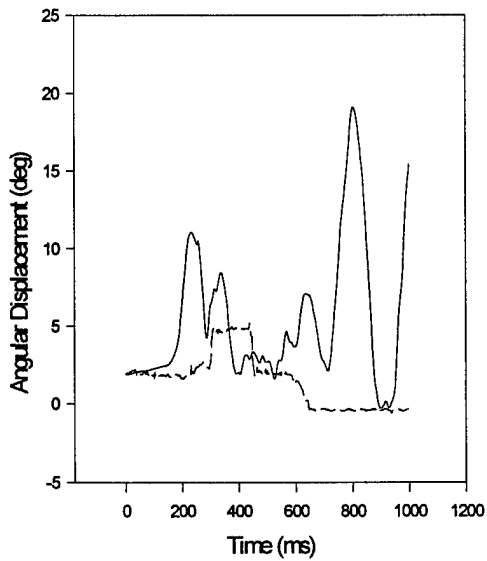
— ATB Model  
-- AMIT 79E-F1

Right Elbow Supination/Pronation



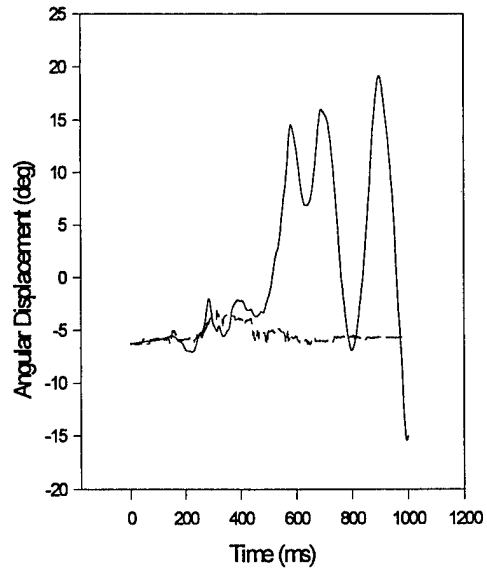
— ATB Model  
-- AMIT 79E-F1

Left Hip Abduction/Adduction



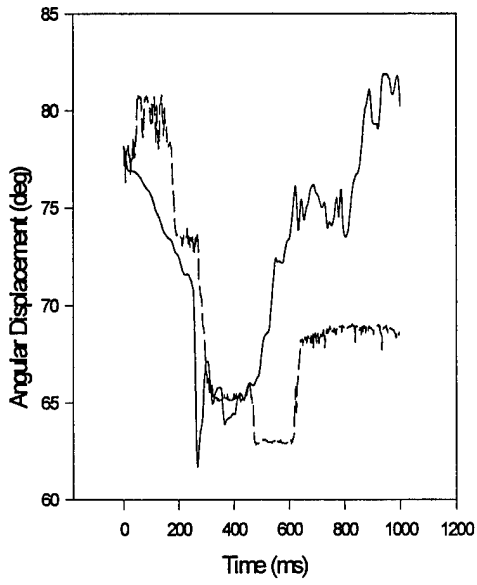
— ATB Model  
-- AMIT 79E-F1

Right Hip Abduction/Adduction



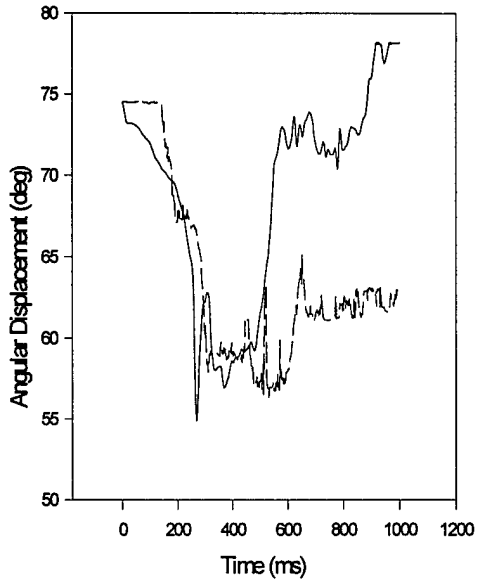
— ATB Model  
-- AMIT 79E-F1

**Left Hip Flexion**



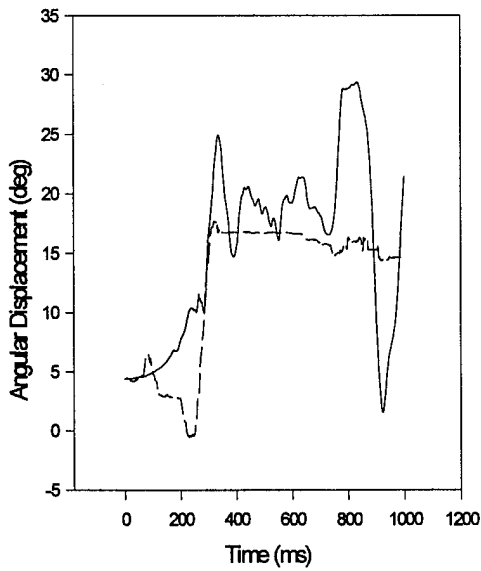
— ATB Model  
- - - AMT 79E-F1

**Right Hip Flexion**



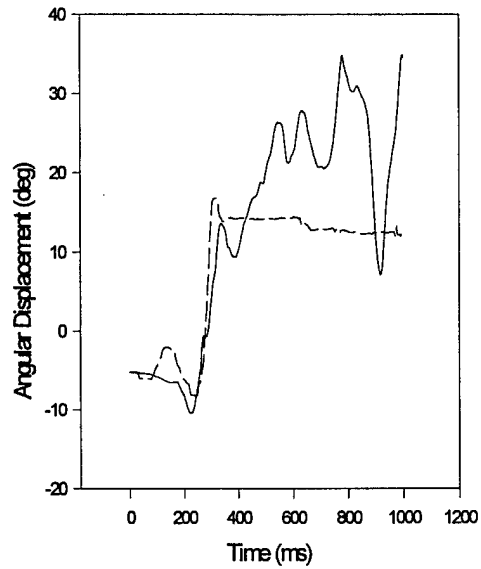
— ATB Model  
- - - AMT 79E-F1

**Left Hip Medial/Lateral**



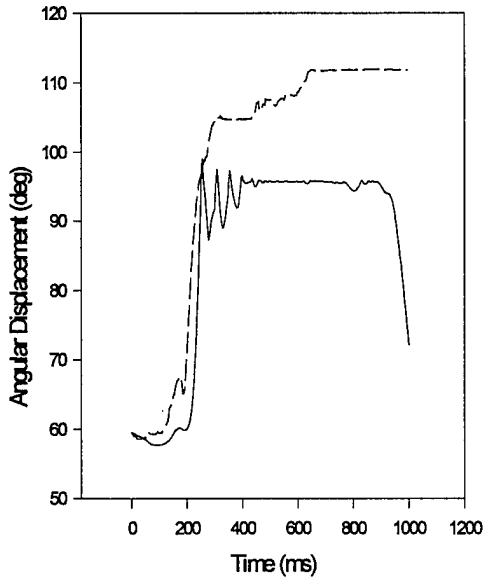
— ATB Model  
- - - AMT 79E-F1

**Right Hip Medial/Lateral**



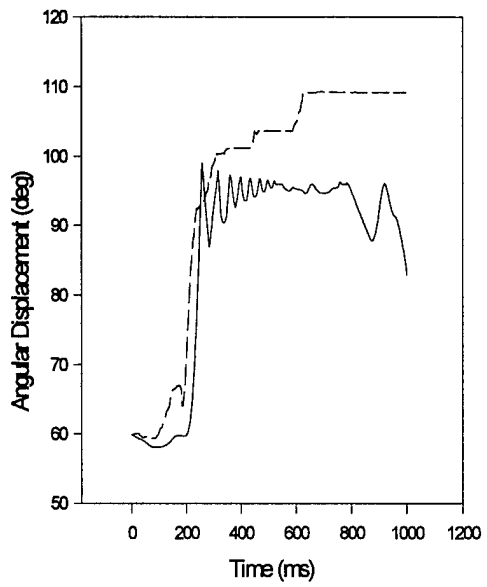
— ATB Model  
- - - AMT 79E-F1

Left Knee Flexion



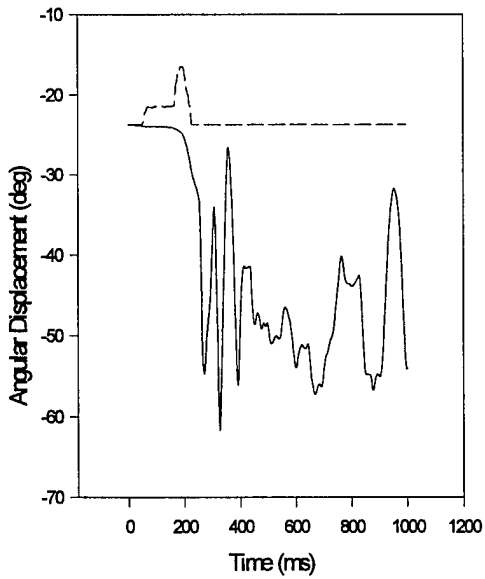
— ATB Model  
-- AMT 79E-F1

Right Knee Flexion



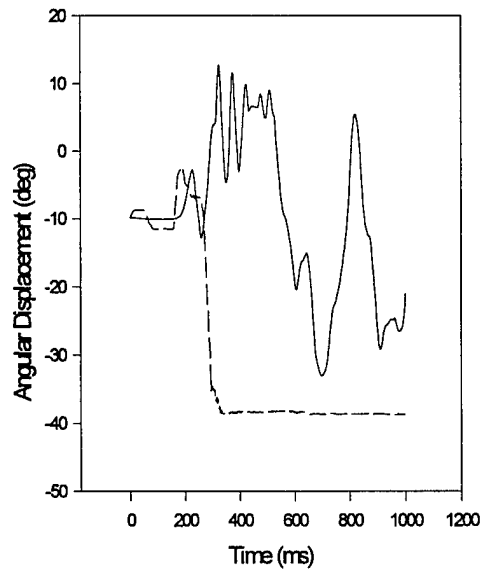
— ATB Model  
-- AMT 79E-F1

Left Knee Medial/Lateral



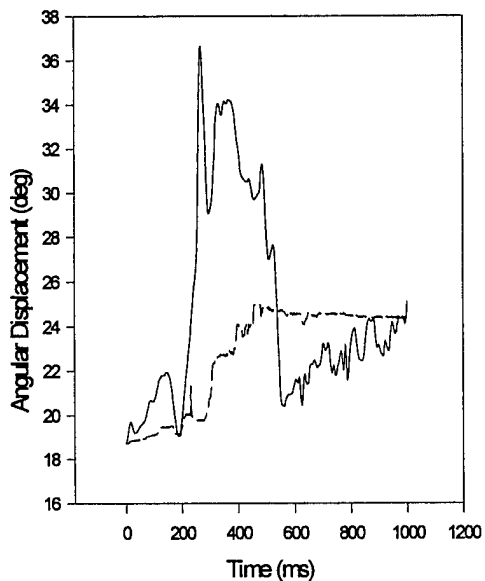
— ATB Model  
-- AMT 79E-F1

Right Knee Medial/Lateral



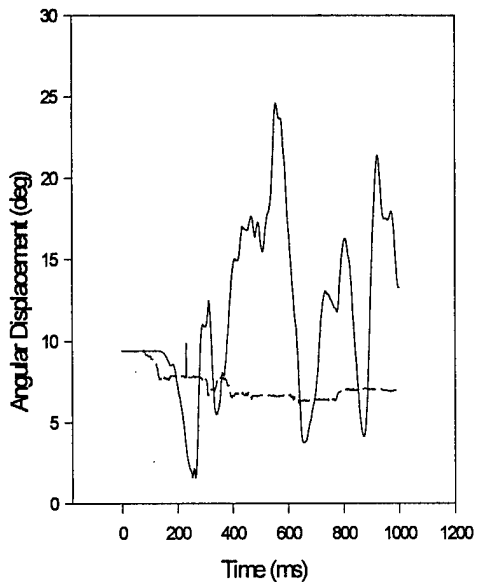
— ATB Model  
-- AMT 79E-F1

Lumbar Pitch



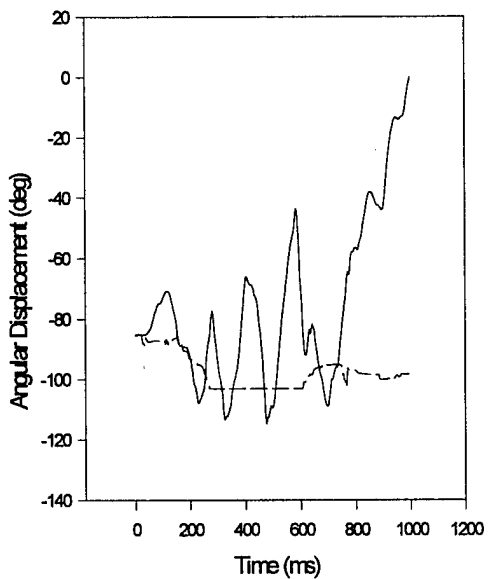
— ATB Model  
-- AMIT 79E-F1

Lumbar Roll



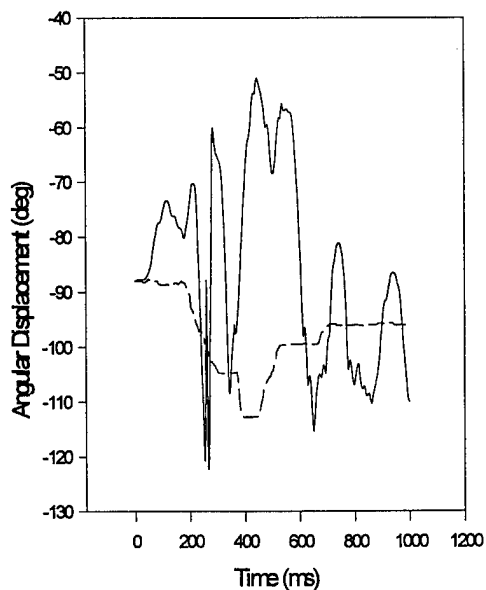
— ATB Model  
-- AMIT 79E-F1

Left Shoulder Abduction/Adduction



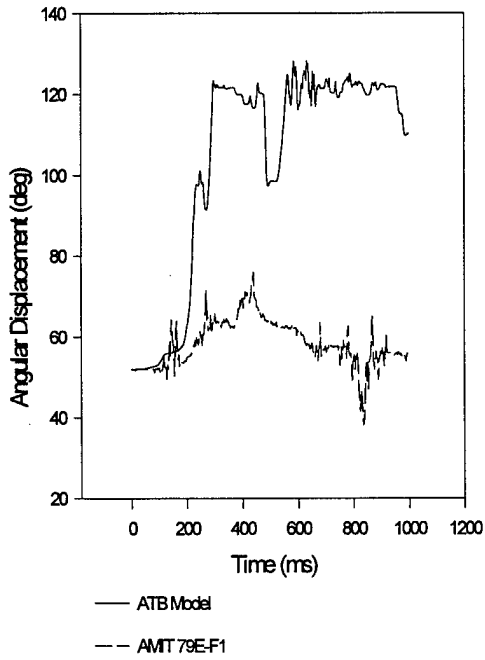
— ATB Model  
-- AMIT 79E-F1

Right Shoulder Abduction/Adduction

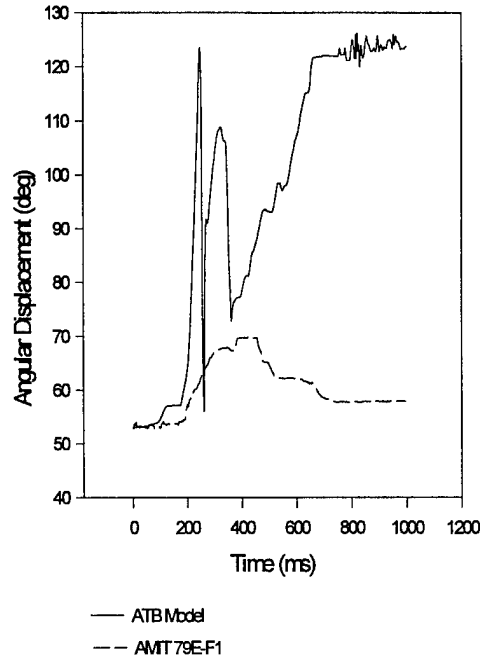


— ATB Model  
-- AMIT 79E-F1

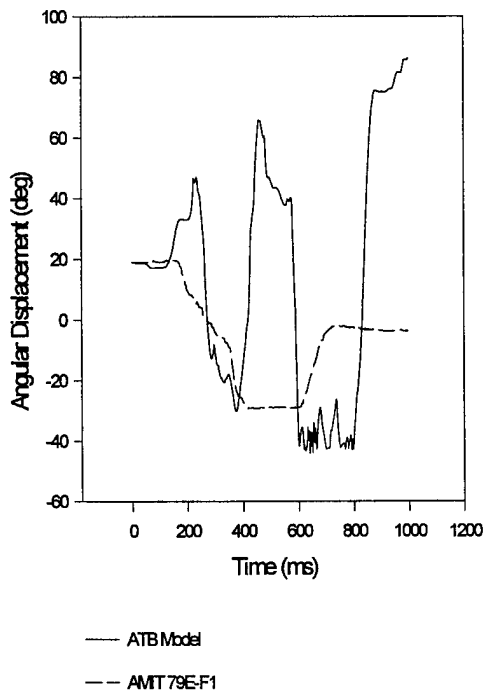
Left Shoulder Coronal Plane Abduction/Adduction



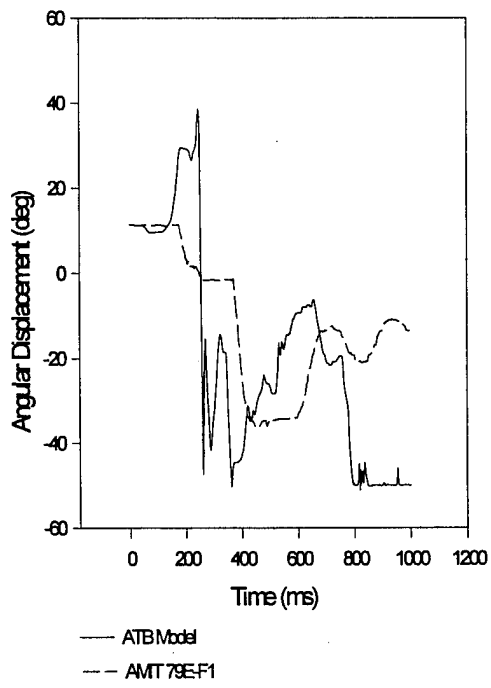
Right Shoulder Coronal Plane Abduction/Adduction



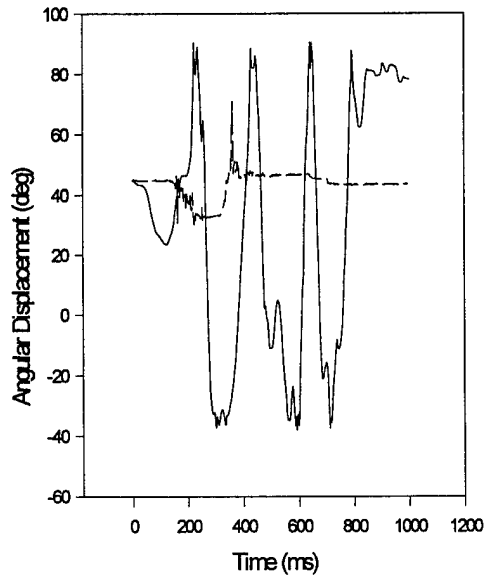
Left Shoulder Flexion



Right Shoulder Flexion

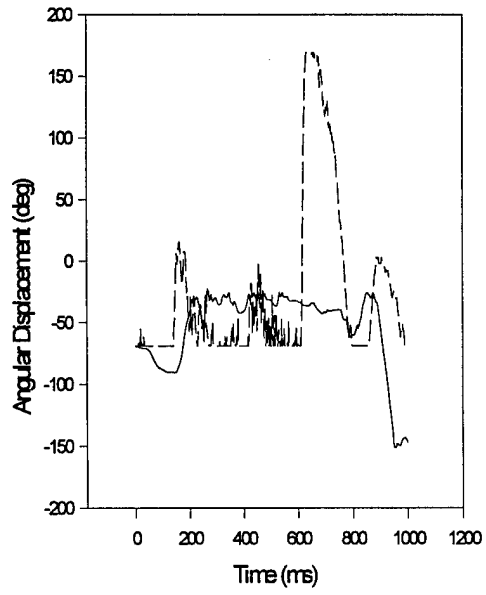


Left Shoulder Medial/Lateral



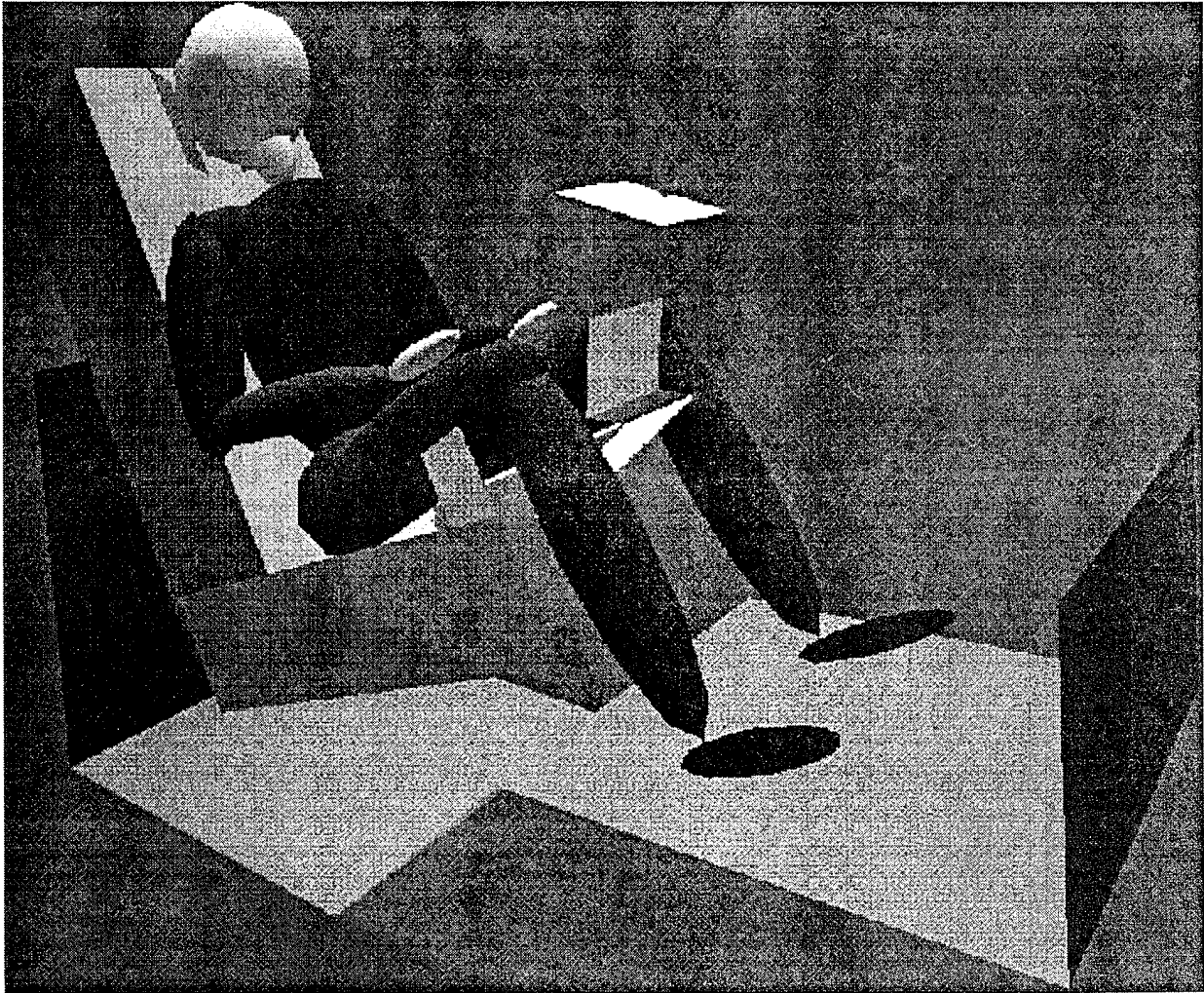
— ATB Model  
-- AMT 79E-F1

Right Shoulder Medial/Lateral

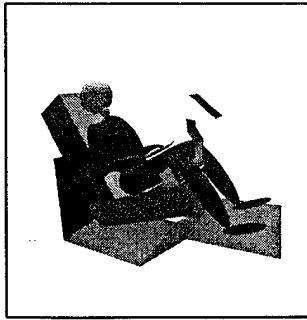


— ATB Model  
-- AMT 79E-F1

APPENDIX Y: ATB Model of ADAM, ACES II Ejection Seat and F-16 Cockpit



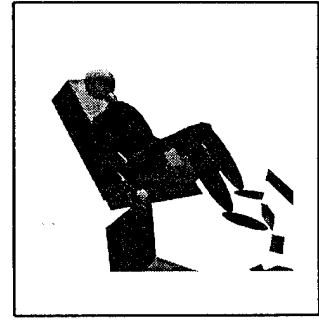
APPENDIX Z: ATB SIMULATION OF AMIT 79E-F1



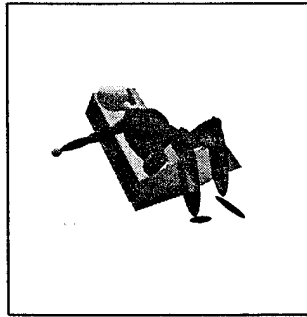
0 ms



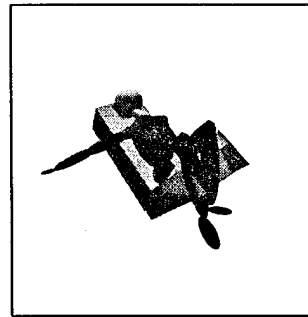
100 ms



200 ms



300 ms



400 ms



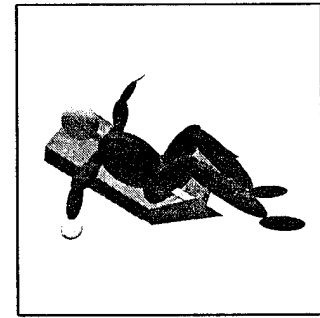
500 ms



600 ms



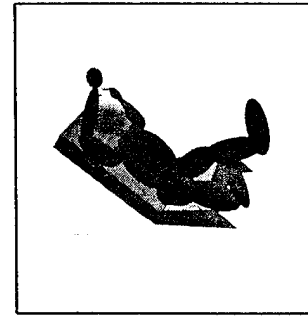
700 ms



800 ms



900 ms



1000 ms

Velocity: 237 m/s (450 KEAS)  
Orientation: Straight & Level  
Temperature: 6.7 deg C  
Pressure: 87700 N/m

## Bibliography

- Albery, Chris. Mechanical Lab Technician 3, Systems Research Laboratory, Inc., Dayton, OH, 1995.
- Bartol, Aileen M., Vernon L. Hazen, Joseph F. Kowlaski, Brian P. Murphy, Richard P. White, Jr. Advanced Anthropomorphic Manikin (ADAM) Final Design Report, February 1985 - June 1989. AAMRL-TR-90-023. Armstrong Aerospace Medical Research Laboratory, Human Systems Center, Air Force Materiel Command, Wright-Patterson Air Force, OH, March 1990.
- Clark, John J., Jr. Chief, Reports Division, Air Force Safety Office, HQ AFSA/JAR, Kirtland AFB, NM, 1995.
- Gragg, C. D. CREST ADAM/MASE Integration Test (AMIT) 79E-G2A. 46th Test Group, Holloman AFB, NM. JON:2868SQ01, 30 April 1993.
- Greenwood, Donald T. Principles of Dynamics (Second Edition). New Jersey: Prentice Hall, 1988.
- Cheg, Huaining. Mechanical Engineer, Systems Research Laboratories, Inc., Dayton, OH, 1995.
- Input Description for the Articulated Total Body Model ATB-IV.5. Biomechanics and Biocommunications Divisions, Armstrong Laboratory, Wright Patterson AFB, OH, July 1994.
- Karner, Art. Data Trend Analysis For Navy Ejections (1976 Through 1989). 31st Annual SAFE Symposium Proceedings, 8-10 November 1993.
- MATHCAD®. Version 5.0 Plus, IBM, disk. Computer Software. Houghton Mifflin Co, 1993.
- MATLAB® With SIMULINK™. MATLAB® version 4.0, SIMULINK™ version 1.2, IBM, disk. Computer software. The MathWorks, Inc., 1984-1993.
- Meyer, Michael J., 1Lt, USAF. Escape Engineer, Aircrew Protection Branch, Vehicle Subsystems Division, Flight Dynamics Directorate, Wright Laboratory, Wright Patterson AFB, OH. Telephone Interview. 3 May 1995.
- Obergefell, Lousie A., PhD. Mechanical Engineer, Vulnerability Assesment Branch, Armstrong Laboratory, Wright Patterson, AFB, OH, 1995.

- Obergefell, Louise A., Annette Rizer. Articulated Total Body (ATB) Model Course. Slides, 23-26 August 1993.
- Obergefell, Lousie A., Thomas R. Gardner, Ints Kaleps, John T. Fleck. Articulated Total Body Model Enhancements. (Volume 2: User's Guide) AAMRL-TR-88-043. Armstrong Aerospace Medical Research Laboratory, Human Systems Center, Air Force Materiel Command, Wright-Patterson Air Force, OH, January 1988.
- Peterson, Brian. Systems Engineering Student (GSE-95D), Air Force Institute of Technology, 1995.
- Plagha, John. Mechanical Engineer, Crew Escape Technologies Program Office, Armstrong Laboratory, Wright Patterson AFB, OH., 1995.
- Rasmussen, Roy R., Jr., John A. Plaga, Ints Kaleps. The Advanced Dynamic Anthropomorphic Manikin - ADAM. Biodynamics and Biocommunications Division, Armstrong Laboratory, Wright Patterson, AFB, OH., 1993.
- Rizer, Annette L., Louise A. Obergefell, Ph.D., Lt David Johnson, Gregory Thompson. Development of a Simulation Database for the Advanced Dynamic Anthropomorphic Manikin (ADAM). System Reseach Laboratories, Inc, Dayton, OH, November 1994.
- Rizer, Annette. Mechanical Engineer, Systems Research Laboratories, Inc., Dayton, OH, 1995.
- Thompson, Greg. Mechanical Lab Technician 3, Systems Research Laboratories, Inc., Dayton, OH, 1995.
- Zegler, R. E., W. J. Adams, G. R. Casteel. Crew Escape Technologies (CREST) Mission Area Requirements Study (MARS) Current and Future Escape Requirements Executive Summary. SAFE Journal, Volume 23, Number1, January - February 1993.

## Vita

Joel John Hagan [REDACTED]. He attended Embry-Riddle Aeronautical University in Daytona Beach, Florida where he earned a Bachelor of Science Degree in Aeronautical Engineering in December of 1990. At this same time he was commissioned as a Second Lieutenant in the United States Air Force. His first assignment, 31 September 1991, was to San Antonio Air Logistics Center. For the first two years of this assignment, he served as an industrial process improvement engineer, experimenting with methods of enhancing the quality of Depot production. For the last year of this assignment, he served as an aerodynamics and performance engineer in which he determined the effects on aircraft performance of specific modifications and repairs to T-37, T-38, F-5, C-5, and QF-106 aircraft. At this same time he provided engineering support to several F-15, F-16, and T-38 accident investigation boards. Following this assignment he attended the Air Force Institute of Technology (AFIT) where he earned a Masters of Science Degree in Aeronautical Engineering in December of 1995. His follow on assignment from (AFIT), 1 January 1996, is to the Phillips Laboratory at Kirtland Air Force Base, New Mexico.

# REPORT DOCUMENTATION PAGE

Form Approved  
OMB No. 0704-0188

Public reporting burden for this collection of information is estimated to average 1 hour per response, including the time for reviewing instructions, searching existing data sources, gathering and maintaining the data needed, and completing and reviewing the collection of information. Send comments regarding this burden estimate or any other aspect of this collection of information, including suggestions for reducing this burden, to Washington Headquarters Services, Directorate for Information Operations and Reports, 1215 Jefferson Davis Highway, Suite 1204, Arlington, VA 22202-4302, and to the Office of Management and Budget, Paperwork Reduction Project (0704-0188), Washington, DC 20503.

<b>1. AGENCY USE ONLY (Leave blank)</b>		<b>2. REPORT DATE</b> December 1995	<b>3. REPORT TYPE AND DATES COVERED</b> Technical Paper; Thesis	
<b>4. TITLE AND SUBTITLE</b>  Validation of the Articulated Total Body Model Data Set Describing the Large Advanced Dynamic Anthropomorphic Manikin			<b>5. FUNDING NUMBERS</b>	
<b>6. AUTHOR(S)</b>  Captain Joel Hagan				
<b>7. PERFORMING ORGANIZATION NAME(S) AND ADDRESS(ES)</b>  Air Force Institute of Technology, WPAFB OH 45433-6583			<b>8. PERFORMING ORGANIZATION REPORT NUMBER</b>  AFIT/GAE/ENR/95D-11	
<b>9. SPONSORING / MONITORING AGENCY NAME(S) AND ADDRESS(ES)</b>  AL/CFBV Wright-Patterson AFB, OH 45433-7521			<b>10. SPONSORING / MONITORING AGENCY REPORT NUMBER</b>	
<b>11. SUPPLEMENTARY NOTES</b>				
<b>12a. DISTRIBUTION / AVAILABILITY STATEMENT</b>  Approved for public release; Distribution Unlimited			<b>12b. DISTRIBUTION CODE</b>	
<b>13. ABSTRACT (Maximum 200 words)</b>  Recent cut-backs in Department of Defense spending have presented a need to augment full-scale ejection seat testing with computer simulation. To this end, the U.S. Air Force's Armstrong Laboratory has developed a data set describing the Advanced Dynamic Anthropomorphic Manikin (ADAM) for use in conjunction with the Articulated Total Body (ATB) model for the purpose of simulating the dynamics of the ADAM during sled track ejections. The purpose of this thesis is to validate the ADAM data set by graphically comparing ADAM joint angular displacements calculated by the ATB model with those measured during ejection seat sled track tests. The tests used for these comparisons are the ADAM/MASE Integration Tests (AMIT) 79E-G2A and 79E-F1. Results of initial comparisons indicate oversimplifications in original joint resistive torque function calculations. These oversimplifications result in excessive joint oscillations as simulated by the ATB model. A certain amount of success in damping these joint oscillations is realized as a result of modifications to these joint resistive torque functions. Overall, the ATB model accurately simulates ADAM motion for the first 400 milliseconds of each simulation. Beyond this time, simulation versus AMIT 79E-F1 test results correlate relatively well. Nonetheless, excessive oscillations in certain joints continue to persist.				
<b>14. SUBJECT TERMS</b>  Manikin, ADAM, Ejection Seat, Modeling, Human Body, Ejection			<b>15. NUMBER OF PAGES</b> 182	
			<b>16. PRICE CODE</b>	
<b>17. SECURITY CLASSIFICATION OF REPORT</b>  UNCLASSIFIED	<b>18. SECURITY CLASSIFICATION OF THIS PAGE</b>  UNCLASSIFIED	<b>19. SECURITY CLASSIFICATION OF ABSTRACT</b>  UNCLASSIFIED	<b>20. LIMITATION OF ABSTRACT</b>  UL	

## GENERAL INSTRUCTIONS FOR COMPLETING SF 298

The Report Documentation Page (RDP) is used in announcing and cataloging reports. It is important that this information be consistent with the rest of the report, particularly the cover and title page. Instructions for filling in each block of the form follow. It is important to *stay within the lines* to meet *optical scanning requirements*.

**Block 1. Agency Use Only (Leave blank).**

**Block 2. Report Date.** Full publication date including day, month, and year, if available (e.g. 1 Jan 88). Must cite at least the year.

**Block 3. Type of Report and Dates Covered.** State whether report is interim, final, etc. If applicable, enter inclusive report dates (e.g. 10 Jun 87 - 30 Jun 88).

**Block 4. Title and Subtitle.** A title is taken from the part of the report that provides the most meaningful and complete information. When a report is prepared in more than one volume, repeat the primary title, add volume number, and include subtitle for the specific volume. On classified documents enter the title classification in parentheses.

**Block 5. Funding Numbers.** To include contract and grant numbers; may include program element number(s), project number(s), task number(s), and work unit number(s). Use the following labels:

<b>C</b> - Contract	<b>PR</b> - Project
<b>G</b> - Grant	<b>TA</b> - Task
<b>PE</b> - Program Element	<b>WU</b> - Work Unit Accession No.

**Block 6. Author(s).** Name(s) of person(s) responsible for writing the report, performing the research, or credited with the content of the report. If editor or compiler, this should follow the name(s).

**Block 7. Performing Organization Name(s) and Address(es).** Self-explanatory.

**Block 8. Performing Organization Report Number.** Enter the unique alphanumeric report number(s) assigned by the organization performing the report.

**Block 9. Sponsoring/Monitoring Agency Name(s) and Address(es).** Self-explanatory.

**Block 10. Sponsoring/Monitoring Agency Report Number.** (If known)

**Block 11. Supplementary Notes.** Enter information not included elsewhere such as: Prepared in cooperation with...; Trans. of...; To be published in.... When a report is revised, include a statement whether the new report supersedes or supplements the older report.

**Block 12a. Distribution/Availability Statement.** Denotes public availability or limitations. Cite any availability to the public. Enter additional limitations or special markings in all capitals (e.g. NOFORN, REL, ITAR).

**DOD** - See DoDD 5230.24, "Distribution Statements on Technical Documents."

**DOE** - See authorities.

**NASA** - See Handbook NHB 2200.2.

**NTIS** - Leave blank.

**Block 12b. Distribution Code.**

**DOD** - Leave blank.

**DOE** - Enter DOE distribution categories from the Standard Distribution for Unclassified Scientific and Technical Reports.

**NASA** - Leave blank.

**NTIS** - Leave blank.

**Block 13. Abstract.** Include a brief (*Maximum 200 words*) factual summary of the most significant information contained in the report.

**Block 14. Subject Terms.** Keywords or phrases identifying major subjects in the report.

**Block 15. Number of Pages.** Enter the total number of pages.

**Block 16. Price Code.** Enter appropriate price code (*NTIS only*).

**Blocks 17. - 19. Security Classifications.** Self-explanatory. Enter U.S. Security Classification in accordance with U.S. Security Regulations (i.e., UNCLASSIFIED). If form contains classified information, stamp classification on the top and bottom of the page.

**Block 20. Limitation of Abstract.** This block must be completed to assign a limitation to the abstract. Enter either UL (unlimited) or SAR (same as report). An entry in this block is necessary if the abstract is to be limited. If blank, the abstract is assumed to be unlimited.